Small angle X-ray scattering studies on proteins under extreme conditions

Dissertation

zur Erlangung des Doktorgrades der Naturwissenschaften
der Fakultät Physik der Technischen Universität Dortmund

vorgelegt von

Martin A. Schroer

September 2011

Contents

1 Introduction

In nature, creatures have evolved that can withstand extreme conditions. Some of these so-called extremophiles can tolerate and even need such environmental conditions as e.g. low or high temperatures, pressures, pH, or salinity [Rothschild and Mancinelli, 2001]. To assure the integrity and function of the cells in these organisms, different mechanisms are present counteracting the external influences. A cell's interior is a complex liquid consisting of different macromolecules like proteins, ribosomes, lipid vesicles, or DNA molecules dissolved in water with many small molecules and ions in it [Voet et al., 2006]. These all might be affected by extreme environments. For instance, in deep sea habitats organisms have to cope with pressures up to 1 kbar which affects e.g. lipid membranes and proteins [Daniel et al., 2006]. The knowledge about the mechanisms of counteracting these external factors might give a better understanding of how life has evolved under such conditions and what conditions are still tolerable for life to exist.

A class of macromolecules present in living cells that is largely influenced by external extreme perturbations are proteins. These biomolecules are made of a linear sequence of different amino acids. The amino acid residues interact which each other and the surrounding water, which leads to a complex three-dimensional structure. This structure formation process is called folding. Proteins fulfill specific functions like catalysis of chemical reactions, signaling inside a cell and between cells, or transport of substances. Essential for most of them is the coupling between their three-dimensional structure and their biological function. Extreme conditions might lead to the loss of their complex structure, so-called unfolding, and thus of their activity.

However, the use of external perturbations can also give access to the details that govern the folding process. As proteins are affected differently depending on the type of external condition, variation of these can be used to explore the contributions of different interactions to the folded state. This approach allows to explore the phase diagram and thus the thermodynamics of a protein [Panick et al., 1999, Lassalle et al., 2000]. For instance, changes of the pH or salt content of a protein solution influence the Coulomb interaction of the amino acids or high pressure affects the protein's volumetric properties [Uversky et al., 1998a, Silva et al., 2001]. These perturbations might lead to unfolding, where the unfolded states can differ in their residual structure. The knowledge of the structure of these states, how this is influenced, and the kinetics of their for-

mation, are essential for a full understanding of the complex process of protein folding [Dill et al., 2008].

In this thesis, proteins in solutions are studied under different types of external conditions by small angle X-ray scattering (SAXS). With SAXS, samples in the nanometer regime can be studied [Feigin and Svergun, 1987, Lindner and Zemb, 2002]. It is therefore well suited to determine the size and shape of proteins and thus to investigate their unfolding due to perturbations. Furthermore, using concentrated solutions it can be used to explore the interactions between proteins. This gives the possibility to learn about the factors that govern interactions in dense protein solutions as they are present in the cell's interior.

In vivo, proteins exist in different shapes and folding states. For instance, there are globular folded proteins, with a compact shape, and more elongated ones with a linear architecture. Also proteins are known to be present in cells that are natively unfolded [Uversky, 2002]. It is therefore interesting to access the different influences of the specific properties of the local and global structure on the protein folding. This can be achieved by employing external perturbations such as pressure and pH. Another approach to study protein folding is the fabrication of mutants of a protein by mutagenesis. For example, mutants with a single amino acid substituted allow one to analyze the influence of the single residue on the protein structure. Using for instance pressure, unfolding can be induced which depends on the specific properties of the amino acid exchanged [Brun et al., 2006]. A combined approach of SAXS and extreme conditions can give insight how local changes affect the global structure. Such measurements were performed on three different types of proteins: a globular, a natively unfolded, and a non-globular linear protein.

Concentrated protein solutions under high pressures serve as simple model systems for the interior of cells in deep sea organism. In order to study the interaction between the macromolecules, SAXS measurements can be employed. These allow to monitor the pressure dependence of the proteins' interaction potential. Moreover, the influence of small biologically relevant molecules known to affect the protein stability especially under high hydrostatic pressures can be studied [Yancey et al., 2002]. Such measurements will allow to get a deeper understanding of the mechanisms established in nature to protect proteins against unfolding. A detailed knowledge on protein-protein interactions is also essential for fabrication of protein crystals necessary for protein structure determination. Finally, interactions between partially folded proteins can lead to special types of aggregates, so-called fibrils, which are suspected to be the source of plaque involved in the pathogenesis of several diseases, including Alzheimer‘s disease and prion diseases [Dobson, 2003, Selkoe, 2003]. In order to learn about these interactions, SAXS measurements were performed on concentrated proteins under high pressure in absence

and presence of small organic molecules to reveal the influence on the protein-protein interaction potential.

The outline of this thesis is as follows:

- In **chapter** 2 the theory of small angle X-ray scattering will be presented in detail. Starting with the general concepts of SAXS, the scattering on diluted and concentrated particle solutions will be discussed.

- **Chapter** 3 contains details about the experimental setups that were used. Furthermore, the general data treatment is presented.

- In **chapter** 4 the experimental studies on different folding states of proteins induced by external perturbations will be discussed. At first, common aspects of protein structure, folding, and stability are presented. Thereafter, the results of the SAXS studies are given. In paragraph 4.2 the influence of an ionizable residue inside a globular protein is studied as a function of pH and pressure. The study in paragraph 4.3 deals with electrostatic effects on a natively unfolded protein. In paragraph 4.4 the features of the folding and unfolding of a non-globular protein are investigated.

- **Chapter** 5 presents results on the protein-protein interaction in highly concentrated protein solutions under high pressures. In paragraph 5.1 proteins in buffer solution are studied for different temperatures and concentrations. In paragraph 5.2 the effects of biologically relevant osmolytes on the pressure-dependent interaction are discussed.

- **Chapter** 6 summarizes the results of the different studies performed. It closes with a short outlook.

2 Fundamentals of small angle X-ray scattering (SAXS)

Whenever studying materials with scattering techniques the in general anisotropic intensity pattern depends on the three-dimensional structure of the scattering objects and on the distances between them. In the case of X-rays as a probe, which is in the focus of this thesis, scattering takes place on the electrons within the sample under investigation. As will be shown later, characteristic distances between the electron positions will give rise to scattering signals at different scattering angles. Thus, detecting the intensity at different angles gives access to distinct length scales.

Concerning interatomic distances in the Ångstrom range as for example between the atoms of molecules in a gas or liquid or in the unit cell of solids, the corresponding scattering signal can be recorded at a scattering angle of several degrees. Hence, in the case of isotropic samples this structure analysis technique is called besides X-ray diffraction (XRD) also wide angle X-ray scattering (WAXS).

Larger structures give rise to scattering at smaller angles. Small angle X-ray scattering (SAXS) can be utilized to study samples of colloidal size, i.e. 1 to 100 nm. Looking at even larger structures besides microscopy techniques ultra small angle X-ray scattering (USAXS) can be used.

As SAXS is the technique of choice to study proteins in solution, which is the main subject of this thesis, this method will be discussed in detail in the following paragraphs. In general, small angle X-ray scattering is well suited to study both disordered structures of colloidal size immersed in an outer matrix, e.g. nanoparticles, polymers, and proteins in solutions or defects and amorphous structures in solids, as well as ordered macromolecular structures as e.g. fibers [Feigin and Svergun, 1987, Stribeck, 2007]. As a consequence, the corresponding two-dimensional scattering pattern is in the former case isotropic whereas for fiber structures an anisotropic intensity signal with a preferred orientation is detectable.

Focusing on disordered systems, the SAXS technique can provide information on the sample size, shape, and the polydispersity, and in the case of concentrated colloidal solutions also on the interparticle interactions. These structures can be interpreted as particle-like inhomogeneities inside a homogeneous matrix.

For a theoretical description of scattering on such types of particles, the finite size as well as the lack of order between them have to be considered.

This chapter is oriented on [Schroer, 2008]. Paragraph 2.1 shows how this type of scattering results in a small angle signal and its consequences for colloidal systems. Paragraph 2.2 deals with the so-called form factor which can be obtained for diluted independent particles and yields information about shape and size. In paragraph 2.3 the consequences of scattering on many non-independent particles, where interparticle interactions are not negligible, will be discussed.

2.1 X-ray scattering at small angles

In order to study the problem of scattering at small angles the typical scattering geometry is described first. A plane and monochromatic electromagnetic wave with wavelength λ_i impinges on the system of interest and excites the electrons within the sample, resulting in the emission of secondary waves. These interfere which each other. The resulting scattered wave with wavelength λ_f is detected at a scattering angle 2Θ at a distance L from the sample.

The incident wave is characterized by the wave vector $\vec{k}_\mathrm{i}$ specifying the direction of propagation. In the same way $\vec{k}_\mathrm{f}$ is introduced for the scattering wave (Fig. 2.1). Its modulus is given as

$$\left|\vec{k}_\mathrm{i}\right| = \frac{2\pi}{\lambda_\mathrm{i}} , \quad \left|\vec{k}_\mathrm{f}\right| = \frac{2\pi}{\lambda_\mathrm{f}} . \tag{2.1}$$

The wave vector transfer $\vec{q}$ describes the difference between incident and scattered wave. It is defined as

$$\vec{q} = \vec{k}_\mathrm{f} - \vec{k}_\mathrm{i} . \tag{2.2}$$

2.1.1 X-ray scattering on a free electron

To describe the scattering process on a sample system theoretically, the scattering strength $f(\vec{q}, E)$ of every atom is needed. This in general complex quantity is a function of both wave vector transfer $\vec{q}$ and the energy E of the radiation and can be written as [Feigin and Svergun, 1987]

$$f(\vec{q}, E) = f_0(\vec{q}) + f'(E) + i \cdot f''(E) . \tag{2.3}$$

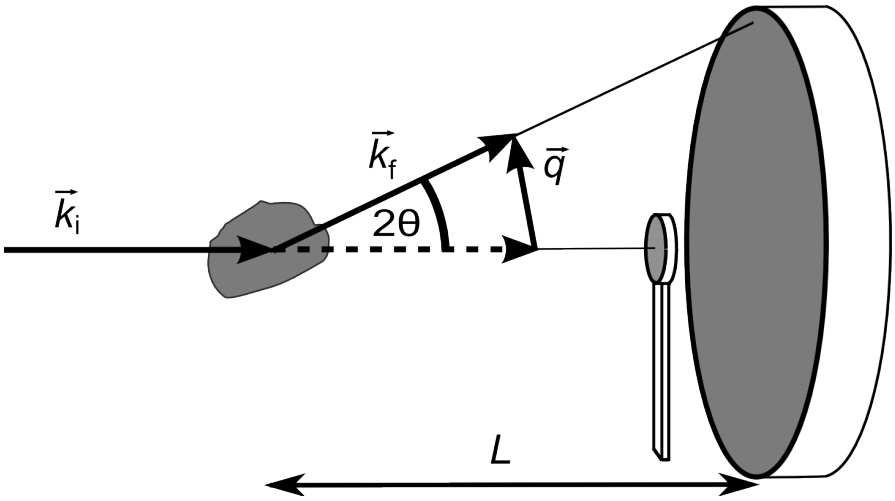

Figure 2.1: *Typical scattering geometry. The incident wave characterized by the wave vector $\vec{k}_i$ impinges on the sample and is scattered and recorded under an angle 2Θ at a distance L. The difference between $\vec{k}_i$ and the wave vector of the scattered wave, $\vec{k}_f$, defines the wave vector transfer $\vec{q}$. Shown is the situation where a two-dimensional resolving detector is utilized. In order to protect the detector from the more intense unscattered, attenuated primary beam, a beam stop is used.*

Herein, $f_0(\vec{q})$ is the form factor of the atom, $f'(E)$ is the dispersion correction, and $f''(E)$ corresponds to the absorption of X-rays. f_0, being a function of the wave vector transfer $\vec{q}$, is the Fourier transform of the electron density of the corresponding atom. Thus, for small q, i.e. $q = |\vec{q}| \to 0$, the atom form factor is equal to the total number Z of the atom's electrons. The two additional contributions $f'(E)$ and $f''(E)$ are related to each other by the so-called Kramers-Kronig relation. The strength of both varies significantly when changing the energy near and above an absorption edge of an element. This gives the chance to perform anomalous small angle X-ray scattering (ASAXS). However, as all samples studied in this thesis are biological samples which consist of atoms whose absorption edges are far below the energy of the incident X-rays (i.e. carbon C, nitrogen N, oxygen O, sulfur S), $f'(E)$ and $f''(E)$ do not have any significant contribution to the scattering signal and will not be discussed further[1] [Schurtenberger, 2002a]. In small angle X-ray scattering only elastic scattering processes are considered, i.e. $\left|\vec{k}_i\right| = \left|\vec{k}_f\right| = \frac{2\pi}{\lambda}$. Hence, the wave vector transfer (eq. (2.2)) for elastic scattering is given as

$$q = |\vec{q}| = \frac{4\pi}{\lambda} \sin\Theta \,. \tag{2.4}$$

[1] In the case of small angle neutron scattering (SANS) the scattering process depends on the scattering length density b of the sample's nuclei. Here the exchange of hydrogen atoms with a negative neutron length density by deuterium atoms with a positive b gives the opportunity for so-called contrast variation or contrast matching.

For elastic scattering q is a unique function of the scattering angle at fixed λ. Contributions of inelastic scattering processes lead to an unstructured background at these angles. Hence, these will not be taken into account.

For SAXS on biological samples such as proteins the relevant contribution of the scattering strength is reduced to $f_0(\vec{0})$, further denoted as f. It is fully sufficient to describe the electrons of the atoms as free and not bound. Thus, the scattering contribution of a single atom at small angles is given as that of a single electron times the electron number Z.

For elastic scattering on a free electron the ratio between scattered intensity I_f and incident intensity I_i is given in dipole approximation by the so-called Thomson scattering formula [Als-Nielsen and McMorrow, 2001]

$$\begin{aligned} \frac{I_\mathrm{f}}{I_\mathrm{i}} &= \left(\frac{e^2}{4\pi\epsilon_0 mc^2}\right)^2 \cdot \frac{1}{L^2} \cdot \frac{(1+\cos^2(2\Theta))}{2} \\ &= \frac{r_0^2}{L^2} \cdot \Pi\left(2\Theta\right) \ . \end{aligned} \tag{2.5}$$

Herein, e denotes the elementary charge, m the electron rest mass, ϵ_0 the vacuum permittivity, c the speed of light, and L the distance from the electron to the point of detection. All constants are combined to the classic electron radius r_0 also known as Thomson scattering length. Its numerical value is $r_0 = 2.82 \cdot 10^{-5}$ Å. The polarization factor $\Pi\left(2\Theta\right)$ takes the radiation characteristic of the electron into account. For small angles, which are considered in this thesis, this factor is $\Pi\left(2\Theta\right) \approx 1$.

2.1.2 The kinematic approximation

Consider a system of electrons characterized by a charge distribution $\rho(\vec{r})$ for which the assumptions in paragraph 2.1.1 are valid. Herein, $\vec{r}$ denotes the spatial variable. If the size of this sample system is much smaller than the sample-to-detector distance, the scattering process can be treated in the so-called far field approximation. If an X-ray with $\vec{k_\mathrm{i}}$ and an electrical field strength of modulus E_i impinges on a sample, the plane wave excites the electrons within the sample resulting in the emission of secondary waves. In the case that the interaction between the electronic system and the electromagnetic wave is weak, these secondary waves will not be scattered again. For a single scattering event the resulting wave with amplitude $E_\mathrm{f}(\vec{r'})$ is given in the kinematic approximation [Pietsch et al., 2004], identical with the first Born approximation [Dawydow, 1981], as

$$E_\mathrm{f}(\vec{r'}) = E_\mathrm{i} \cdot e^{i\vec{k_\mathrm{i}}\cdot\vec{r'}} + E_\mathrm{i} \cdot \frac{e^{ik_\mathrm{i}\cdot r'}}{r'} \cdot r_0 \cdot \int_\mathrm{Vol} \rho(\vec{r})\ e^{i\,\vec{q}\cdot\vec{r}} d^3r \ . \tag{2.6}$$

The first term on the right-hand side corresponds to a non-interacting plane wave. This primary beam will be masked in an experiment by the use of a beam stop. The second term is the scattering contribution. Any infinitesimal element $\rho(\vec{r})d^3r$ of the sample system is the source of a spherical wave. These spherical waves interfere and are detected at a distance L. The so-called scattering amplitude is mathematically equal to the Fourier transform of the charge distribution. An example for this relation is the aforementioned atomic form factor $f_0(\vec{q})$. The scattering amplitude is defined as

$$A(\vec{q}) = r_0 \cdot \int_{\mathrm{Vol}} \rho(\vec{r})\ e^{i\vec{q}\cdot\vec{r}} d^3r\ . \tag{2.7}$$

The product of the Thomson scattering length r_0 and the charge density $\rho(\vec{r})$ is known as scattering length density. In this thesis all further considerations of the scattering process will start from the scattering amplitude $A(\vec{q})$.

At this point the so-called differential scattering cross section $\frac{d\sigma}{d\Omega}(\vec{q})$ is introduced. It is given as

$$\frac{d\sigma}{d\Omega}(\vec{q}) = A(\vec{q}) \cdot A^*(\vec{q})\ . \tag{2.8}$$

$A^*(\vec{q})$ denotes the complex conjugate of the scattering amplitude. The differential scattering cross section characterizes the number of photons scattered into the volume element $d\Omega$ relative to the incoming flux.

The scattering intensity is the physical quantity measured in a scattering experiment. It is given as

$$I(\vec{q}) = I_0\ \frac{1}{L^2}\ \frac{d\sigma}{d\Omega}(\vec{q})\ . \tag{2.9}$$

$I_0 = E_{\mathrm{i}}^2$ is the intensity of the incident beam.

The scattering signal is a real number, i.e. the imaginary part specifying the phase relations cancels. Due to this so-called phase problem it is not possible to get direct access to the electron distribution by a simple inversion of the intensity profiles recorded in a scattering experiment [Als-Nielsen and McMorrow, 2001]. This problem is present for all scattering techniques employing X-rays for structure analysis.

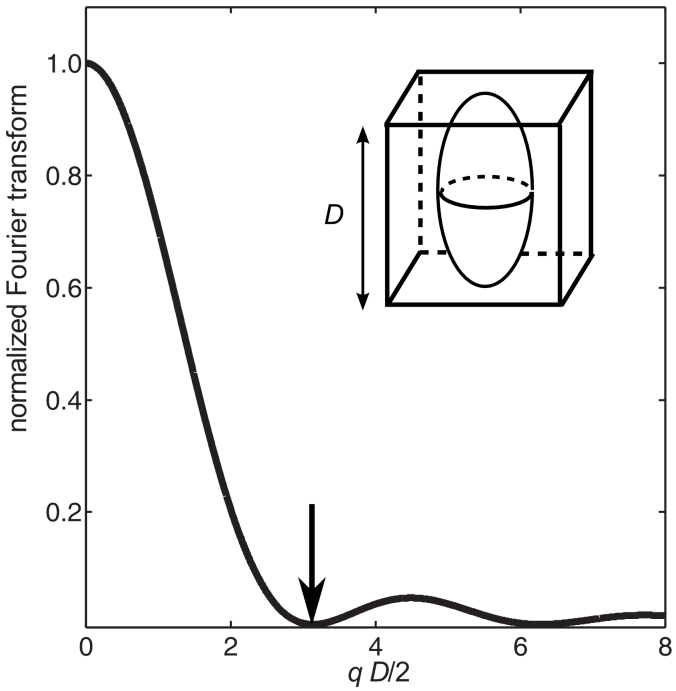

Figure 2.2: *Normalized Fourier transform of a function which is constant in the interval 0 to D and serves as a model for a cube. The first root of the scattering curve is tagged by an arrow. In the inset, the position of a particle inside the cube is shown.*

2.1.3 Length scale estimations

As the scattering amplitude $A(\vec{q})$ is related to the electron distribution via a Fourier transformation, a relation between the typical system dimension D and the corresponding q-range where the scattering function is most pronounced can be given. In the following, consider scattering on a single particle with constant electron density ρ having roughly the same dimension in all directions. In order to estimate the wave vector transfer q_c where the scattering curve has a characteristic structure, the particle is set into a cube whose edge length D is equal to the maximum particle diameter. For this equivalent cube the scattering amplitude is calculated. As the Fourier transform factorizes with the space dimensions only the one-dimensional case has to be considered.

For the edge of the cube the normalized scattering amplitude is given as

$$A(q) = r_0 \cdot \frac{\sin\left(q \cdot \frac{D}{2}\right)}{q \cdot \frac{D}{2}} \,. \tag{2.10}$$

A characteristic feature of the corresponding intensity curve (Fig. 2.2) is its first root at $\frac{q_c \cdot D}{2} = \pi$. In an experiment the q-range close to this q_c should be detected. This yields the following relation

$$q_c = \frac{2\pi}{D} \,. \tag{2.11}$$

Thus, the larger the particle, the smaller the corresponding characteristic q-range.

In the case of scattering on small, globular proteins, typical length scales are 2.5 to 4.4 nm, which corresponds to a q-range of 1.4 to 2.5 nm^{-1}. Thus, in a SAXS experiment on protein solutions a q-range from roughly about 0.1 up to 3.5 nm^{-1} should be detected. Employing eq. (2.4) with a typical wavelength of $\lambda = 0.1$ nm the corresponding scattering angles 2Θ are 1.3 ° and 2.3 °, respectively. This order of magnitude justifies the assumptions made above and gives the technique its name.

2.1.4 Scattering on complex particles

The general formulation of the scattering amplitude, eq. (2.7), is used in this paragraph to describe the scattering from complex particles. With this term large macromolecules as well as inclusions in solids with size in the nanometer regime are denoted.

Consider the scattering signal of identical particles with volume V_p and charge density $\rho^{(\mathrm{p})}(\vec{r})$. The description of a particle by a continuous charge distribution instead of its scattering strength f is valid if its size is large compared to internal structure inhomogeneities [Porod, 1982].

These particles are placed unorderedly in a sample volume hit by an incident X-ray. The term "unordered" states that all orientations of the particles have the same probability and that no preferred orientation exists. Within this sample volume a mean number $\bar{N}$ of particles is excited to scatter [Guinier and Fournet, 1955]. As in this system no long range order exist, the distribution of particles is isotropic. The total charge distribution can be written as

$$\rho(\vec{R}) = \sum_{j=1}^{\bar{N}} \rho^{(\mathrm{p})}(\vec{R} - \vec{R_j}) \; . \tag{2.12}$$

Herein, $\vec{R_j}$ denotes the center of particle j. As depicted in Fig. 2.3, $\vec{R} = \vec{R_j} + \vec{r}$. Hence, the differential cross section is given as

$$\begin{aligned} \frac{d\sigma}{d\Omega}(\vec{q}) &= r_0^2 \cdot \left\{ \sum_{j=1}^{\bar{N}} e^{i\vec{q}\cdot\vec{R_j}} \int_{V_\mathrm{p}} \rho_j^{(\mathrm{p})}(\vec{r}) \; e^{i\vec{q}\cdot\vec{r}} d^3r \right\} \cdot \left\{ \sum_{k=1}^{\bar{N}} e^{-i\vec{q}\cdot\vec{R_k}} \int_{V_\mathrm{p}} \rho_k^{(\mathrm{p})}(\vec{r'}) \; e^{-i\vec{q}\cdot\vec{r'}} d^3r' \right\} \\ &= r_0^2 \cdot \sum_{j,k=1}^{\bar{N}} e^{i\vec{q}\cdot\left(\vec{R_j}-\vec{R_k}\right)} \int_{V_\mathrm{p}} \int_{V_\mathrm{p}} \rho_j^{(\mathrm{p})}(\vec{r}) \rho_k^{(\mathrm{p})}(\vec{r'}) e^{i\vec{q}\cdot\left(\vec{r}-\vec{r'}\right)} \; d^3r \; d^3r' \; . \end{aligned} \tag{2.13}$$

The terms of the double sum with the same index $j = k$ correspond to scattering on one and the same particle. Those terms with $j \neq k$ reflect scattering on two different particles and are thus due to interference. This interference term depends on the inter-

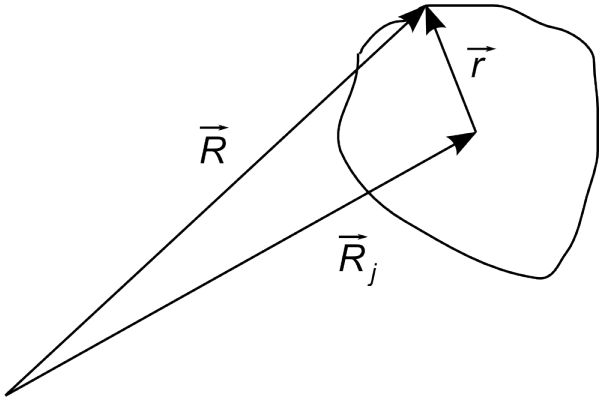

Figure 2.3: *Schematic drawing of the different vectors used in the calculations.*

particle distance which itself is a function of interactions between the particles. Thus, this term characterizes the particle-particle interaction.

Decomposing the sums results in

$$\frac{d\sigma}{d\Omega}(\vec{q}) = r_0^2 \cdot \left\{ \bar{N} \left|F(\vec{q})\right|^2 + \sum_{j=1}^{\bar{N}} \sum_{k \neq j}^{\bar{N}} F_j(\vec{q}) \cdot F_k^*(\vec{q})\ e^{i\,\vec{q}\cdot(\vec{R_j}-\vec{R_k})} \right\} , \tag{2.14}$$

with

$$F_j(\vec{q}) = \int_{V_\mathrm{P}} \rho_j^{(\mathrm{p})}(\vec{r})\ e^{i\,\vec{q}\cdot\vec{r}}\ d^3r\ . \tag{2.15}$$

The so-called form amplitude $F_j(\vec{q})$ is the Fourier transform of the charge distribution $\rho_j^{(\mathrm{p})}(\vec{r})$ of particle j and characterizes its size and shape.

The two quantities $F(\vec{q})$ and $\left|F(\vec{q})\right|^2$ refer to scattering on ordered particles that have a special arrangement to each other. However, this is not the case for colloidal particles in liquid solution, which are in the focus of this thesis. These particles obey Brownian motion and move diffusively through the region irradiated by the X-rays. For this type of systems ergodicity is assumed, i.e. there is no difference between temporal reorientation of a single particle and different orientations of many particles [Spalla, 2002]. Instead of eq. (2.14) the differential cross section statistically averaged over all orientations, $\frac{d\sigma}{d\Omega}(q) := \left\langle \frac{d\sigma}{d\Omega}(\vec{q}) \right\rangle_\Omega$, is calculated[2].

[2] $\langle\cdot\rangle_\Omega$ denotes the statistical average over all orientations. For a given function $f(\vec{q})$ it is explicitly given as

$$\langle f(\vec{q})\rangle_\Omega = \frac{\int_0^{2\pi}\int_0^{\pi} f(q,\theta,\phi)\sin(\theta)\,d\theta\ d\phi}{4\pi} ,$$

with θ and ϕ denoting the solid angles.

It is given as

$$\frac{d\sigma}{d\Omega}(q) = r_0^2 \cdot \left\{ \bar{N} \left\langle |F(\vec{q})|^2 \right\rangle_\Omega + \left\langle \sum_{j=1}^{\bar{N}} \sum_{k \neq j}^{\bar{N}} F_j(\vec{q}) \cdot F_k^*(\vec{q}) \; e^{i\,\vec{q}\cdot(\vec{R_j}-\vec{R_k})} \right\rangle_\Omega \right\} . \qquad (2.16)$$

This term is exact for monodisperse particles. To further go on with the calculations, the right term on the right-hand side has to be averaged over all orientations. Therefor, it is assumed that particle distance and orientation are not correlated. Thus, a particle's orientation in space does not have any influence on how far another particle is separated. This so-called decoupling approximation is valid for not too highly concentrated solutions [Kotlarchyk and Chen, 1983, Kaler, 1995]. The form amplitudes $F_j(\vec{q})$ are uncorrelated, can be averaged independently, and, hence, factorize. This gives

$$\left\langle \sum_{j=1}^{\bar{N}} \sum_{k \neq j}^{\bar{N}} F_j(\vec{q}) \cdot F_k^*(\vec{q}) \; e^{i\,\vec{q}\cdot(\vec{R_j}-\vec{R_k})} \right\rangle_\Omega = \left\langle F(\vec{q}) \right\rangle_\Omega^2 \cdot \left\langle \sum_{j=1}^{\bar{N}} \sum_{k \neq j}^{\bar{N}} e^{i\,\vec{q}\cdot(\vec{R_j}-\vec{R_k})} \right\rangle_\Omega . \qquad (2.17)$$

In contrast to the first term in eq. (2.16), where the product of the form amplitudes is averaged, here the product of the averaged quantity is computed. Both quantities are equal in the case of centrosymmetric particles.

The interference term averaged over all orientations is equivalent to scattering on point scatterers distributed in space each emitting a q-dependent intensity $\langle F(\vec{q}) \rangle_\Omega^2$. Thus, the interference term can be written in the isotropic case as [Hansen and McDonald, 1986]

$$\left\langle \sum_{j=1}^{\bar{N}} \sum_{k \neq j}^{\bar{N}} e^{i\,\vec{q}\cdot(\vec{R_j}-\vec{R_k})} \right\rangle_\Omega = \frac{\bar{N}^2}{V} \; 4\pi \int_0^{V^{1/3}} r^2 \; g(r) \frac{\sin(qr)}{qr} dr \; . \qquad (2.18)$$

V denotes the volume irradiated by the X-rays. Herein, the radial pair distribution function $g(r)$ has been introduced. This function quantifies the system's order. The integral is basically the Fourier transform of $g(r)$ averaged over all orientations. For systems without any long-range order, as it is the case in the present discussion, it is

$$\lim_{r \to \infty} g(r) \to 1 \; . \qquad (2.19)$$

Additional properties of $g(r)$ will be given in paragraph 2.3.

Writing the integrand in eq. (2.18) as $g(r) - 1 + 1$ gives two integrals. The first one is

$$\int_0^{V^{1/3}} r^2 \; (g(r) - 1) \, \frac{\sin(qr)}{qr} dr \; ,$$

being non-zero for those r only at which short-range order is present. Thus, the upper

integration boundary can be set to infinity.

The second integral is basically the three-dimensional Fourier transform of the irradiated volume

$$\int_0^{V^{1/3}} r^2 \, \frac{\sin(qr)}{qr} dr \, .$$

As this volume is much larger than the colloidal particles its corresponding scattering signal will be most pronounced at very small angles (see paragraph 2.1.3) which is not detectable at all. Hence, this scattering contribution needs not to be considered anymore [Guinier and Fournet, 1955].

In summary it is

$$\frac{d\sigma}{d\Omega}(q) = r_0^2 \, \bar{N} \cdot \left\{ \left\langle |F(\vec{q})|^2 \right\rangle_\Omega + \langle F(\vec{q}) \rangle_\Omega^2 \, \frac{\bar{N}}{V} \cdot 4\pi \int_0^\infty r^2 \, (g(r) - 1) \, \frac{\sin(qr)}{qr} dr \right\} \, . \tag{2.20}$$

In order to arrange this term more clearly, the so-called form factor of a particle

$$P(q) = \left\langle |F(\vec{q})|^2 \right\rangle_\Omega \tag{2.21}$$

as well as the structure factor

$$S(q) = 1 + 4\pi \, \frac{\bar{N}}{V} \int_0^\infty r^2 \, (g(r) - 1) \, \frac{\sin(qr)}{qr} dr \tag{2.22}$$

are introduced. $P(q)$ is a function of the size and shape of the particle and $S(q)$ is characterized by the interactions between the particles.

This gives

$$\frac{d\sigma}{d\Omega}(q) = r_0^2 \, \bar{N} P(q) \cdot \{1 + \beta(q) \cdot (S(q) - 1)\} \, , \tag{2.23}$$

with

$$\beta(q) = \frac{\langle F(\vec{q}) \rangle_\Omega^2}{\left\langle |F(\vec{q})|^2 \right\rangle_\Omega} \, . \tag{2.24}$$

In the case of centrosymmetric particles, it is $\beta(q) = 1$. Thus, the signal is proportional to the product of form factor and structure factor.

In order to have a compact notation also for less symmetric particles the effective

structure factor is additionally introduced as[3] [Kotlarchyk and Chen, 1983, Kaler, 1995]

$$S_{\text{eff}}(q) = 1 + \beta(q) \cdot (S(q) - 1) \ . \tag{2.25}$$

The scattered intensity of a system of monodisperse particles detected at a distance L is given as

$$I(q) = I_0 \ \frac{r_0^2}{L^2} \cdot \bar{N} \cdot P(q) \cdot S_{\text{eff}}(q) \ . \tag{2.26}$$

As can be seen on eq. (2.26) the scattering signal does not depend on the orientation of q. Due to the different orientations of the particles, information on the spatial order is lost.

2.1.5 The SAXS signal

In principle, all information on the system of interest are given in the form factor $P(q)$ and the effective structure factor $S_{\text{eff}}(q)$. However, in an experiment two additional contributions have an influence on the detected SAXS signal. These are absorption and contrast.

The absorption of X-rays results in a reduction of the intensity. In general, absorption takes place in all matter penetrated by the beam. In the case of macromolecules in solution the dominant contribution of absorption will be due to the solvent as long as the number of the particles per volume, $n = \frac{\bar{N}}{V}$, in the sample is small. As the beam of a spot size A passes the sample volume of thickness d, the transmission T of the sample is given in the small angle approximation as [Lindner, 2002]

$$T = e^{-\mu d} \ . \tag{2.27}$$

Herein μ is the linear absorption coefficient of the solvent.

Up to this point the calculations were performed for particles in vacuum. However, in a real experiment they are dissolved, i.e. are embedded in a matrix. Thus, the form factor depends on the difference between the electron distributions of the solvated macromolecule and the solvent. As the solvent molecules are much smaller than the colloidal particle, their electron density ρ_{s} averaged over the volume of the solvated particle can be treated as constant. Scattering on a volume V containing a single

[3] A similar relation holds for the case of spherical polydisperse particles.

macromolecule and solvent only gives

$$A_{\mathrm{c}}(\vec{q}) = r_0 \int_{V_{\mathrm{P}}} \rho^{(\mathrm{p})}(\vec{r})\; e^{i\,\vec{q}\cdot\vec{r}}\; d^3r + \rho_{\mathrm{s}} \cdot r_0 \int_{V-V_{\mathrm{P}}} e^{i\,\vec{q}\cdot\vec{r}}\; d^3r \qquad (2.28)$$
$$= r_0 \int_{V_{\mathrm{P}}} \Delta\rho(\vec{r})\; e^{i\,\vec{q}\cdot\vec{r}}\; d^3r + \rho_{\mathrm{s}} \cdot r_0 \int_{V} e^{i\,\vec{q}\cdot\vec{r}}\; d^3r\;,$$

introducing the contrast $\Delta\rho(\vec{r}) = \rho^{(\mathrm{p})}(\vec{r}) - \rho_{\mathrm{s}}$.

If there are no correlated density fluctuations in the solvent, the second term in eq. (2.28) corresponds to the undetectable forward scattering, i.e. all scatterers in the sample are in phase [Goodisman and Brumberger, 1973]. In this case the scattering intensity is the square of the first term. In the case of correlations in the solvent the second term gives a detectable signal. For small angle scattering on water the signal is a constant in the relevant q-range being proportional to the isothermal compressibility [Orthaber et al., 2000]. Calculating the square of the amplitude results in a mixing term that can give an additional contribution [Goodisman and Brumberger, 1973]. However, these terms should be negligible in the relevant q-range [Carpenter and Mattice, 1977].

The contrast dependent form factor $P_{\mathrm{c}}(q)$ is given as

$$P_{\mathrm{c}}(q) = \left\langle \left| \int_{V_{\mathrm{P}}} \Delta\rho(\vec{r})\; e^{i\,\vec{q}\cdot\vec{r}}\; d^3r \right|^2 \right\rangle_{\Omega}\;. \qquad (2.29)$$

Comparing the average electron density of a protein, $\bar{\rho}_{\mathrm{P}} \approx 420\ \frac{\mathrm{electrons}}{\mathrm{nm}^3}$, to that of pure water, $\rho_{\mathrm{s}} \approx 334\ \frac{\mathrm{electrons}}{\mathrm{nm}^3}$, demonstrates the contrast-induced reduction of the scattering signal [Svergun and Koch, 2003]. In order to obtain a good signal-to-noise ratio either the sample needs to be exposed to the X-ray beam for a longer time or a source with a higher intensity has to be used. The last point is fulfilled by third generation synchrotron light sources.

In a real SAXS experiment the detected scattering intensity is instead of eq. (2.26) given by

$$I(q) = I_0\, \frac{r_0^2}{L^2} \cdot T \cdot A \cdot d \cdot n \cdot P_{\mathrm{c}}(q) \cdot S_{\mathrm{eff}}(q)\;. \qquad (2.30)$$

The incident intensity I_0, the sample-to-detector distance L, the transmission T, the beam size A, and the sample thickness d are determined by the beam properties and the experimental setup. $P_{\mathrm{c}}(q)$ and $S_{\mathrm{eff}}(q)$ contain information on the studied system. Thus, the form factor as well as the structure factor will be discussed in detail in the following paragraph.

2.2 The form factor

Here, the case of diluted solutions is considered. Following eq. (2.22), as $\frac{\bar{N}}{V} = n$ is assumed to be small, this means

$$\lim_{n \to 0} S(q) \to 1 \ , \tag{2.31}$$

i.e. the scattering signal of $\bar{N}$ independent scattering particles is detectable.

Neglecting those parameters which are determined by the experimental setup the scattering curve is equal to the particle form factor $P_{\mathrm{c}}(q)$. The form factor's properties will be discussed now in more detail.

2.2.1 Scattering from geometrical bodies

According to eq. (2.29) the form factor is given by the square of the Fourier transform of the charge density difference between particle and solvent averaged over all possible orientations. In the following the contrast, if not mentioned explicitly, is taken as constant and thus the index in $P_{\mathrm{c}}(q)$ is dropped.

In the case of discrete scatterers the form factor according to Debye is given by [Debye, 1915]

$$P(q) = \sum_j \sum_k f_j f_k \frac{\sin(q r_{jk})}{q r_{jk}} \ . \tag{2.32}$$

Herein r_{jk} denotes the distance between two point-like scatterers with scattering strength f_j and f_k. Averaging over all orientations results in the decay of the scattering signal with increasing wave vector transfer q. In principle the Debye formula can always be used when the exact atomic positions are known.

As this condition is not alway fulfilled the Fourier transform of a continuous charge distribution has to be calculated. However, instead of using the exact $\rho(\vec{r})$, usually the averaged charge density $\bar{\rho}$ of the particle is employed. As this quantity is constant the determination of the form factor reduces to the calculation of the Fourier transform and its orientation average. Often macromolecules and nanoparticles are modeled by simple geometrical bodies for which the form factor can be calculated.

In the following list the form factors of some typical geometrical bodies normalized to the respective volumes are given.

- sphere with radius R [Guinier and Fournet, 1955]

$$P_{\mathrm{S}}(q) = |F_{\mathrm{S}}(qR)|^2 = \left[3\,\frac{\sin(qR) \;-\; qR\,\cos(qR)}{q^3R^3}\right]^2 \tag{2.33}$$

- hollow sphere with inner radius R_{i} and outer radius R_{o} [Mittelbach, 1964]

$$P_{\mathrm{HS}}(q) = \frac{\left[R_{\mathrm{o}}^3 F_{\mathrm{S}}(qR_{\mathrm{o}}) - R_{\mathrm{i}}^3 F_{\mathrm{S}}(qR_{\mathrm{i}})\right]^2}{(R_{\mathrm{o}}^3 - R_{\mathrm{i}}^3)^2} \tag{2.34}$$

- ellipsoid of revolution with semiaxes a and b [Mittelbach and Porod, 1962]

$$P_{\mathrm{RE}}(q) = \int_0^1 F_{\mathrm{S}}^2(q\sqrt{a^2 + x^2\cdot(b^2 - a^2)})\;dx \tag{2.35}$$

- triaxial ellipsoid with semiaxes a, b, and c [Mittelbach and Porod, 1962]

$$P_{\mathrm{TE}}(q) = \int_0^1\int_0^1 F_{\mathrm{S}}^2\,(q\;r(x,y))\,dxdy\;; \tag{2.36}$$
$$r(x,y) = \sqrt{\left(a^2\cos^2(\frac{\pi x}{2}) + b^2\sin^2(\frac{\pi x}{2})\right)\cdot(1-y^2) + c^2y^2}$$

- cylinder with radius R and height H ($J_1(x)$ denoting the first order Bessel function) [Guinier and Fournet, 1955]

$$P_{\mathrm{C}}(q) = \int_0^{\pi/2}\left[\frac{2J_1(qR\sin\alpha)}{qR\sin\alpha}\frac{\sin(qH\cos\alpha/2)}{qH\cos\alpha/2}\right]^2\sin\alpha\;d\alpha \tag{2.37}$$

Except for the form factor of a sphere the integrals are only numerically solvable due to the averaging process. A comprehensive list of various different form factors can be found in [Pedersen, 2002].

For extremely anisotropic particles such as long thin rods or flat discs the scattering amplitudes can be separated into a diameter factor and a length factor. For these the averaging and thus the integration can be done independently [Porod, 1982]. For rods the cylinder axis is much longer than the diameter and thus the form factor separates into scattering from a quasi-one-dimensional object, i.e. the long axis, and a quasi-two-dimensional object, i.e. the much smaller diameter. In the case of discs the length relations are reversed, i.e. the quasi-two-dimensional object is much larger. For these

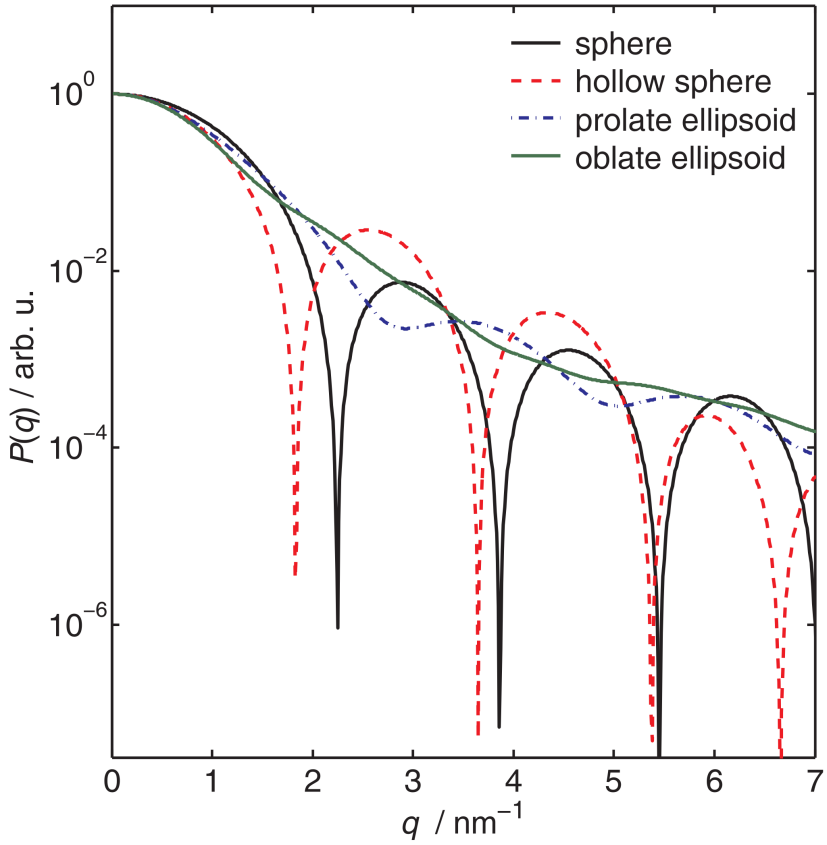

Figure 2.4: *Form factors of various geometrical bodies with identical volume. The following values were used to calculate the curves: sphere $R = 2.0$ nm; hollow sphere $R_\mathrm{i} = 1.2$ nm, $R_\mathrm{o} = 2.1$ nm; prolate ellipsoid of revolution $a = 1.5$ nm, $b = 3.6$ nm; oblate ellipsoid of revolution $a = 3.0$ nm, $b = 0.9$ nm.*

types of particles the form factor can thus be written for large q as

$$P_\mathrm{anisotropic}(q) = \text{const. } q^{-p}\, I_\mathrm{cs}(q)\ , \tag{2.38}$$

wherein the constant includes the geometrical size of the larger object, i.e. cylinder axis for the rod and diameter for the disc. Depending on the dimension of the larger part, the power law exponent p has a characteristic value. It is $p = 1$ for rods and $p = 2$ for discs. Hence, dimensionality is reflected in the power of the decay of the form factor. In the following paragraphs these relations will be discussed more generally again.

Now it will be focused on less anisotropic particles. Fig. 2.4 depicts some form factors of different geometrical bodies. Although the same volume was assumed, significant differences are detectable. In the case of bodies with spherical symmetry the form factor has sharp minima. These are absent for less symmetrical bodies. Due to the finite resolution in a SAXS experiment, these pronounced minima will not be detectable. However, differences between distinct objects will be observed as long as the shape and size are not too similar.

As is shown by this example, the scattering curve depends not only on the particle size but is also a function of the shape of the scatterer. An unique interpretation of the curves is delicate and in principle also impossible as the information is lost during the orientation averaging. Objects with spherical symmetry can be distinguished from those with a strong asymmetric shape but differences in the scattering curves of a homogeneous sphere and a hollow sphere are less obvious.

2.2.2 The radial pair-distance distribution function

As shown previously, the form amplitude $F(\vec{q})$ is the Fourier transform of the charge density $\rho(\vec{r})$. Now it will be discussed how the Fourier transform of the form factor $P(q)$ is related to the electron distribution function and if additional information can be obtained by this.

Using eq. (2.15) $|F(\vec{q})|^2$ can be written as

$$\begin{aligned} |F(\vec{q})|^2 &= \int_{V_\mathrm{P}} \int_{V_\mathrm{P}} \rho(\vec{r'})\ \rho(\vec{r'}+\vec{r})\ e^{i\,\vec{q}\cdot\vec{r}} d^3r'\ d^3r \\ &= \int_{V_\mathrm{P}} \gamma(\vec{r})\ e^{i\,\vec{q}\cdot\vec{r}} d^3r\ . \end{aligned} \tag{2.39}$$

Herein the mutual auto-correlation function [Glatter, 2002],

$$\gamma(\vec{r}) = \rho(\vec{r}) * \rho(-\vec{r}) = \int_{V_\mathrm{P}} \rho(\vec{r'})\rho(\vec{r'}+\vec{r})\ d^3r' \tag{2.40}$$

is introduced, which is also called Patterson function [Feigin and Svergun, 1987]. Mathematically this is the self-convolution of the charge density $\rho(\vec{r})$.

Averaging over all orientations gives for the form factor $P(q)$

$$P(q) = 4\pi \int_0^\infty \gamma(r)\ r^2\ \frac{\sin(qr)}{qr}\ dr\ . \tag{2.41}$$

$\gamma(r) = \langle \gamma(\vec{r}) \rangle_\Omega$ is the so-called characteristic function [Debye and Bueche, 1949] [Porod, 1951, Porod, 1952]. For homogeneous particles it is a function of shape only.

The geometrical interpretation of $\gamma(\vec{r})$ and $\gamma(r)$ can be best demonstrated for a sphere with constant charge density. For this spherically symmetric example both functions are identical. The characteristic function describes the volume that two spheres have in common as a function of the distance r of the centers (Fig. 2.5).

Similar to the form factor the sphere is one of the few bodies for which the characteristic function is given in an analytical form. The characteristic function of a sphere

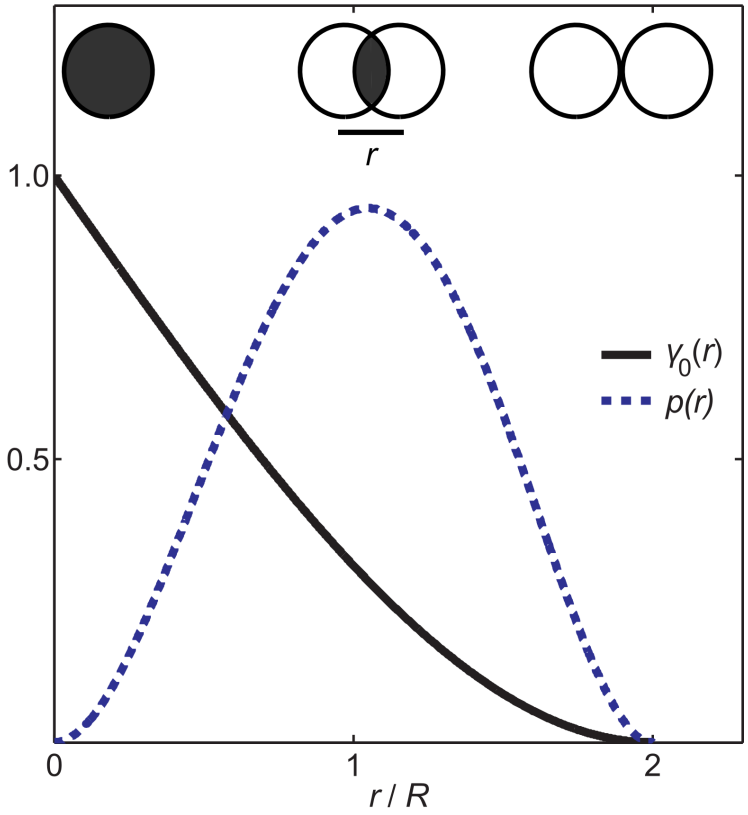

Figure 2.5: *The normalized characteristic function $\gamma_0(r)$ and the radial pair-distance distribution function $p(r)$ of a sphere with radius R. The corresponding geometrical interpretation is shown additionally.*

divided by the volume V_S is given as [Porod, 1948]

$$\gamma_0(r) = \frac{\gamma(r)}{V_S} = 1 - \frac{3}{4}\frac{r}{R} + \frac{1}{16}\left(\frac{r}{R}\right)^3 . \tag{2.42}$$

For $r = 0$, both spheres overlap. The shared volume is $V_S = \frac{4}{3}\pi R^3$ and thus $\gamma_0(0) = 1$. With increasing distance of the centers the overlapping volume reduces. At a characteristic distance $D_{\max}$, the maximum particle extension, the shared volume vanishes, i.e. $\gamma(D_{\max}) = 0$. In the case of a sphere $D_{\max}$ is obviously the diameter.

For particles without spherical symmetry the volume in common depends on the orientation of the two bodies to each other. The averaging process thus takes place over all possible orientations between the particles. It is noteworthy that the form factor is given by averaging $\gamma(\vec{r})$ and not by the averaged charge density $\rho(r)$.

Instead of the characteristic function the radial pair-distance distribution function is often used

$$p(r) := \gamma(r) r^2 . \tag{2.43}$$

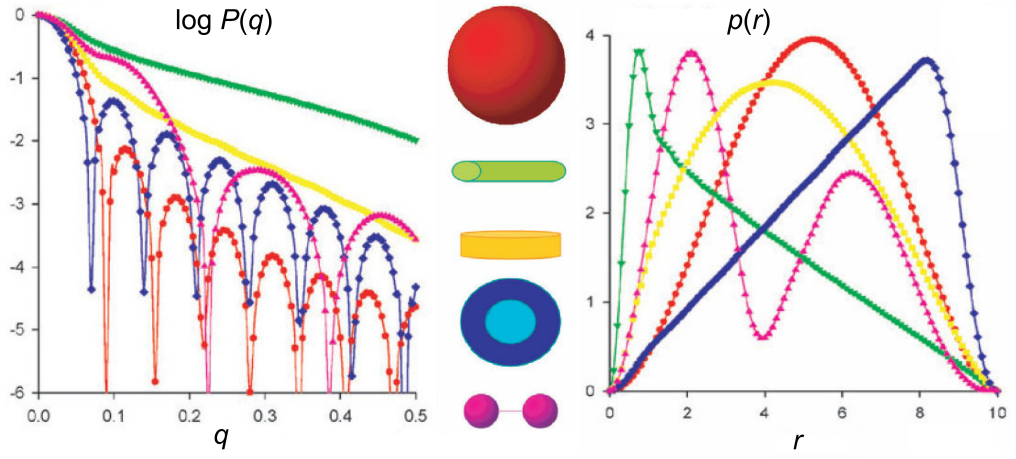

Figure 2.6: *Comparison of the scattering curves (left) and radial pair-distance distribution functions (right) for different geometrical bodies with same $D_{\max}$. Shown are the curves for a sphere, a long rod, a flat disc, a hollow sphere, and a dumbbell. Adapted with permission from [Svergun and Koch, 2003] (doi: 10.1088/0034-4885/66/10/R05); IOP publishing Ltd. Copyright (2003).*

For homogeneous particles $p(r)$ also has a geometrical interpretation. Consider two arbitrary points within the particle volume. Then $4\pi p(r)$ is the probability that the distance between them is equal to r [Kratky and Porod, 1948, Porod, 1948].

Fig. 2.5 depicts the radial pair-distance distribution function of a sphere. It vanishes at $r = 0$ and $r = 2R$. A pronounced maximum is present at $\frac{r}{R} \cong 1.049$, i.e. roughly for the radius of the sphere. Noteworthy is the nearly symmetrical shape of the curve. For nonspherical bodies without any cavities the curve is asymmetrical and the position of the maximum is at smaller r [Glatter, 1979].

The form factor can be written as

$$P(q) = 4\pi \int_0^{D_{\max}} p(r)\, \frac{\sin(qr)}{qr}\, dr\ . \tag{2.44}$$

Conversely, $p(r)$ can be determined theoretically from the form factor obtained by a SAXS experiment by inverse Fourier transform

$$p(r) = \frac{1}{2\pi^2} \int_0^{\infty} P(q)\ q\ r\ \sin(qr)\ dq\ . \tag{2.45}$$

However, this implies the continuous detection of the scattering intensity over the whole q-space which will be not realized in a real experiment. Due to the finite spatial resolution of the detectors, a discrete data set is obtained instead. Additionally, the experimental setup limits the accessible q-range.

Instead of performing a direct transformation, an indirect Fourier transform is carried out. Therefor the exact $p(r)$ is approximated by a finite sum $p_{\mathrm{A}}(r) = \sum_{i=1}^{N} c_i S_i(r)$ of

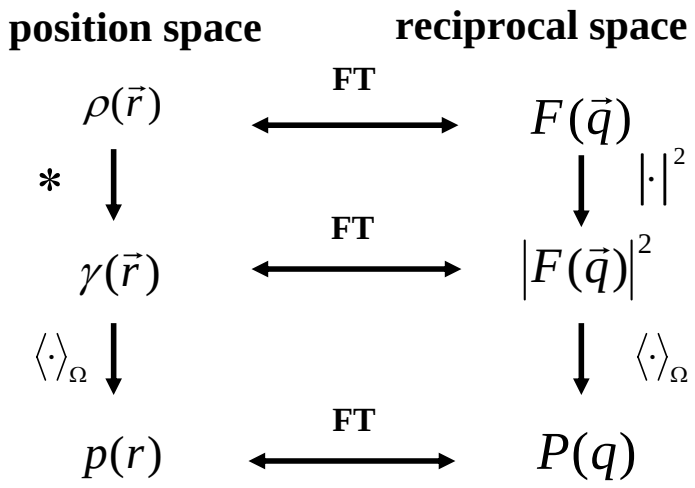

Figure 2.7: *General relations between different functions introduced for SAXS on particles. "FT" denotes Fourier transformation.*

appropriate splines $S_i(r)$ with yet not fixed coefficients c_i. Fourier transformation of $p_\mathrm{A}(r)$ gives the approximate function $P_\mathrm{A}(q)$. The coefficients are obtained by refinement of $P_\mathrm{A}(q)$ to the experimental data [Glatter, 1977]. With this approach both a fit to the experimental data as well as the pair-distance distribution function are obtainable. A program which utilizes this approach is GNOM [Svergun, 1992]. This was employed for the data analysis in this thesis.

Fig. 2.6 depicts the scattering curves and the radial pair-distance distribution function for various different geometrical bodies. The difference between a homogeneous sphere and a hollow sphere, for example, is in the $p(r)$ representation more pronounced than in the SAXS signal as previously mentioned. The shift of the maximum in the $p(r)$ curves of a sphere, a flat disc, and a long rod to smaller r is characteristic of the differences between three-dimensional and quasi-two- and quasi-one-dimensional structures [Glatter, 1979].

Negative values of $p(r)$ exist for particles in solution if there are regions of different charge density inside the particle whose contrasts have different signs [Glatter, 1979].

Although the radial pair-distance distribution function contains the same information as the form factor, the shape of $p(r)$ gives a better access to the particle shape. Besides knowledge of the shape also the maximum particle extension D_max is obtainable.

Fig. 2.7 summarizes the transformation properties of the various functions introduced. It can be distinguished between quantities that depend on $\vec{r}$ or r and describe the structure in position space and those depending on $\vec{q}$ or q and are related to the reciprocal space.

2.2.3 Scattering on less compact structures: Random coils and fractals

Until now the form factors of compact geometrical bodies were discussed, which serve as valuable models for scattering on variously shaped nanoparticles and even for folded proteins. However, polymers or unfolded proteins can not be appropriately characterized by compact bodies. A better description can be obtained using chain-like structures as e.g. the Gaussian random coil [Kirste and Oberthür, 1982, Calmettes et al., 1994, Schurtenberger, 2002b]. This model is an example for mass fractals. Hence, in this paragraph the form factor of a random coil as well as scattering on fractal structures will be discussed.

It will be started with the simplest coil model, the so-called Gaussian random coil [Kirste and Oberthür, 1982, Schurtenberger, 2002b]. Consider a linear chain consisting of N elements of length a without any interaction between the segments. Furthermore, the probability of finding one chain element as a function of distance from another one should be given by Gaussian statistics which is the case for large N. Mathematically this chain model can be described by a random walk. Introducing the radius of gyration of the chain

$$R_{\mathrm{g}} = \sqrt{\frac{1}{N}\sum_{j=1}^{N}\langle (r_j - r_{\mathrm{cm}})^2\rangle} \tag{2.46}$$

with r_{cm} the center of mass of the chain and $\langle\cdot\rangle$ the average of the probability of finding a chain element, the form factor of this Gaussian random coil following Debye [Debye, 1947] is given as

$$P_{\mathrm{RC}}(q) = N\frac{2}{x^2}\left(e^{-x} - 1 + x\right) \tag{2.47}$$

with $x = q^2R_{\mathrm{g}}^2$. In deriving this so-called Debye function, besides the orientation average, also an average over the Gaussian distribution function has to be performed in eq. (2.32). For large q the Debye function has a characteristic asymptotic q^{-2} dependence.

More realistic chain models take into account chemical details such as bonding angles (freely rotating chain) or chain flexibility (Kuhn model, worm-like chain model). Especially the last-mentioned model of a so-called persistent chain describes a continuous transition of the chain from rod-like to coil-shaped with increasing chain length [Kirste and Oberthür, 1982]. As a consequence the corresponding form factor shows besides the asymptotic behavior of random coil at even higher wave vector transfers a q^{-1} dependence which is characteristic of a rod. In addition, due to the cross-section term (see eq. (2.38)) the chemical structure of the chain becomes important

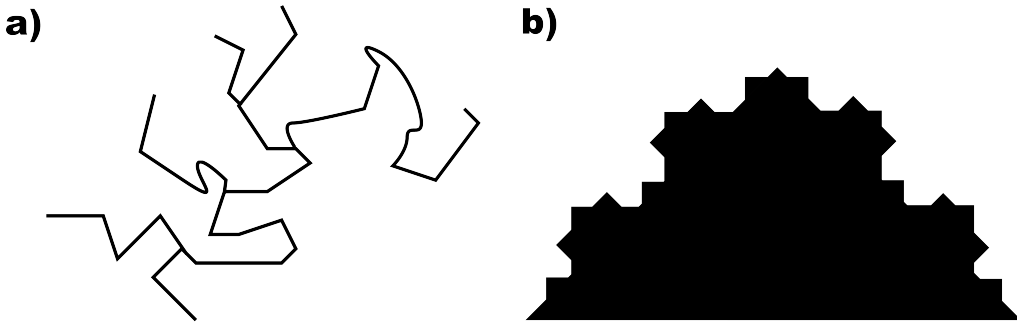

Figure 2.8: *Schematic drawing of the two types of fractals: a) Mass fractal. b) Surface fractal.*

[Calmettes et al., 1994].

Interactions both between the chain elements as well as with the solvent also affect the structure of the chain. Without going into details the major effect of these interactions relevant here is the change of the power law exponent p. Whereas $p = 2$ is the case for the random coil, $p < 2$ reflects a swollen polymer due to more favorable interaction with the solvent than with the chain, i.e. excluded volume interactions are present. $p > 2$ corresponds to a collapsed chain as is the case for a polymer in a poor solvent [Kirste and Oberthür, 1982, Beaucage, 1996].

Summarizing scattering on chain-like structures leads to a different type of form factor with the Debye equation (2.47) as the most simple scattering formula. Analyzing the high q dependence of the scattering curves of chain-like systems will give a deeper insight into the structure even when no proper model is available.

The chain models introduced so far are part of a special class of geometrical objects called mass fractals. As the concept of fractals serves as a description for many different structures especially in the mesoscopic length regime, the basic concepts and subsequent scattering on these types of objects will be discussed now shortly.

Fractal objects or fractals are characterized by a non-integer dimension, i.e. in contrast to common geometrical bodies such as a line, a square, or a cube with Euclidean dimensions d of 1, 2, and 3, respectively, these special types of objects have a broken d [Takayasu, 1990, Bunde and Havlin, 1991, Gouyet, 1996].

Mathematically, fractal objects have the nature of showing self-similarity. This means by magnifying a part of a fractal the same structure as the original one is obtained. In other words, this type of system has no characteristic length scale. Evidently, this property is not present in real physical or biological materials as the size of the molecules or atoms gives a lower limit. In addition, the characteristic size ξ of the quasi-fractal itself gives the upper border. However, the concept of fractals within this length regimes has been used successfully for the description of very different objects, such as polymers, neurons of the nerve system, clouds, or the shore lines of lakes.

Fig. 2.8 exemplary shows two schematic drawings of fractals. In order to obtain a reasonable measure for these objects, a tiling of the fractal in Fig. 2.8a) with a minimum number $N(r)$ of spheres with radius r is considered exemplarily. The total volume of the sphere gives an estimation of the fractal's volume [Schmidt, 1991]. The fractal dimension D is introduced as [4]

$$N(r) \propto r^{-D} \; . \tag{2.48}$$

As with decreasing radius r and thus enhancing number of spheres the tiling becomes finer, in the limit of infinite r a measure for quantifying the fractal is introduced, i.e.

$$D = \lim_{r \to \infty} \frac{\ln(N(r))}{\ln(\frac{1}{r})} \; . \tag{2.49}$$

For a straight line the fractal dimension is $D = 1$ and for a square $D = 2$. Depending on the special form of the fractal, a characteristic dimension is introduced in this way.

Two important types of fractals are mass fractals and surface fractals (Fig. 2.8). Mass fractals, such as polymers as previously mentioned or similar dendritic structures, are objects for which the following relation between mass $M_{\mathrm{m}}(r)$ and fractal dimension D_{m} holds

$$M_{\mathrm{m}}(r) \propto r^{D_{\mathrm{m}}} \; . \tag{2.50}$$

Surface fractals can be used to describe rough interfaces and surfaces such as e.g. defects and voids in solids. The relation between surface area $A_{\mathrm{s}}(r)$ and fractal dimension D_{s} is given by

$$A_{\mathrm{s}}(r) \propto r^{2-D_{\mathrm{s}}} \; . \tag{2.51}$$

The dimensions of these two fractals have characteristic values. For mass fractals $D_{\mathrm{m}} \leq 3$ and for surface fractals $2 \leq D_{\mathrm{s}} \leq 3$ [Schmidt, 1991].

These special dimensions give rise to a characteristic behavior of the scattering curve for $q > 1/\xi$. Following Sinha [Sinha, 1989] for the case of mass fractals, we introduce a pair correlation function $t(r) := \langle \rho(r')\rho(r+r') \rangle$ describing the electronic distribution wherein the average is taken over an ensemble of fractals with the asymptotic form [Sinha, 1989, Schmidt, 1991]

$$t(r) \propto r^{D_{\mathrm{m}}-3} \; . \tag{2.52}$$

[4] More precisely this is the definition of the so-called capacity dimension [Takayasu, 1990]. Other definitions of relevant fractal dimensions can be found e.g. in [Takayasu, 1990, Bunde and Havlin, 1991].

Inserting in eq. (2.39) this gives rise to scattering at large q as

$$P(q) \propto q^{-D_\mathrm{m}} \; . \tag{2.53}$$

In a similar way the large angle behavior for surface fractals reads [Bale and Schmidt, 1984, Schmidt, 1991]

$$P(q) \propto q^{6-D_\mathrm{s}} \; . \tag{2.54}$$

A recent summary of various scattering functions of fractal systems can be found in [Sinko et al., 2008].

As D_m as well as D_s only can take the values mentioned above, scattering of fractals gives rise to a characteristic decay power p and thus mass fractals and surface fractals can be distinguished. It is $1 < p < 3$ for mass fractals and $3 < p < 4$ for surface fractals [Martin and Hurd, 1987]. In particular the results of the scattering on the chain models is obtained again.

2.2.4 Asymptotic behavior of the form factor

As shown in the previous paragraph on fractals, the asymptotic behavior of the form factor yields special information about the structures under investigation. Thus, different objects can be identified and distinguished from each other even if the whole scattering curve can not be refined. Hence, the asymptotic properties of the form factor $P(q)$ will now be discussed.

Consider the form factor at small wave vector transfer q. Expanding the term $\frac{\sin(qr)}{qr}$ in eq. (2.41) for small q and identifying this with the representation of the Gaussian function the so-called Guinier approximation [Guinier and Fournet, 1955]

$$\lim_{q \to 0} P(q) = P(0) \; \mathrm{e}^{-\frac{1}{3} R_\mathrm{g}^2 \; q^2} \tag{2.55}$$

is obtained. Herein R_g is the radius of gyration, already introduced previously for chains (eg (2.46)). A more general definition is given by [Feigin and Svergun, 1987]

$$R_\mathrm{g}^2 = \frac{\int_{V_\mathrm{P}} \rho(\vec{r}) \; r^2 \; d^3r}{\int_{V_\mathrm{P}} \rho(\vec{r}) \; d^3r} = \frac{\int_0^{D_\mathrm{max}} p(r) \; r^2 \; dr}{2 \int_0^{D_\mathrm{max}} p(r) \; dr}. \tag{2.56}$$

Analogous to the moment of inertia in mechanics the radius of gyration describes the electronic extent of the studied particles. In the following list R_g is given for some geometrical bodies [Mittelbach, 1964] and the random coil [Kirste and Oberthür, 1982].

- sphere with radius R

$$R_{\mathrm{g,S}} = \sqrt{\frac{3}{5}} R \tag{2.57}$$

- hollow sphere with inner radius R_{i} and outer radius R_{o}

$$R_{\mathrm{g,HS}} = \sqrt{\frac{3}{5}} \sqrt{\frac{R_{\mathrm{o}}^5 - R_{\mathrm{i}}^5}{R_{\mathrm{o}}^3 - R_{\mathrm{i}}^3}} \tag{2.58}$$

- ellipsoid of revolution with semiaxis a and b

$$R_{\mathrm{g,RE}} = \sqrt{\frac{2a^2 + b^2}{5}} \tag{2.59}$$

- triaxial ellipsoid with semiaxis a, b, and c

$$R_{\mathrm{g,TE}} = \sqrt{\frac{a^2 + b^2 + c^2}{5}} \tag{2.60}$$

- cylinder of elliptical cross-section with semi-axis a and b and height H

$$R_{\mathrm{g,EC}} = \sqrt{\frac{a^2 + b^2}{4} + \frac{H^2}{12}} \tag{2.61}$$

- random coil with number of chain elements N and element length a

$$R_{\mathrm{g,RC}} = \sqrt{\frac{N}{6}} a \tag{2.62}$$

As is obvious from the Guinier approximation the scattering curve for small q is only a function of the typical extent of the particle and does not depend on its shape. Thus, the form factors of two different bodies such as a sphere and a cube having the same R_{g} show the similar curve form in this q-regime.

Employing eq. (2.55) gives a way to determine the radius of gyration from the data points of a scattering curve at small q. Plotting $\ln I(q)$ versus q^2 for small wave vector transfer a straight line should be obtained. From the corresponding slope of this so-called Guinier plot R_{g} can be calculated.

Usually the range of validity of the Guinier approximation is assumed to be $R_{\mathrm{g}} \cdot q_{\max} \leq 1$ [Guinier and Fournet, 1955]. Herein, $q_{\max}$ denotes the maximum wave vector transfer

of the data point which can be still used for fitting. In the case of proteins it has been shown that the approximation can even be used for $R_g \cdot q_{max} \leq 1.3$ [Kataoka et al., 1995]. If the radial pair-distance distribution function $p(r)$ is known, the radius of gyration can also be calculated using eq. (2.56).

$P(0)$ describes the case that all secondary waves are scattered in phase from the electrons inside the particle resulting in a maximum amplification of the scattering intensity at vanishing q. Using eq. (2.29) and neglecting the contrast $P(0)$ reads

$$P(0) = (\bar{\rho}\, V_p)^2 = N_P^2 \,, \tag{2.63}$$

i.e. the total number N_P of electrons within the sample. For macromolecules in solution the mean electron density $\bar{\rho}$ has to be replaced by the contrast factor $\Delta\rho$.

The contribution of forward scattering is not directly measurable as it is superimposed by the much more intensive primary beam which is masked by the beam stop. However, employing the Guinier approximation it can be extrapolated if the intensity recorded by the detector is on an absolute scale.

For large q the asymptotic behavior has already previously been discussed for highly anisotropic particles (eq. (2.38)) and fractal objects (paragraph 2.2.3). To complete this the case of compact, less anisotropic particles is considered now. Following Porod and by ignoring rapid oscillating terms one finds for the form factor at large wave vector transfer [Porod, 1951, Porod, 1952]

$$P(q) = 2\pi\, \frac{\bar{\rho}^2\, S}{q^4} \tag{2.64}$$

wherein S denotes the particles' surface. This so-called Porod q^{-4} behavior is valid for homogeneous bodies with negligible curvature. Taking into account the surface curvature results in an additional q^{-6} term [Kirste and Porod, 1962].

For macromolecules such as proteins which can be approximated by geometrical bodies the distribution of electrons within the particle gives rise to additional scattering signals at higher q [5]. This inhomogeneous electron density distribution which can be also interpreted as density fluctuations leads to deviations from the Porod power law behavior [Sobry and Ciccariello, 2002].

The following list summarizes the different, most relevant power law exponents p and the corresponding structures introduced so far which give rise to this high q asymptotic behavior.

[5] In other words, at high q the internal structure of the macromolecule, especially proteins, leads to a WAXS signal [Fischetti et al., 2003].

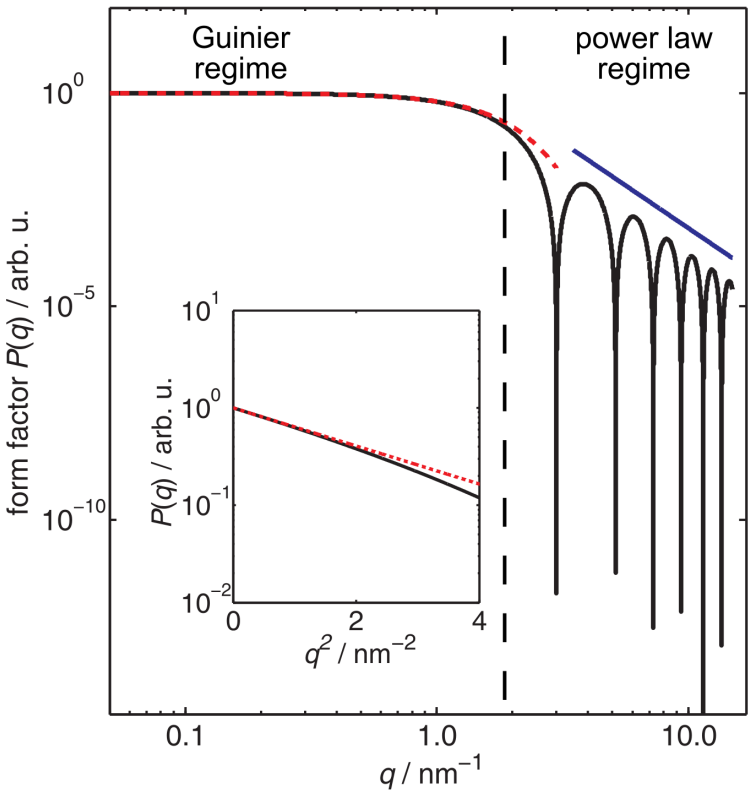

Figure 2.9: *Form factor of a sphere ($R = 1.5$ nm, solid curve) as well as the result of the corresponding Guinier approximation (dashed curve) and power law decay (solid line). The radius of gyration R_g is 1.2 nm, the power law exponent p is 4. As can be seen for small q up to about 1.0 nm^{-1} the Guinier approximation is in accord with the exact form factor. This is visualized in the Guinier plot (inset).*

- $p = 4$: homogeneous, compact body (Porod case)
- $3 < p < 4$: surface fractal
- $1 < p < 3$: mass fractal
- $p = 2$: random coil
- $p = 2$: flat disc
- $p = 1$: long rod

Figure 2.9 exemplarily depicts the form factor of a sphere together with the corresponding curve of the Guinier approximation (eq. (2.55)) given for small q. Additionally, the power law dependence of the Porod case is shown by the straight line at large wave vector transfer. Besides the oscillations a q^{-4} decay is present. In the inset the Guinier plot visualizes the range of validity of the approximation.

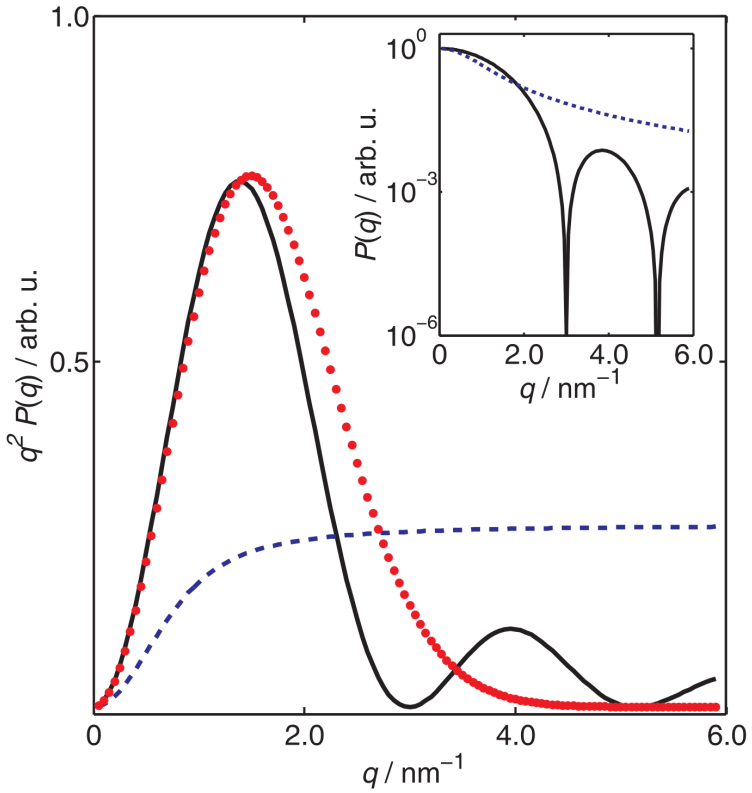

Figure 2.10: *Kratky plot of a sphere ($R = 1.5$ nm) and a Gaussian random coil ($R_g = 1.7$ nm, dashed curve). Additionally, the curve using the Guinier approximation of the sphere is plotted as well (dotted curve). The inset depicts the form factors of sphere and random coil.*

Summarizing the general asymptotic behavior, the form factor of any structure with a characteristic correlation length ξ can be described for small q by a Gaussian behavior and for high q by a power law decay [Beaucage, 1995].

A special application of the different power law decays is used in the so-called Kratky plot [Kratky, 1982]. Here, the wave vector transfer q is plotted versus $q^2 \cdot P(q)$. As the scattering curve of a random coil has a q^{-2}-asymptotic behavior at high q values, a plateau will be visible whereas the form factor of a compact particle has a stronger decay leading to a maximum. Thus, in this representation polymers and unfolded protein can be distinguished from colloids and folded proteins [Kataoka et al., 1995, Semisotnov et al., 1996].

Figure 2.10 shows the Krakty plot of a sphere and a random coil. The plateau in the case of the coil is clearly visible. In contrast the curve for the sphere shows a pronounced first maximum. The higher order maxima at larger q will not be present for less symmetric particles such as ellipsoids of revolution which are often used to model the shape of simple proteins. The form factors of both objects are given in the inset. Additionally, the Kratky plot of the curve of the Guinier approximation is depicted. Its

maximum is shifted toward larger q than that of the exact form factor. However, at least an approximate value for the radius of gyration of compact particles can be obtained from the position of the maximum. Consider the Guinier approximation is valid up to those wave vector transfers where a maximum in the Kratky plot is present. Then the position of the maximum is given by

$$q_{\max} = \frac{\sqrt{3}}{R_{\mathrm{g}}} \,. \tag{2.65}$$

Thus, by plotting the scattering curve in this representation and determining the peak position one is able to obtain a very first estimation of the size of the particle studied.

Another application of the power law behavior which at least should be mentioned is the so-called Porod plot, i.e plotting q versus $q^4 \cdot P(q)$. For homogeneous, compact bodies a characteristic plateau will be present at large q.

For completeness a quantity which takes into account the whole scattering curve of a particle is introduced finally. The so-called Porod invariant [Porod, 1951] of a homogeneous particle is given as [Feigin and Svergun, 1987]

$$Q = \int_0^\infty P(q)\; q^2 \; dq = 2\pi^2 \; \bar{\rho}^2 \; V_{\mathrm{p}} \,. \tag{2.66}$$

The invariant is proportional to the whole scattering intensity. It does only depend on the particle volume and the mean electron density and not on the particle's shape. If Q as well as the forward scattering intensity $P(0)$ (eq. (2.63)) are determined, the volume V_{p} can be calculated.

2.2.5 Polydispersity

Until now monodisperse systems wherein all particles have the same shape and size were considered. For diluted solutions of native proteins where no aggregation occurs the assumption of monodispersity is valid [Svergun and Koch, 2003]. In order to determine the contribution of differently sized particles, polydisperse solutions will be discussed shortly. Therefor, a particle size distribution $D(R)$ is introduced. The premises are such that the decoupling approximation is valid [Kotlarchyk and Chen, 1983, Kaler, 1995]. Thus, the form factor and the effective structure factor can be considered separately. The detectable intensity is then given as [Pedersen, 2002]

$$I(q) \propto \bar{\rho}^2 \int_0^\infty D(R)\; V(R)^2 \; P(q,R) \; dR \,. \tag{2.67}$$

Herein $V(R)$ denotes the volume and $P(q,R)$ the form factor to the parameter R characterizing the size. For polydisperse spheres R corresponds to the radius. Using proper

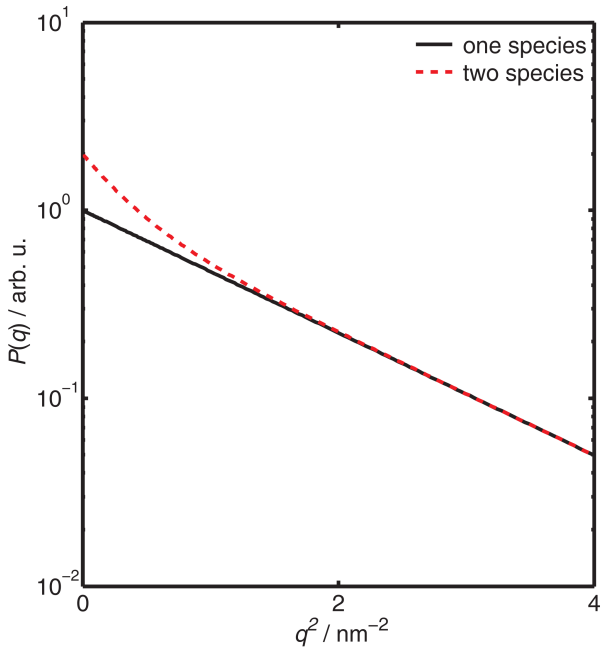

Figure 2.11: *Guinier plot for the scattering curves of monodisperse particles with radius of gyration $R_g = 1.5$ nm (solid line) and for a equal mixture of particles with $R_g = 1.5$ nm and $R_g = 3.0$ nm (dashed line). In the case of polydispersity a nonlinear increase at small q is present.*

distribution functions $D(R)$ and particle shapes the scattering curves can be modeled with this approach.

The presence of polydispersity leads to smearing out of sharp structures of the form factor, e.g. the minima. For example, scattering on differently sized spheres is similar to scattering from monodisperse ellipsoids [Hosemann, 1939].

In order to detect polydispersity in a SAXS experiment the Guinier plot can be analyzed. Instead of a straight line which can be seen for monodisperse solutions, a nonlinear decrease at small q occurs in polydisperse systems [Guinier and Fournet, 1955].

This is exemplarily shown in Fig. 2.11. Here, the Guinier plot for a particle with radius of gyration R_g is depicted for which it is assumed that it can be fully described by the Guinier approximation in the given q-range. This curve is compared to the SAXS signal of a superposition of similar particles with R_g and $2R_g$. For diluted protein solutions such a nonlinear shape indicates the presence of aggregates.

2.3 The structure factor

Until now the case of diluted particle solutions has been discussed. For scattering on concentrated solutions the interactions between the particles can not be ignored anymore. These give rise to an additional interference effect which contributes also to the scattering signal. The scattering intensity can then be described by the formula of Guinier and Fournet (eq. (2.20)) [Guinier and Fournet, 1955]. In the case of spherical particles eq. (2.20) reduces to the scattering formula of Zernike and Prins [Zernike and Prins, 1927]

$$I(q) \propto \bar{N} \cdot P(q) \cdot \left[1 + 4\pi\ n \int_0^\infty r^2\ \left(g(r) - 1\right) \frac{\sin(qr)}{qr} dr\right] . \tag{2.68}$$

This equation is the starting point of all following considerations. For anisotropic particles as well as in the case of polydispersity the decoupling approximation has to be used instead [Kotlarchyk and Chen, 1983, Kaler, 1995].

The term in square brackets on the right-hand-side of eq. (2.68) is equal to the structure factor $S(q)$ (eq. (2.22)). The radial pair distribution function $g(r)$ describes the thermodynamics of a macroscopic system, i.e. the thermodynamical potentials and the equation of state, in terms of the microscopic particle-particle interactions [Hansen and McDonald, 1986]. Here its definition will be given in the framework of the statistical mechanics description used for simple liquids. This concept assumes particles with spherical symmetric and non-saturating interactions which is realized e.g. for liquid inert gases, some molecules like methane, or particularly in liquid metals [Croxton, 1975]. Notable, liquid water is not a simple liquid due to the presence of a hydrogen bond network. The concept of simple liquids can also be used for macroions in solution, i.e. charged colloids in a solvent like water with much smaller contra- and co-ions added, if the solvent is treated as a continuous background characterized by its dielectric permittivity, which is the so-called primitive model. If the small ions are assumed to be point-like leading to a screening of the macroion charges but have no additional chemical influence, one speaks of the one-component macrofluid model [Schmitz, 1993, Klein, 2002, Curtis and Lue, 2006]. For the following considerations this course-grained description for the particles in solution is used. For a detailed derivation of these concepts and their consequences and applications the reader is referred to e.g. [Croxton, 1975, Hansen and McDonald, 1986]. Short general surveys can be found in [Klein, 2002, Nägele, 2008].

Consider the system of $\bar{N}$ particles can be described by the hamiltonian $\mathcal{H}_{\bar{N}}\left(\overrightarrow{r^{\bar{N}}}, \overrightarrow{p^{\bar{N}}}\right)$ wherein $\overrightarrow{r^{\bar{N}}}$ denotes the 3 $\bar{N}$ coordinates and $\overrightarrow{p^{\bar{N}}}$ the 3 $\bar{N}$ momenta of the particles. Besides the kinetic contribution to the hamiltonian, $\mathcal{H}_{\bar{N}}\left(\overrightarrow{r^{\bar{N}}}\right)$ is especially a function of the total potential energy $V_{\bar{N}}\left(\overrightarrow{r^{\bar{N}}}\right)$. Together with the corresponding grand canon-

ical partition function Ξ and the activity z[6] the so-called m-particle density function $n^{(m)}\left(\overrightarrow{r^m}\right)$ is introduced as

$$n^{(m)}\left(\overrightarrow{r^m}\right) = \frac{1}{\Xi}\sum_{\bar{N}\geq m}^{\infty}\frac{z^{\bar{N}}}{(\bar{N}-m)!}\int e^{-\beta V_{\bar{N}}\left(\overrightarrow{r^{\bar{N}}}\right)}d^{\bar{N}-m}r\ . \tag{2.69}$$

Herein, it is $\beta = \frac{1}{\mathrm{k_B}T}$ with the Boltzmann constant $\mathrm{k_B}$ and the temperature T. With this definition of $n^{(m)}\left(\overrightarrow{r^{\bar{N}}}\right)$ the m-particle distribution function is given as

$$g^{(m)}\left(\overrightarrow{r^m}\right) = \frac{n^{(m)}\left(\overrightarrow{r^m}\right)}{\prod_{j=1}^{m} n^{(1)}(\overrightarrow{r_j})}\ . \tag{2.70}$$

In the absence of external fields and for isotropic pair potentials, i.e. $V_{\bar{N}}\left(\overrightarrow{r^{\bar{N}}}\right) = \sum_{j>k}^{\bar{N}} V(r_{jk})$, the pair distribution function is defined as $g(r) = g^{(2)}(r)$.

$g(r)$ is the relative probability for finding two particles separated by a distance r and it thus characterizes the deviations of the system of interest from an ideal gas [Croxton, 1975]. In this completely unordered system the particles do not have any spatial correlations. Thus, for scattering on an ideal gas there is no interference contribution from the particles at different positions detectable as the phase relation between the secondary waves is randomly distributed. Hence, the ideal gas is characterized as $g(r) = 1$. As liquids possess a short range order within a correlation length ξ, the radial pair distribution function obeys $g(r) \neq 1$. For $r > \xi$ there is no order anymore resulting in $g(r) \to 1$. This demonstrates that $g(r)$ is related to the interaction between the particles. However, as can be seen on eq.'s (2.69) and (2.70), the pair distribution function depends on the contributions of the other (N-2) particles. In order to relate the distribution functions in a manageable way to the actual particle interactions, various approaches and approximations have been formulated (see e.g. [Croxton, 1975, Hansen and McDonald, 1986]). A special way to solve the aforementioned problem is based on the integral equation method. The basic concept will be discussed shortly here as its application is often employed for analyzing the structure factor of colloidal solutions.

Introducing the total correlation function $h(r) = g(r) - 1$, the so-called Ornstein-

[6] The activity is defined in terms of the chemical potential μ as

$$z = \Lambda^{-3}\ \exp(\beta\mu)$$

wherein the thermal de Broglie wavelength Λ is used.

Zernike integral equation is defined as [Ornstein and Zernike, 1914]

$$h(r) = c(r) + n \int c\left(\left|\vec{r} - \vec{r'}\right|\right)\ h(r')d^3r\ , \tag{2.71}$$

wherein $c(r)$ is the direct correlation function. The Ornstein-Zernike equation states that the total correlation between two particles is given as the sum of the direct correlation between them as well as the indirect interaction involving additional particles. This indirect correlation is expressed by the convolution term on the right-hand side of eq. (2.71). By insertion of the definition of $h(r)$ iteratively into this term, the indirect correlation is presented by the contributions of the direct correlation with a third particle, a forth particle and so on. This is the starting point for various approximation to determine $h(r)$ and $g(r)$ and thus to the thermodynamics of the system in terms of the pair interaction potential. Some relevant so-called closure relations connecting $c(r)$ with $g(r)$ and $V(r)$ will be given below. These allow, in combination with the Ornstein-Zernike equation (2.71), to calculate an approximation for the radial pair distribution function. Prior to that, some general properties of the structure factor will be given.

Fourier transformation of eq. (2.71) and insertion into eq. (2.22) gives the following general relation between the structure factor $S(q)$ and the Fourier transform $c(q)$ of the direct correlation function

$$S(q) = \frac{1}{1 - nc(q)}\ . \tag{2.72}$$

Thus it is $nc(q) \leq 1$, as $S(q) \geq 0$.

Especially for small and large wave vector transfers general expressions can found. For small q the structure factor of a liquid is given as

$$\lim_{q \to 0} S(q) \to n\ \mathrm{k_B}\ T\ \kappa_T = \frac{\left\langle \bar{N}^2 \right\rangle - \left\langle \bar{N} \right\rangle^2}{\bar{N}}\ . \tag{2.73}$$

Herein κ_T denotes the isothermal compressibility [Hansen and McDonald, 1986]. Thus, for very small q the scattering contribution results from the density fluctuations within the macroscopic sample. For colloidal particles in solution the small q limit is given by the osmotic compressibility $\chi_T = \frac{1}{n}\left(\frac{\Pi}{n}\right)_T^{-1}$ wherein Π denotes the osmotic pressure [Grimson, 1983]. For large q it is

$$S(q) \to 1\ . \tag{2.74}$$

In order to solve the Ornstein-Zernike equation a connection between the direct correlation function $c(r)$, the radial pair distribution function $g(r)$ and accordingly the total correlation function $h(r)$, and the pair interaction potential $V(r)$ has to be found.

Depending on the type (attractive or repulsive), strength, and range of the potential as well as the particle density n, different closure relations can be formulated to yield the best approximation to the problem. For these and the respective potentials either analytical or numerical solutions can be found. In the list below the most important approximation for colloidal particles in solution, especially for proteins, are summarized.

- Mean-spherical approximation (MSA)

$$c_{\mathrm{MSA}}(r) = -\beta V(r)\ , r > \sigma \tag{2.75}$$

- Percus-Yevick (PY) closure relation

$$c_{\mathrm{PY}}(r) = \left[1 - e^{\beta V(r)}\right] g(r) \tag{2.76}$$

- Hypernetted-chain (HNC) approximation

$$c_{\mathrm{HNC}}(r) = -\beta V(r) + h(r) - \ln\left[1 + h(r)\right] \tag{2.77}$$

- Random phase approximation (RPA): If the interaction potential can be divided into a short-ranged reference part $V_{\mathrm{ref}}(r)$ with exact structure factor $S_0(q)$ and a perturbation part $V_{\mathrm{pert}}(r)$, the structure factor is given as ($V_{\mathrm{pert}}(q)$, Fourier transform of $V_{\mathrm{pert}}(r)$)

$$S_{\mathrm{RPA}}(q) = \frac{S_0(q)}{1 + n\beta S_0(q) V_{\mathrm{pert}}(q)}\ ,\ \text{for}\ n\beta S_0(q) V_{\mathrm{pert}}(q) > -1 \tag{2.78}$$

The PY approximation is best suited for short-range interactions whereas the HNC approximation gives better results for long-range repulsive interactions. The MSA can be used for interactions in the midrange and works quite well for moderate particle densities. It has the advantage that there exist analytical solutions to various interaction potentials [Hansen and McDonald, 1986, Nägele, 2008]. The RPA can be used for moderately charged particles where only a weak perturbation is present [Grimson, 1983, Narayanan and Liu, 2003].

The most basic interactions between colloidal particles is the sterical repulsion as these can not interpenetrate each other. This interaction between hard spheres thus is used for many different simulation studies to predict the structure and stability of liquid systems and their phase transitions. For example, the so obtained structure factors serve

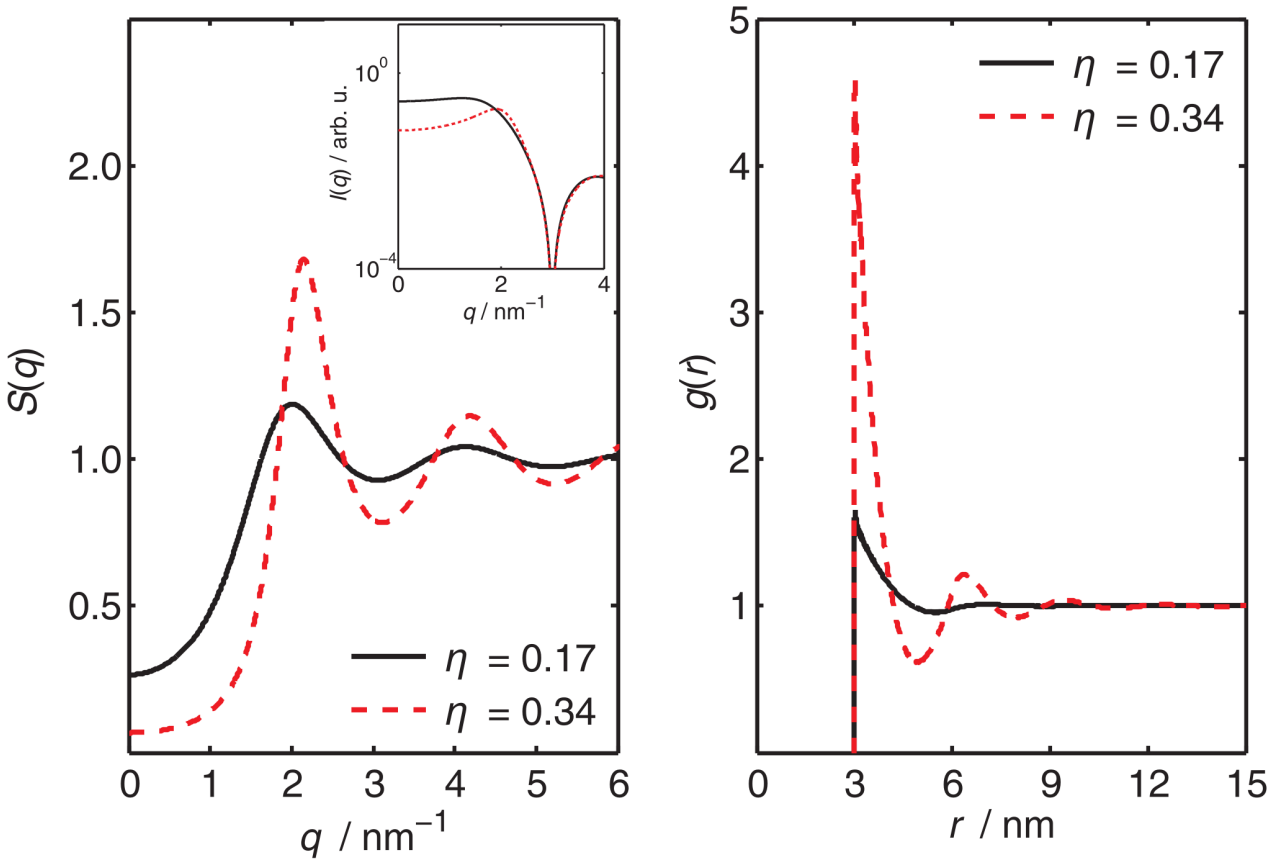

Figure 2.12: *Left: Structure factor $S(q)$ of a system of hard spheres (diameter $\sigma = 3.0$ nm) calculated in PY approximation for two volume fractions η. The inset shows the total scattering intensity of a system of spheres. Right: Corresponding pair distributions functions $g(r)$.*

as criteria to determine the quality of the results of the solutions to the Ornstein-Zernike equations with the different closure relations. The hard sphere interaction potential can be written as

$$\begin{aligned} V_{\mathrm{HS}}(r) &= \infty \,, & r < \sigma \\ &= 0 \,, & r > \sigma \end{aligned} \tag{2.79}$$

wherein σ denotes the particle diameter. For this type of interaction, it is $g(r) = 0$ for $r < \sigma$, as there can be no correlations for distances smaller than the diameter at which two impenetrable particles touch each other. As the structure as well as the thermodynamics of the hard sphere system for given diameter are only determined by the particle density n, the volume fraction $\eta = \frac{1}{6}\pi n\sigma^3$ is typically used to characterize this system.

For the hard sphere interaction an analytical solution within the PY approximation can be found [Nägele, 2008]. The left side of Fig. 2.12 shows the calculated structure factors for two different volume fractions. With increasing η the extrema of $S(q)$ shift to higher q and the limit $\lim_{q\to 0} S(q)$ decreases due to a change of the compressibility. In the inset the full scattering intensity $I(q)$ for this system of interacting spheres is shown. The contribution of the structure factor causes the presence of a so-called correlation peak which is more pronounced for higher volume fractions. Notable, the position of the correlation peak is at smaller q values than the first maximum of corresponding structure factor. On the right side of Fig. 2.12 the related radial pair distribution functions $g(r)$ are depicted[7]. As η is increased, the maximum at the contact distance σ increases, the extrema become more pronounced, and shift to small r.

Whereas the model of interacting hard sphere serves as the starting point to describe the structure of many simple liquids and colloids, in most systems additional interactions have a significant influence on their properties. The following list summarizes different, frequently used pair interaction potentials which are especially employed to model the interactions between proteins in solution. For all of these an additional hard sphere interaction due to the impenetrability is assumed.

[7] These can be obtained by inversion of eq. (2.22)

$$g(r) = 1 + \frac{1}{2\pi^2 n}\int_0^\infty (S(q) - 1)\,\frac{\sin(qr)}{qr}\; q^2\; dq \,.$$

- Square well potential with attraction depth Δ and range $\delta\sigma$ [Sharma and Sharma, 1977, Zhang et al., 2007]

$$\begin{aligned} V_{\mathrm{SW}}(r) &= -\Delta, && \sigma \leq r \leq \delta\sigma \\ &= 0\ , && r > \delta\sigma \end{aligned} \tag{2.80}$$

- 1-Yukawa-type potential with potential strength J and range d which can be either repulsive or attractive [Hayter and Penfold, 1981, Hansen and Hayter, 1982, Malfois et al., 1996, Zhang et al., 2007]

$$V_{\mathrm{1Y}}(r) = J \cdot \sigma\ \frac{\exp\left(-\frac{r-\sigma}{d}\right)}{r} \tag{2.81}$$

- 2-Yukawa-type potential with repulsion strength J_{r} and range d_{r} and attraction strength J_{a} and range d_{a} [Liu et al., 2005]

$$V_{\mathrm{2Y}}(r) = J_{\mathrm{r}} \cdot \sigma\ \frac{\exp\left(-\frac{r-\sigma}{d_{\mathrm{r}}}\right)}{r} - J_{\mathrm{a}} \cdot \sigma\ \frac{\exp\left(-\frac{r-\sigma}{d_{\mathrm{a}}}\right)}{r} \tag{2.82}$$

All these interaction potentials consist of a hard core repulsion as well as an effective attraction due to dispersion forces and/or an effective electrostatic repulsion. Especially the 2-Yukawa-type potential $V_{\mathrm{2Y}}(r)$ consisting of all three interaction contributions is an abbreviated version of the so-called Derjaguin-Landau-Verwey-Overbeek (DLVO) potential [Israelachvili, 1985], which fully reads [Tardieu et al., 1999]

$$\begin{aligned} V_{\mathrm{DLVO}}(r) =& V_{\mathrm{C}}(r) + V_{\mathrm{vdW}}(r) \\ =& \frac{e^2}{4\pi\epsilon_0\epsilon_{\mathrm{r}}}\ \frac{Z_{\mathrm{eff}}^2}{\left(1+0.5\frac{\sigma}{\lambda_{\mathrm{D}}}\right)^2}\frac{\exp\left(-\frac{r-\sigma}{\lambda_{\mathrm{D}}}\right)}{r} - J \cdot \sigma\ \frac{\exp\left(-\frac{r-\sigma}{d}\right)}{r}\ , \end{aligned} \tag{2.83}$$

for $r > \sigma$.

Herein, ϵ_{r} denotes the relative permittivity of the solvent, J the strength of attraction and d its range. The Debye screening length $\lambda_{\mathrm{D}} = (\epsilon_0\epsilon_{\mathrm{r}}\mathrm{k_B}\ T)\ (e^2\ \sum_i n_i z_i^2)^{-1}$ characterizes the strength of the decay of the electrostatic interaction as a function of distance and depends on the amount n_i of ion species i per volume and its charge z_i. In this model proteins are approximated as dielectric bodies with an effective charge Z_{eff}. The different side chains of the amino acids on the protein surface can be charged depending

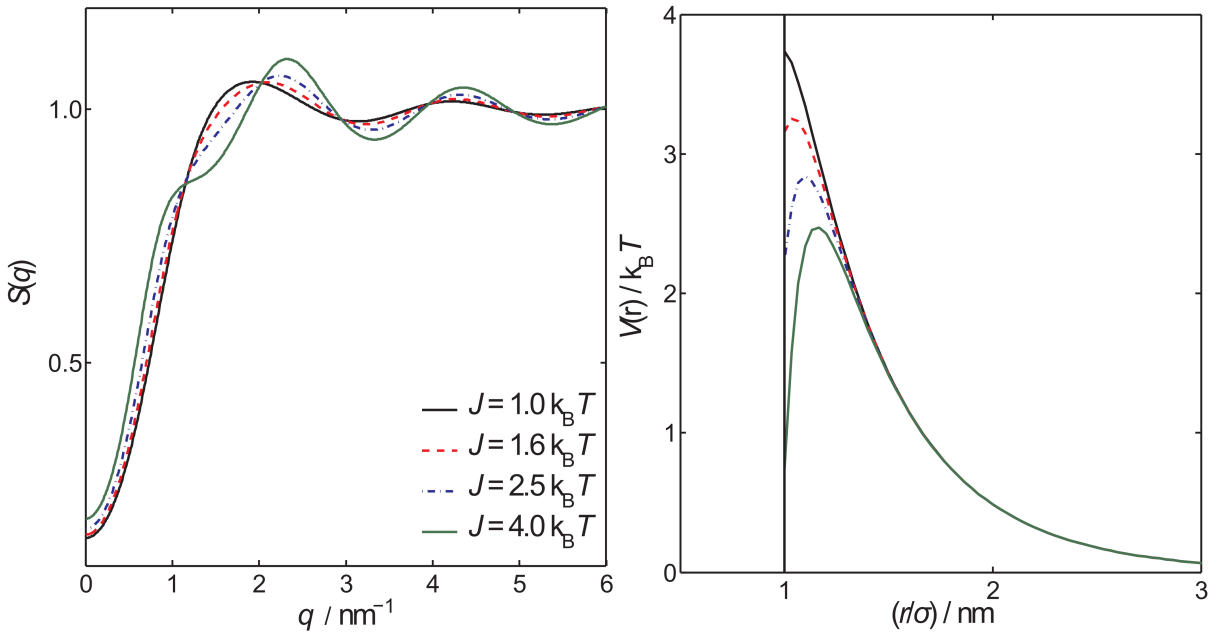

Figure 2.13: *Left: Structure factor $S(q)$ for spherical particles ($\sigma = 3.0$ nm, $\eta = 0.10$) assuming a DLVO potential calculated in MSA. The strength of the repulsion is kept constant whereas the attraction strength J is varied. For details see text. Right: Corresponding interaction potentials.*

on the solution's pH value. The effects of hydrogen bonds as well as the hydrophobic interactions are not directly included into this type of interaction. To some extent their influence, together with the van der Waals interaction, will be reflected by the attraction part which sums up all attractive interactions. As the DLVO is deduced in the framework of the one-component macrofluid model the different chemical nature of the anions and cations is neglected which, however, has a significant influence on the protein-protein interaction for concentrated salt solution [Curtis and Lue, 2006]. This so-called Hofmeister effect depends on the ratio between the solution's pH value and the protein's isoelectric point pI[8] and influences the stability of proteins in solution as well as the protein solution's stability.

Exemplary, on the left side of Fig. 2.13 the structure factors $S(q)$ for particles (diameter $\sigma = 3.0$ nm, volume fraction $\eta = 0.10$) interacting via the DLVO potential (eq. (2.83)) are shown for different attraction strength J. These were calculated in MSA using the MATLAB® code of [Liu et al., 2005][9]. Four cases are depicted. For $J = 1.0$ $k_B T$ the attraction is smaller than the repulsion, for $J = 1.6$ $k_B T$ these are equal, and for $J = 2.5$ $k_B T$ and 4.0 $k_B T$ the attraction is stronger. The corresponding interac-

[8] The isoelectric point, pI, is the pH value where the proteins effective charge Z_{eff} vanishes. For pH < pI the protein is positively charged, at pH > pI it is negatively charged.

[9] For the repulsive part an effective charge of $Z_{\text{eff}} = 8$ and the permittivity of water $\epsilon_r = 78.85$ is assumed. The screening length λ_D is 1.9 nm and the attraction range d is 0.3 nm. Such a type of long-range repulsion and short-range attraction is typical for colloidal interactions.

tion potentials are depicted on the right side of Fig. 2.13. For stronger repulsion as well as for equal strength, the structure factor has a pronounced first maximum and a shape similar to that of the pure hard sphere system (Fig. 2.12). The absence of a cancellation of the two interactions is due to the different interaction ranges. Increasing the attraction, the curves maxima and minima shift to higher q. Additionally, a shoulder evolving into another maximum with increasing J appears at small q which is called cluster peak in literature [Broccio et al., 2006, Kim et al., 2011]. In the corresponding $V(r)$ curves, a maximum becomes present which subsequently shifts to larger r and drops in height. Despite of its shortcomings this type of interaction potential is frequently used to describe the small angle scattering data of concentrated protein solutions [Javid et al., 2007a, Javid et al., 2007b, Shukla et al., 2008, Sinibaldi et al., 2008].

Experimentally, the structure factor is implicitly given by the scattering intensity

$$I(q) \propto P(q) \cdot \{1 + \beta(q) \cdot (S(q) - 1)\}\,, \tag{2.84}$$

wherein $\beta(q)$ is the factor due to the decoupling (eq. (2.24)). If the form factor $P(q)$ is determined additionally by measuring the SAXS signal of a diluted particle solution $I_0(q)$ and if $\beta(q)$ can be calculated for example by modeling the particle form by a simple geometrical body, $S(q)$ can be obtained by refinement of the data. Therefore, a proper liquid state model discussed above has to be employed [10].

[10] In the case of centrosymmetric particles $S(q)$ can be also determined directly via

$$S(q) = \frac{c_0\, I(q)}{c\, I_0(q)}\,.$$

Herein, c_0 and c denote the low and the high particle concentration, respectively.

3 Experimental Setup

Within the framework of this thesis, small angle X-ray scattering experiments were performed at different synchrotron radiation facilities. In this chapter these experimental setups will be discussed. A typical SAXS endstation will be described first (paragraph 3.1). Afterwards the different SAXS beamlines will be discussed shortly (paragraph 3.2). Subsequently a description of the high pressure equipment employed is given (paragraph 3.3). The chapter ends with a discussion about general data treatment (paragraph 3.4). This chapter is oriented on [Schroer, 2008].

3.1 General outline of a SAXS setup

The setup of a typical small angle scattering experiment can be subdivided into five essential parts: the X-ray source, the beam optics before the sample, the sample environment, the section between sample and detector, and the detector itself. A schematic drawing of such a setup is given in Fig. 3.1. In the following the setup for SAXS experiments at a synchrotron radiation facility is described.

A SAXS beamline can either be attached to a bending magnet or to a wiggler or an undulator. The advantage of the latter two types of insertion devices is their high photon flux and the lower horizontal divergence. The so produced synchrotron radiation is polychromatic. Using a monochromator a single wavelength can be selected from the emitted synchrotron radiation spectrum.

The monochromatic X-ray beam is usually passing through a system of three slits. A slit is an arrangement of four knife edges that are controlled separately to define the beam profile. They are made of high Z material, like for example tungsten, in order to assure complete absorption of the impinging X-rays. For most of the X-ray diffraction experiments two slits are already sufficient as they lead to a properly collimated beam.

The slits themselves are a source of scattering, which becomes significant at small angles. As the beam hits the slits, diffraction can be recorded as an asymmetric pattern in the detector signal. This background is enhanced by scattering contributions due to the surface roughness of the knife edges [Le Bolloc'h et al., 2002]. Such a type of parasitic scattering is present for small angles close to the primary beam. For most diffraction experiments the low q-regime is not relevant so that this type of scattering

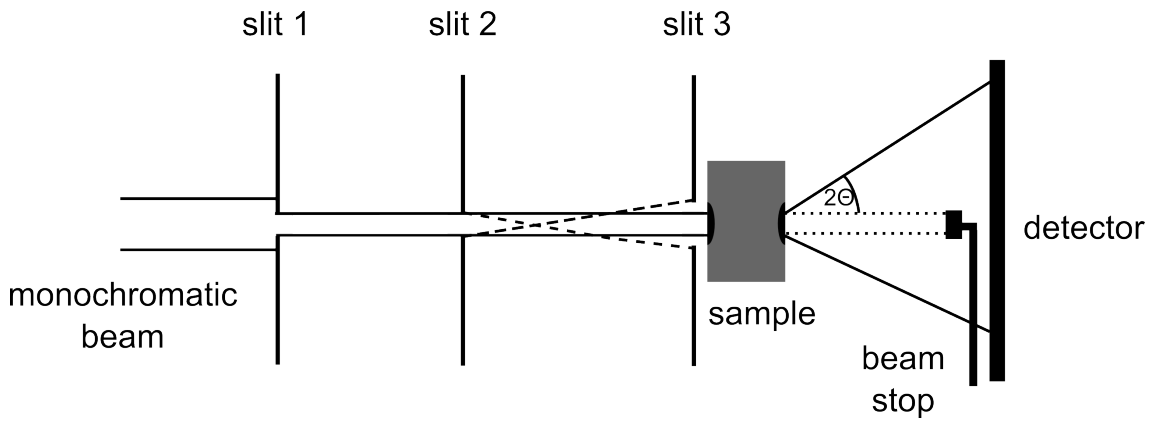

Figure 3.1: *Schematic drawing of a typical setup for SAXS experiments. Additional to the collimated direct beam impinging on the sample and the transmitted beam stopped by the beam stop (dotted line), the contributions of parasitic scattering on the slits (dashed line) as well as of the small angle scattering are shown.*

can be masked by a large-area beamstop. However, in the case of small angle scattering this type of parasitic scattering must be removed as it is superimposed on the actual signal of interest, which is typically weak. Thus, a third guard slit is employed, which should be located close to the sample. Its knife edges must be very close to the collimated primary beam to remove the parasitic scattering but must not be hit by it which would lead to an undesired scattering contribution again. Following this approach the parasitic scattering can be removed sufficiently [Wignall et al., 1990].

Subsequent to the slit system is the actual sample environment. Depending on the requirements of the experiment, appropriate sample containers, e.g. capillaries or cells, are used. The size of the sample container depends on the wavelength. For liquid samples like nanoparticles or proteins in solution the sample thickness must be chosen in a way that a sufficient amount of material is present to receive a detectable signal. At the same time the thickness must not be too large as otherwise the approximation of a single scattering event loses validity. From eq. (2.27) and eq. (2.30) the transmitted scattering intensity is proportional to

$$I \propto d \cdot e^{-\mu d} \,. \tag{3.1}$$

The maximum of the transmitted scattering signal is obtained when the following relation between sample thickness d and the wavelength dependent linear absorption coefficient is fulfilled [Lindner, 2002]

$$\mu_{\mathrm{opt}}(\lambda) = \frac{1}{d} \,. \tag{3.2}$$

If the sample thickness is fixed, the wavelength should be chosen so that $\mu(\lambda)$ is in

accord with eq. (3.2) if this is compatible with the requirements for a proper beamline operation. For scattering on aqueous protein solutions the absorption is mainly due to the solvent. Thus, the absorption coefficient of water can be used for calculations.

The transmitted primary beam as well as the actual scattering contribution both leave the sample. As the SAXS signal is much weaker than the primary beam, a sensitive detector has to be employed. In order to protect it against destructive overexposure, the transmitted beam is masked by a beamstop usually made of lead or tungsten. Avoiding to neglect a large part of the signal of interest the beamstop should be not larger than mandatory to fully remove the primary beam.

As the wavelength is fixed either due to the beamline requirements or the sample thickness and the aperture of the sample environment is in general constant, the detectable q-range is determined by the sample-to-detector distance. It has to be chosen sufficiently to ensure to obtain the characteristic features of the sample's scattering curve.

The scattered intensity of proteins in solution is weak due to the small contrast between them and the solvent. Thus, employing two-dimensional resolving area detectors is of advantage. As for these systems the SAXS signal is isotropic, azimuthal averaging gives an adequate signal strength and suppresses the contribution of statistical noise. Besides the gain in time also anisotropies due to reflexions or scattering contributions of compounds of the beamline optics can be seen on a two-dimensional resolving detector.

Additionally to slit scattering also scattering on air gives rise to the parasitic background. Furthermore, the X-ray is also partially absorbed by the air resulting in a decrease of intensity. Thus, it is necessary to evacuate as much sections the beam passes as possible. For most beamlines this is realized for the sections between source point and the sample as well as between sample and detector.

3.2 Beamlines

In this paragraph the setup of the different SAXS endstations where experiments were performed are described shortly. More detailed descriptions can be found in the corresponding literature on the beamlines as well as on the respective web pages.

3.2.1 BL9 (DELTA)

The electron storage ring DELTA (Dortmunder Elektronen-Speicherring-Anlage, Dortmund, Germany) is a third generation synchrotron radiation facility with a maximum electron energy of 1.5 GeV. The typical ring current is 130 mA with a life time of ca. 10 hours [Krywka et al., 2007]. Besides several bending magnets and two undulators

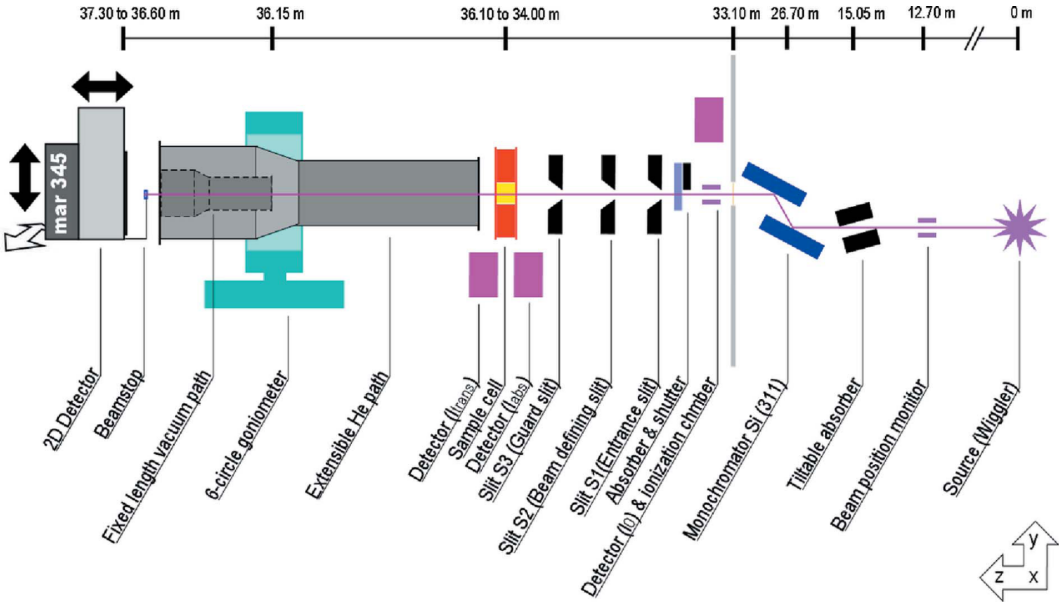

Figure 3.2: *Schematic outline of the SAXS setup at BL9 of DELTA [Krywka et al., 2007]. Copyright IUCr: http://journals.iucr.org/. Received with permission.*

providing synchrotron radiation, there is a superconducting asymmetric wiggler (SAW). Connected to the latter are three beamlines: BL8, BL9, and BL10.

At the multipurpose BL9 different experimental setups can be realized. Besides X-ray diffraction (XRD), gracing incidence diffraction (GID), X-ray reflectivity (XRR), and X-ray standing waves (XSW) measurements SAXS experiments can also be performed [Krywka et al., 2006, Krywka et al., 2007, Paulus et al., 2008]. A schema of the SAXS setup, which is not permanently installed, is given in Fig. 3.2.

Employing a Si(311) double crystal monochromator an X-ray energy between 4 keV and 30 keV can be utilized, which fully covers the range required for typical SAXS studies. With the second monochromator crystal a horizontal focus of 1.0 mm can be obtained. In the vertical direction the beam width typically is 1 - 2 mm. At a photon energy of $E = 10$ keV the flux is $5 \cdot 10^7 \frac{\text{photons}}{\text{s mm}^2 \text{ mA}}$ [Krywka et al., 2007]. Passing the slit system the primary beam hits the sample resulting in a SAXS signal. The distance between sample and detector is connected by a rigid evacuated flight tube with a length of 1.1 m. The backmost tube opening has a diameter of 200 mm. Due to this, a part of the active area of the two-dimensional detector (diameter: 345 mm) is shadowed. The detector installed is a MAR345 image plate detector with selectable pixel size (100 x 100 μm^2, 150 x 150 μm^2). A detailed description of the SAXS setup on beamline BL9 is given in [Krywka et al., 2007, Krywka, 2008]

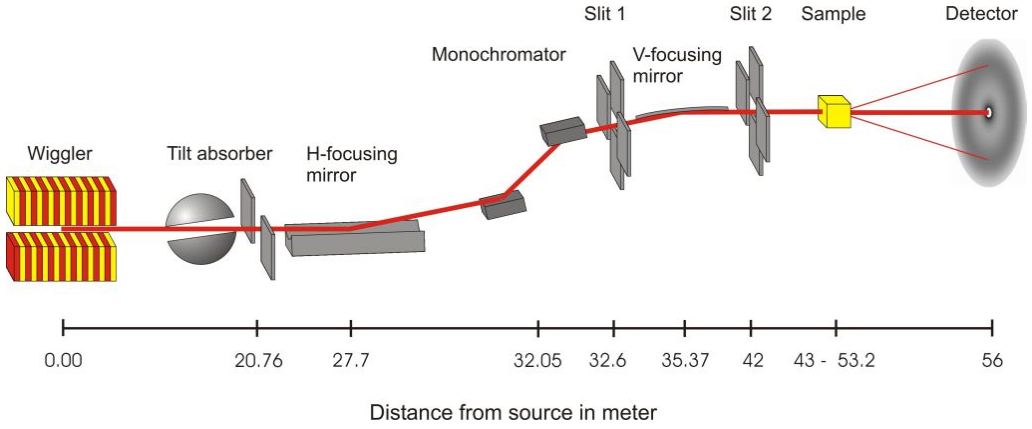

Figure 3.3: *Schematic outline of beamline BW4, HASYLAB. Reprinted with permission from [Timmann et al., 2009]. Copyright (2009), American Institute of Physics.*

3.2.2 BW4 (HASYLAB)

The Doris III positron storage ring of HASYLAB (Hamburger Synchrotronlabor) at DESY (Deutsches Elektronen-Synchrotron, Hamburg, Germany) with a ring current of 130 mA provides synchrotron radiation for 33 beamlines of which beamline BW4 is dedicated to small angle X-ray scattering techniques. Employing a Si(111) double crystal monochromator this wiggler beamline is usually operated at a fixed energy of 8.979 keV. The total photon flux is $6.5 \cdot 10^{10}$ $\frac{\text{photons}}{\text{s mm}^2 \text{ (100 mA)}}$ [Timmann et al., 2009]. The usual focused beam size is 0.4 x 0.4 mm^2, which can be further reduced by the use of beryllium compound refractive lenses to 65 x 35 μm^2 [Roth et al., 2006].

The layout of beamline BW4 is given in Fig. 3.3. Due to the flexible positioning of the sample stage, sample-to-detector distances in the range from 0.1 m to 12.4 m can be realized [Roth et al., 2006, Perlich et al., 2010]. Thus, a large q-range is accessible at BW4. Besides SAXS also WAXS and USAXS as well as gracing incidence small angle X-ray scattering (GISAXS), gracing incidence ultra-small angle X-ray scattering (GIUSAXS), and GID measurements can be performed. A photodiode has been installed inside the beamstop to record the transmitted intensity. For detection of the scattering signals two different area detectors were used. The MARCCD165 detector has an active area of 165 mm diameter made of 2048 x 2048 pixels of 79.1 μm size. Additionally, a Pilatus 300K with an active area of 83.8 x 106.5 mm^2 has been used (number of pixels: 487 x 619; pixel size: 172 x 172 μm^2).

3.2.3 ID02 (ESRF)

The ESRF (European Synchrotron Radiation Facility, Grenoble, France) posseses the SAXS dedicated undulator beamline ID02. Using a Si(111) double crystal monochromator energies in the range of 8 to 17 keV are accessible. The maximum incident intensity

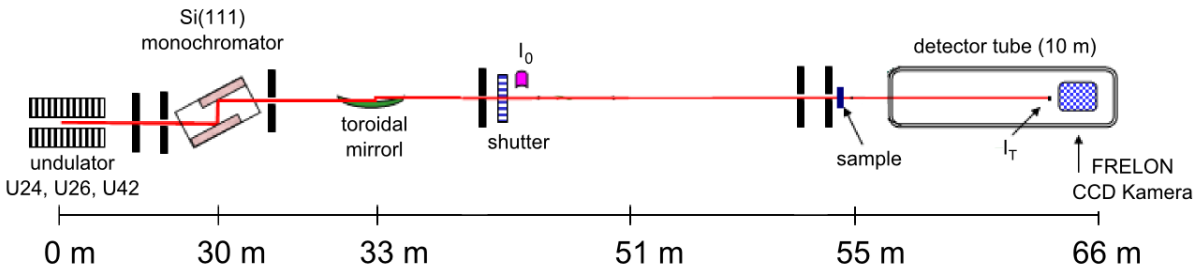

Figure 3.4: *Schematic outline of the high brilliance beamline ID02, ESRF. Adapted from [Beamline ID02, 2011].*

is 10^{13} $\frac{\text{photons}}{\text{s (100 mA)}}$ at a photon energy of 12.5 keV. Thus, the exposure times of biological samples can be reduced to several milliseconds. Focusing the beam gives a profile of 0.2 x 0.4 mm^2 (vertical x horizontal) [Narayanan et al., 2001].

The layout of the beamline is schematically shown in Fig. 3.4. The source of the synchrotron radiation are three undulators (U24, U26, U42). Besides various slits and count monitors a toroid mirror is employed for beam focusing. Detection of the scattering signals is achieved using a FRELON CCD camera. Its active area has a diameter of 230 mm and is made of 1024 x 1024 pixels. The camera is installed in a 12 m long evacuated tube where it can be moved freely. In such a way, the sample-to-detector distance can be changed from 1 m to 10 m. Inside the beamstop a diode is implanted allowing detection of the transmitted beam, which serves as the normalization signal. Besides SAXS experiments also WAXS and USAXS measurements can be performed at ID02.

3.3 High pressure setup

A large part of the studies done in the framework of this thesis were performed on protein solutions under high hydrostatic pressure conditions. Therefor, a high pressure setup employing a custom built sample cell for SAXS experiments, constructed and built by C. Krywka [Krywka, 2008, Krywka et al., 2008], was used.

The high pressure setup, shown in Fig. 3.5, consists of a unit for pressure generation, special high pressure tubing for connecting, the sample cell, and a pressure detector. The high pressure pump, valves, high pressure tubing, and additional supply were purchased from NOVA Swiss®. As high pressure transmitting medium deionized water is used.

The pumping unit consists of a hand spindle pump, a water reservoir, and a special valve for separating the reservoir, which is under ambient pressure conditions, from the high pressure system

The high pressure sample cell is made of stainless steal into which the actual sample carrier is placed. It was designed to withstand pressures up to 7 kbar. For the studies

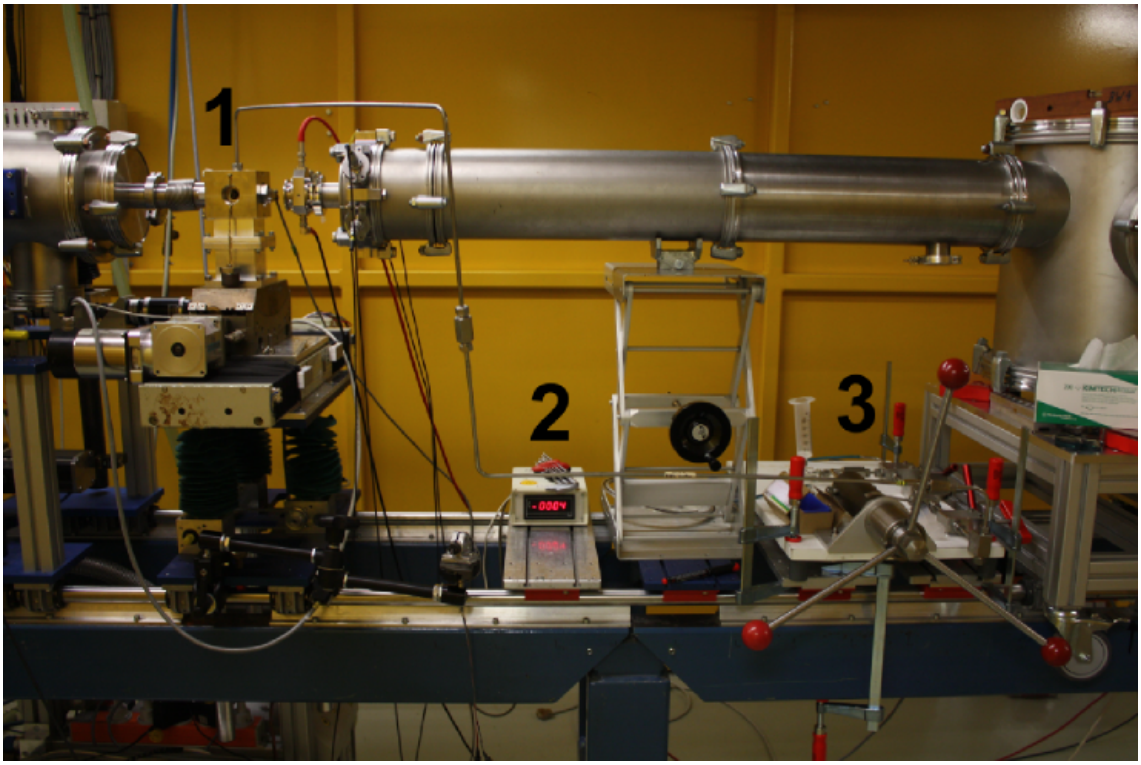

Figure 3.5: *Photograph of the high pressure setup installed at BW4, HASYLAB. (1) High pressure sample cell. (2) Display of the high pressure sensor. (3) Pumping unit.*

performed within this thesis usually pressures up to 4 kbar were employed.

In Fig. 3.6 technical drawings and a photograph are shown. Three large holes were drilled into the massive steel block. Those two facing each other are housing the window holders that are passed by the X-rays. The third inlet allows to place in the sample carrier. In addition, the cell has two grooves for connecting to the high pressure tubing and to the pressure sensor. On the backside there are two grommets to join the cell to a heat bath for tempering the sample cell via an internal water channel.

As X-ray windows two flat diamonds of type IIa (1.0 mm thickness, 6.0 mm diameter) are employed. These so-called Poulter-type windows are glued on special window holders with epoxy glue to assure fixed positions at low pressure [Sherman and Stadtmuller, 1987, Krywka, 2008]. At high pressures, the windows are kept fixed due to the pressure transmitting water. The two diamond windows are separated 2 mm from each other. Into this gap the sample carrier is placed (thickness 1.6 mm, Fig. 3.6b)). This is made of gold-coated copper or steel with Kapton® (polyimide) foil as window material[1]. The sample carriers can be charged with a liquid sample volume of 55 μl and are sealed by a nylon screw (M 2.5). These carriers can be easily removed from the sample cell and a fast change of samples can be performed without removing the diamond windows.

[1]It has to be noted that both the glue as well as the Kapton® foil have a finite thickness (Fig. 3.6c)). Thus, the original made sample carriers had to be made slightly thinner in thickness.

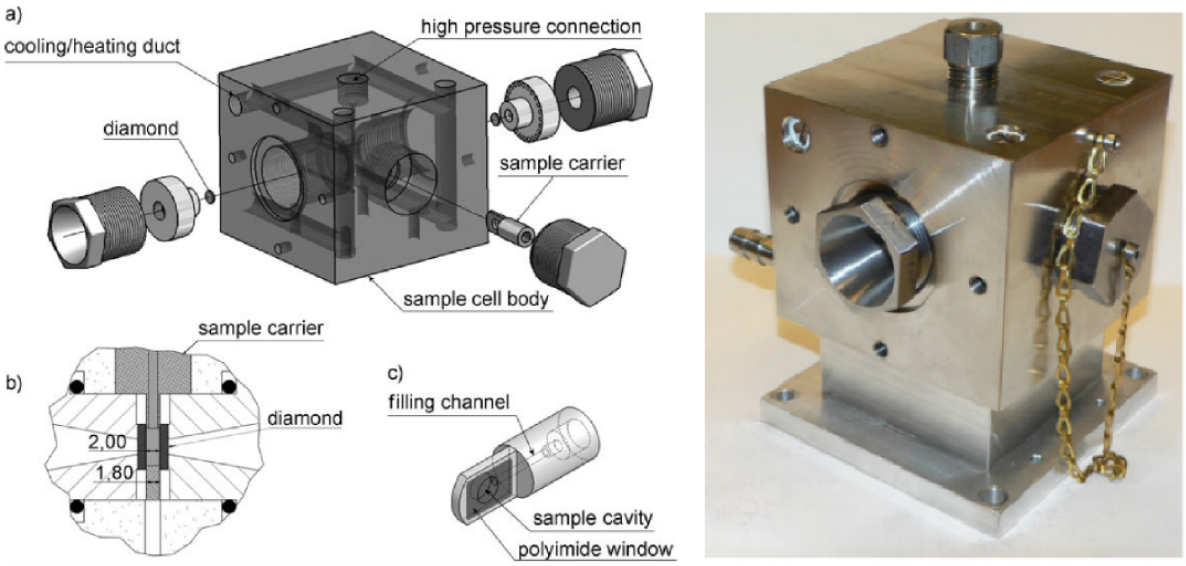

Figure 3.6: *Left: a) Scheme of the high pressure sample cell. b) Sketch of the sample carrier placed between the two diamonds. c) Sample carrier. Taken from [Krywka et al., 2008]. Copyright Wiley-VCH Verlag GmbH & Co. KGaA. Reproduced with permission. Right: Photograph of the sample cell. Taken from [Krywka, 2008]*

Keeping the diamonds at a fixed position avoids the change of the background signal as they also give rise to an anisotropic scattering signal.

To keep the cell tight at high pressures, the window holders are equipped with O-rings made of Viton® that form the seal between the holders and the cell. The window holders are pressed onto the O-ring by use of additional box nuts. The inlet for the sample carrier is sealed by a large plug equipped with an O-ring[2].

3.4 Basic data treatment

Herein, a short description of the basic treatment of the data obtained by small angle X-ray scattering experiments on protein solution is given.

As stated previously, two-dimensional resolving area detectors are employed in general for SAXS experiments. These have the advantage that a whole scattering pattern can be obtained in short time thus reducing the exposure durations. Besides a general gain in time, the damage of the sample due to radiation can be reduced. Furthermore, any anisotropy of the scattering signal can be detected.

As a first step a calibration of the sample-to-detector distance, the beam position on the detector as well as of its rotation and tilt has to be performed. Therefor, silver behenate ($CH_3(CH_2)_{20}COOAg$) has been used as a calibrate. This standard has a powder diffraction pattern with regular ($00l$) reflexions corresponding to a lattice plane

[2]The dimensions of the O-rings are: sample carrier 11 x 3 mm, window holder 13 x 3 mm.

distance of 58.380 Å giving rise to a diffraction signal at small angles [Huang et al., 1993]. After a proper calibration has been made, one-dimensional scattering curves can be calculated by azimuthally averaging of the two-dimensional scattering pattern. For both calibration and transformation the software package Fit2D has been employed [Hammersley et al., 1996]. In advance to the averaging it should be checked that there are no anisotropies or additional scattering signals from the window material. These have to be masked out previously.

Even for concentrated protein solutions the SAXS signal is weak. Therefore, the proper background has to be subtracted from the scattering curve. To perform this background correction, the sample carrier is filled with the corresponding buffer solution, which is used for the protein sample. By subtracting the scattering signal of the buffer also the parasitic scattering contributions from slits and air as well as that of the window material (i.e. Kapton® and diamond) will be removed. For this background correction both protein and buffer signal need to be normalized. Therefor, either the transmitted, attenuated primary beam or the total integrated scattering signal can be used. For the first one a so-called active beamstop, i.e. a diode placed inside of the beamstop, has to be used. Such a device is present at the beamlines BW4 and ID02. Alternatively, the totally integrated scattering signal which is recorded with a two-dimensional resolving detector can be utilized. This has been done for the data obtained at BL9. As both normalization signals have transmitted the sample, no absorption corrections need to be done.

However, irrespective of the type of normalization signal, it has been found that an additional constant number g which is close to unity has to be multiplied for each data set to obtain proper background subtraction. The scattering signal solely from the proteins in solution, $I_{\mathrm{p}}(q)$, is thus given by

$$I_{\mathrm{p}}(q) = \frac{I_{\mathrm{p+s+bkg}}(q)}{\mathrm{N}_{\mathrm{p+s+bkg}}} - g \cdot \frac{I_{\mathrm{s+bkg}}(q)}{\mathrm{N}_{\mathrm{s+bkg}}} \tag{3.3}$$

wherein $I_{\mathrm{p+s+bkg}}(q)$ and $I_{\mathrm{s+bkg}}(q)$ is the scattering signal from the protein solution with background and from the buffer solution with background, respectively, and $\mathrm{N}_{\mathrm{p+s+bkg}}$ as well as $\mathrm{N}_{\mathrm{s+bkg}}$ the corresponding normalization signals.

A proper number g can be either found by trial-and-error and comparison with the refinement of the experimental data which has been done for concentrated solutions where the structure factor has a significant contribution to the SAXS signal. Alternatively for diluted solutions of globular particles, the quality of the background subtracting can be checked from the corresponding Kratky plot (see chapter 2.2.4). Fig. 3.7 exemplarily shows how the scattering signal looks like for different numbers g. It has been found

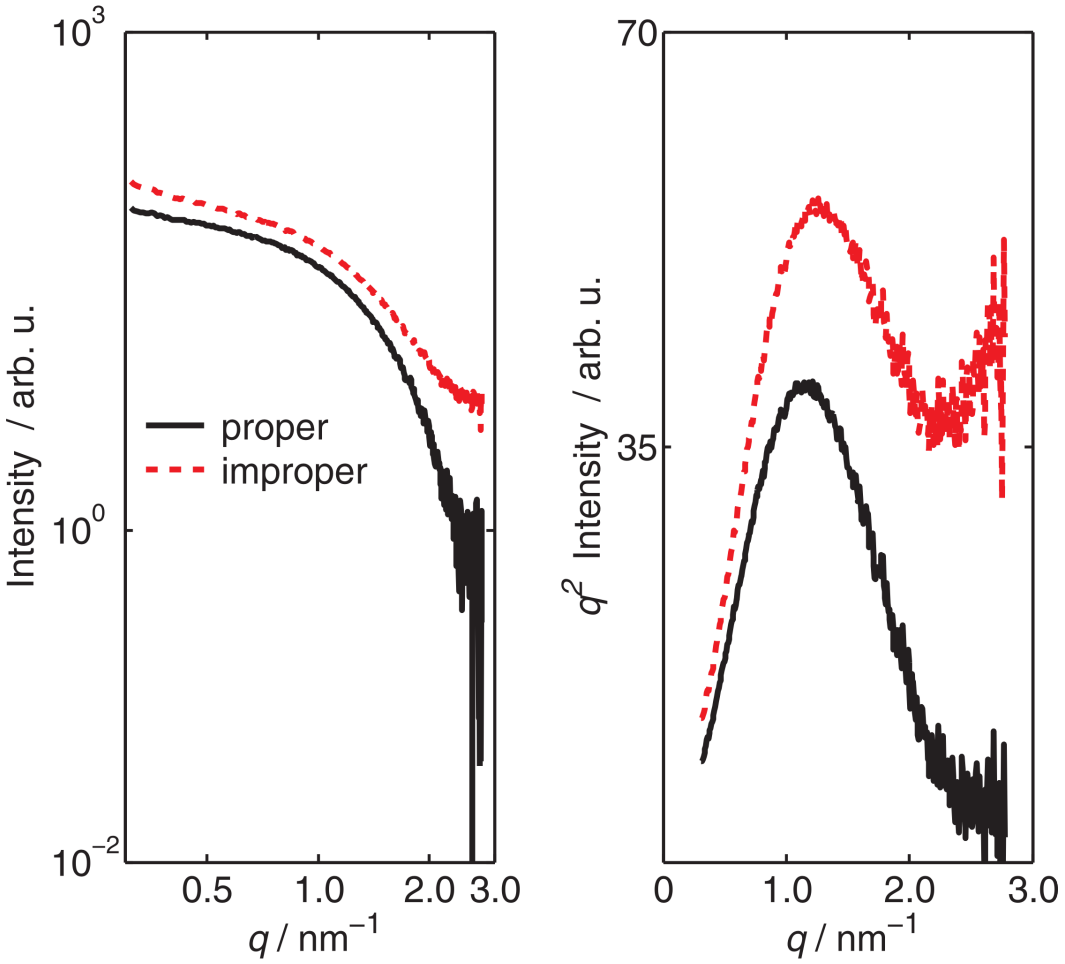

Figure 3.7: *Demonstration of a proper background subtraction for a 5 mg/ml solution of the protein lysozyme ($pH = 7$, $T = 25\,^\circ C$). Left: Scattering curves for proper (black solid curve) and improper (red dashed curve) background subtraction. Right: In the corresponding Kratky plot the quality of the subtraction can be seen better.*

that this number should be best chosen such that the curve in the Kratky plot (Fig. 3.7, right) has a sharp maximum and the minimum is close to zero. The criterion does not hold for unfolded or partially folded proteins as there will be not pronounced maxima. However, also in these cases the Kratky representation can be used for background subtraction. This is equivalent to the fact, that both curves should have a similar scattering intensity for high q as the protein contribution to the SAXS signal becomes weak at larger angles.

4 SAXS studies on different folding states of proteins induced by extreme conditions

For many years different questions on the protein folding process have been in the focus of research. Among these is that of how proteins adopt their three-dimensional structure within milliseconds to seconds starting from a linear polypeptide chain. Also it was asked if there exists a prediction of the native form from the amino acid sequence [Dill and Chan, 1997, Dobson et al., 1998, Dobson, 2003, Dill et al., 2008]. The complex interplay between different interactions leads to the heterogeneous three-dimensional folded structure of proteins that consists of ordered and disordered regions. Among these interactions are steric repulsion, Coulomb interactions, van der Waals interactions, hydrophobic interactions, hydrogen bonding, and covalent bonds between the protein's amino acid residues. In addition, the interaction with the solvent has a major influence.

Up to now many different concepts were developed to describe the thermodynamics, kinetics, and the structural evolution of the folding process using a large diversity of experimental techniques, computational studies, and theoretical calculations. One of the most accepted concepts is the folding funnel [Bryngelson et al., 1995, Brooks et al., 2001]. Within this energy landscape model, the folding process can be described as a reduction of the conformational entropy by a decrease of the total free energy.

Applying extreme conditions can change this energy landscape and thus gives access to folding state ensembles and folding kinetics [Dill and Chan, 1997, Silva et al., 2001]. These conditions can be heat, high pressure, change of the pH value of the solution, or the addition of special cosolvents leading either to stabilization or destabilization. If one defines "extreme" as "as affecting the protein's stability", also mutations in the protein's amino acid sequence can be counted amongst these.

Several experimental techniques to detect different structural changes that are induced by these types of perturbations emerged. They can give a deeper insight in and better understanding of the complex interplay of the different interactions that give rise to protein stability and folding. Among these experimental methods are spectroscopic, thermodynamic, and scattering techniques, which all probe different structural

and energetic aspects [Winter and Noll, 1998, Allen, 2008].

Fluorescence and nuclear magnetic resonance (NMR) spectroscopy measurements yield information on the protein structure on the atomic level where local changes can be detected. Measuring the circular dichroism (CD) and the Fourier transform infrared (FTIR) spectrum reveals special structures known as secondary structure elements. Using differential scanning calorimetry (DSC) and pressure perturbation calorimetry (PPC), quantities characterizing the thermodynamics of the protein solutions are obtained. Scattering techniques like small angle scattering on diluted protein solutions are sensitive to the tertiary structure, i.e. the compactness of proteins, and its change induced by perturbations. The information that can be obtained notably by SAXS are discussed in detail in chapter 2.

For this thesis small angle X-ray scattering was the technique of choice to study changes of the global protein structure induced by different external perturbations. This approach allows to get an insight into how microscopic interactions give rise to the protein shape and thermodynamic stability. For instance, the influence of internal charges or point mutations can, depending on their properties, cause structural changes and also stabilization or destabilization. Depending on the type of external perturbations, proteins are influenced differently. For example, high pressure will lead to a reduction of the total volume and thus allows to study the plasticity of proteins. Changing the protein solution's pH value affects the protein surface charges as well as internal ionizable residues if these are present. These effects were in the focus of the presented SAXS studies.

More precisely, SAXS measurements on diluted solutions of different proteins (wild type staphylococcal nuclease (SNase) and different mutants of this protein; the ankyrin repeat of the Notch receptor) were performed in the presence of such extreme conditions. Among these were high hydrostatic pressure, different pH values, addition of cosolvents as well as combinations of those. The present chapter describes the results of these SAXS experiments. The outline is as follows.

In paragraph (4.1) the general structure of proteins is described. Subsequently the model for the folding process and the thermodynamics of two-state folding proteins will be discussed. Special attention therein is given to the effects of different perturbations.

After this general section, the results of three studies on different types of proteins will be discussed. Therein, external perturbations allowed to influence the protein structure and thus to access specific characteristics of the respective protein types.

In paragraph 4.2 the results of a SAXS study on a globular protein with an ionizable residue in the interior are presented. Depending on the charge state of this single residue the protein plasticity of the staphylococcal nuclease variant Δ-PHS/V66K was probed by pressure perturbations. Comparison with the corresponding background variant Δ-

PHS allowed to distinguish specific effects that can be assigned to the presence of the single ionizable residue and its properties.

Paragraph 4.3 deals with another mutant of the protein SNase, T62P, which resembles features of a so-called natively unfolded protein. In this SAXS study its compactness was analyzed as a function of the solution's pH value and salt content and compared with that of the wild type variant. This approach allowed to get insight into the influence of electrostatic interactions on the unfolded state of a protein.

In paragraph 4.4 high pressure SAXS measurements are presented on a non-globular protein, the ankyrin repeat domain. Herein, unique features of the folding and unfolding of this type of protein were explored.

4.1 Proteins

4.1.1 Protein structure

Proteins are a large class of biological macromolecules that fulfill specific needs in all living cells and organisms. Depending on their biological function different types of proteins can be found. Structure proteins like collagen give stability, others like hemoglobin transport small molecules. Some proteins, like insulin, act as hormones and others are involved into cell signaling and energy transfer processes. For most of the proteins known today there is a strong correlation between their biological function and their three-dimensional structure, i.e. their native folded state. However, some members of a class of proteins, the so-called natively unfolded proteins, are assumed to function in the disordered state. Others undergo a transition into the ordered state to function but exist otherwise as disordered coils [Uversky, 2002, Dyson and Wright, 2005]. The different structural hierarchies in these biomolecules will be discussed shortly. This presentation follows references [Voet et al., 2006] and [Löffler et al., 2007].

Proteins are special types of polymers consisting of amino acids. There are 20 so-called proteinogenic amino acids which most proteins are made of. These small molecules are derivatives of carboxylic acids wherein an amino-group (-NH_2) is substituted on the central carbon atom (C^{α}) [Löffler et al., 2007]. Beside the amino- and the carboxyl-group (-COOH) also a hydrogen and an additional side chain are attached to it. The zwitterionic amino acids differ in the type of their side chains which can be differentiated in size and ionic properties. In the following, the 20 proteinogenic amino acids are listed in terms of their side chains' polarity [Voet et al., 2006, Löffler et al., 2007]. In brackets, the corresponding three-letter- and one-letter-abbreviation is given.

- amino acids with nonpolar side chains
  - glycine (Gly, G), alanine (Ala, A), valine (Val, V), leucine (Leu, L), isoleucine (Ile, I), methionine (Met, M), proline (Pro, P), phenylalanine (Phe, F), tryptophan (Trp, W)
- amino acids with uncharged polar side chains
  - serine (Ser, S), threonine (Thr, T), asparagine (Asn, N), glutamine (Gln, Q), tyrosine (Tyr, Y), cysteine (Cys, C)
- amino acids with acidic side chains
  - aspartic acid (Asp, D), glutamic acid (Glu, E)
- amino acids with basic side chains
  - lysine (Lys, K), arginine (Arg, R), histidine (His, H)

Connecting the carboxyl-group of one amino acid to the amino-group of another one by a peptide bond, a polypeptide is formed. The so created (-N-C^{α}-C-N-C^{α}-C-)-sequence is the backbone of the polypeptide. Depending on the length of these amino acid chains, actual peptides and proteins are defined. Roughly, one speaks of a protein from a number of 40 amino acids [Voet et al., 2006]. As the polypeptide backbone is present in all proteins the properties and functions are related to the different side chains [Löffler et al., 2007]. More precisely, it is the amino acid sequence that is essential for determining the biological function of the protein. This sequence is called the primary structure of the protein. In Fig. 4.1a) a polypeptide with a length of six amino acids is shown as a representation of the primary structure. Therein, R_1 - R_6 denote (different) side chains.

Special interactions between different parts of the polypeptide chain give rise to the three-dimensional structure of the protein. First, due to the steric repulsion of two adjacent amino acids the conformation of the chain is reduced to special angles between the chain elements that can be obtained from a so-called Ramachandran plot [Voet et al., 2006]. The formation of hydrogen bonds between the different parts of the polypeptide backbone that are in contact and not stericly forbidden leads to special structure elements known as the protein's secondary structures. Frequent representatives of this class are the α helix and the β sheet which are depicted in Fig. 4.1b). On the left side an α helix is shown with the corresponding hydrogen bonds (dotted lines). On the right side two strands of an antiparallel β sheet also with hydrogen bonding are

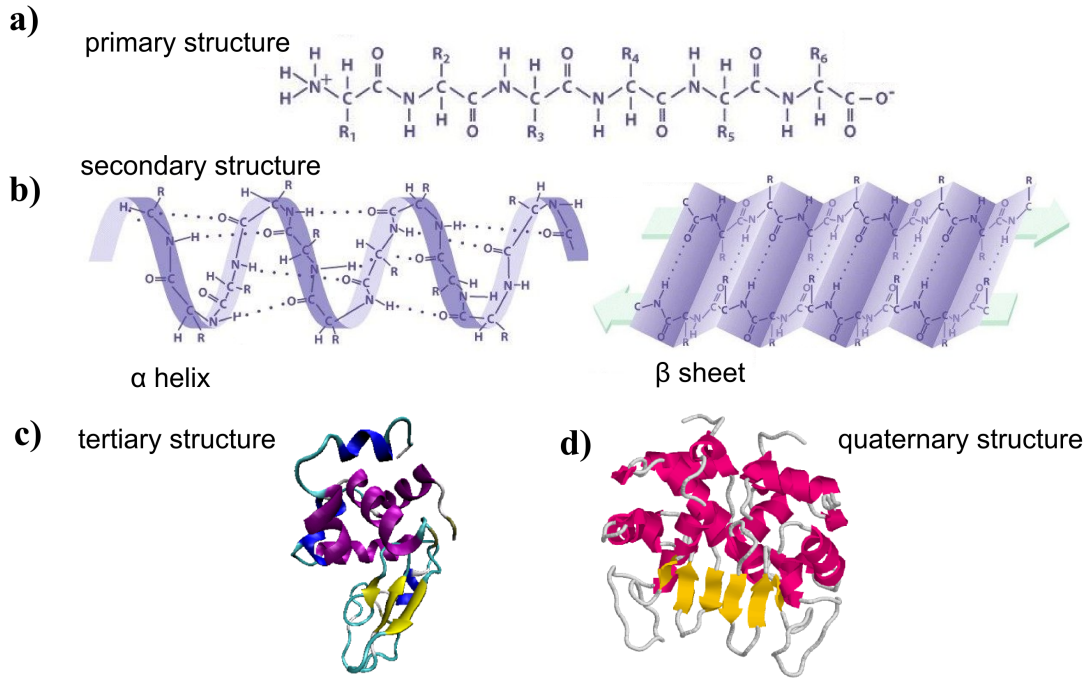

Figure 4.1: *Different hierarchical structures in proteins. a) Primary structure: Polypeptide chain. b) Secondary structure elements: (Left) α helix. (Right) Antiparallel β sheet. c) Tertiary structure: Folded protein with different secondary structure elements present. d) Quaternary structure: Association of two tertiary structure subdomains. Adapted from [Oregon State University, 2008].*

presented. Typically, such types of antiparallel strands are connected by a small loop.

In fibrous proteins like structure proteins, repetition of certain amino acids within the sequence gives rise to a periodical structure such as the triplet helix of collagen. Such highly ordered structured regions are missing in globular proteins. Herein, special domains with secondary structure elements are present as well as regions with turns and loops and disordered parts. Different interactions between the amino acid side chains lead to the formation of a compact protein with its biological function (see 4.1c)). Hydrophobic interactions mostly between the nonpolar amino acid residues result in the formation of a hydrophobic core which is separated from the surrounding solvent. This structure is additionally stabilized by van der Waals interactions, hydrogen bonds, covalent bonds in form of disulfide bridges, and some ionic interactions inside the protein, the so-called salt bridges. Therefore, usually those amino acid residues with charged polar side chains are directed outwards of the protein toward the solvent forming the protein surface. However, internal ionizable groups are present in those proteins that are involved in energy transduction processes such as H^+-transport [Yoshikawa et al., 1998] or light-activated processes [Luecke et al., 1999]. In conclusion, the polar side chains can be found both inside and outside of the protein [Voet et al., 2006, Löffler et al., 2007]. Within the folded protein there are special groupings of secondary structure elements.

These are called supersecondary structures. Examples of these are the β hairpin, i.e. an arrangement of antiparallel β sheets connected by a turn, and the β barrel, i.e. extended β sheets that are rolled up. For larger proteins consisting of a single polypeptide chain there are often more folded globular clusters, the so-called structural domains, which are commonly related to actual biological function of the protein [Voet et al., 2006, Löffler et al., 2007].

Proteins consisting of more than one polypeptide chain and thus of two and more associate subunits are said to have a quaternary structure. This type is typical for large proteins. Some larger proteins with catalytic activity also posses so-called prosthetic groups which are essential for their biological function. These often contain metal atoms. An example of a protein with quaternary structure is depicted in Fig. 4.1d).

Protein structures can be obtained by X-ray crystallography measurements with resolution of about an Ånstrom [Winter and Noll, 1998, Voet et al., 2006, Allen, 2008]. Today, there exist specialized beamlines at synchrotron radiation facilities that are dedicated to structural biology which are often fully automated. Furthermore, due to the use of dedicated software packages, a three-dimensional electron density map is directly obtainable after a diffraction pattern has been detected. However, to achieve this the presence of proper protein crystals is required. Crystallization is often not possible for special proteins such as membrane proteins. Furthermore, to avoid radiation damages, protein crystals need to be cooled down. Thus, the so obtained structure might deviate from the biological relevant one in the liquid solvent[1]. Molecular details of proteins in solution can be obtained by NMR spectroscopy. However, the shortcoming of this technique is that it is limited to smaller proteins [Svergun and Koch, 2003].

To complement those information obtained by crystallography and NMR measurements or, if these information are absent, to study the protein structure at all, other spectroscopic and scattering techniques can be utilized. As already mentioned shortly in the introduction to this chapter, fluorescence spectroscopy can give insight into the local chemical environment of the fluorophore. Within proteins, amino acids with aromatic site chains, like phenylalanine, tyrosine, and tryptophan, serve as intrinsic fluorophores, whereof tryptophan has the largest fluorescence yield [Winter and Noll, 1998]. Structural information on secondary structure elements can be obtained using circular dichroism (CD) and the Fourier transform infrared (FTIR) spectroscopy.

By employing small angle scattering, information on the general three-dimensional shape of the protein can be obtained. As the resolution of this technique is lower than that of diffraction studies due to the smaller q-range as well as the averaging process, no atomic details can be resolved. However, information on the protein's envelope are

[1] However, this seems to be not the case for most proteins [Voet et al., 2006].

accessible. Different software packages have been developed that allow to calculate the three-dimensional models ab initio from the scattering signal. For example, the programs DAMMIN and its more recent version, DAMMIF, restore the low-resolution shape of a protein by assuming a random configuration of dummy atoms and comparing the corresponding scattering curve with the experimental data [Svergun, 1999, Franke and Svergun, 2009]. By use of different criteria the program searches for those dummy atom structures by a simulated annealing process that coincidence best with the data. For details, see the references [Svergun, 1999, Franke and Svergun, 2009]. Note that using neutrons as the probe, labeling of subdomains can give additional information [May, 2002].

4.1.2 Protein folding

In living cells, proteins are synthesized on the ribosomes as linear chains. Involving various macromolecules like molecular chaperones, the natively folded protein with its biological function is created in vivo [Ellis and Hartl, 1999]. However, the work of Anfinsen and colleagues on the reversible un- and refolding of the protein ribonuclease showed that the folding can also be observed in vitro and that the native protein structure is a thermodynamical stable state [Anfinsen, 1973, Dill and Chan, 1997]. This folded state depends on the amino acid sequence and the solutions conditions but not on the folding kinetics [Anfinsen, 1973, Dill et al., 2008]. This result opened the way for studying various proteins regarding their stability. Soon the question arose how a protein can fold within milliseconds although a random search of the polypeptide for its native structure would last an astronomical time, i.e. the so-called Levinthal paradox [Dobson et al., 1998]. This apparent contradiction can be solved when there is not a random process but a special folding pathway between an unfolded state and a folded state connected by intermediate states. During the study of these folding pathways it was experimentally found that not only on-pathway intermediates but also off-pathway intermediates can exist. It was pointed out that there is not a single way but multiple parallel pathways for protein folding [Harrison and Durbin, 1985]. Therefore, instead of using the concepts of folding pathways and defined states, a statistical energy landscape approach was developed wherein state ensembles are present [Bryngelson et al., 1995]. This energy landscape representation predicting a funnel-like shape is currently the mostly accepted model for describing the protein folding process.

The underlying concept of the energy landscape representation assumes that the folding process can be described by the free energy of the polypeptide in solution, taking into account all intramolecular interactions and those with the solvent molecules as a function of a few proper order parameters, like the radius of gyration or the frac-

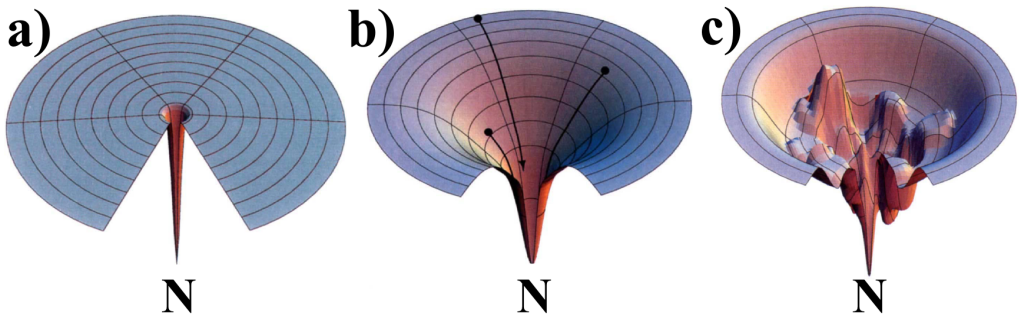

Figure 4.2: *Different energy landscapes. "N" denotes the native state. a) Levinthal "golf course" landscape. b) Smooth folding funnel. c) Rough folding funnel. Adapted with permission from Macmillan Publishers Ltd: [Nature Structural Biology] [Dill and Chan, 1997], copyright (1997).*

tion of native contacts [Bryngelson et al., 1995, Dobson et al., 1998, Dill et al., 2008]. In terms of the energy landscape, the unfolded state is characterized by occupying the largest conformational space whereas the folded state has the lowest one. Folding then can be understood as a reduction of configuration space by a subsequent decrease of the total free energy. In terms of a landscape picture one could think of a downhill process. Furthermore, this funnel-like representation can describe the heterogeneity of the folding process that has been observed for some proteins [Dill et al., 2008].

Fig. 4.2 shows different schemes of energy landscapes types. Note, that herein only the effective or internal interaction energy is depicted on the vertical axis, i.e. the contribution of the configurational entropy on the total free energy is missing. In Fig. 4.2a) the so-called Levinthal "golf course" landscape is shown. If there are no interactions and only a random folding process, a flat energy landscape is present with only one steep minimum. To reach this, an unrealistic large time would be needed. An idealized folding landscape is shown in Fig. 4.2b). In such an energy landscape the protein would be funneled down from a random chain to its native folded form. Such smooth folding funnels are realistic for small, single domain proteins. For larger proteins the energy landscape becomes more rough (Fig. 4.2c)). Therein, local minima and maxima are present reflecting intermediate and transition state ensembles. These are the bottlenecks for folding. A local minimum corresponds to intermediate states that are characterized as being already partially folded. Such a kinetic intermediate state is separated from the global minimum by an energy barrier. The shape of such a landscape is reflected in the kinetics of the folding process. Taking into account the configurational entropy contribution, the resulting free energy landscape can have a broad minimum at higher energies also for the folding landscape in Fig. 4.2b). This minimum is separated by a barrier from the native state minimum. This means that also for a single domain protein kinetic transition state ensembles are present

[Dinner et al., 2000]. As the free energy depends both on the internal interactions as well as on the configurational entropy, changes of the temperature, the solvent composition, and pressure or changes due to mutations will result in a different folding landscape [Dobson et al., 1998, Leeson et al., 2000, Silva et al., 2001]. Folding energy landscapes can be e.g. obtained by using proper computer simulations and calculations such as lattice models. These evidently lack an atomistic description but reflect the essential features of the energy landscape [Bryngelson et al., 1995, Dinner et al., 2000].

Using the landscape model, the folding and unfolding kinetics that are accessible in an experiment are reflecting the landscape's roughness [Bryngelson et al., 1995] [Hyeon and Thirumalai, 2003, Chavez et al., 2004]. Single domain proteins with a smooth energy surface show a single-exponential decay in their folding kinetics corresponding to two-state-folding. This means that only two structural states, namely the unfolded and the native, exist which are connected by a kinetic folding transition state ensemble and it is the entropic bottleneck that gives rise to the last one. For proteins with rough landscapes multi-exponential relaxations have been determined reflecting a more complex folding behavior.

Different types of states, either kinetic or structural, have been assumed to be present during the protein folding. For two-state folding proteins the location of the transition state ensemble can be either more close to the unfolded state or to the folded one. In the first case small nucleus, foldings cores, or wet molten globules are present [Dinner et al., 2000]. If the transition state is closer to the native protein, one speaks of the dry molten globule state [Dinner et al., 2000, Baldwin et al., 2010]. In more detail, there are some proteins with a transition state ensemble with localized structures in the interior with only partially folded secondary structure elements, and others where the whole set of secondary structure is already completely present [Barrick, 2009]. Also there are states that are polarized, i.e. that are structured on some sites and not on others [Barrick, 2009]. Evidently, such states differ in compactness and degree of hydration. Recently, the existence of a stable dry molten globule state as a commonplace structural intermediate in protein folding has been proposed [Baldwin et al., 2010].

To obtain an insight into the molecular details that give rise to the existence of either transition state ensemble, experiments on proteins wherein specific amino acids were replaced by mutagenesis are performed [Fersht and Daggett, 2002, Mitra et al., 2007]. These locally perturb the structure and thus can influence the folding kinetics. Additionally, the proteins stability can be changed. To test this change of stability different ways to unfold proteins can be used. Depending on the type of global perturbation different unfolded states have been reported. Such means of unfolding and thus of testing protein stability are high and also low temperatures, high pressures, low and high pH values as well as addition of cosolvents, like urea or guanidine hydrochloride. These can change

the free-energy landscape and thus the folding kinetics as well as the thermodynamics of the protein. To this end a thermodynamical description will be given for the most important case of two-state folding proteins in the next subsection. This will allow to understand how the thermodynamical parameters temperature, T, and pressure, p, can cause unfolding.

4.1.3 Protein stability

The folded state of a protein is only slightly more stable than the unfolded one at physiological conditions [Voet et al., 2006]. A free energy for unfolding of about 0.4 kJ/mol per amino acid has been reported reflecting the balance and complex interplay between the different interactions involved. To describe the thermodynamics of a two-state folding protein the knowledge of the temperature and pressure dependence is mandatory [Kauzmann, 1987]. If the solution conditions are similar for both the folded and unfolded state, a thermodynamical description can be given in terms of the Gibbs free energy $G(p,T)$. Following Hawley [Hawley, 1971], the difference $\Delta G(p,T)$ between the unfolded and folded state reads [Winter et al., 2007]

$$\begin{aligned}\Delta G(p,T) =& \Delta G_0 - \Delta S_0(T-T_0) - \Delta C_\mathrm{P}\left[T\left(\ln\frac{T}{T_0}-1\right)+T_0\right] \\ &+ \Delta V_0(p-p_0) + \frac{\Delta\tilde{\kappa}}{2}(p-p_0)^2 + \Delta\tilde{\alpha}(p-p_0)(T-T_0)\ .\end{aligned} \tag{4.1}$$

Herein, S denotes the entropy, C_P the heat capacity, $\tilde{\kappa} = (\frac{\partial V}{\partial p})_T$ the compressibility factor, and $\tilde{\alpha} = (\frac{\partial V}{\partial T})_p$ the thermal expansion factor. The last two quantities are related to the isothermal compressibility κ_T and thermal expansion coefficient α_p via $\tilde{\kappa} = -V\kappa_T$ and $\tilde{\alpha} = V\alpha_p$, respectively. "$\Delta$" denotes the change between unfolded and folded states of the quantities and the index "0" an arbitrary reference point. Equilibrium between both states is present for $\Delta G(p,T) = 0$ [Heremans and Smeller, 1998]. Then, the transition line in the p,T-diagram has an elliptical shape which is shown in Fig. 4.3[2]. This shape is a result of the differences of the second order terms C_P, $\tilde{\kappa}$, and $\tilde{\alpha}$ between the unfolded and folded state. More precisely it is due to the differences in the volumetric and entropic fluctuations as these thermodynamic parameters can be expressed as $\langle S-\langle S\rangle\rangle^2 = \mathrm{k_B}C_\mathrm{P}$, $\langle V-\langle V\rangle\rangle^2 = \mathrm{k_B}TV\kappa_T$, and $\langle SV-\langle S\rangle\langle V\rangle\rangle = \mathrm{k_B}TV\alpha_p$, wherein terms in brackets indicate ensemble averages [Heremans and Smeller, 1998]. Notewor-

[2]More precisely, expanding the term in square brackets in eq. (4.1) in the vicinity of the reference point leads to

$$T\left(\ln\frac{T}{T_0}-1\right)+T_0 = \frac{(T-T_0)^2}{2\,T_0}$$

giving the formula of an ellipse [Smeller, 2002].

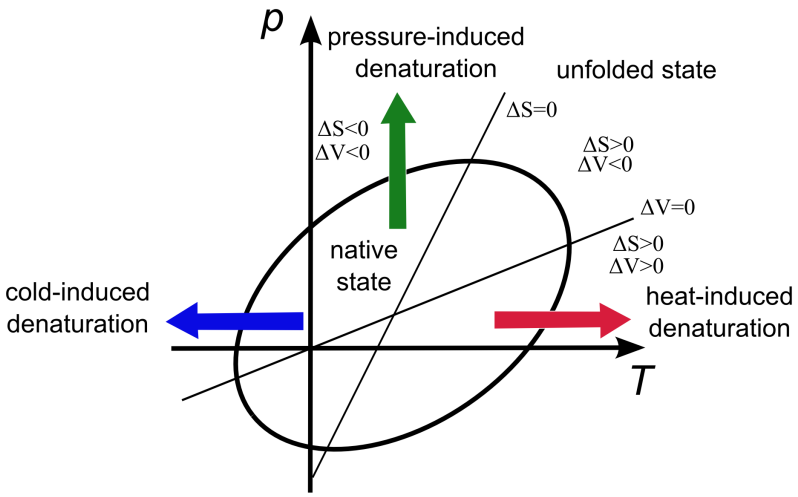

Figure 4.3: *Scheme of a typical elliptically shaped pressure-temperature stability diagram. Protein stability is present for $\Delta G(p,T) > 0$. Increase as well as decrease of temperature and increase of pressure leads to protein unfolding. Also shown are the lines of vanishing entropy and volume change. Thus, regions are present where unfolding is accompanied by different ΔS and ΔV.*

thy, all these quantities describe the hydrated protein, i.e. the presence of the hydration layer has an essential contribution to the thermodynamics of a protein. For instance, as a first approximation the change of entropy ΔS as well as of the volume ΔV can be decomposed into contributions from the protein and from the hydration layer [Winter et al., 2007].

Within the derivation of eq. (4.1) it has been assumed that the parameters do not change significantly with pressure or temperature [Smeller, 2002, Winter et al., 2007]. If these dependencies are also taken into account, additional terms are present in eq. (4.1) which lead to a distortion of the ellipse.

Knowledge of all the different thermodynamic parameters present in eq. (4.1) for the unfolding of a protein allows to calculate the free-energy landscape and thus the p,T- stability diagram [Lassalle et al., 2000, Ravindra and Winter, 2003]. Therefor, a combination of different experimental techniques is needed. Especially by employing techniques like DSC, PPC, and densitometry, the heat capacity C_P, thermal expansion coefficient α_p, and the relative volume change $\frac{\Delta V}{V}$ as well as the apparent specific volume can be obtained [Seemann et al., 2001, Ravindra and Winter, 2003]. Furthermore, ultrasonic velocimetry studies give access to the adiabatic compressibility κ_S, which is related to the isothermal compressibility via $\kappa_T = \kappa_S + \alpha_p^2 T/(\rho C_p)$ wherein ρ is the density of the protein solution [Heremans and Smeller, 1998]. Thus, in principle a full description of the thermodynamics of two-state folding proteins can be obtained using this approach which was done e.g. for the small protein staphylococcal nuclease (SNase). The corresponding calculated p,T-stability diagram was in accord with exper-

imental data [Panick et al., 1999, Ravindra and Winter, 2003].

Fig. 4.3 shows that there are different ways to induce the unfolding of proteins. Either increasing as well as decreasing of temperature leads to unfolding. Furthermore, high pressure also can unfold proteins. Whereas changing the temperature results in a simultaneous change of total energy and volume, pressure solely affects the system's volume [Silva et al., 2001]. Following Le Chatelier's principle, increasing pressure favors the state with the least volume. Therefore, using high pressure as a perturbation the influence of volumetric changes like hydrophobic packing on the protein stability can be studied. In the following, general aspects of pressure will be discussed.

Pressures up to 10 kbar do not affect the primary and secondary structure as there is no change of covalent bonds and only non-covalent interactions are influenced [Boonyaratanakornkit et al., 2002, Meersman et al., 2006]. Thus, in this range pressure leads to a destabilization of tertiary and quatenary structures, only. The threshold for unfolding depends on the protein and its internal structure like the presence of disulfide bonds. Typical values, which are experimental accessible can range from about 1 kbar to 7 kbar and above that [Smeller, 2002, Winter et al., 2007]. When releasing pressure the most proteins refold reversible [Perrett and Zhou, 2002, Winter et al., 2007]. The pressure-induced denatured state is more compact than the temperature-induced one which is reflected by a much smaller radius of gyration [Panick et al., 1998]. Furthermore, for the pressure-induced unfolded state secondary structure elements are still present in protein which is not the case for heat. This is due to the fact that pressures promote hydrogen-bond formation [Boonyaratanakornkit et al., 2002]. Pressure also leads to the dissociation of protein aggregates which are usually present for heat-induced unfolding [Silva et al., 2001, Perrett and Zhou, 2002].

The volume of unfolding ΔV, i.e. the volume difference between the unfolded and folded state, is small and negative. Typical values are less than 1% [Royer, 2002]. Different contributions to this can be defined. These are changes of the cavity volume in protein interior, i.e. regions of imperfect protein packing, of the volume due to interactions with the hydration water, and of the thermal volume reflecting the thermal fluctuations of the protein. The van der Waals volume, i.e. sum of the volume of the constituent atoms, does not evidently change between the two folding states [Chalikian and Breslauer, 1998, Meersman et al., 2006]. ΔV has been found to decrease as a function of temperature which can be understood by the different thermal expansion coefficients of the unfolded and folded protein and thus due to the different temperature dependence of the volume change contributions [Mitra et al., 2006]. Moreover, the volume of unfolding can even change its sign at high temperatures, i.e. the unfolded states has a larger volume than the folded state. As a consequence of this pressure leads to

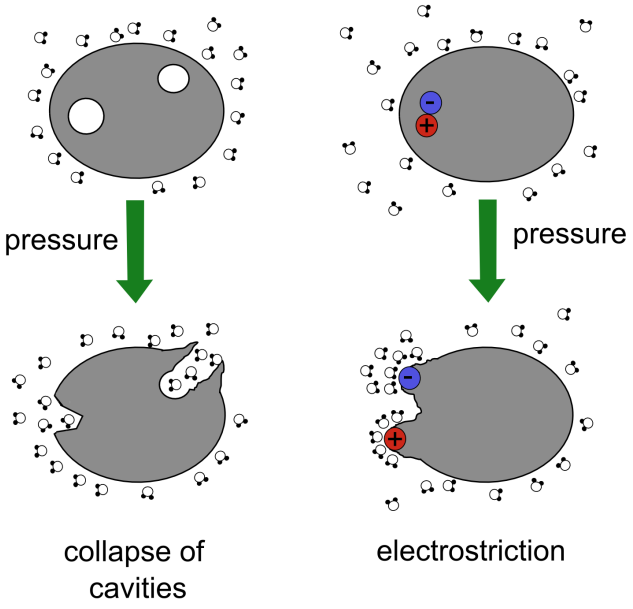

Figure 4.4: *Schematic drawing of two mechanisms that contribute to the volume reduction in pressure-induced unfolding. Left: Collapse as well as opening of internal cavities can give access to the surrounding water molecules. Right: Exposure of polar residues and dissociation and exposure of paired charged residues leads to electrostriction.*

a stabilization of the folded protein at high temperatures. In the p,T-stability diagram this is reflected by a positive slope of the $\Delta G(p,T) = 0$ line on the high temperature end [Royer, 2002].

Mechanisms for pressure-induced unfolding leading to a volume reduction are the collapse of internal cavities, void volumes, and packing defects [Frye and Royer, 1998, Royer, 2002] (Fig. 4.4 left). Exposure of polar residues as well as dissociation and exposure of paired charged residues present in the interior can also lead to a decrease of volume by electrostricton (Fig. 4.4 right). This however might not be the dominant mechanism as most charged residues are already located on the protein's surface [Frye and Royer, 1998]. Furthermore, also the hydrophobic interaction might change at high pressures leading to unfolding. Computer calculations on methane molecules have shown that in presence of pressure the direct interaction between the molecules is destabilized relative to the indirect water mediated interactions [Hummer et al., 1998]. Thus, pressure driven insertion of water molecules can result in a weakening of hydrophobic interactions and concomitant unfolding.

The mechanism of pressure-induced unfolding depends on the actual structure of a protein. For instance, for the protein SNase it has been shown in a series of experiments using different cavity mutants, i.e. mutants wherein a single amino acid in the interior was replaced by differently sized others, that the main mechanism is the collapse of void volumes [Royer et al., 1993, Frye et al., 1996, Vidugiris et al., 1996,

Frye and Royer, 1998]. Generally, pressure-induced unfolding results in an insertion of water molecules into the proteins interior which was observed experimentally and by computer simulations for example for SNase [Lassalle et al., 2000, Paliwal et al., 2004, Sarupria et al., 2010]. Thus, this type of unfolded state is characterized as swollen, hydrated, and partially unfolded [Meersman et al., 2006].

In contrast to a still partially compact pressure-induced unfolded state, the heat-induced unfolded state is nearly lacking any residual secondary structure and can be described in some cases as a random coil. However, for other proteins some residual structure is present [Matthews, 1993]. Here, the entropy driven unfolding is due to a transfer of the nonpolar groups from the hydrophobic core into the water [Baldwin, 1986, Hummer et al., 1998]. Thus, a different mechanism of unfolding resulting in a different unfolded state ensemble is present.

As is reflected in Fig. 4.3 proteins can also unfold at low temperatures. Often these transitions are beyond the freezing point of water. In order to access cold-induced unfolding, pressure is employed as under these conditions the freezing temperature of water is reduced [Winter et al., 2007]. Inspection of the p,T-stability diagram shows that the cold-induced denaturation similar as the pressure-induced one is volume change driven and the unfolded state is thus expected to be more compact that the heat-induced one [Smeller, 2002].

The presence of special cosolvents in a protein solution can also influence the protein stability [Timasheff, 1993]. Thus, besides pressure and temperature also changes of the chemical potential affects the protein folding. Depending on the effect on the stability two different types of additives can be defined. Kosmotropic cosolvents are those that increase the protein stability whereas chaotropic cosolutes lead to destabilization. Typically, these substances are small molecules. However, also different salts can, beyond the sole screening effect, lead to protein (de-)stabilization. The so-called Hofmeister series characterizes the influence of the different anions and cations on the protein stability [Baldwin, 1996, Curtis and Lue, 2006].

The stabilizing effect of kosmotropic molecules is due to so-called preferential exclusion. As the interaction between the cosolvent and the protein is disfavored in comparison to interaction with the surrounding water, the interaction interface will be reduced as much as possible. Therefore, the compact folded state is preferred and the kosmotrope is excluded from the protein surface. Alternatively, the mechanism is called preferential hydration as this surface is stronger hydrated. Kosmotropic cosolvents are for example sugars or polyhydric alcohols like sucrose or glycerol. In more detail, for some molecules like sugars this mechanism is independent of the chemical nature of the protein surface and a result of steric exclusion and a perturbation of the protein's surface tensions [Timasheff, 1993]. For others, like polyols, it is due to the solvophobic effect,

i.e. the interaction of these molecules with the water network leading to hydrogen bond formation, making interactions with the protein even less favorable [Timasheff, 1993].

In contrast, chaotropic molecules or denaturants destabilize proteins by preferential binding, i.e. direct interactions between these molecules are favorable. As a consequence the unfolded state offering the largest interaction interface is preferred. Common chaotropes used for protein studies are urea and guanidine hydrochloride.

Furthermore, there exist some biological relevant molecules which serve to balance cellular osmosis like trimethylamine N-oxide (TMAO) or hypotaurine in deep sea organisms like sharks [Yancey et al., 2002, Yancey, 2005]. The effect of these biological osmolytes is to protect the organisms against osmolytic stresses. For example, within these animals TMAO counteracts the destabilizing effect of urea.

Drastic changes of the pH value away from the protein's isoelectric point, i.e. the pH value where a protein has vanishing effective charge, can also lead to unfolding. As the number of surface charges increases with decreasing pH value, the Coulomb repulsion can cause so-called acid denaturation [Dill, 1990]. Similarly but with the opposite sign of the surface charges high pH values also induce unfolding. For many proteins the acid denatured state is less unfolded than the heat-induced unfolded state or those unfolded by urea or guanidine hydrochloride. Moreover, depending on the presence of ions added to the protein solution different species of unfolded state have been reported [Fink et al., 1994].

Besides these global means to influence and thus study the protein stability, changes of the amino acid sequence by mutagenesis affect the protein stability in a well located way [Alber, 1989, Matthews, 1993]. For instance, different types of amino acid substitutions as well as deletions can enhance or decrease the protein stability. A biological example of how a single mutation can lead to destabilization is the substitution of glycine by alanine in type I collagen which is the molecular origin of osteogenesis imperfecta (brittle-bone disease). Herein, this mutation disrupts the helical structure of the fiber protein leading to a destabilization of the collagen structure [Voet et al., 2006, Löffler et al., 2007]. As a rough finding, the critical amino acid whose substitution may lead to a change in stabilization are generally inaccessible to the solvent in the folded state [Alber, 1989]. Changes by mutations can affect both the folded and the unfolded states in terms of structure and stability.

To test protein stability and thus to shed light into the underlying interactions, combinations of the different means of modulation introduced in this section can be combined. For instance to achieve pressure-induced unfolding for stable proteins which would not unfold in the pressure range covered by a respective sample cell, addition of denaturants will lower the pressure of unfolding. Especially in this particular case, the destabilizing effects of pressure and cosolvents are additive [Perrett and Zhou, 2002]. However, differ-

ent ways of unfolding lead to diverse unfolded states as mentioned for heat-, cold-, and pressure-induced unfolding. This should be kept in mind, when comparing differently denatured states.

4.2 High pressure SAXS study on the influence of an internal charge on the protein stability

In living organisms proteins with ionizable residues in their interior are involved in energy transfer processes. Even though the burying of such an amino acid in a hydrophobic environment is energetically disfavored, which should result in destabilizing the folded state, nature has produced such types of proteins. Some examples of these are cytochrome c oxidase, an enzyme which has a key role in cell respiration [Yoshikawa et al., 1998], bacteriorhodopsin, which functions as a light driven ion-pump [Luecke et al., 1999], or the photoactive yellow protein, which transforms light into mechanical energy [Hendriks et al., 1999]. Furthermore, studying configurational changes induced by varying the charge state within proteins can give a better understanding of partially unfolded protein states present in the folding process. Thus, using proteins with substituted ionizable residues allows to map the folding energy landscape [Zheng and Sosnick, 2010].

Previous studies on proteins wherein different amino acids have been substituted with ionizable residues by mutagenesis have shown that for the amino acids lysine, aspartic acid, and glutamic acid present in a protein's hydrophobic interior, the respective pK_a is shifted in such a way that the residues are neutral at physiological pH [Isom et al., 2008]. The explanation of this shift has been under debate. The mechanism leading to this could be the penetration of long-lived water molecules into the hydrophobic core close to the ionizable residue as this is charged. Alternatively, local conformational changes in its vicinity could be the molecular reason for the shift in the pK_a value [Damjanovic et al., 2005, Denisov et al., 2004]. The high tolerance of proteins for ionizable residues in their interior has lead recently to the speculation that this could be a general property of stable proteins and not only of specialized ones [Isom et al., 2008, Isom et al., 2011].

These types of studies have mostly been performed on different variants of the protein staphylococcal nuclease (SNase). For some of its mutants it was shown that water penetration can be ruled out leaving conformational changes as the reason for its tolerance of ionizable residues. In order to access these structural changes globally and to get a deeper insight into the protein packing at either charge states, high pressure SAXS measurements where performed on two mutants of the protein staphylococcal nuclease. The hyperstable mutant Δ-PHS and its single residue mutant Δ-PHS/V66K, wherein an ionizable residue has been inserted into the hydrophobic core, have been investigated. In the present section the results of this SAXS study will be presented.

The whole study on the two SNase mutants has been performed within a collaboration of the groups of Prof. M. Tolan (TU Dortmund), Prof. R. Winter (TU Dortmund),

Prof. C.A. Royer (Univerisité de Montpellier), Prof. B. Garcia-Moreno (The Johns Hopkins University), and Prof. K. Akasaka (Kinki University). The presented results were already published as: R. Kitahara, K. Hata, A. Maeno, K. Akasaka, M. Chimenti, B. Garcia-Moreno E., M.A. Schroer, C. Jeworrek, M. Tolan, R. Winter, J. Roche, C. Roumestand, K. Montet de Guillen, C.A. Royer (2011). Structural plasticity of staphylococcal nuclease probed by perturbation with pressure and pH. *Proteins: Structure, Function and Bioinformatics* 79:1293-1305.

The outline of this section is as follows. At first, the protein SNase and the mutants used will be described. Thereafter, the results of the SAXS measurements at different pH values and pressures will be discussed in detail. This section ends with a comparison of this data with the results of NMR experiments performed by the collaborating groups and a summary.

4.2.1 Staphylococcal nuclease and its mutants

Herein, the protein staphylococcal nuclease and its mutants will be described shortly. Parts of this presentation are oriented on [Schroer, 2008].

The protein staphylococcal nuclease (SNase) consists of 149 amino acids and has a molecular weight M_w of 16809 Da. It has no disulfide bonds resulting in a low thermodynamic stability. Furthermore, it has a single tryptophan residue at position 140. Its isoelectric point is at pI = (9,62 ± 0,03) [Heins et al., 1967]. This extracellularly enzyme of the bacteria *Staphylococcus Aureus* is a Ca^{2+}-dependent 5'-phosphodiesterase catalyzing the hydrolytic cleavage of DNA as well as RNA. It has both exo- and endonuclease activity [Tucker et al., 1978, Cotton et al., 1979], meaning that the nucleic acids are removed from a terminal side as well as cleaved within the polynucleotide [Voet et al., 2006]. There are two bacteria strains, the V8 and the Foggi strain, from which it can be derived. The Foggi strain variant of *S. Aureus* which differs from the V8 variant only at position 124 is used mostly. The three-dimensional structure of the protein is depicted in Fig. 4.5a). The most relevant structures are the three α helices and five β strands forming a β barrel [Hynes and Fox, 1991]. The hydrophobic core of SNase is made out of this β barrel and two helices. The complete crystallographic data reveals that SNase contains 26.2 % helices, 24.8 % β sheets in form of the barrel, 7.4 % extented chains, 24.8 % turns and loops, 8.7 % unordered chains, and 8.1 % is uncertain [Panick et al., 1998]. In the native folded state a radius of gyration R_g between 16.3 to 17.1 Å has been reported [Panick et al., 1998, Paliwal et al., 2004].

SNase has served as a model protein for exploring the phase diagram as it unfolds at a moderately accessible pressure of 2 kbar at ambient temperatures [Panick et al., 1998]. The pressure-induced unfolding is completed at a pressure of 3 kbar. Its pressure-

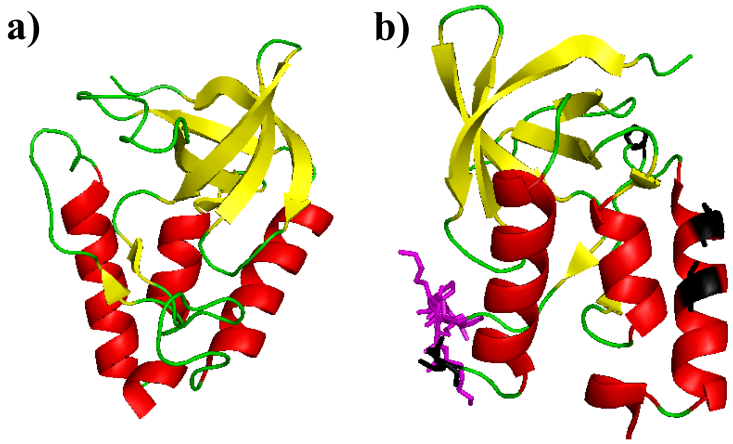

Figure 4.5: *a) Ribbon diagram of staphylococcal nuclease (SNase) (pdb file [RCSB Protein Data Bank, 2000] 1EY0 [Chen et al., 2000]) drawn with PyMOL [Schrödinger, LLC, 2008]. The β strains are shown in yellow, the α helices in red, and loose parts in green. The five β strains forming a β barrel and the two α helices on the right side form the protein's hydrophobic core. b) Structure of wild type SNase to visualize the deviations from the Δ-PHS variant. The amino acids that have been removed (purple) and changed (black) in the hyperstable variant are presented as sticks.*

temperature free-energy landscape was fully obtained [Panick et al., 1999] [Lassalle et al., 2000, Ravindra and Winter, 2003], reflecting its justified description as a two-state folder. Heat-induced unfolding sets in at 45 °C and is completed at about 55 °C with a melting temperature T_m of 53 °C [Panick et al., 1998, Byrne and Stites, 2007]. The pressure-induced unfolded state has a radius of gyration, R_g, of about (36 ± 1) Å which is similar to that of the chemically denaturated one (R_g = (37.2 ± 1.2) Å in 8 M guanidine hydrochloride [Kohn et al., 2004]) but smaller than the heat-induced unfolded one (R_g = (45 ± 2) Å [Panick et al., 1998]). The latter having only very little secondary structure elements resembles a random coil. SNase is native within the pH range of 5.0 to 8.0 [Uversky et al., 1998a]. The acid-induced unfolded state of SNase is not completely unfolded but has residual structure [Carra et al., 1994]. For refolding of this state by addition of salts, three different partially folded intermediates have been reported whose formation depends on the type of anion used [Uversky et al., 1998a].

As the presence of an internal ionizable amino acids leads to a destabilization of a protein, instead of the wild type (WT) form of SNase its hyperstable version called Δ-PHS has been used as the reference protein. Within this a single residue has been replaced by mutagenesis. To achieve stability, the residues 44-49 of WT SNase have been deleted and the following substitutions have been performed in the nuclease gene: G50F, V51N, P117G, H124L, and S128A [Garcia-Moreno et al., 1997]. This notation means, that e.g. the glycine (G) residue at position 50 has been exchanged by phenylalanine (F). The one-letter code of the amino acids has been given in the list of amino acids in

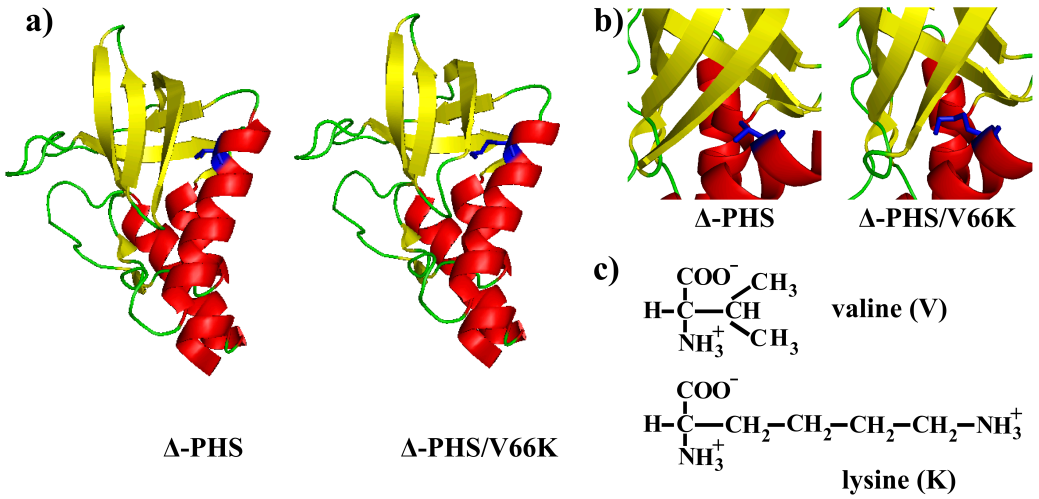

Figure 4.6: *a) Ribbon diagram of SNase variants Δ-PHS (pdb file 3BDC [Castaneda et al., 2009]) and Δ-PHS/V66K (pdb file 3HZX [Karp et al., 2010]) drawn by PyMOL [Schrödinger, LLC, 2008]. The residue at position 66 of Δ-PHS and Δ-PHS/V66K, valine and lysine, respectively, located in the hydrophobic core is shown in blue in the stick representation. b) Enlargement of the hydrophobic pocket wherein the residue 66 is buried. c) Covalent structure of valine and lysine.*

paragraph 4.1.1. The residues that are different in Δ-PHS from WT SNase have been marked in Fig. 4.5b) in the wild type structure.

In this hyperstable variant the valine residue 66 has been substituted by lysine. This internal lysine group is fully buried in the hydrophobic core of the Δ-PHS/V66K variant at neutral pH values as has been determined by crystallographic data [Isom et al., 2008]. No water molecule has been found in the vicinity of this lysine side chain either at cryo or room temperature [Schlessman et al., 2008]. Crystals of the Δ-PHS/V66K variant at a lower pH value of 4.7 can not be grown. However, crystallization can be achieved for the PHS/V66K variant, wherein only the three substitutions P117G, H124L, and S128A have been made. For the so obtained crystal at a low pH value, the backbone is unaffected but the residue is disordered [Karp et al., 2010]. In Fig. 4.7a) the structure of both variants, Δ-PHS and Δ-PHS/V66K, are shown. The amino acid substituted between these variants is depicted blue. This can be seen in more detail in the corresponding enlargement (Fig. 4.7b)). The chemical formula of valine and lysine are shown as well (Fig. 4.7c)).

4.2.2 Results of the high pressure SAXS study

Small angle X-ray scattering measurements under high pressures were performed on the two SNase mutants at two different pH values to study the influence of internal charges on the protein stability. The pH values were chosen such that the Lys-66 residue in

Δ-PHS/V66K was either charged or uncharged. The Δ-PHS background protein was measured as a reference as the Val-66 residue is not ionizable.

The high pressure SAXS measurements were performed at BL9, DELTA, and BW4, HASYLAB. The different parameters of the experimental setups are summarized in Table 4.1. Using the high pressure equipment described in section 3.3 the pressure range from 1 bar to 3 kbar has been covered in steps of 1 kbar at ambient temperature (T = 20 °C). The pressure value in the sample cell was kept constant for the whole pressure range. For higher pressures, changes of about 0.1 kbar were present within the exposure time. Protein concentrations c_P of 3.5 - 5.0 mg/ml were used to simultaneously obtain a significant scattering intensity and avoid an appearance of the structure factor in the SAXS signal.

The pK_a value of the Lys-66 residue in this variant was found to be at a pH value of 5.7 [Garcia-Moreno et al., 1997]. This value is much smaller than that of the pure amino acid in water. As lysine is an amino acid with a basic side chain, at pH values below the pK_a it is positively charged and above uncharged. Therefore, the measurements were performed at pH values of pH 4 and pH 6 for Δ-PHS/V66K, and pH 4 and pH 7 for Δ-PHS.

In order to keep the pH value constant, a buffer solution is usually used for protein studies. Different buffer salts exist which have different characteristic ranges where these are working properly. When applying high pressures to a solution, care has to be taken in the choice of the buffer salts, as most buffers do not keep the solution's pH fixed under these conditions. Therefore, special buffer substances are used. The common high pressure buffers are bis-Tris (bis(2-hydroxyethyl)iminotris(hydroxymethyl)methane, pK_a = 6.5, pH range: 5.8 - 7.2) and Tris (tris(hydroxymethyl)aminomethane, pK_a = 8.1, pH range: 7.0 - 9.1) [Lide, 2003]. In usual buffers the (de-)protonation leads to a change in the number of formal charges, e.g. for a phosphate buffer it is: $HP0_4^{2-} + H_2O \rightleftharpoons PO_4^{3-} + H_3O^+$. In contrast, the number of formal charges is kept constant in bis-Tris and Tris, i.e. $TrisH^+ + H_2O \rightleftharpoons Tris + H_3O^+$ [Neuman et al., 1973]. As electrostriction reduces the total volume, application of pressure results in an increase of formal charges and thus shifts the equilibrium, resulting in a pH change for the first example. Since there is no change of the charge for bis-Tris and Tris in the (de-)protonation process, pressure does not have an influence on the pH value for these buffers.

Therefore, a 25 mM Tris buffer was used for pH values of 6 - 7. As this buffer solution does not keep the pH value constant at pH 4.5, a 15 mM sodium acetate buffer was used instead. All buffers were adjusted using concentrated hydrochloric acid.

Changing the pressure also influences the un- and refolding kinetics of proteins. As has been shown by pressure jump studies on wild type (WT) SNase whose folding

	BL9, DELTA	BW4, HASYLAB
detector	MAR345 image plate	Pilatus 300K
number of pixels	2400 x 2400	487 x 619
wavelength λ / Å	1.239	1.3808
exposure time / s	1800	1200
q-range /nm^{-1}	0.3 - 3.5	0.2 - 2.8

Table 4.1: *Synopsis of the different parameters of the SAXS measurements at the two beamlines. Given are the type of area detector, the number of its pixels, the wavelength λ, the typical exposure time, and the accessible q-range.*

can be described by a single exponential relaxation profile, an increase of pressure is accompanied by an increase of the relaxation time for unfolding [Panick et al., 1998, Panick et al., 1999, Woenckhaus et al., 2001]. For instance, completely unfolding is observed after a time of 1 h with a corresponding relaxation time of 14 min for a positive jump from 1.5 kbar to 3.0 kbar [Woenckhaus et al., 2001]. In contrast, a negative jump from 4 kbar to 1 bar is much faster with a relaxation time of 4.5 s. Therefore, care has also to be taken for performing experiments under static pressure conditions when increasing the pressure. The waiting time between the pressure increase and the beginning of exposure has to be properly chosen. The unfolding process should be already largely completed as the detected SAXS intensity would change with time otherwise. As the scattering intensity is accumulated in the detector over the exposure time, a change of the protein structure would result in a SAXS curve being the integral of all form factors present within that time. Such a curve can hardly be analyzed. As the major changes of the relaxation process occur within the relaxation time, the waiting time should be at least longer than this. However, it should be short enough to perform experiments within feasible time. Notable, for SNase Δ-PHS mutants with an ionizable residue at position 66, like Δ-PHS/V66K studied in this thesis, it was shown that an increase in pressure results in a decrease of the relaxation time [Brun et al., 2006]. Therefore, the corresponding scan was started 20 min after a pressure increase.

The experimentally obtained SAXS curves for both proteins at the two respective pH values are depicted in Fig. 4.7 for different pressures. Using the program GNOM the azimuthally averaged and background corrected scattering data points were fitted to obtain the corresponding radial pair-distance distribution function $p(r)$. This approach however does only work if the protein has a globular shape, i.e. it is not unfolded. In Fig. 4.7, these refinements are shown as solid lines for those data, where a globular protein is present. The scattering curves are shifted for clarity. Nevertheless, as the density of water becomes larger under high pressure conditions, the contrast between protein and solvent is reduced which results in a decrease of scattering intensity and an

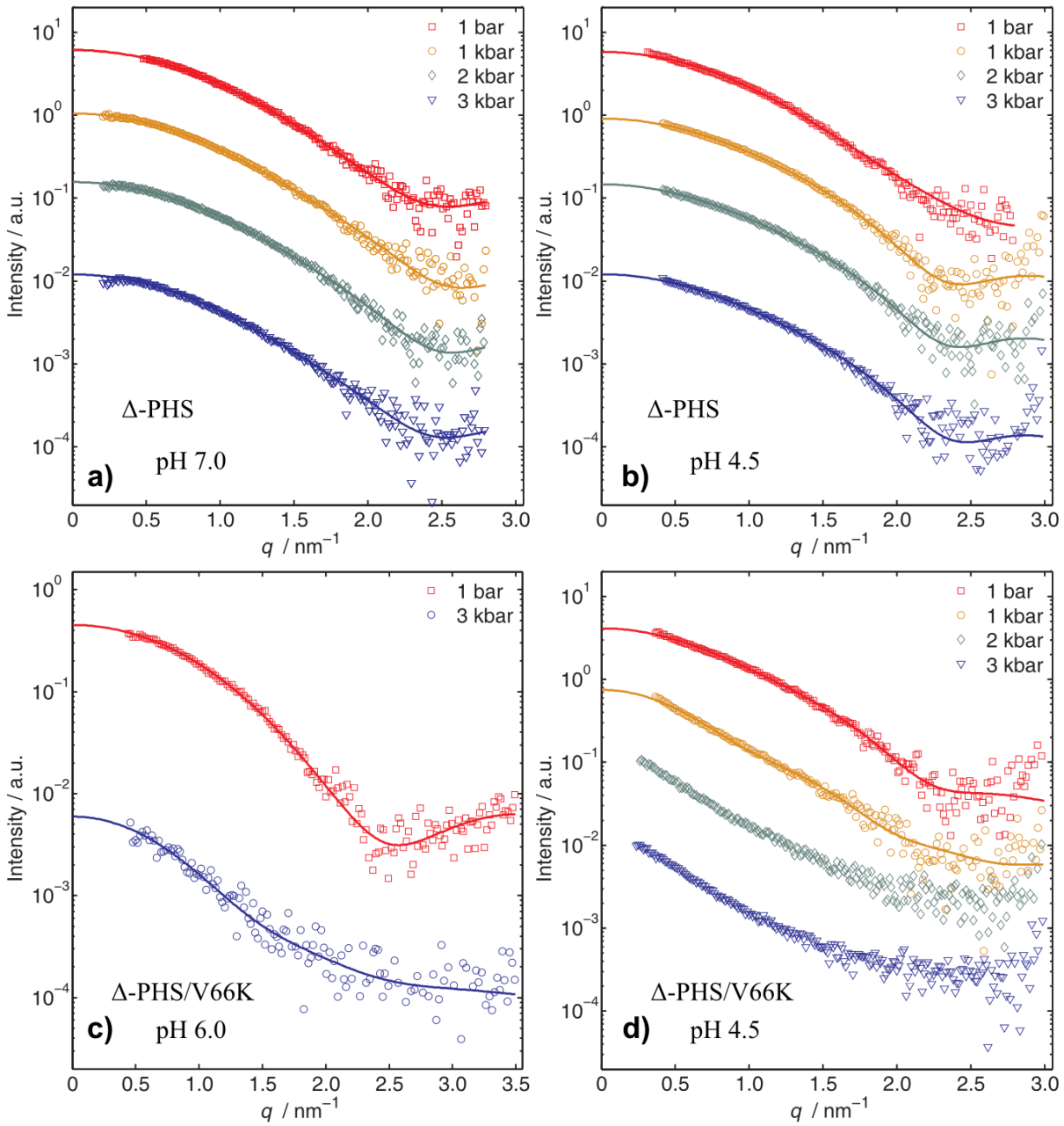

Figure 4.7: *SAXS curves for the SNase mutants at different pH values as a function of pressure. a) Δ-PHS at pH 7.0. b) Δ-PHS at pH 4.5. c) Δ-PHS/V66K at pH 6.0. d) Δ-PHS/V66K at pH 4.5. Experimental data points are shown as symbols, solid lines are the corresponding refinements. Note the different q-range for c) as the data were obtained at another experimental endstation. It was averaged over 4 data points.*

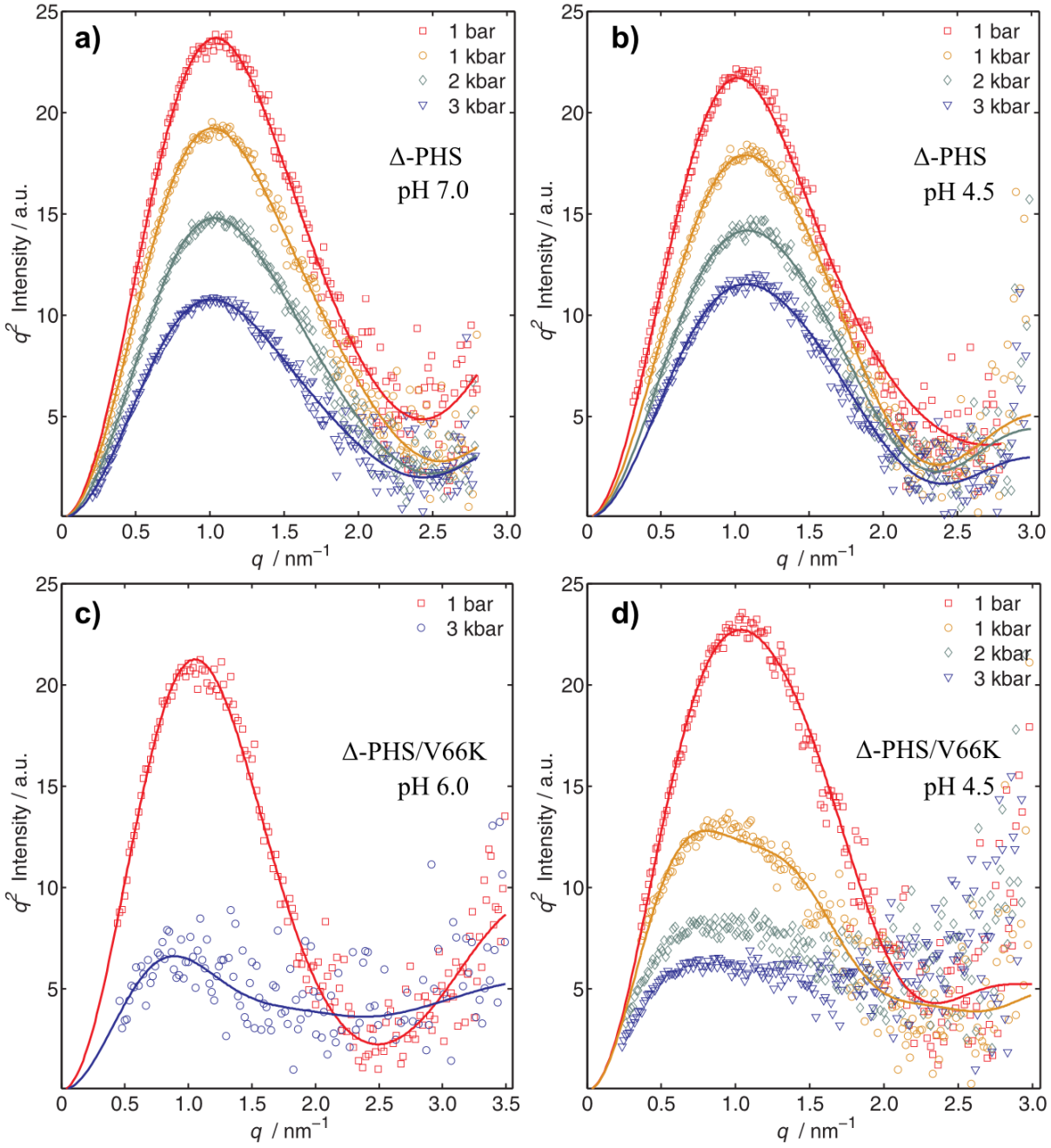

Figure 4.8: *Kratky plot (q vs. $q^2I(q)$) of the SNase mutants at different pH values as a function of pressure. a) Δ-PHS at pH 7.0. b) Δ-PHS at pH 4.5. c) Δ-PHS/V66K at pH 6.0. d) Δ-PHS/V66K at pH 4.5. Note the different q-range for c). It was averaged over 4 data points.*

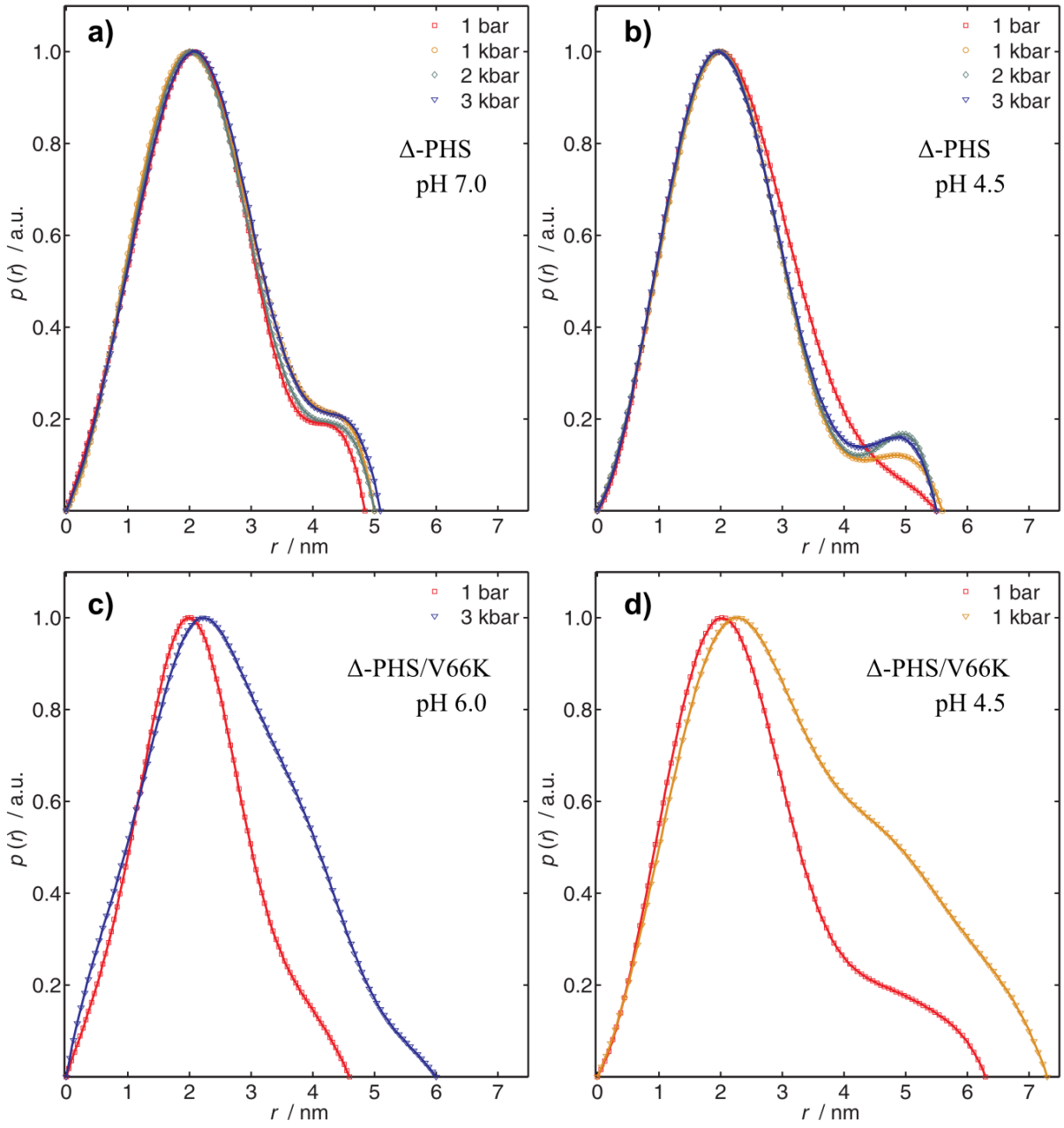

Figure 4.9: *Radial pair-distance distribution function p(r) of the SNase mutants at different pH values as a function of pressure. a) Δ-PHS at pH 7.0. b) Δ-PHS at pH 4.5. c) Δ-PHS/V66K at pH 6.0. d) Δ-PHS/V66K at pH 4.5.*

Variant	Experimental condition	R_g / Å
Δ-PHS	1 bar, pH 7.0	16.9 ± 0.5
Δ-PHS	3 kbar, pH 7.0	17.9 ± 0.4
Δ-PHS	1 bar, pH 7.0 + 2.0 M GuHCl	16.7 ± 0.3
Δ-PHS	3 kbar, pH 7.0 + 2.0 M GuHCl	29.7 ± 2.0
Δ-PHS	1 bar, pH 4.5	17.6 ± 0.8
Δ-PHS	3 kbar, pH 4.5	17.5 ± 0.8
Δ-PHS/V66K	1 bar, pH 6.0	16.2 ± 0.4
Δ-PHS/V66K	3 kbar, pH 6.0	19.7 ± 0.2
Δ-PHS/V66K	1 bar, pH 4.5	18.0 ± 0.5
Δ-PHS/V66K	3 kbar, pH 4.5	30.2 ± 2.0

Table 4.2: *Values of the radius of gyration, R_g, for the SNase variants at different solution conditions for 1 bar and 3 kbar.*

accompanied decline of the signal-to-noise ratio.

The Δ-PHS variant is folded at all pressures at pH 7.0 (Fig. 4.7a)) and pH 4.5 (Fig. 4.7b)). This can be seen in more detail when plotting the SAXS data in the Kratky representation (q vs. $q^2I(q)$, Fig. 4.8). Herein, a pronounced maximum is present that keeps its position constant as the pressure is raised. The globular, folded shape present under all conditions can be seen on the corresponding $p(r)$ curves (Fig. 4.9). Therein, the position of the maximum, which is at r = (20.0 ± 1.0) Å, does neither change with pH nor with pressure. For pH 7.0 also there is no change of the curves' shapes. Decreasing it from pH 7.0 to 4.5 results in a slight increase in the protein's size as is reflected from the value of the maximum extension D_{max} from (48.5 ± 1.0) Å to (55.0 ± 1.0) Å. At this pH value the changes in shape of the curves as pressure rises is not significant as to attribute it to structural changes.

These findings are in accord with the values of the radii of gyration, R_g (table 4.2), obtained by the Guinier approximation for small q (eq. (2.55)). Therein, the R_g values at 1 bar and 3 kbar for all solution conditions studied are summarized. At ambient pressures changing pH does not change the radius of gyration within the experimental error. The obtained values of R_g = (16.9 ± 0.5) Å at pH 7.0 and R_g = (17.6 ± 0.8) Å at pH 4.5 are similar to that of WT SNase at pH 5.5 (R_g between 16.3 to 17.1 Å [Panick et al., 1998, Paliwal et al., 2004]) as is the D_{max} value for the hyperstable variant at pH 7.0. Thus, the absence of amino acids in Δ-PHS due to mutagenesis compared to the wild type protein does not have a detectable effect on the SAXS curve for the protein in solution. Similar values were found for two other Δ-PHS variants, Δ-PHS/V66A and Δ-PHS/V66Y, wherein the Val-66 has been replaced by alanine and tyrosine, respectively [Schroer et al., 2010]. Increasing pressure does not change significantly the radius of gyration. The slight increase in R_g for pH 7.0 at 3 kbar might reflect some

local changes but is far to small to be attributed to any type of unfolding. At pH 4.5 even no effect is present.

This SAXS data on the Δ-PHS background variant confirms its stability over the whole pH range studied. A decrease of the pH to pH 4.5 results in a slight increase of size. Any further change present in Δ-PHS/V66K thus can be attributed to the presence of the ionizable residue Lys-66 and on its properties and interactions.

At ambient pressures Δ-PHS/V66K is folded both at pH 6.0 at which the Lys-66 residue is uncharged as well as in the charged state at pH 4.5 as can be seen from the scattering curves (Fig. 4.7c,d)) and the corresponding Kratky plots (Fig. 4.8c,d). The radial pair-distance distribution function, $p(r)$, for the uncharged state has a similar shape as that of the background variant at pH 7.0. Only a slightly smaller $D_{\max}$ value of (46.0 ± 1.0) Å is present which is in accord with a smaller R_g = (16.2 ± 0.4) Å (table 4.2). In the uncharged state the Lys-66 residue was reported to be located in the hydrophobic core both for the crystal and the solution structure [Schlessman et al., 2008, Takayama et al., 2008]. This is consistent with these SAXS results.

Changing the pH value to pH 4.5 at which the lysine at position 66 is charged, both the radius of gyration and $D_{\max}$ increase as the protein becomes more extended. Furthermore, the corresponding $p(r)$ curve is much broader still having its maximum at r = (20.0 ± 1.0) Å. The observed increase can be related to some extent to a slight increase in size observed already for the background protein at lower pH values. However, the differences in the pair-distribution functions between Δ-PHS and its V66K variant are only attributed to the charged lysine residue. Thus, this SAXS data at ambient pressure indicates the presence of two conformational structures of the protein Δ-PHS/V66K due to the two different charge states. As the amino acid forms a part of a helix with the location of the side chain inside the hydrophobic core the different structures should be attributed to local changes of the protein conformation. This assumption is confirmed by results of NMR spectroscopy on Δ-PHS/V66K and ab initio modeling of the SAXS data presented here [Kitahara et al., 2011]. Previous experimental [Karp et al., 2010, Chimenti et al., 2011] and molecular simulation studies [Damjanovic et al., 2005, Damjanovic et al., 2007, Damjanovic et al., 2008] also reported on small structural changes on ionization of the side chain.

A similar result for the radius of gyration was also found for Δ-PHS/V66R, wherein arginine is present at position 66, which also has a basic side chain [Schroer et al., 2010]. At ambient conditions, its radius of gyration is R_g = (18.9 ± 0.5) Å which is even a little bit larger than the radius of gyration of the Lys-66 variant at pH 4.5 (R_g = (18.0 ± 0.5) Å). The presence of arginine at a position next to the hydrophobic core destabilizes the protein dramatically and leads to structural reorientation in the neighborhood of

this residue [Damjanovic et al., 2008, Schroer et al., 2010]. Therefore and in contrast to Δ-PHS/V66K the pK_a of this residue is not shifted but has a similar value as the free amino acid [Damjanovic et al., 2008].

To test the pressure stability and thus the protein plasticity depending on the two different charged states, Δ-PHS/V66K was also studied under high pressure by SAXS for both pH values. With this approach differences in the packing structure of Δ-PHS and its Lys-66 variant due to the substitution as well as by the different degree of hydration of the lysine residue are accessible as different types of packing are differently pressure susceptible.

For the uncharged state at pH 6.0 the scattering has only been determined at 3 kbar. The SAXS profile (Fig. 4.7c)) differs from that at ambient pressures indicating structural changes. However, this unfolded state still possesses some compactness as can be seen from its Kratky plot (Fig. 4.8c)) wherein a small maximum shifted to a lower q-value is present. The corresponding $p(r)$ curve calculated using GNOM is depicted in Fig. 4.9c). This unfolded state which has been also observed by fluorescence spectroscopy measurements at similar conditions [Brun et al., 2006] is characterized by a radius of gyration of $R_g = (19.7 \pm 0.2)$ Å which is much smaller than that of the pressure-induced unfolded state of WT SNase ($R_g = (36 \pm 1)$ Å [Panick et al., 1998]). Thus, even though the insertion of lysine into the hydrophobic core decreases the conformational stability of hyperstable Δ-PHS, the V66K variant can be described as a condensed chain.

When the Lys-66 residue is charged at pH 4.5, pressure-induced unfolding already sets in at 1 kbar and is completed at 2 kbar (Fig. 4.7d)). The corresponding Kratky plots show a broad maximum shifted to smaller q-values at $p = 1$ kbar (Fig. 4.8d)). The pair-distance distribution function still can be obtained, but is much broader than at ambient pressures with a maximum extent $D_{max} = (73.0 \pm 3.0)$ Å (Fig. 4.9d)). Furthermore, the position of the maximum of $p(r)$ is at larger r. For higher pressures, a plateau is present in Kratky plot indicating unfolding. Thus, the $p(r)$ curve can not be obtained from the data within the given q-range. The radii of gyration of the unfolded state (table 4.2) are similar to that of pressure-induced WT SNase and thus much larger than at pH 6.0. This means that due the different charged states within Δ-PHS/V66K, different pressure-induced unfolded states are existing. Whereas the unfolded state at pH 6.0 possesses a certain degree of compactness, at pH 4.5 the protein is in a typical pressure-unfolded state. Noteworthy however, this state still can not be described as a random coil.

Summarizing the results of the SAXS study described above, the radii of gyration of the different species studied are compared in Fig. 4.10. Fig. 4.10a) shows a Guinier

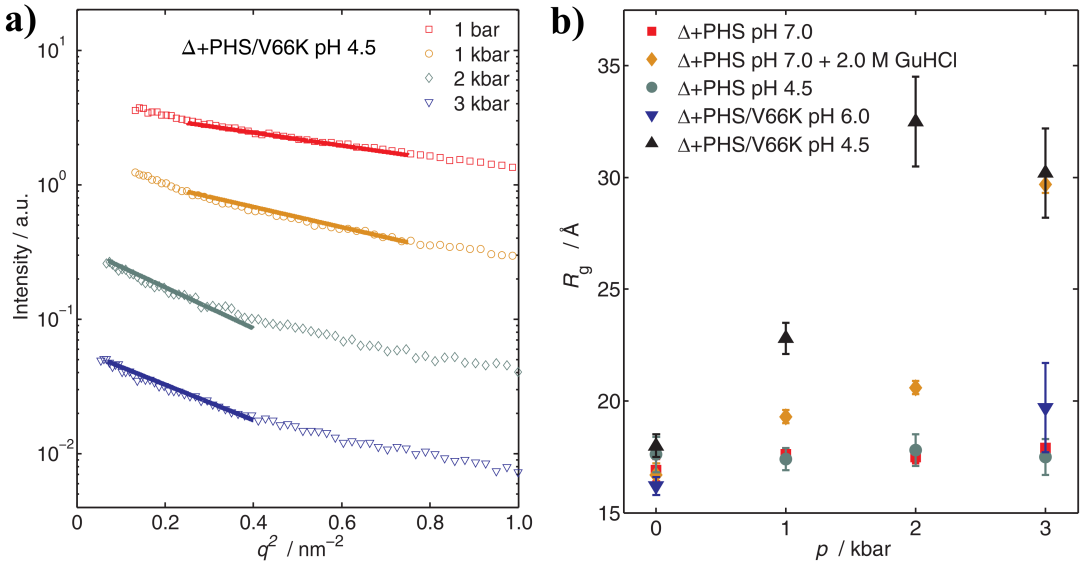

Figure 4.10: *a) Guinier plot of Δ-PHS/V66K at pH 4.5 as a function of pressure. Symbols are the experimental data, solid lines the corresponding refinement. b) Radius of gyration, R_g, as a function of pressure, p, for the SNase variants at different solution conditions.*

plot of the scattering data of Δ-PHS/V66K obtained at different pressures as herein the largest changes are present. The solid lines are the refinements plotted in the q-range used for fitting. Fig. 4.10b) shows the different R_g plotted as function of pressure. Additionally, in order to induce unfolding of the hyperstable variant at high pressures at pH 7.0, 2.0 M guanidine hydrochloride (GuHCl, CH_5N_3·HCl) was added to the protein solution for destabilization. Under these conditions unfolding sets in already at 1 kbar. At 3 kbar, the highest pressure measured at within the present study, a R_g-value of (29.7 ± 2.0) Å is obtained. As this value is comparable to that of the pressure-induced unfolded states of WT SNase as well as of Δ-PHS/V66K at pH 4.5 it seems that the unfolding process is completed at 3 kbar. This is in accord with previous fluorescence spectroscopy measurements performed at similar conditions [Brun et al., 2006]. The SAXS results on Δ-PHS in 2.0 M guanidine hydrochloride solution are also given in table 4.2 and Fig. 4.10b). Fig. 4.10b) reflects that at ambient pressures there are slight structural differences for Δ-PHS and Δ-PHS/V66K at the two different pH values studied. These are more pronounced for the Lys-66 variant and can be attributed to changes induced by the charged state of the residue in the region of the helix wherein it is located. With increasing pressure, unfolded states at $p = 3$ kbar are present for Δ-PHS at pH 7.0 with 2.0 M GuHCl added, Δ-PHS/V66K at pH 4.5, and Δ-PHS at pH 6.0. Whereas the first two variants have a R_g common for pressure-induced unfolded states of SNase, the latter is characterized by a greater compactness. No unfolding was detected for the hyperstable variant in pure buffer.

4.2.3 Discussion and Conclusion

The previously discussed SAXS measurements have been performed within a collaboration of different groups introduced at the beginning of the present section. In framework of this, nuclear magnetic resonance (NMR) spectroscopy measurements were conducted at ambient and high pressure at both proteins Δ-PHS and Δ-PHS/V66K at similar solution conditions. The experimental details of these measurements as well as the data analysis can be found in the corresponding publication (see [Kitahara et al., 2011]). Here, only the general results of these will be given and discussed in comparison to the aforementioned SAXS data.

Previous NMR studies on the hydrogen exchange behavior of the Lys-66 variant at ambient pressure already showed that at pH 7.0 the thermodynamic stability is reduced due to the substitution of the residue [Takayama et al., 2008, Chimenti et al., 2011]. In the charged state, the region close to the residue is influenced leading to an increase of local structural fluctuations [Chimenti et al., 2011]. These findings are supported by the recent results.

At ambient pressure, accompanied to the ionization of the lysine residue, conformational exchanges have been detected, particularly in the β barrel, for timescale longer than milliseconds. The dynamics of both charge states were also probed. There was no effective influence of the insertion of the lysine residue and its ionization on the dynamics in the picosecond to nanosecond compared to the background variant. Furthermore, for Δ-PHS at pH 6.5 and 4.5 no conformational exchange was detected on a microsecond to millisecond timescale reflecting it stability. A similar finding was found for Δ-PHS/V66K at pH 6.0. In contrast, for the ionized state conformation exchange at that timescale was detected for residues in the β barrel and in the helix wherein the Lys-66 residue is located. In these two parts of the protein those residues are located that lead to its drastic destabilization compared to the background variant.

Increasing the pressure up to 2 kbar, structural changes of the reference protein obtained by NMR spectra at pH 6.3 are small which is in accord with the SAXS results. Similar changes also were recorded for Δ-PHS/V66K except for the helix and barrel regions which are attributed to pressure-induced conformational fluctuations on the sub-microsecond timescale.

At pressures of 3 kbar at pH 6.3 changes in the corresponding NMR spectra reflect unfolding of the whole protein. Similar findings have been reported for fluorescence spectroscopy studies [Brun et al., 2006]. The unfolding process takes place on a timescale larger than milliseconds.

The SAXS results give insight into the static global shape of the different folding states present and the NMR data into the dynamics of the local protein structure. In

combination, both techniques allow to access the different structural and dynamical consequences of burying the ionizable residue Lys-66 into the hydrophobic core of the hyperstable Δ-PHS. At either of the two pH values or pressures studied, no significant differences were detected for Δ-PHS by both techniques. Only the addition of 2.0 M GuHCl leads to pressure-induced unfolding.

Thus, for Δ-PHS/V66K at ambient pressure structural changes between the two charge states can be fully attributed to the Lys-66 residue. In the uncharged state, there are only small differences to the background protein present in the SAXS data. This is in accord with the corresponding crystal structures of both SNase variants showing no significant changes upon exchange of residue 66 [Karp et al., 2010]. At pH 4.5, the protein is more extended as the lysine is charged. Accompanied to this is a change in the conformational exchange in the β barrel and the helix, i.e. in regions close of the residue. Thus, a conformational change is trigged by the ionization of Lys-66. Previous computer simulation and experimental studies are in agreement with these findings [Damjanovic et al., 2008, Chimenti et al., 2011]. Furthermore, the burying of lysine instead of valine at position 66 and especially its ionization leads to destabilization. To get insight into how the substitution of valine by the larger amino acid lysine changes the protein packing and thus the volumetric properties and how the protein plasticity depends on the charge state of the residue, the effect of high pressures on the protein in solution was studied. For pressures up to 2 kbar, only changes in the region close to Lys-66 are present which is also affected by ionization of lysine at ambient conditions. The size of the side chain of valine in protein interiors is 73.3 Å^3, that of the lysine side chain is 106.2 Å^3 [Harpaz et al., 1994]. Thus, the Lys-66 variant should be less pressure sensitive as the packing inside the hydrophobic should be denser. The hydration of this lysine residue however leads to an even larger volume decrease. Therefore, a possible transition in a more open, hydrated state might give rise to the pressure-induced changes observed by NMR. Notable, the β barrel and the helix are affected either by low pH values as well as high pressures.

Pressure-induced unfolding for the neutral state is completed at 3 kbar as is reflected by the NMR data. The pressure-induced unfolded state at pH 6.0, however, possesses a high degree of compactness as its radius of gyration is much smaller than that of WT SNase under similar conditions. This residual compactness might be attributed to stabilizing interactions in the hydrophobic core present in the hyperstable background variant Δ-PHS but not in the wild type protein [Kitahara et al., 2011]. In contrast, in the charged state of Δ-PHS/V66K pressure unfolding sets in already at 1 kbar and is finished at 2 kbar with a pressure-induced unfolded state that is similar to that of the wild type protein as well as to that of Δ-PHS with a denaturant added.

In the presented SAXS study on the SNase mutants Δ-PHS and Δ-PHS/V66K it is shown how a combined approach of the two different types of perturbations (pH and pressure) helps to shed light into the consequences of burying an ionizable residue into a protein's hydrophobic core. Depending on its charge state different structural changes are present influencing its stability significantly. By comparing the Lys-66 mutant with the background protein these findings can be attributed solely to the lysine residue and its interactions with the other residues as well as with the surrounding solvent. For Δ-PHS/V66K different folded and unfolded states were detectable by small angle scattering that, depending on the solution pH, were distinguished by their degree of compactness. In combination with site-specific structural and dynamical information detected by NMR spectroscopy, those regions that are strongly influenced by pH and pressure were localized given rise to global structure obtained by SAXS [Kitahara et al., 2011]. Thus, subtle changes within the protein structure lead to its high tolerance against insertion of ionizable residues like they are present in biologically relevant proteins. And also subtle variations of the solution condition like herein the change of pH drastically influence the thermodynamics of these types of proteins.

4.3 Electrostatic effects on the structure of a natively unfolded protein

In order to get a full understanding of protein folding a detailed knowledge not only of the folded state is mandatory but also of the structure and interactions present in the unfolded state ensemble. The relevance of residual structure of this ensemble as well as of its degree of compactness for the folding process are still open questions that need to be answered [Sosnick and Barrick, 2011]. To study the structural properties of the unfolded state ensemble of a protein, in general high amounts of destabilizing cosolvents like urea or guanidine hydrochloride are added. These induce unfolding of the protein but also affect the denatured state as well. Instead of this, it would be more preferable to investigate the unfolded state in pure buffer solution without additives. There exists a class of proteins known as natively unfolded or intrinsically disordered which are unfolded under native conditions. These are promising models for studying some general aspects of flexible, dynamical protein states.

Natively unfolded proteins can be distinguished from natively folded ones by having a less complex amino acid sequence. They consist to a large part of so-called disorder-promoting residues, which are polar and charged amino acids, and lack order-promoting residues, i.e. bulky hydrophobic ones [Dyson and Wright, 2005, Uversky, 2009]. As a consequence, natively unfolded proteins possess a low degree of mean hydrophobicity and a high mean net charge [Uversky et al., 2000, Uversky, 2002]. There are roughly three different subclasses of these types of proteins, the so-called collapsed intrinsically disordered proteins, intrinsic premolten globes, and intrinsic coils which differ in their degree of compactness and residual structure [Uversky, 2002, Uversky, 2009]. The last two ones are also known as extended intrinsically disordered proteins. General features of this class of proteins and special examples can be found e.g. in [Dyson and Wright, 2005, Uversky, 2009]. One finding is that binding of special ligands induces a disorder-to-order transition of some natively unfolded proteins into a folded state. This complex formed is characterized by a high specificity but relative low affinity [Dyson and Wright, 2005]. Dissociation of the protein-ligand complex results in unfolding of the protein again. As unfolded polypeptides are cleavaged by so-called proteases within organisms, the function of these proteins is highly controllable. Thus, in living cells intrinsically disordered proteins are involved in different signaling and regulatory processes.

As in this type of highly destabilized proteins Coulomb interactions play a major role, variation of the solution's ionic strength by changing the solution pH value as well as the addition of salts will cause structural changes. Thus, probing the protein compactness by means of SAXS as a function of pH will shed light into structural features of the unfolded protein state.

A model substance for an unfolded protein state is the T62P variant of staphylococcal nuclease which is already unfolded due to a single point mutation at ambient solution conditions. SNase itself has a high isoelectric point and a relatively low intrinsic hydrophobicity giving rise to its low thermodynamic stability. It thus falls in between the two classes of natively unfolded and stable proteins [Nishimura et al., 2001].

In a previous simulation study the influence of electrostatic interactions on the unfolded state of SNase has been investigated for different models of the unfolded state ensemble [Fitzkee and Garcia-Moreno E., 2008]. These results were compared to H^+-titration curves of the T62P variant. This theoretical study showed that Coulomb interactions play an important role for the unfolded state, especially for pH values far away from the isoelectric point leading to a further increase of the already large expansion of the protein. In order to compare these findings with experimental data, SAXS measurements have been performed.

In more detail, in the present study, the influence of the solution's pH value on the three-dimensional protein structure of the intrinsically disordered SNase mutant T62P was investigated and compared to the wild type protein. In addition, the influence of the amount of salt on the pH dependence was monitored. This study has been part of a collaboration between the groups of Prof. M. Tolan (TU Dortmund), Prof. R. Winter (TU Dortmund), and Prof. B. Garcia-Moreno (The Johns Hopkins University).

The outline of this section is as follows. At first, after a short description of the SNase mutant and the experimental parameters, the effect of the pH value on the structure of the protein T62P at a fixed salt concentration will be discussed. This will be compared to the influence on the wild type protein WT SNase. Thereafter, SAXS data of the proteins at two other salt concentrations will be presented to explore in more detail the influence of the ionic strength. The section ends with a summary and discussion.

4.3.1 pH dependence of the protein compactness

The proteins studied are the wild type of staphylococcal nuclease (WT SNase) which has been described in section 4.2.1 and its T62P mutant. Due to the substitution of threonine which is located at position 62 in a helix by proline this SNase variant is highly destabilized [Baskakov and Bolen, 1998a]. Fig. 4.11 shows an enlargement of the structure of WT SNase wherein the Thr-62 residue is observable. As is reflected by its structure, proline disturbs the helix formation within the protein. The nitrogen atom of the amino group is part of a rigid ring structure which hinders the rotation of the backbone and thus inhibits the formation of the helical structure [Löffler et al., 2007]. As a consequence, the T62P variant is already unfolded in pure buffer solution at pH 7.0 [Baskakov and Bolen, 1998b]. By this special type of point mu-

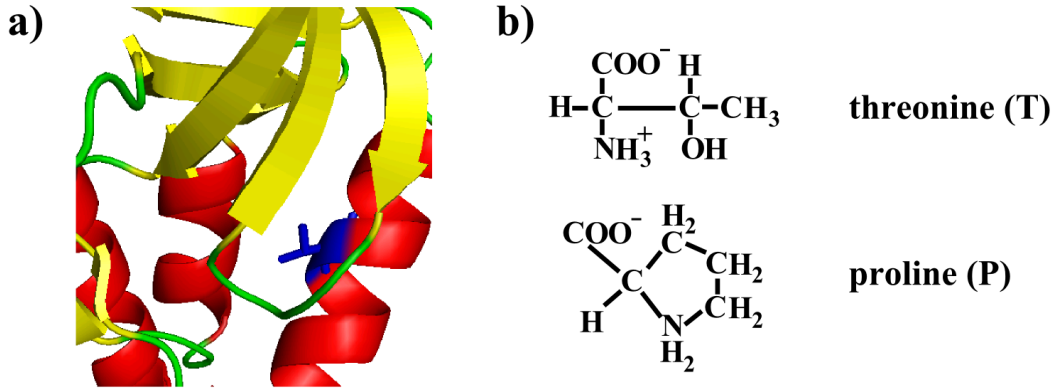

Figure 4.11: *a) Enlargement of the structure of WT SNase (pdb file 1EY0 [Chen et al., 2000]) in the ribbon presentation drawn by PyMOL [Schrödinger, LLC, 2008]. Shown is threonine residue 62 (blue sticks) which is located in a helix. In the T62P mutant, this residue has been replaced by proline. b) Covalent structure of threonine and proline.*

tation an intrinsically unfolded protein is manufactured, i.e. the folded state is largely destabilized. Addition of the destabilizing agent urea to T62P leads to a continuous increase of the protein's extent with amount of cosolvent without evidence of a co-operative unfolding transition which is a typical feature for a natively unfolded protein [Baskakov and Bolen, 1998b]. Notable, addition of the osmolyte trimethylamine N-oxide to a solution of T62P leads to its folding into a native-like state with a large degree of enzymatic activity not present in pure buffer solution [Baskakov and Bolen, 1998a]. For low pH values, SNase theoretically should have a large positive charge (+40 elementary charges) [Fitzkee and Garcia-Moreno E., 2008]. Therefore, variation of the solutions ionic strength by changing the pH value and the salt content will affect the unfolded state of T62P.

The influence of the pH value on the structure of the two proteins was studied by SAXS measurements performed on beamline BL9 of DELTA. The experimental parameters are given in Tab. 4.3. The high pressure sample cell described in section 3.3 was used. Instead of using diamonds as the window material, holders with Kapton® windows which absorb X-rays only little were used for measurements at ambient pressures.

The protein concentrations used were 5 mg/ml. SAXS measurements were performed at ambient temperature. As a broad range of pH values from 2.0 to 7.0 was covered, different types of buffers were used which are summarized in Tab. 4.4. For pH 4.5 to pH 6.0 sodium acetate ($NaCH_3COO$) and for pH 6.5 to pH 7.0 HEPES (N-(2-Hydroxyethyl)piperazine-N'-(2-ethanesulfonic acid)) were employed. For pH values smaller than 4.5 no buffer was used. To these buffers solutions different amounts of sodium chloride (NaCl) were added (10 mM, 100 mM, 1 M). Furthermore, for some

detector	MAR345 image plate
number of pixels	2400 x 2400
wavelength λ / Å	1.239
exposure time / s	1800
q-range /nm^{-1}	0.3 - 4.0

Table 4.3: *Experimental parameters of the SAXS setup used at beamline BL9, DELTA.*

pH range	buffer
2.0 - 4.0	none
4.5 - 6.0	sodium acetate (25 mmol/l)
6.5 - 7.0	HEPES (25 mmol/l)

Table 4.4: *List of the buffers used for different pH values.*

samples sodium sulfate (Na_2SO_4) was used instead. For all solutions the pH values were adjusted using concentrated hydrochloric acid (HCl).

In Fig. 4.12 the scattering curves of T62P and WT SNase in a 100 mM NaCl solution as a function of pH are shown in a double logarithmic and a Kratky plot. For both proteins a pH dependence of the form factor is detectable.

In a low pH range from 2.0 to 4.5 the SAXS curves of T62P changes drastically (Fig. 4.12a)) which can be also seen in the corresponding Kratky plot (Fig. 4.12b)). For pH 2.0 - 3.0 the scattering intensity resembles that of a random coil. Refinements to the data with the random coil scattering function (eq. (2.47)) are shown as solids lines. Increasing the pH value the protein becomes more compact as a maximum occurs in the Kratky plot. This becomes slightly narrower with increasing pH. For higher pH values (5.0 - 7.0) this effect continues (Fig. 4.12c), d)).

The results of respective measurements on the wild type protein are shown in Fig. 4.12e) and f). Herein, also a pH dependent increase of compaction of SNase is detectable. Its degree of compaction is much higher due to its larger stability than that of the T62P variant. For pH 2.0 the refinements of the data with the random coil model are given in Fig. 4.12e), and f) as well. The agreement of the experimental data points with the model fit is not as good as for T62P. Thus, although SNase is unfolded under this condition, it can not be fully described as a random coil in contrast to its natively unfolded variant. With increasing pH value WT SNase folds. At pH 4.0 the folding is completed as no significant changes occur for larger pH (6.0, 7.0). The scattering curves can be refined using the program GNOM, reflecting its compact structure. The SAXS signal of the protein at pH 3.0 can be attributed to the presence of a partially folded state.

For completeness the radial pair-distance distribution function for T62P at low pH

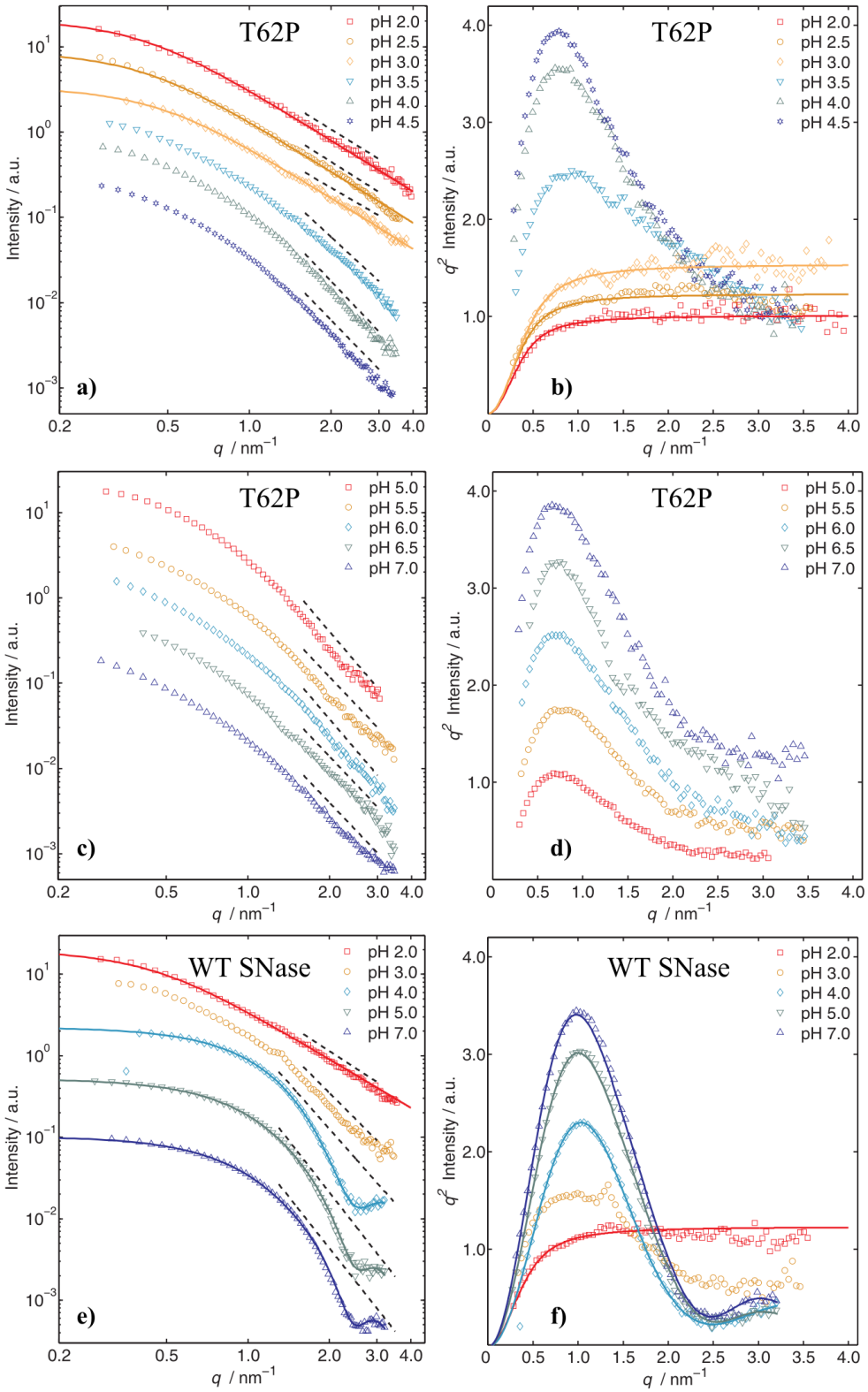

Figure 4.12: *SAXS curves of T62P and wild type SNase solutions (both with 100 mM NaCl added) for different pH values in a double logarithmic plot and the corresponding Kratky plot. a), b) Curves of T62P for pH 2.0 - pH 4.5. c), d) Curves of T62P for pH 5.0 - pH 7.0. e), f) Curves for WT SNase for pH 2.0 - pH 7.0. Solid lines are refinements to the data. Dashed lines mark the power law decay regime. Curves are shifted for clarity. It was averaged over nine data points.*

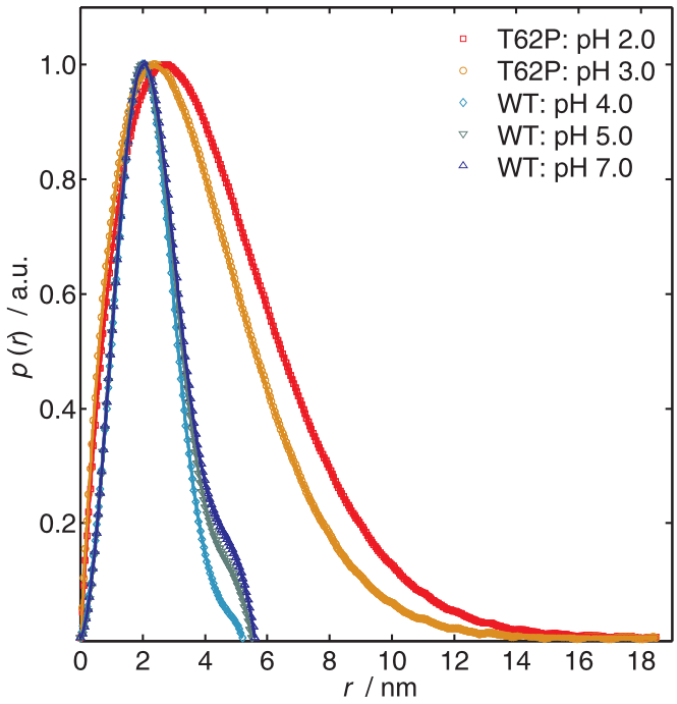

Figure 4.13: *Radial pair-distance distribution function, $p(r)$, for T62P at low pH and WT SNase at moderate pH for a 100 mM NaCl solution. The wild type protein is folded, whereas in case of the mutant a random coil is present.*

and for WT SNase at moderate pH is depicted in Fig. 4.13. At these conditions the whole SAXS curves could be refined. In case of wild type SNase, the $p(r)$ curve was obtained using the program GNOM and corresponds to the refinement shown in Fig. 4.12e) and f). For the mutant, the pair-distance distribution function was computed from the random coil scattering curve using eq. (2.45). As visible, the $p(r)$ function of a random coil is much broader and more asymmetric than that of the globular protein. The maximum extent, $D_{\max}$, of the random coil is between 130 and 140 Å. In contrast, the $D_{\max}$ value for the folded WT SNase is much smaller (52 to 55 Å). The slight change of this with pH might be attributed to minor changes in the three-dimensional structure but should not be overestimated. Notable, the shape, the extent, and the position of the maximum are similar to those of the $p(r)$ curves obtained for the hyperstable mutant 4.2.2.

To analyze the SAXS curves in more detail especially for those pH values, where the data can be refined neither with a random coil model nor with a compact model, the radii of gyration of both proteins were obtained using the Guinier approximation. The results are shown in Fig. 4.14a).

For the wild type protein, the radius of gyration decreases with increasing pH until at pH 4.0 a constant value is reached. For pH 2.0 - 3.0 it is unfolded but differs in degree

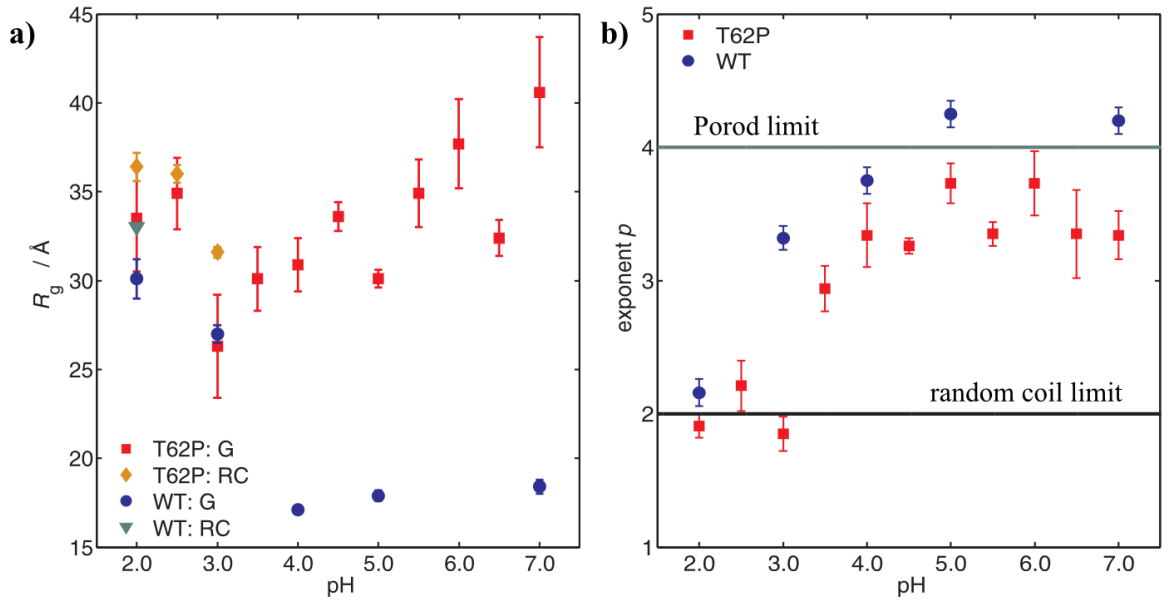

Figure 4.14: *Parameter obtained for T62P and WT SNase in a 100 mM NaCl solution as a function of pH value. a) Radius of gyration, R_g, of the proteins as a function of pH. Herein, "G" and "RC" denote values obtained by using the Guinier approximation and by refinement using the random coil scattering function, respectively. b) Power law exponent, p, as a function of pH. The data points used are marked in Fig. 4.12. The values for the limiting cases of the Porod law and the random coil are given as solid lines.*

of compaction. Thus, decreasing the protein's charge leads to different unfolded species. The results of the refinement to the random coil scattering function is also given in Fig. 4.14a). At pH 4.0 SNase is folded. Slightly different R_g values for higher pH might be attributed to local structural changes due to the different surface charges. However, in terms of compactness the protein does not change within the pH range of 4.0 - 7.0. This finding for WT SNase is in accord with previous studies [Uversky et al., 1998a].

In the case of T62P at pH 2.0 under the same solution conditions the radius of gyration is to some extent larger than that of the wild type protein although it has a larger experimental error. Increasing the pH value to 3.5 results in a decrease of the R_g to a value of (30.1 ± 1.8) Å. As the pH value increases toward the isoelectric point the number of charged residues is decreased resulting in a reduced Coulomb repulsion. Except for pH 3.0, the result of the refinement to the random coil scattering function is similar to that of the Guinier analysis. For pH values larger than pH 4.0 an increase of the radius of gyration for T62P is present. At pH 7.0 it is $R_g = (40.6 \pm 3.1)$ Å which is even larger than the result at pH 2.0. Whereas for low pH smaller than 3.5 the larger radius of gyration can be attributed to a fully unfolded protein which is supported by the refinement, with increasing pH a more compact structure of T62P should be present as is reflected by the respective Kratky plots. Notable, as the proteins were in a 100 mM

NaCl solution aggregation, especially formation of dimers, must be taken into account.

In order to shed more light into the pH dependence oof the structure of both proteins, the high q-region of the scattering curves was analyzed in more detail. As can be seen in the double logarithmic plots in Fig. 4.12, the SAXS signal shows a power law decay for larger wave vector transfer. These parts of the data were refined to obtain the corresponding power law exponents. In Fig. 4.12, the respective curves are shown as dashed lines. In the case of WT SNase, at higher pH values where the protein is already folded and the form factor thus shows an oscillation, the exponent p was obtained by calculating the tangent of the curve. The results of the power law analysis are given in Fig. 4.14b) (see chapter 2.2.4 for an overview of the different types of exponents).

For WT SNase at pH 2.0 the power law exponent is close to that of a random coil. Increasing the pH value, p increases until it reaches a value slightly larger than the Porod limit at pH 5.0. For pH 3.0, $p = 3.3 \pm 0.1$ is that of a surface fractal. This is in accord with the interpretation already derived from pH dependence of the radius of gyration. Thus, at pH 3.0 the protein can be described to be in an intermediate state of folding. This shows that the folding of SNase as a function of pH can be described in terms of the power law exponent as well.

The results of the Guinier analysis of T62P were not fully clear. Therefore, the respective exponent p was obtained (Fig. 4.14b)). For pH 2.0 - 3.0, this protein has a p value close to that of a random coil, i.e. under these conditions it is unfolded. With increasing pH larger than pH 3.0 the power law exponent increases. At first there is a steep increase to $p = 2.9 \pm 0.2$, corresponding to an extended surface fractal. For higher pH values, p slightly becomes larger but does not reach a value of 4. Under these conditions the protein shows features of a more compact surface fractal. Thus, as a function of pH T62P undergoes a transition from a random coil state to a collapsed natively unfolded protein state at high pH values [Uversky, 2009].

In terms of these findings, the pH dependence of the radius of gyration for T62P can be understood as follows. As p is about 2 for pH smaller than 3.0, the protein is unfolded. Thus, the size of the R_g at these solution conditions is reflecting the unfolded state of the SNase mutant. Changing the pH value in this range does not change p but the radius of gyration. In contrast, for the wild type protein a decrease of R_g is accompanied by a increase in p at pH 3.0 as a partially folded state is present. Two possible explanations for a similar type of structure, i.e. p, with different size, i.e. R_g, for T62P might be given. Either there is a slight difference between the unfolded state as the Coulomb repulsion is decreased from pH 2.0 to pH 3.0 or dimer formation is present also at low pH values which changes as a function of pH. Employing different concentrations of NaCl will allow to change the degree of dimerization if present. However, taking into

account the large error of R_g this discrepancy should not be overestimated.

With beginning of compaction of T62P at pH 3.5 - 4.0 the minimum of R_g is due to the presence of the properly monomeric protein in a partially folded state. The increase of the radius of gyration with pH thus is due to the increase in number of dimers. As the Coulomb repulsion between the proteins is reduced the amount of dimers should increase. Maybe the presence of a partially folded state with a hydrophobic core which is at least to some extent exposed to the solvent favors the dimerization. Due to the hydrophobic interactions between these species, they might attract each other when being in close contact leading to dimer formation even though WT SNase has a low intrinsic hydrophobicity only. As dimers are probably present at a protein concentration of $c_P = 5$ mg/ml, using lower concentrations should avoid their formation.

In summary, for a solution of the natively unfolded protein T62P with 100 mM NaCl added an increase in compaction was detectable with increasing pH. Whereas it is unfolded at low pH resembling a random coil, for higher pH values it can be described as collapsed. Characterizing the scattering curves by their power law exponent for large q values gives additional information to the Guinier analysis. The latter approach fails to give reliable information in the case of oligomerization.

4.3.2 Influence of different salt concentrations

In order to get a deeper insight into the influence of salt added to the solution on the pH dependence of the protein structure, additional SAXS measurements were performed. Using two different NaCl solutions (10 mM, 1 M) the effect of dimer formation could be influenced as well.

SAXS data for T62P were recorded for selected pH values at both low and high NaCl concentrations. Additionally, the scattering from WT SNase was detected at pH 2.0 for these conditions as well. The results of the experiments for both salt concentrations are shown in Fig. 4.15.

Fig. 4.15a) and b) reflect that for a low salt content the T62P variant is unfolded for pH 2.0 - 4.0 as is the wild type protein for pH 2.0. The corresponding scattering curves can not be refined using the random coil model. Increasing the pH value to pH 4.0 and above that, the Kratky plot of scattering curves of the T62P mutant shows a broad maximum. Thus, also for lower salt concentrations, an increase of compactness with increasing pH value is present for this natively unfolded protein.

For the sodium chloride concentration of 10 mM, the screening of the protein's charges exposed to the solvent due to the ions is reduced compared to the previous data. Thus, the Coulomb repulsion between these charges will be stronger at this solution condition which should result in an increase of the protein's size in the unfolded state. In addi-

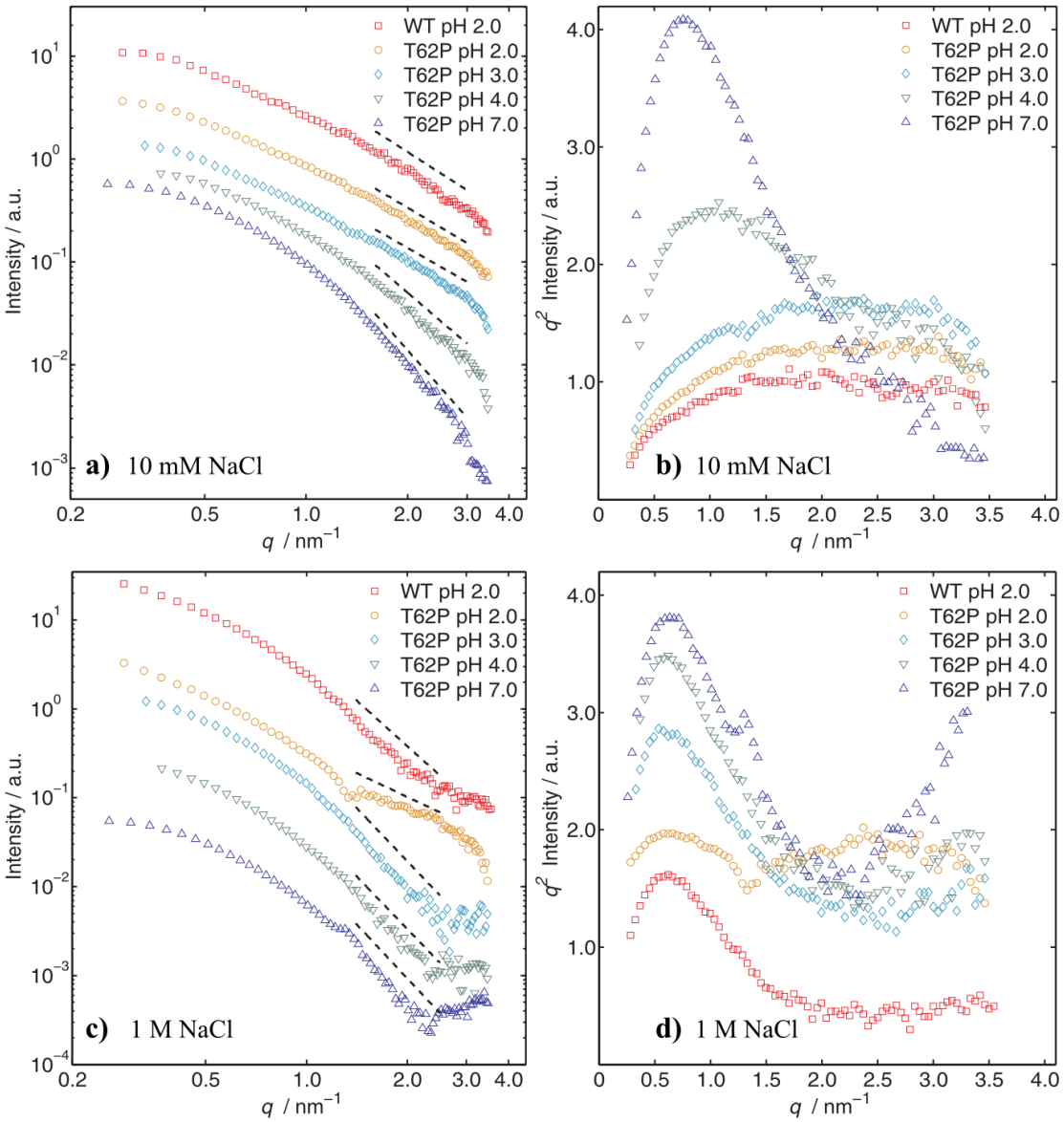

Figure 4.15: *Scattering curves for T62P and WT SNase as function of pH for different NaCl concentrations. a) Double logarithmic plot for 10 mM NaCl added. b) Corresponding Kratky plot. c) Double logarithmic plot for 1 M NaCl added. d) Corresponding Kratky plot. Data where averaged over 9 points. Curves are shifted for clarity. Dashed lines mark the power law decay regime.*

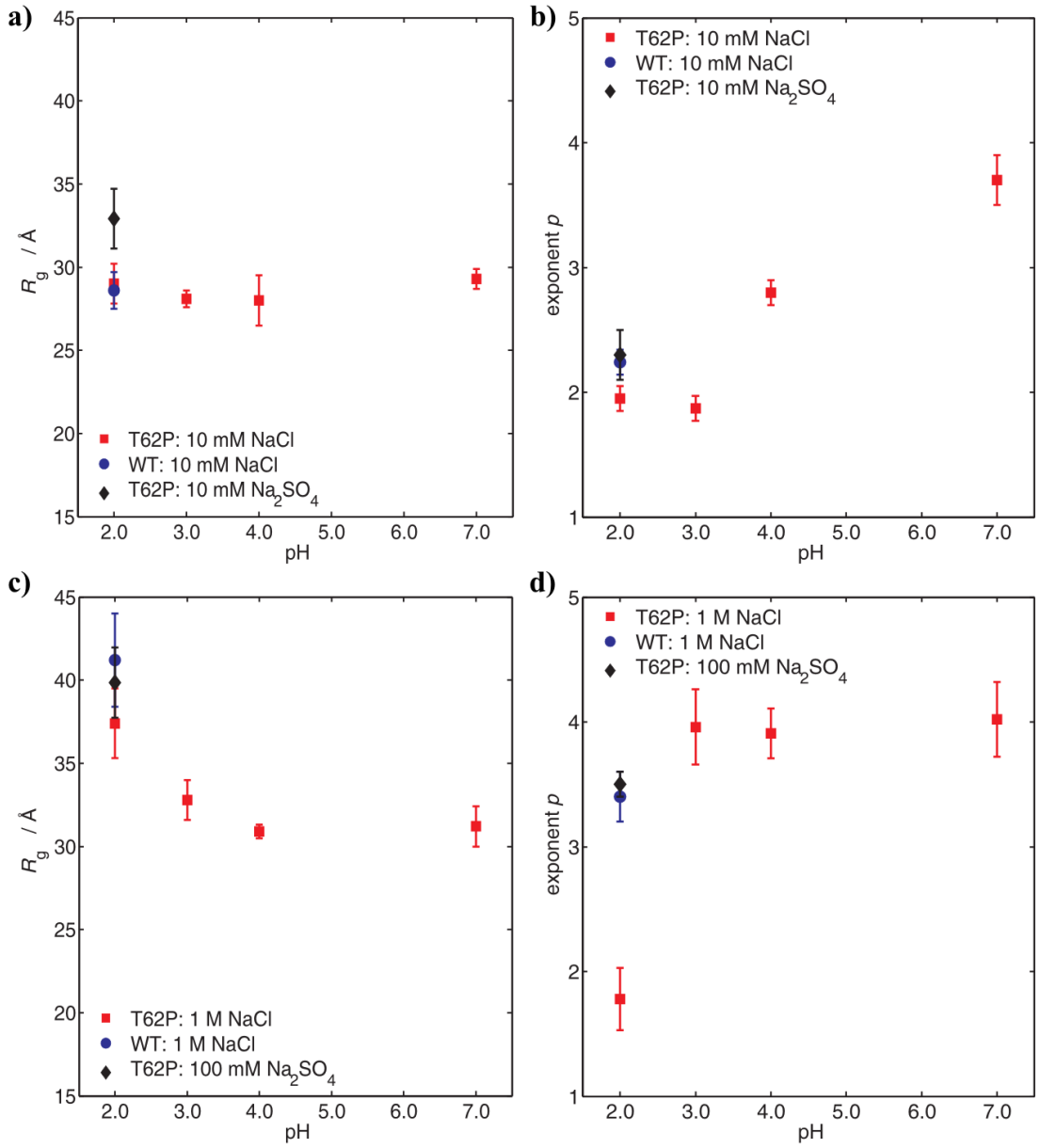

Figure 4.16: *a) Radii of gyration for T62P and WT SNase as a function of pH for 10 mM NaCl. Also shown is the result for T62P in a 10 mM Na_2SO_4 solution. b) Corresponding power law exponents. c) Radii of gyration for 1 M NaCl added to the protein solutions as well as for 100 mM Na_2SO_4 added. d) Corresponding power law exponents.*

tion, the attraction between the proteins is reduced lowering the propensity for dimer formation. To analyze this, the radii of gyration as well as the power law exponent have been determined. These are depicted in Fig. 4.16a) and b).

For WT SNase there is only a slight decrease in R_g from (30.1 ± 1.1) Å for 100 mM NaCl to (28.6 ± 1.1) Å for 10 mM NaCl. Similarly, the power law exponent does not change. Thus, for the wild type protein no significant influence of reducing the salt concentration is present. In the case of T62P there is nearly no pH dependence of the radius of gyration detectable for the lower salt concentration. A R_g value between 28 to 29 Å is present for any pH value. Interestingly, the power law exponent shows a similar dependence as for the 100 mM NaCl solution.

These findings indicate that the presence of sodium chloride of a concentration of 10 mM to 100 mM does not have a significant influence on the pH dependent degree of compactness. The differences in the radii of gyration of the mutant for both solutions at high pH values might be attributed to the presence of dimers. As the amount of NaCl is increased, the Coulomb repulsion is reduced and more dimers of the protein in collapsed state may form. A similar effect might also be presented for T62P for pH values smaller than pH 4.0. With decreasing pH value the number of chloride ions increases as the number of protons H^+ does in the solution. Therefore, it seems probable that besides the protonation of the residues, which leads to the increase of surface charges and thus unfolding, also the accompanied increase in chloride ions has an effect on these charges. A similar effect of anions of an acid has been reported for acid-induced folding of proteins. In a protein solution of low ionic strength decreasing the pH value first leads to denaturation close a pH value of pH 2.0. A further increase of the acid concentration leads to an increase of secondary structure again [Goto et al., 1990a, Goto et al., 1990b]. Measurements on acid-denatured proteins in solutions with the salt of the respective acid added showed the same effect. It was suggested that the anions are binding to the charged groups of the unfolded proteins at low pH values [Goto et al., 1990b]. As this reduces the Coulomb repulsion, refolding is induced as well as the propensity for aggregation is enhanced [Goto et al., 1990a]. Such a behavior has also been found for wild type SNase [Fink et al., 1993, Uversky et al., 1999].

Thus, at moderate ionic strengths like in the case of 100 mM NaCl the combined effect of anions of the acid as well as of the salt leads to a particular dimerization also at low pH values. This is not observed for the 10 mM NaCl solution probable due to the low salt content. It should be noted that whereas for high pH values the possible dimerization is between collapsed states, for low pH values this effect is between fully unfolded proteins.

Using high salt concentrations of 1 M NaCl, both WT SNase as well as the T62P variant show a certain degree of compactness for all pH values (see the scattering curves

in Fig. 4.15c) and the corresponding Kratky plots in d)). For the mutant at pH 2.0 the Kratky plot indicates the presence of different species in solution. A broad maximum attributed to partially folded state as well as a plateau indicative for random coil like states are present. For higher pH values, a single maximum is present. The increase of the scattering signal for T62P at pH 7.0 for large q is due to problems in the background subtraction.

The corresponding radii of gyration and the power law exponents are shown in Fig. 4.16c) and d). For WT SNase it is $R_g = (41.2 \pm 2.8)$ Å indicating the presence of dimers in the solution at high salt concentrations. These are partially folded as is reflected by the power law exponent. In the case of T62P a similar pH dependence of the radius of gyration is present as for the 100 mM NaCl solution with the exception for pH 7.0. At this value the R_g is smaller than that for the moderate salt concentration. Maybe a different degree of dimerization is present in this case. The power law exponent for T62P suggests that the protein resembles features of a compact particle. In contrast to the lower salt concentrations, 1 M NaCl solution already leads to compactness at pH 3.0 which is somewhat higher than for the other concentrations. Increasing pH does not give a further increase of p, i.e. the process of structural collapsing is already finished.

Exemplary SAXS curves were also measured for T62P at pH 2.0 with two different amounts of Na_2SO_4 (10 mM, 100 mM) to test the influence of a divalent anion. The respective R_g and p values are added in Fig. 4.16. For the lower concentration results comparable to that of the 100 mM NaCl are obtained. In the case of the 100 mM Na_2SO_4 solution an even larger radius of gyration as in the case of 1 M NaCl is present reflecting a possible higher amount of dimers. In addition, a power law exponent similar to that of the WT protein in 1 M NaCl solution indicates the presence of a partially folded species. In general, the effect of sodium sulfate on the protein structure is increased in comparison to sodium chloride. Similar findings have been reported previously for refolding of acid-denaturated WT SNase by anions [Uversky et al., 1998a]. This ion specific effect is due to the large electroselectivity of divalent ions compared to the monovalent ones [Goto et al., 1990b]. Thus, binding of SO_4^{2-} is more preferred than that of Cl^-.

4.3.3 Summary and Discussion

The presented study on WT SNase and its T62P mutant which is natively unfolded shows the influence of the solution's pH value and the salt concentration on the protein structure. T62P serves as a model for the unfolded state of SNase. Due to the mutation of a single residue it is not folded at native conditions. Thus, the effects of different ionic strength on the unfolded state can be studied in the absence of denaturing agents.

The SAXS measurements on WT SNase in 100 mM NaCl solution were performed as a reference to the actual study on the T62P variant. WT SNase is folded within pH range from 5.0 to 7.0. Decreasing the pH, the protein unfolds and resembles a surface fractal object. This unfolding process is completed at pH 2.0. At this condition, it has a larger radius of gyration compared to the folded state (R_g = (30.1 ± 1.1) Å for pH 2.0, R_g = (17.1 ± 0.1) Å for pH 7.0) as well as a small power law exponent (p = 2.2 ± 0.1 for pH 2.0, p = 4.2 ± 0.1 for pH 7.0). Changing the salt concentration for the unfolded state at pH 2.0 from 100 mM to 10 mM NaCl showed no significant effect. An enhancement to 1 M, however, leads to the formation of aggregates which are most probable dimers, as is reflected by the increase of the radius of gyration. Accompanied is an increase of compactness, as p becomes larger.

The explanation of this finding is as follows. For acid-unfolded WT SNase the addition of salts induces folding into different partially folded intermediate states, the so-called A states [Uversky et al., 1998a]. Depending on the type of anion three A states exist which differ in their degree of folding. If chloride or sulfate ions are added to the solution the A_1 is present which is 50 % folded, has considerable secondary structure, and is relatively compact but lacks tertiary structure [Uversky et al., 1998a]. The amount of anions needed to induced folding depends on their valance. Due to electroselectivity, divalent anions bind more preferentially to the charges of the protein than monovalent ones [Goto et al., 1990b]. Addition of trifluoroacetate (TFA) and trichloroacetate (TCA) induces folding to the more structured A_2 and A_3 states, respectively, from which the latter has the highest degree of folding [Uversky et al., 1998a]. For these partially-folded SNase intermediates it has been found that their association either due to high salt or protein concentrations induces folding [Uversky et al., 1998b, Uversky et al., 1999]. Especially for the A_1 state, lacking a maximum in the corresponding Kratky plot revealed from SAXS studies, the formation of dimers and oligomers causes an increase in compactness. Thus, the large radius of gyration and the value of p indicating surface fractal-like structures in a 1 M NaCl solution can be understood by the formation of dimers of SNase in the A_1 state. These results on SNase are thus in good agreement with previous studies [Fink et al., 1993, Uversky et al., 1998a, Uversky et al., 1999].

The measurements on the T62P mutant were performed to study the influence of

electrostatic effects on the denatured state. For all conditions studied, the radius of gyration is always larger than that of the wild type protein. Furthermore, no compact folded state was detectable in terms of the power law exponent except for the highest salt concentration. These findings reflect the unfolded character of this variant which is in accord with previous results [Baskakov and Bolen, 1998a, Baskakov and Bolen, 1998b, Isom et al., 2008]. Another general finding is the large propensity of T62P to form dimers in comparison to WT SNase. The degree of aggregation significantly depends on the ionic strength of the solution as could be seen by variation of the salt content.

For the lower sodium chloride concentration studied (10 mM NaCl), there is no serious change of the radius of gyration as the pH value is changed. However, at a pH value of 4.0 T62P becomes more compact as is revealed by the Kratky plot and the power law exponent. Thus, there seems to be a pH induced transition into a folding intermediate state apparently without change in the protein size. Two possible interpretations can be formulated. Either there is already dimer formation present at this low salt concentration due to the amount of protein in solution as the pH value is raised. This leads to association induced folding as in the case of WT SNase intermediates. Alternatively, some specific structure of T62P is formed having a certain degree of compactness but a large electronic extent.

When increasing the salt concentration (100 mM NaCl), aggregate formation is present both for low and moderate pH values. For a pH value smaller than 4.0 most probable dimers are present as the R_g is increased compared to the lower NaCl solution at similar conditions. A possible mechanism for this enhancement in amount of aggregation with decrease of pH might be the binding of chloride ions to the charged residues. This would lead to a decrease in Coulomb repulsion between the unfolded proteins. The source of the anions are both the salt as well as the hydrochloric acid added. No dimer formation has been observable for the lower salt concentration at low pH values as the amount of anions was probable too low.

The aggregation due to anion binding at low pH values has been already proposed previously [Goto et al., 1990a]. In contrast to the wild type protein [Uversky et al., 1998b, Uversky et al., 1999], however, there is no folding accompanied by this aggregation as the power law exponent is close to a value of 2. Thus, it seems there are differences in the actual dimer formation process between SNase and its T62P variant. This might be attributed to the different amount of hydrophobic subdomains exposed to the solvent as well as the number of actually charged residues. Theoretically, there should be no difference in the intermolecular interaction between WT SNase and T62P for the completely unfolded state as these are only differing at a single residue. However, if there is some kind of residual structure existing in either of the two proteins at low pH value, these interaction might be different. Notable, for a fully unfolded WT SNase using 6 M guani-

dine hydrochloride a radius of gyration of (37.2 ± 1.2) Å was found [Kohn et al., 2004], which is larger than any value obtained for T62P and SNase within the presented study. Therefore, it is likely that the T62P variant is not completely unfolded but possesses such a type of residual structure as it is the case for the wild type protein. Furthermore, it has been pointed out that there are special arrangements of unfolded proteins that resemble features of a random coil as it is revealed by e.g. SAXS, but still possess some type of structural elements [Fitzkee and Rose, 2004]. The unequal amount of aggregate formation for the WT SNase and T62P at similar protein concentrations and solution conditions might be attributed as a weak indication of the presence of different types of residual structure.

With increasing pH larger than 3.5 the mutant begins to fold and the degree of aggregation rises again. Here, aggregation is most probably induced due to screening of the protein charges and not only direct binding as the number of charged residues is reduced with rising pH. Accompanied is an increase in the degree of folding as for the lower salt concentration. This might be either due to reduced intramolecular repulsion as for the wild type protein or association-induced folding.

For a sodium chloride concentration of 1 M, a compact state of the mutant is already present at lower pH values. Different types of folding states seem to be existing at pH 2.0. At this salt concentration a similar amount of aggregation as for the 100 mM NaCl solution is present with the exception of pH 7.0. Here, most probable some type of precipitation must have happened as large aggregates formed at the high salt amount. Finally, using a Na_2SO_4 the influence of electroselectivity on T62P could be demonstrated.

This study on the T62P variant shows that it is most probable that aggregation for different ionic strengths and protein concentrations are present. As reflected by the results of the Guinier analysis these unequal degrees of oligomerization are influenced by the actual solution conditions. Different mechanisms for these findings have been proposed above that are present for folding intermediates of WT SNase. Despite of the presence of aggregation, information of the structure of T62P and the effect of electrostatic interactions were found.

Both, the value of the R_g between 28.1 to 29.0 Å as well as that of the power law exponent p of 1.9 to 2.0 suggest that in a pH range from 2.0 to 3.0 and at a NaCl concentration of 10 mM T62P is present in a monomeric unfolded state. Notable, the radius of gyration is much smaller than that obtained by recent simulations using different types of unfolded ensembles for T62P [Fitzkee and Garcia-Moreno E., 2008]. Therein, R_g has been calculated as a function of pH excluding and including electrostatic interactions. Due to this, it seems that there is some type of residual structure present

in this unfolded SNase variant. This interpretation is in accord with the results for fully chemically unfolded SNase [Kohn et al., 2004] and the concept that random coil-features and residual structure do not rule out each other [Fitzkee and Rose, 2004].

Increasing pH leads to a rise of the protein compaction similar as in presence of large amounts of salt. This indicates structure formation as the electrostatic repulsion is reduced. If this effect is equivalent to that of WT SNase, i.e. due to changes in the intramolecular interaction, or due to association-induced folding between intermediates, can not be decided on basis of the presented study.

Furthermore, the higher propensity of T62P for aggregate formation might be attributed to a low content of residual structure. As was shown for the intermediate states of SNase A_1, A_2, and A_3, the affinity to dimer and oligomer formation decreases with the degree of structure [Uversky et al., 1999]. A similar effect might thus also be valid for T62P.

In summary, variation of ionic strength has a significant influence on structure formation and interactions of the natively unfolded T62P mutant. It can not be fully decided if these are coupled. Therefore, additional measurements employing different techniques will help to solve this. Nevertheless, a structural transition was observed for this variant by means of SAXS. Even for those conditions where no refinement of the whole scattering curve could be performed, the combination of the Guinier and the power law exponent allowed to derive information about the electrostatic effects on the structure of an intrinsically disordered protein.

4.4 Pressure effects on the structure of a non-globular repeat protein

Up to now, unfolding of small, globular, single domain proteins was studied. A characteristic of these is their compact structure. As a consequence of their three-dimensional fold, residues which are separated in the primary structure, i.e. the amino acid sequence, may be in close contact in the folded state. Thus, modular changes in the sequence like deletions can strongly affect the folding process. A linear relation between the primary structure and the folded state however is present in repeat proteins. These can be described as polypeptides consisting of repeat units made out of helices. These proteins have an elongated structure and a long hydrophobic core. Recently, the so-called ankyrin domain of the *Drosophila* Notch receptor was studied in detail regarding its structure and folding at ambient pressure conditions [Zweifel and Barrick, 2001b, Mello and Barrick, 2004, Mello et al., 2005]. In order to access the pressure-induced unfolding and its dependence on the concentration of destabilizing urea added, SAXS measurements were performed and will be described below.

This study on the ankyrin repeat domain has been performed within a collaboration between the groups of Prof. M. Tolan (TU Dortmund), Prof. R. Winter (TU Dortmund), Prof. C.A. Royer (Univerisité de Montpellier), and Prof. D. Barrick (The Johns Hopkins University). The presented results were already published as: J.-B. Rouget, M.A. Schroer, C. Jeworrek, M. Pühse, J.-L. Saldana, Y. Bessin, M. Tolan, D. Barrick, R. Winter, C.A. Royer (2010). Unique features of the folding landscape of a repeat protein revealed by pressure perturbation. *Biophysical Journal* 98:2712-2721.

The outline of this section is as follows. First, the protein studied will be shortly introduced. Thereafter, the high pressure SAXS data will be presented. The present section ends with a summary of the results obtained with other techniques within this collaboration and a discussion.

4.4.1 The ankyrin domain of the *Drosophila* Notch receptor

The ankyrin domain of the *Drosophila* Notch receptor studied is made out of 213 residues [Rouget et al., 2010] and consists of seven so-called ankyrin repeats (Fig. 4.17a)). The molecular weight is about 28 - 30 kDa [Zweifel and Barrick, 2001a]. A single ankyrin repeat is 33 residues long and is made out of two antiparallel α helices which are connected by a short loop [Zweifel and Barrick, 2001a, Zweifel et al., 2003]. Two of these repeats are linked by a long loop. In Fig. 4.17b) the ankyrin repeat can be seen.

In general the ankyrin domain is part of the transmembran Notch receptor present in metazoans which is essential for the so-called Notch signaling pathway. With this

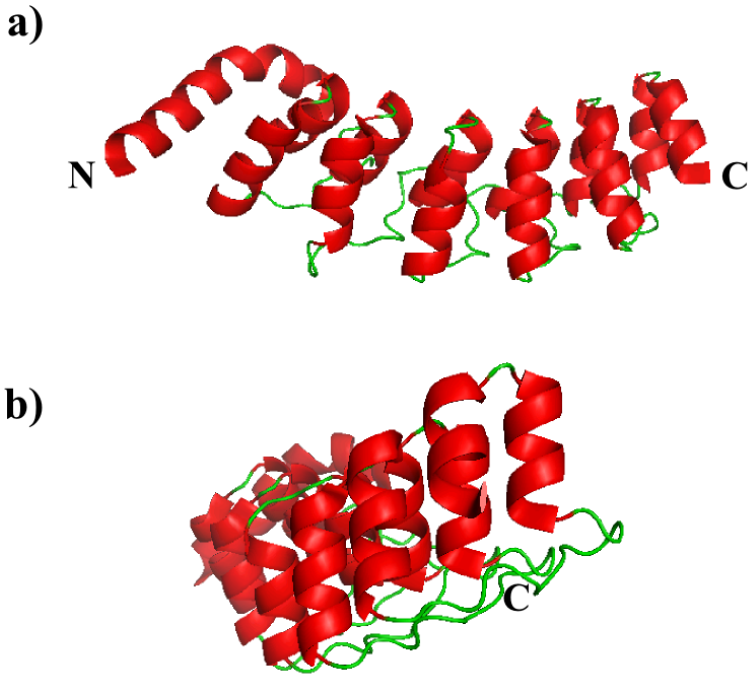

Figure 4.17: *Ribbon diagram of the ankyrin repeat domain of the Drosophila Notch receptor (pdb file 1OT8 [Zweifel et al., 2003]) drawn with PyMOL [Schrödinger, LLC, 2008]. a) Frontal view. The domain contains seven ankyrin repeats from which the first N-terminal one is disordered. b) Side view. Herein, the ankyrin domain consisting of two α helices with a short loop can be seen more clearly.*

receptor, signals between two cells are communicated to regulate the fate of the cells [Zweifel and Barrick, 2001a, Zweifel et al., 2003]. Different sequences for ankyrin repeats and ankyrin domain are known which however show a quite similar secondary and tertiary structure.

The investigated repeat protein is that from *Drosophila melanogastor* and consists of six tandem repeats meeting the ankyrin consensus sequence and a seventh putative C-terminal repeat with lower similarity [Zweifel and Barrick, 2001a, Zweifel et al., 2003]. A tryptophan residue is located in the fifth repeat [Zweifel et al., 2003]. The N-terminal repeat does not have a regular fold but is disordered (the very left in Fig. 4.17a)). The putative repeat has been shown to be essential for increasing the protein stability [Zweifel and Barrick, 2001b, Zweifel et al., 2003]. For the seven repeat long variant, unfolding sets in at 2.8 M urea at ambient pressure [Zweifel and Barrick, 2001b]. Kinetic studies at ambient pressure indicate a discrete pathway with an intermediate present [Mello et al., 2005, Bradley and Barrick, 2006]. Finally its folding landscape has been revealed as well [Mello and Barrick, 2004]. For more details, the reader is referred to the literature.

	BL9, DELTA	BW4, HASYLAB
detector	MAR345 image plate	MARCCD165
number of pixels	2400 x 2400	2048 x 2048
wavelength λ / Å	1.239	1.3808
exposure time / s	1800	1200
q-range /nm^{-1}	0.3 - 3.5	0.3 - 3.0

Table 4.5: *Synopsis of the different parameters of the SAXS measurements at the two beamlines. Given are the type of area detector, the number of its pixels, the wavelength λ, the typical exposure time, and the accessible q-range.*

4.4.2 High pressure SAXS on the ankyrin repeat domain

Small angle scattering measurements were performed on the ankyrin repeat domain to study structural changes induced by hydrostatic pressure in presence of different urea concentrations. The SAXS experiments were conducted at beamline BL9, DELTA, and BW4, HASYLAB. The experimental parameters are given in Tab. 4.5. High pressure conditions were achieved using the sample cell described in chapter 3.3. With this, a pressure range from 1 bar to 3 kbar was covered. The pressure value in the vessel was kept constant for the whole pressure range. For higher pressures changes of about 0.1 kbar were present within the exposure time.

Protein concentrations of 7.8 - 11.0 mg/mL were used to obtain a proper scattering signal within reliable time avoiding a contribution of a structure factor to the SAXS signal. To keep the pH value constant, a 50 mM Tris buffer was employed at pH 7.5[3]. From the pure buffer stock solution, two solutions with urea (CH_4N_2O) added (2.0 M, 2.2 M) were made. The measurements were performed at ambient temperature (T = 24 °C). After decreasing the pressure, aggregates of the unfolded protein were detected. However, no aggregates were present at high pressure as under these conditions aggregate formation is inhibited [Perrett and Zhou, 2002].

The determined SAXS curves of the repeat domain in different solutions are depicted in Fig. 4.18 as a function of pressure. The scattering signal of the protein in pure buffer at ambient pressure shown in Fig. 4.18a) clearly has a different shape than that of a small globular protein. This can be seen when comparing this curve with that of folded WT SNase (see Fig. 4.12e)).

With increasing pressure, changes in the scattering curves are visible indicating structural rearrangements of the protein. These also depend on the solution's properties. For instance, variation the urea concentration from 2.0 M to 2.2 M results in a much steeper decay of the scattering intensity as a function of q.

[3]For details on the buffer, see section 4.2.2.

The solid lines are fits to the data using the program GNOM which allows to access the corresponding radial pair-distance distribution functions $p(r)$. In order to obtain this function, the following condition between the maximum extent of the protein, $D_{\max}$, and the minimum q value, $q_{\min}$ that has been obtained for the form factor has to be fulfilled [Svergun, 1992, Svergun et al., 2009]

$$q_{\min} \cdot D_{\max} \leq \pi \; . \tag{4.2}$$

If this condition is not met, a ringing in the corresponding refinement to the scattering data might occur. Especially for the high pressure conditions in presence of the largest urea concentration this might be present. However, this can already be seen as an indication of major structural changes leading to a larger extent of the protein.

The scattering curves are shown in the Kratky plot in Fig. 4.19. In case of the protein in pure buffer solution (Fig. 4.19a)), pressure does not induce unfolding as is indicated by the presence of a maximum in this representation. As the pressure is increased a shift of the position of the maximum occurs which might be attributed to some slight structural changes within the protein. However, these are not large enough to lead to unfolding. The increase of the signal for higher q value at 2 and 3 kbar should not be overestimated, as under high pressure conditions the background subtraction becomes challenging for low protein concentrations due to the reduction in contrast.

Addition of 2.0 M urea to the protein solution effects its stability against high pressure conditions significantly (Fig. 4.19b)). At ambient pressure the maximum is much broader than for the pure buffer solution. This persists for $p = 1$ kbar. For higher pressures the protein is unfolded as the maximum is absent.

Increasing the urea concentration only slightly to 2.2 M affects the scattering curves much stronger than one would expect (Fig. 4.19c)). For 1 bar and 1 kbar, a maximum as for the 2.0 M urea solution is present. This is much broader, which indicates a more flexible, less well defined folded state. For higher pressures, no clear maximum is visible as there is insufficient q space detected. This is due to the fact that the protein extensively unfolds and thus becomes much larger and is not properly resolvable anymore. Therefore, the refinement is not as sound as for the previous data.

In Fig. 4.20 the corresponding $p(r)$ curves are depicted. For the protein in pure buffer solution the sole effect of pressure is a slight shift of the maximum of the curves as the maximum extent keeps constant to values between 94 to 98 Å. In principle this finding could be indicative of a transition from an ellipsoid particle to more spherical one. As the repeat protein has an elongated linear form the interpretation of the 1 bar curve

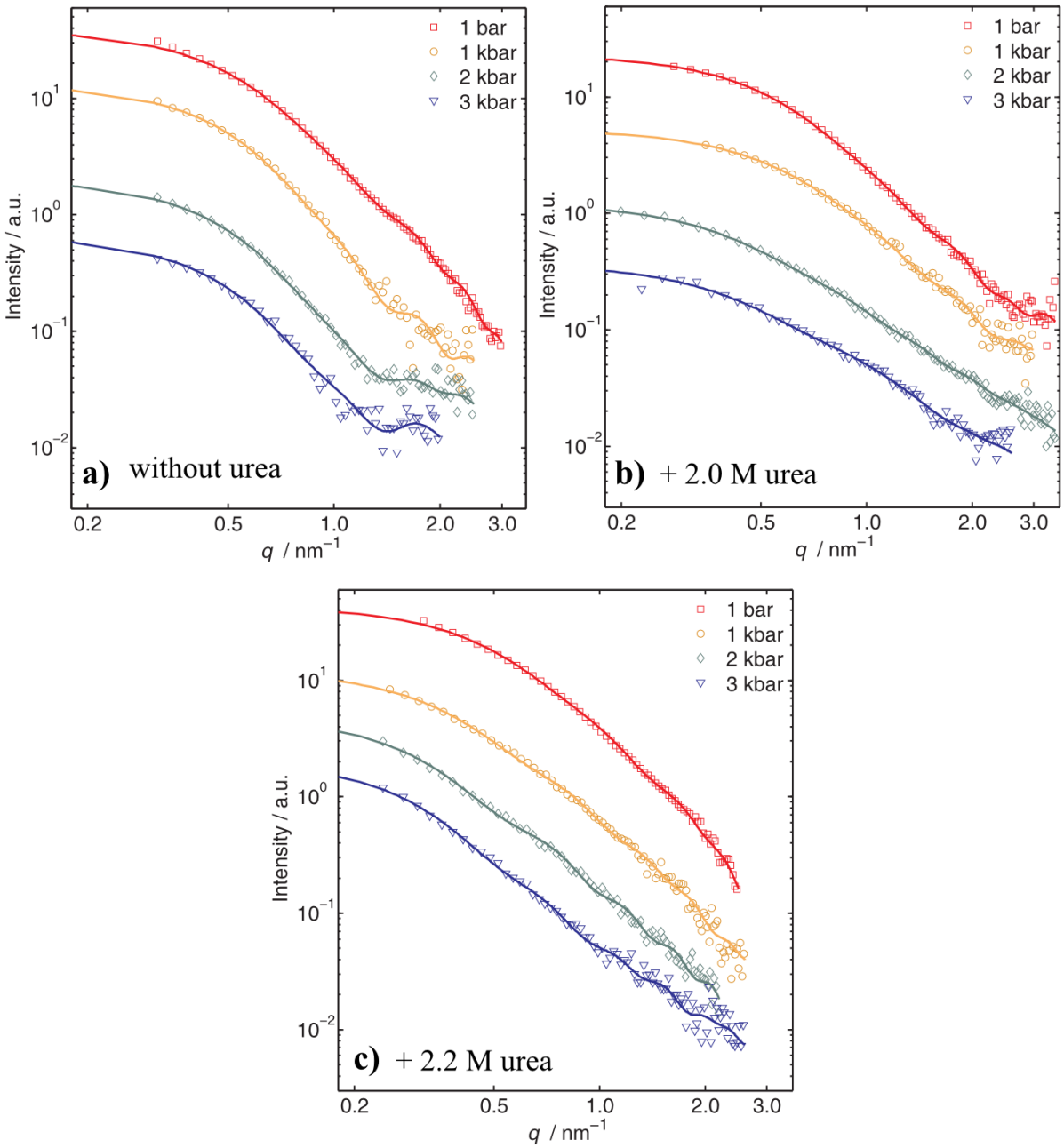

Figure 4.18: *SAXS curves of the ankyrin repeat domain of the Notch receptor as a function of pressure for different urea concentrations. a) In pure buffer solution. b) In buffer solution with 2.0 M urea added. c) In buffer solution with 2.2 M urea added. Solid lines are refinements to the data using GNOM. It was averaged over 10 data points.*

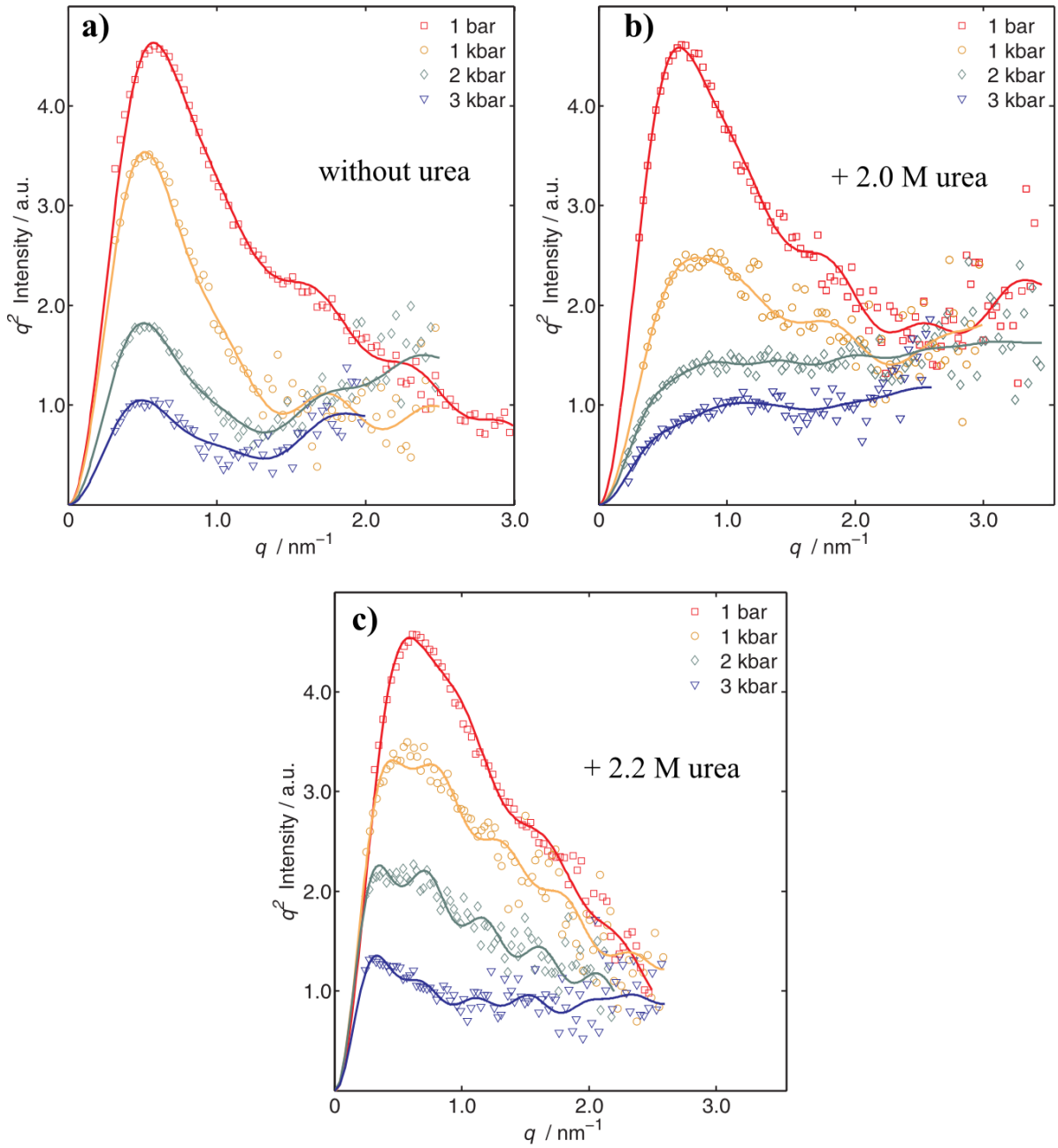

Figure 4.19: *Kratky plot of the ankyrin repeat domain of the Notch receptor as a function of pressure for different urea concentrations. a) In pure buffer solution. b) In buffer solution with 2.0 M urea added. c) In buffer solution with 2.2 M urea added. Solid lines are refinements to the data using GNOM. It was averaged over 10 data points.*

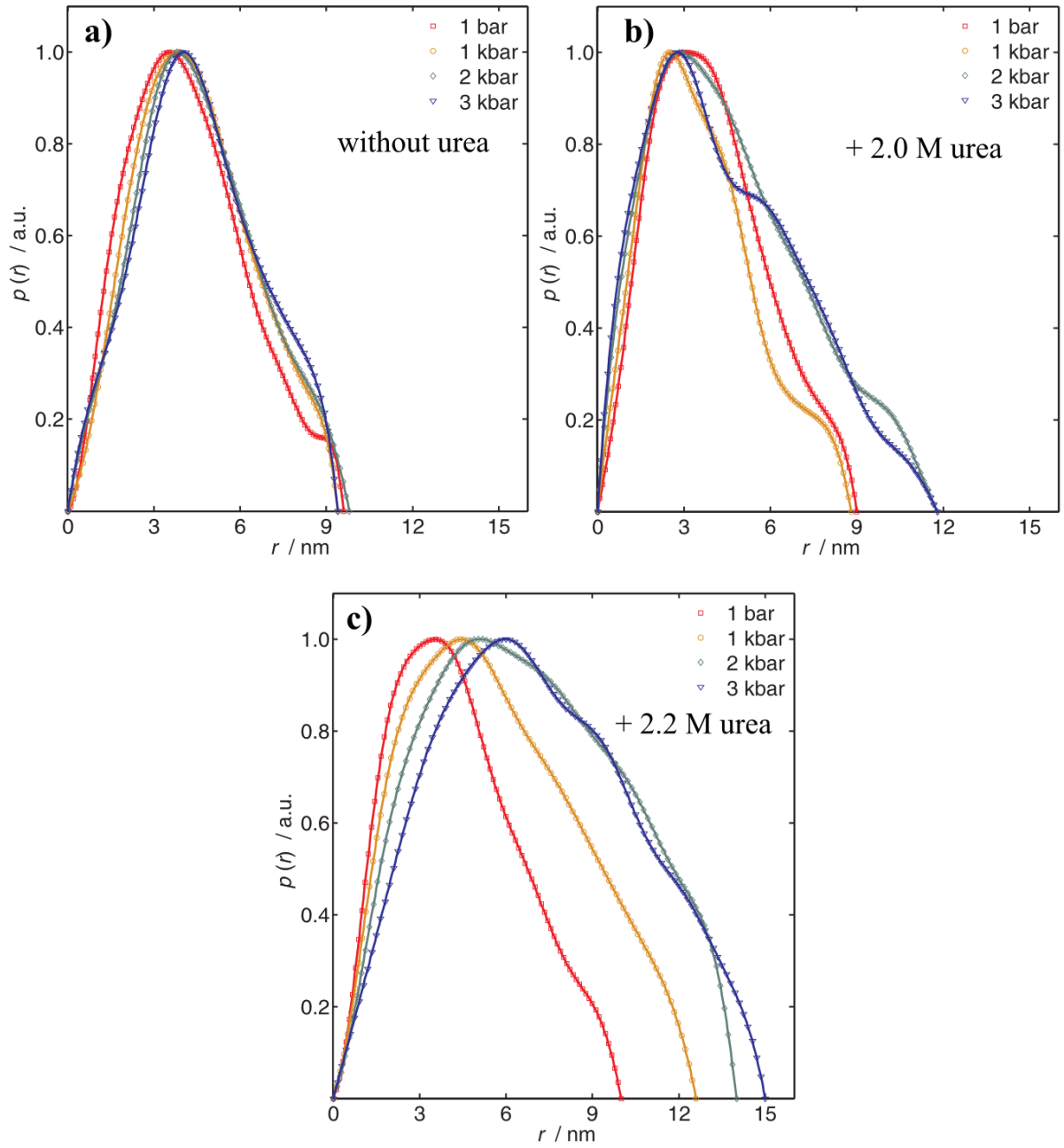

Figure 4.20: *Radial pair-distance distribution function p(r) of the ankyrin repeat domain of the Notch receptor as a function of pressure for different urea concentrations. a) In pure buffer solution. b) In buffer solution with 2.0 M urea added. c) In buffer solution with 2.2 M urea added.*

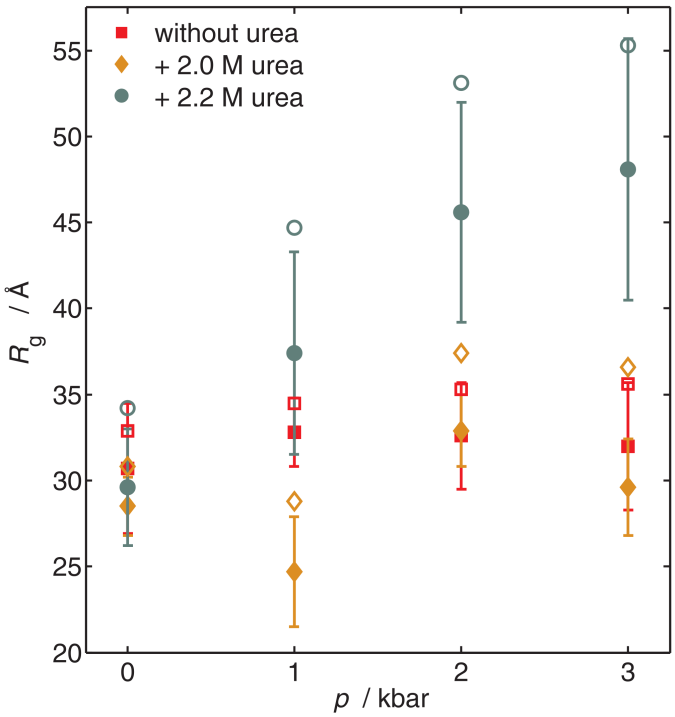

Figure 4.21: *Radius of gyration, R_g, of the ankyrin repeat domain of the Notch receptor as a function of pressure for different urea concentrations. Full symbols mark results obtained using the Guinier approximation, open symbols those obtained using $p(r)$.*

is in accord herewith. The change with pressure might be the indication of a slight compaction particular to its structural flexibility.

For the repeat protein in 2.0 M urea solution a somewhat more compact structure is present at 1 bar and 1 kbar (D_{max} between 88 to 90 Å). For higher pressures, the protein becomes unfolded as the $p(r)$ function becomes much broader ($D_{max} = (118 \pm 3)$ Å). This result corresponds to the finding of the analysis of the Kratky plot. Increasing the urea content to 2.2 M leads to even broader curves. Already at 1 kbar, the shape of the $p(r)$ is indicative of unfolding. Increasing pressure leads to an even larger extent. Care should be taken with the exact value of these special curves as the determination of $p(r)$ depends on the accessible q-range as described above. However, the general trend of this result is obvious.

This can be also seen when looking at the different radii of gyration as a function of pressure (Fig. 4.21). Herein, the R_g were determined using the Guinier approximation (eq. (2.55), full symbols) as well as employing $p(r)$ and eq. (2.56)(open symbols)[4]. For

[4]The experimental error for the Guinier analysis results was obtained by variation of the q-range used for the linear regression in the corresponding ($\ln I(q)$ vs. q^2) plot. For the determination of R_g via the radial pair-distance distribution function no proper criterion for a reliable error calculation was found. However, it is reasonable to assume that it is of the same order than that of the Guinier analysis.

all data points shown, the result of the Guinier analysis is always smaller than that of the other approach. Taking into account the previous comment on determination of $p(r)$, this deviation is not surprising. However, the general trends as well as the order of the R_g value are similar.

For the protein in pure buffer there is no change of the radius of gyration as a function of pressure present within the experimental error (R_g between 30.7 to 32.8 Å). Addition of 2.0 M urea has only a small effect on the R_g value. For $p = 1$ kbar only a deviation between the size in pure solution is present indicating possible slight structural changes. For 2.2 M urea in solution a significant pressure dependence is detectable. Starting with $R_g = (29.6 \pm 3.4)$ Å at ambient pressure, at 3 kbar a value of $R_g = (48.1 \pm 7.6)$ Å. Thus, in terms of the radius of gyration an increase of the structural size is seen for the 2.2 M urea solution but not for 2.0 M.

The presented SAXS study on the ankyrin repeat domain of the Notch receptor was conducted to study the combined effects of urea and high pressures on the protein's plasticity and thus its hydration. The findings can be summarized as follows. For the protein in pure buffer solution, no unfolding is detectable. Only some possible minor structural changes might be present as indicated by the radial pair-distance distribution function. Notable, at ambient pressure, the non-globular structure is detectable in the SAXS signal.

A 2.0 M urea solution destabilizes the protein and leads to pressure-induced unfolding. This sets in at a pressure of 2 kbar as is reflected by the corresponding Kratky plots and the $p(r)$ function. However, no increase in the radius of gyration as a function of pressure is found.

Addition of slightly more urea (2.2 M) induces more structural changes. When looking at the Kratky plots no clear conclusion of the folding state can be given as neither a maximum nor a plateau are unambiguously detectable. The refinement is complicated by the small q-range present. This has to be kept in mind, when interpreting the results on the $p(r)$ curves. However, as a general trend unfolding already at 1 kbar can be found. This is also in account with the pressure dependence of the radius of gyration for this urea concentration. Thus, the SAXS data reveals different folding states for the ankyrin repeat protein induced by a slight change in urea concentration.

4.4.3 Discussion and Conclusion

The previously presented SAXS measurements were part of a collaboration. Within this different experimental techniques were used to study the influence of high pressures on the ankyrin repeat domain of the *Drosophila* Notch receptor. In the present section the results of the other techniques (fluorescence spectroscopy, Fourier transform infrared (FTIR) spectroscopy) will shortly be summarized and discussed together with the SAXS data. More details about these techniques and the data analysis can be found in the corresponding publication (see [Rouget et al., 2010]).

The fluorescence spectroscopy measurements probed the pressure dependence (0 - 3.5 kbar) of the average wavelength of the fluorescence signal of the single tryptophan (Trp) residue as a function of urea concentration and temperature. For urea concentrations within 1.9 to 2.4 M, a pressure-induced red shift of the fluorescence emission showing a plateau value was observed for different temperatures (12 °C, 20 °C, 25 °C) indicating unfolding. Notable, this plateau significantly depends on the urea concentration. Increasing the amount of this destabilizing cosolvent is accompanied by a stronger red shifted emission plateau value. This indicates an enhanced degree of solvent accessibility of the Trp residue. For the largest urea concentration studied the same average wavelength was obtained as for a fully solvent accessible tryptophan moiety [Rouget et al., 2010]. The complete analysis of this data shows that the pressure-induced unfolding of the ankyrin repeat domain is a two state folding process. The volume of unfolding, i.e. the volume difference between the folded and the unfolded state does not depend on the urea concentration. Finally, a pressure-temperature phase diagram similar to that of globular proteins (see Fig. 4.3) is present [Rouget et al., 2010].

The FTIR spectroscopy measurements probed the dependence of the secondary structure elements on pressure and urea concentration. For pure buffer solution an about 25 % loss of α helical content was found over a pressure range from 2.5 to 6 kbar indicating unfolding. As the SAXS measurements were only performed up to a pressure of 3 kbar, no pressure-induced unfolding was detectable with that technique for the protein in buffer solution. For a 2.0 M urea concentration a decrease of the same amount of helical content was found already at lower pressures (within 1.5 - 4.5 kbar). Increasing the amount of urea to 2.35 M, a decrease of secondary structure elements was already present at ambient pressure. Increasing the pressure to $p = 4$ kbar results in a 35 % loss of α helical content. Even though pressure decreases the amount of secondary structure elements in the repeat protein in presence of urea, this effect is not as strong as that on the tertiary structure as revealed by SAXS and fluorescence spectroscopy. With these techniques, a larger increase of the radius of gyration and a fully exposed Trp residue were detected. Therefore, the FTIR results indicate residual secondary structure also at high pressure conditions [Rouget et al., 2010].

In order to access information also on kinetics and thus on the transition state ensemble (TSE) of the repeat protein, also pressure-jump studies were performed from the collaborators. The pressure-induced unfolding process can be described as a single relaxation process indicative for two-state folding. The result of this study is that for low temperatures ($T = 12$ °C) the volume of the TSE is much closer to the folded state than to the unfolded. This indicates the presence of a dry molten globule state similar to that obtained for globular proteins. A more detailed analysis however shows that the thermal expansivity of the TSE is equal to that of the unfolded state. This means that the repeat protein's TSE resembles some features characteristic for the folded state and some for the unfolded state. This indicates that in the TSE a compact state similar to the folded one is present which however is lacking native contacts [Rouget et al., 2010]. This can be interpreted as a unique feature of this type of linear repeat protein.

In summary, the following findings of the repeat protein were obtained. In pure buffer, no pressure-induced unfolding is present for pressures smaller than 2.5 kbar. Addition of urea leads to pressure-induced unfolding. Notable, slight changes of the urea concentration from 2.0 M to 2.2 M have a significant effect on the unfolded state which becomes more expanded, possesses a fully exposed Trp residue, and has a decreased content of α helices. However, the volume change is unaffected by the amount of this destabilizing agent being solely attributed to the pressure-induced unfolding process, i.e. the collapse of void volumes which is independent of urea. A recent pressure study on variants of the repeat protein where different ankyrin repeats were deleted supports these findings [Rouget et al., 2011]. The effect of urea reflects the large plasticity of the unfolded state clearly seen by the complex results of the SAXS data. Similarly, the study on the kinetics reveals the high plasticity of the TSE.

Repeat proteins possess a linear architecture with a local topology, i.e. amino acids in close contact in the amino acid sequence are also close to each other in the folded state, which is different for globular proteins. Albeit this different structure, the presented high pressure study on the non-globular, linear repeat protein shows that it resembles general properties of a globular protein. However, also unique features of this class of macromolecules were found.

5 High pressure effects on protein-protein interactions

Interactions between proteins in solution play an essential role in nature, especially in living cells. In detail, the cell's cytosole is a highly concentrated solution containing many different types of macromolecules like proteins, lipid vesicles, ribosomes, or DNA molecules [Voet et al., 2006], occupying 20 - 30 % of the interior volume of the cell [Ellis, 2001]. Therein, protein concentrations up to 200 - 300 mg/mL are present [Ellis, 2001]. As a consequence, there is a large steric exclusion of the macromolecules within the cells. This macromolecular crowding affects the equilibria and rate constants of reactions of the macromolecules [Ellis and Minton, 2003, Hall and Minton, 2003]. For instance, the presence of large amounts of crowding agents induces refolding of denatured proteins [Ellis, 2001]. Thus, solely due to steric exclusion the properties of concentrated protein solutions are changed. More complex interactions at the different specific locations in the cell's interior give rise to the particular function of proteins. Notable, interactions between particularly unfolded proteins is also known to be essential for several severe diseases, such as the Alzheimer disease [Dobson, 2003, Selkoe, 2003].

Protein-protein interactions do not only play a crucial role in living organisms but give rise to a complex concentration - temperature phase diagram of protein solutions [Curtis and Lue, 2006]. Within this, different transitions are present such as gel transitions at high protein concentrations or metastable liquid-liquid phase separation. For instance, cooling down a homogeneous, concentrated protein solution or the addition of salts induces a phase separation into a highly concentrated protein solution which is immersed in a diluted one [Muschol and Rosenberger, 1997, Dumetz et al., 2008]. A detailed knowledge of a protein solution's concentration - temperature phase diagram is essential for protein crystallization as there is only a small fraction of the phase diagram where proper crystals can be obtained [Asherie, 2004, Curtis and Lue, 2006]. These are however necessary for the determination of the protein structure by diffraction measurements.

To access in a very simplified way these interactions between proteins in solution, different experimental and simulation studies have been performed. For instance, X-ray scattering techniques in combination with liquid state theory have been previously used

to study the interaction between proteins in solution. Small angle scattering on concentrated protein solutions has been shown to be a powerful tool to access the interaction between these macromolecules. As described in chapter 2.3, SAXS as well as SANS can be used to extract the interaction potentials of colloidal particles such as proteins. This approach was exploited largely exploring the interactions between different model proteins and the influences of several parameters.

For instance, the effects of temperature [Malfois et al., 1996, Bonnete et al., 1999], pH value [Boyer et al., 1999], different types and amounts of salts [Narayanan and Liu, 2003, Zhang et al., 2007] as well as cosolvents [Niebuhr and Koch, 2005, Javid et al., 2007b, Sinibaldi et al., 2007], and aggregation [Javid et al., 2007a, Stadler et al., 2010] were studied in great detail. Recently, it was shown that the addition of trivalent salts induces so-called reentrant condensation [Zhang et al., 2008, Zhang et al., 2010]. Using this special effect of that type of salts allowed to grow high quality crystals [Zhang et al., 2011]. Even the presence of protein clusters in solution was proposed [Stradner et al., 2004] which however is still a matter of debate [Shukla et al., 2008, Cardinaux et al., 2011, Liu et al., 2011].

Notable however, the effect of high pressure on the protein-protein interaction is largely unexplored [Ortore et al., 2009]. In order to shed more light on the effect of this thermodynamical parameter on concentrated protein solution, and thus modeling conditions met in organisms living in deep sea environments [Rothschild and Mancinelli, 2001, Daniel et al., 2006], SAXS measurements were performed. The results of these studies will be presented in this chapter.

In paragraph 5.1 the results of a SAXS study on the influence of high pressures on the protein-protein interaction in concentrated lysozyme solutions is given. The effect of different small biologically relevant molecules, so-called osmolytes, on the pressure-dependence is presented in paragraph 5.2.

5.1 Nonlinear pressure dependence of the interaction potential of concentrated lysozyme solutions

In the present section the results of SAXS measurements on concentrated lysozyme solutions will be discussed. This study was part of a collaboration between the groups of Prof. Tolan and Prof. Winter (both TU Dortmund). The results have been published as: M.A. Schroer, J. Markgraf, D.C.F. Wieland, Ch.J. Sahle, J. Möller, M. Paulus, M. Tolan, R. Winter (2011). Nonlinear Pressure Dependence of the Interaction Potential of Dense Protein Solutions. *Physical Review Letters* 106, 178102.

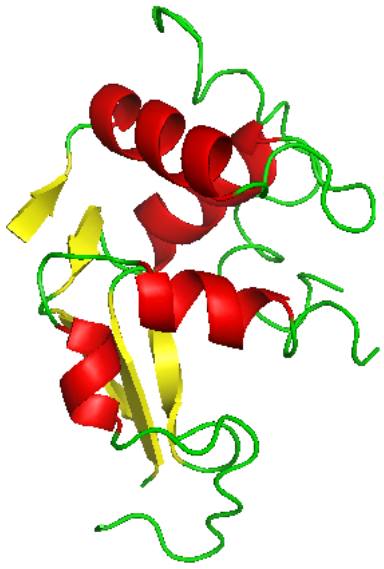

Figure 5.1: *Ribbon diagram of HEW lysozyme (pdb file 6LYZ [Diamond, 1974]) drawn by PyMOL [Schrödinger, LLC, 2008]. The β strains are shown in yellow, the α helices in red, and loose parts in green.*

The high pressure SAXS measurements were conducted at beamline BW4, HASYLAB, and ID02, ESRF. The experimental parameters of the two setups are given in Tab. 5.1. Owing to the different brilliances of the two beamlines, the exposure time at ID02 was significantly smaller. Using the high pressure sample cell, a pressure range from 1 bar to 4 kbar was covered in 500 bar steps. For the highest pressure conditions a pressure drop of about 0.1 kbar occurred within an exposure time of 20 min. SAXS measurements were performed at three temperatures (5 °C, 15 °C, 25 °C). Different protein concentrations were used to test the effect of pressure on the lysozyme structure and on the interactions between the macromolecules. The pH value was adjusted to pH 7 using concentrated hydrochloric acid. In order to keep the pH value constant also at high pressure conditions, a 25 mM bis-Tris buffer solution was used.

Lysozyme is a small protein serving as a bactericidal agent. It hydrolyzes the β-(1,4)

	BW4, HASYLAB	ID02, ESRF
detector	MARCCD165	FRELON CCD
number of pixels	2048 x 2048	1024 x 1024
wavelength λ / Å	1.381	0.995
exposure time / s	1200	0.05
q-range /nm^{-1}	0.3 - 2.9	0.2 - 3.2

Table 5.1: *Synopsis of the different parameters of the SAXS measurements at the two beamlines. Given are the type of area detector, the number of its pixels, the wavelength λ, the typical exposure time, and the accessible q-range.*

glycosidic bonds of the glycopeptides present in the bacterial cell walls thus leading to their osmotic collapse [Löffler et al., 2007]. It is present in many cells and in the secrets of vertebrates like tears, mucus, and saliva. Due to its high availability, the most widely studied lysozyme variant is that from hen egg white (HEW) [Voet et al., 2006]. This variant consists of 129 amino acids and has a molecular weight of $M_{\mathrm{W}} = 14.6$ kDa [Voet et al., 2006]. Its isoelectric point pI is 11 [Kuehner et al., 1999]. The ribbon representation is shown in Fig. 5.1 wherein its four α helices and three β sheets are visible. Notable, due to the presence of four disulfide bonds, lysozyme is a highly stable protein. The HEW lysozyme sample used for the whole SAXS study was purchased from Roche GmbH, Mannheim.

In order to check that no pressure-induced unfolding of the protein occurs, SAXS measurements on diluted lysozyme solutions ($c_{\mathrm{P}} = 5$ mg/mL) were performed for the whole pressure and temperature range covered. In Fig. 5.2 the results for a temperature $T = 25$ °C are shown exemplarily. The scattering curves were refined using the form factor of a prolate ellipsoid of revolution (eq. (2.35)). As is reflected by the scattering curves (Fig. 5.2a)) and the corresponding Kratky plots (Fig. 5.2b)), this geometrical model describes the data properly within the given q-range. Furthermore, no unfolding is present as can be seen on the radius of gyration, R_{g}, as a function of pressure (Fig. 5.2c)). Additional Fourier transform infrared (FTIR) spectroscopy measurements under the same solution conditions performed within the collaboration show no pressure-induced changes in the protein structure up to 5 kbar (for details, see [Schroer et al., 2011]). Fully unfolding of lysozyme has been reported to set in not until 7 kbar even at a low pH value of 2.0 [Maeno et al., 2009]. Thus, any change of the scattering curves for the concentrated solutions with pressure can be attributed to changes of the protein-protein interaction as unfolding has been ruled out.

The results of the measurements on a concentrated lysozyme solution ($c_{\mathrm{P}} = 100$ mg/mL) are depicted in Fig. 5.3. A pronounced correlation peak is visible which is attributed to the presence of a structure factor, $S(q)$. The solid lines are the fits to the data. The refinement was performed as follows.

The scattering curves were treated in the decoupling approximation (eq. (2.84)), i.e.

$$I(q) \propto P(q) + \langle F(\vec{q}) \rangle_{\Omega}^{2} \cdot (S(q) - 1) \ . \tag{5.1}$$

Therein, the form factor $P(q)$ of the protein was approximated by that of a prolate ellipsoid of revolution (eq. (2.35)) which is a good assumption as can be seen on Fig.

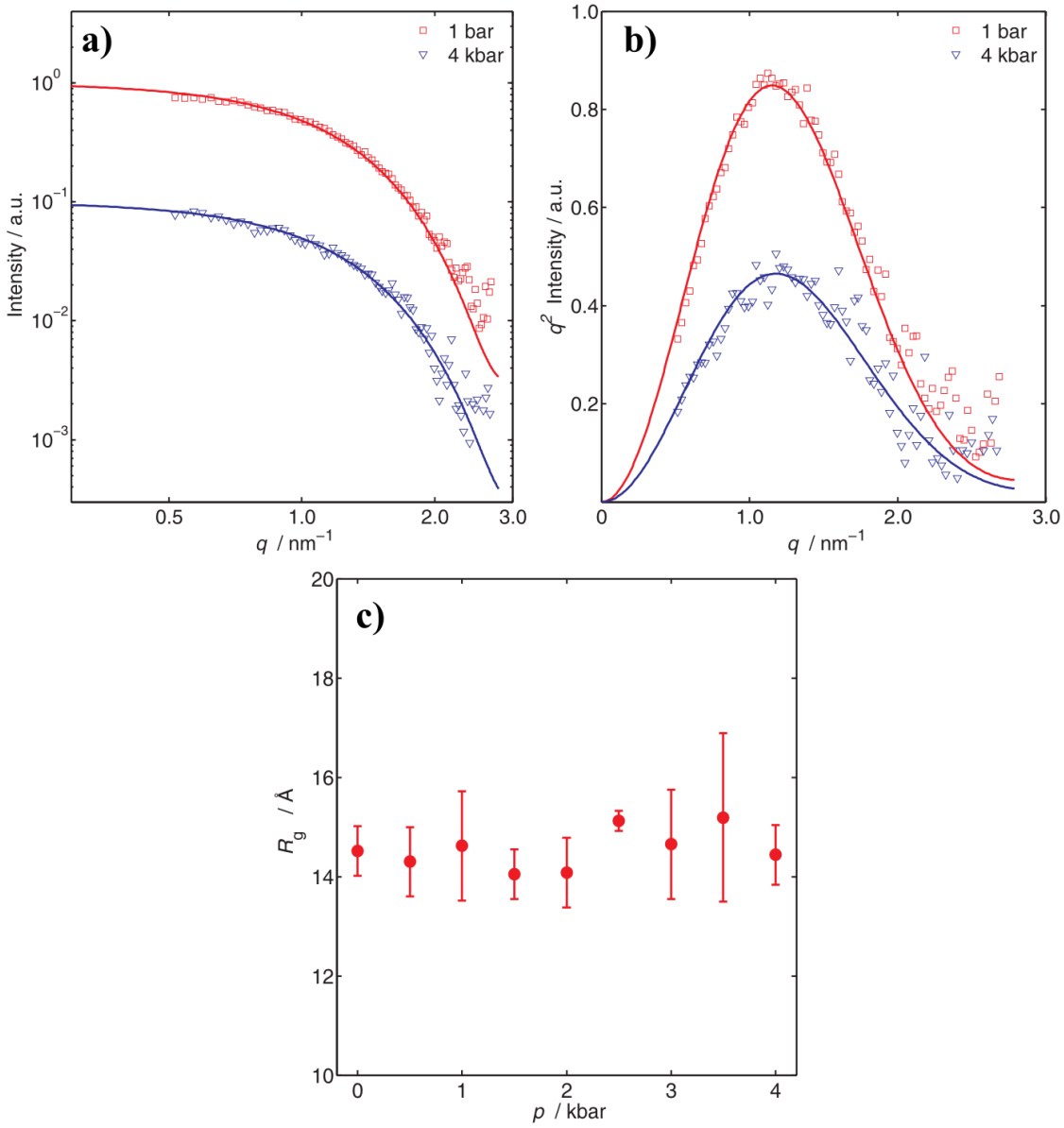

Figure 5.2: *Results of small angle X-ray scattering on a diluted lysozyme solution (c_P = 5 mg/mL) at T = 25 °C as a function of pressure. a) SAXS curves in double logarithmic representation. b) Kratky plot. Solid lines are refinements to data using the form factor of a prolate ellipsoid of revolution. Refinement parameter: R_g = 14.7 Å, a = 15.0 Å(1 bar). R_g = 14.5 Å, a = 14.5 Å(4 kbar). It was averaged over 3 data points. c) Radius of gyration, R_g, as a function of pressure. No pressure-induced unfolding is present.*

5.2. Furthermore, for this geometrical body the term $\langle F(\vec{q})\rangle_\Omega$ can be written explicitly as

$$\langle F(\vec{q})\rangle_\Omega = \int_0^1 F_\mathrm{S}(q\sqrt{a^2 + x^2 \cdot (b^2 - a^2)})\; dx \tag{5.2}$$

wherein F_S is defined as in eq. (2.33)[1]. Refinement parameters were the radius of gyration, R_g, and the minor semiaxis, a, which were determined as $R_\mathrm{g} = (14.8 \pm 0.5)$ Å and $a = (15.5 \pm 0.5)$ Å, respectively. Using eq. (2.59), the major semiaxis is $b = (24.4 \pm 1.6)$ Å and thus the total volume $V = \frac{4\pi}{3}a^2 b = (255.3 \pm 23.6)$ Å^3.

To extract the interaction potentials from the scattering curves, the structure factor was modeled by a DLVO potential in mean spherical approximation (MSA) using the MATLAB® code of [Liu et al., 2005] for a 2-Yukawa type potential which is available from the authors (for details on the different types of interaction potentials and closure relations see chapter 2.3). Recalling the repulsive, screened Coulomb part, $V_\mathrm{C}(r)$, and the attractive, van der Waals-like parts, $V_\mathrm{vdW}(r)$, of the DLVO potential, and keeping in mind the hard sphere repulsion, these are given for $r > \sigma$ as

$$V_\mathrm{C} = \frac{e^2}{4\pi\epsilon_0\epsilon_\mathrm{r}} \; \frac{Z^2}{\left(1 + 0.5\frac{\sigma}{\lambda_\mathrm{D}}\right)^2} \frac{\exp\left(-\frac{r-\sigma}{\lambda_\mathrm{D}}\right)}{r} \tag{5.3}$$

and

$$V_\mathrm{vdW} = -J \cdot \sigma \; \frac{\exp\left(-\frac{r-\sigma}{d}\right)}{r} \; . \tag{5.4}$$

Therein, besides the elementary charge e and the vacuum permittivity ϵ_0 which are constants, different parameters are present which were treated as follows for the refinement process.

The dielectric number of the solution, ϵ_r, and thus the Debye screening length, λ_D, depend on the solutions properties. For ϵ_r the pressure dependence of water at $T = 25$ °C was used which is given in reference [Floriano and Nascimento, 2004]. This was also used for λ_D taking into account also the number of ions in the solution due to the buffer salt.

The protein's effective charge Z was set to 8 which corresponds to the value for pH 7 obtained previously [Kuehner et al., 1999]. Z was assumed to be constant within the

[1]Note the different order of integration and squaring between $P(q)$ and $\langle F(\vec{q})\rangle_\Omega^2$.

pressure range studied as the pH value does not change using a pressure-insensitive buffer solution.

The protein's diameter σ and the range of attraction d were refined for the whole data set. The values used are $\sigma = (29.9 \pm 0.5)$ Å and $d = (2.7 \pm 0.2)$ Å. Thus, the only free parameter that was used for the refinement of each data set was the strength of attraction J. With this approach, the SAXS curves can be properly described (Fig. 5.3a)).

A detailed inspection of the scattering data shows a slight shift of the correlation peak with increasing pressure up to 2 kbar to higher q values. Such a monotonic shift with pressure was reported previously for pressure up to 1.5 kbar [Ortore et al., 2009]. By further increasing the pressure, this effect is inverted. This can be seen better when plotting the position of the correlation peak, q_{corr}, as a function of pressure in Fig. 5.3b). q_{corr} is related to the inverse of the average distance between the proteins in solution. Thus, for pressures below 2.0 kbar the increase of q_{corr} reflects the compression of protein solution. At higher pressures, the average distance becomes larger again as the pressure rises. As the form factor does not change with pressure, this finding is attributed to differences in the structure factor. Therefore, $S(q)$ as obtained from the refinement is shown in Fig. 5.3c) for selected pressures. Pressure-induced changes can be seen on the peak position and height of the first two peaks. To show the effect of pressure more clearly, the difference $\Delta S(q) = S(q)_{\mathrm{p}} - S(q)_{1\mathrm{bar}}$ is depicted in Fig. 5.3d). The typical error for the whole data is shown by three errorbars exemplarily. These were obtained by calculating the difference between two data sets of the same sample solution obtained on the two different beamlines. Although the pressure-induced effects are small, the nonmonotonic pressure dependence reflected by the $\Delta S(q)$ curves is larger than the statistical error between two independent measurements.

With the approach used it is possible to obtain the pressure-dependent interaction potential between the lysozyme molecules in solution. In Fig. 5.4a) a typical interaction potential $V(r)$ is depicted together with the different contributions to it. Especially the meaning of the strength of attraction J can be seen, i.e. the depth of the attractive part of the interaction potential close to the protein surface.

As all parameters of the repulsive part of the interaction potential either are independent of pressure (σ, Z) or show a monotonic dependence (ϵ_{r}, λ_{D}), the nonlinear pressure effect is solely due to changes of the attractive part. More precisely, as the range of attraction d is assumed to be constant, it is the strength of attraction J that gives rise to the pressure dependence. This is shown in Fig. 5.4b) for three different temperatures. With increasing pressure, J decreases until a pressure of 1.5 - 2.0 kbar is reached. A further rise in pressure leads to an increase of J. Thus, a minimum in

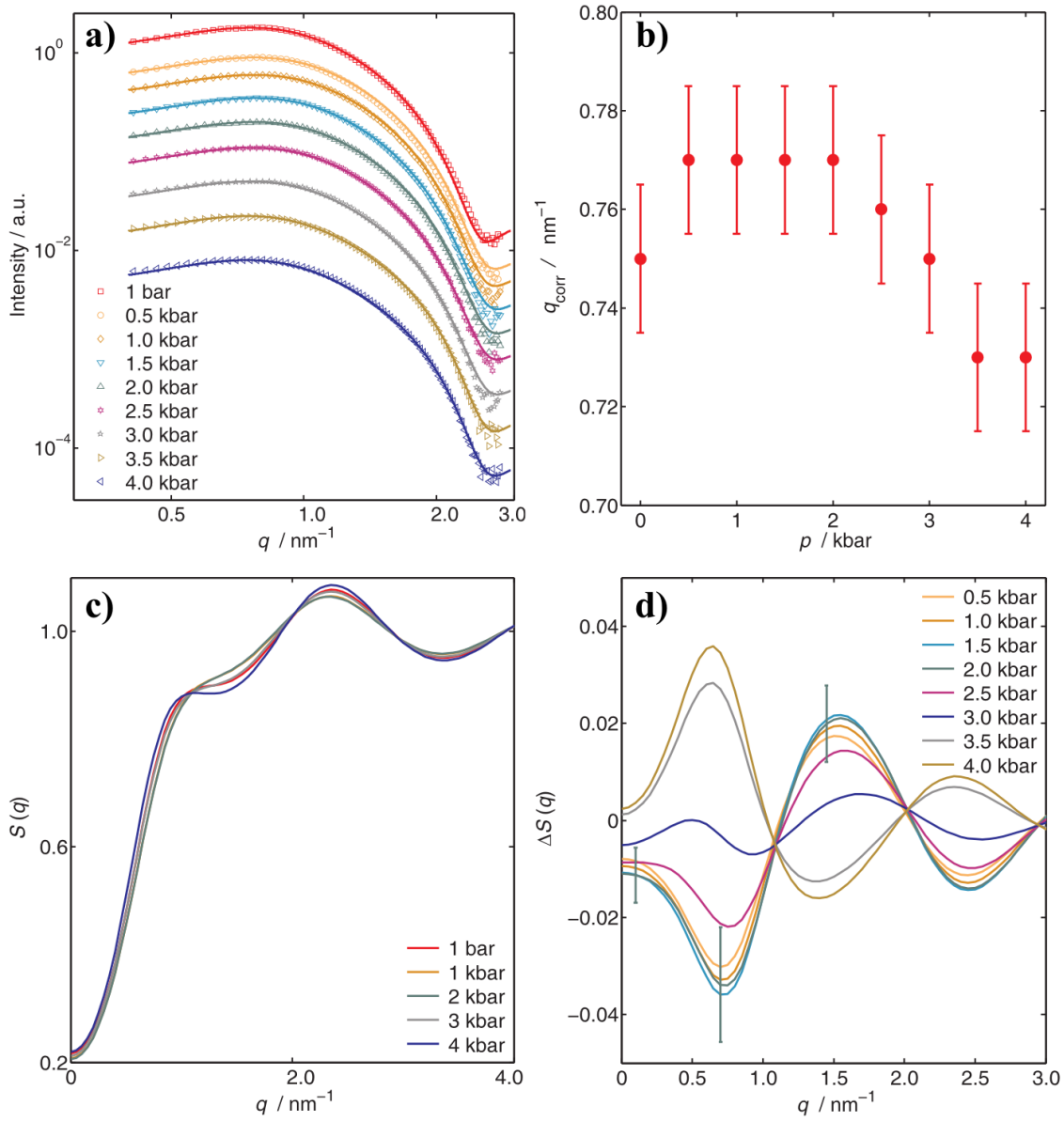

Figure 5.3: *Results of SAXS measurements on a concentrated lysozyme solution (c_P = 100 mg/mL) as a function of pressure for T = 25 °C. a) SAXS curves in double logarithmic representation. Solid lines are refinements to the data. It was averaged over 3 data points. b) Position of the correlation peak, q_{corr}, as a function of pressure. c) Structure factor, $S(q)$, obtained from the refinement. d) Difference $\Delta S(q) = S(q)_p - S(q)_{1bar}$.*

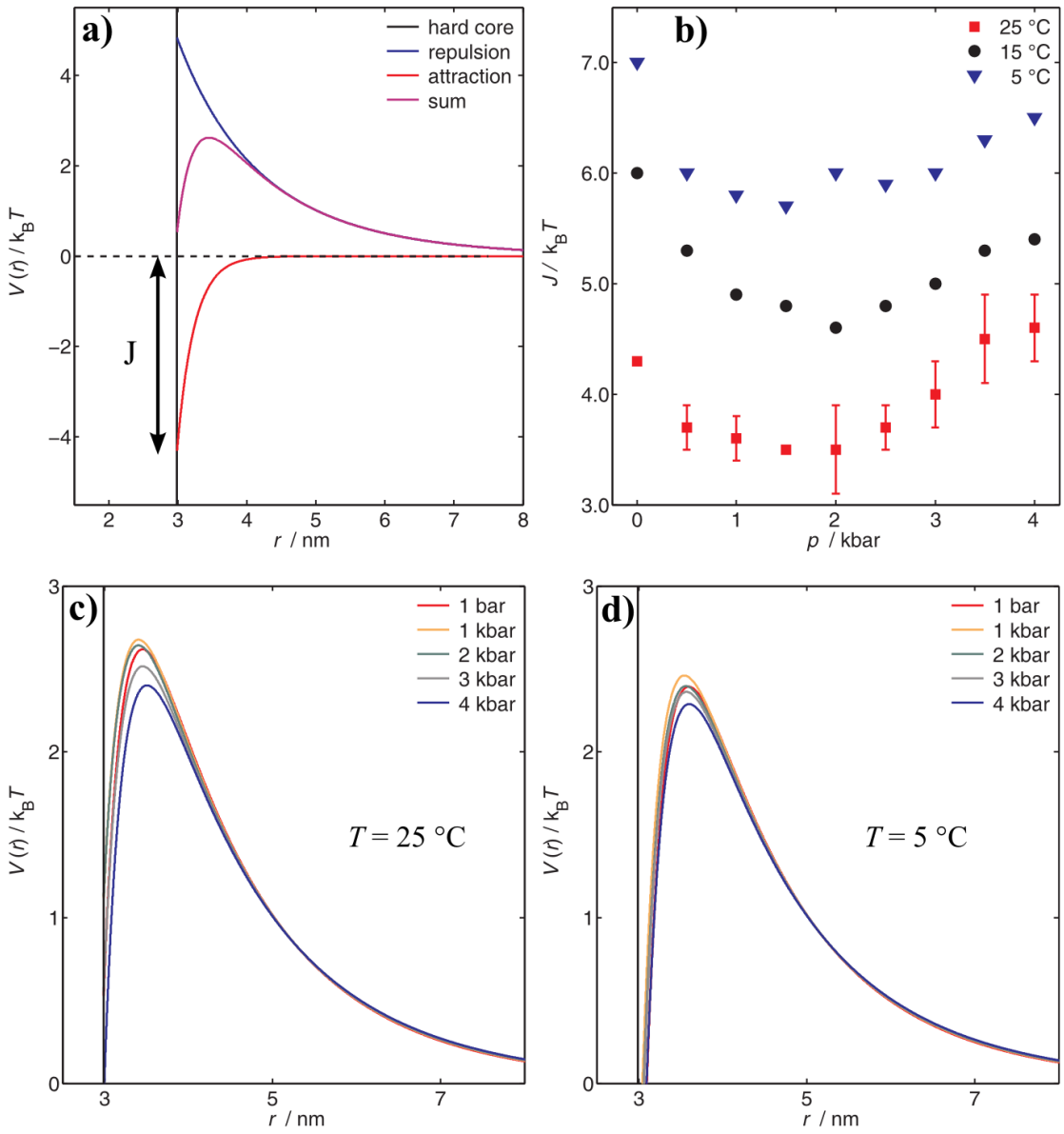

Figure 5.4: *a) Schematic drawing of the different contributions to the interaction potential. b) Strength of attraction, J, for $c_P = 100$ mg/mL for different temperatures as a function of pressure. Pressure dependent interaction potential for c) $T = 25\,^{\circ}C$ and d) $T = 5\,^{\circ}C$. Straight black lines mark the hard core repulsion.*

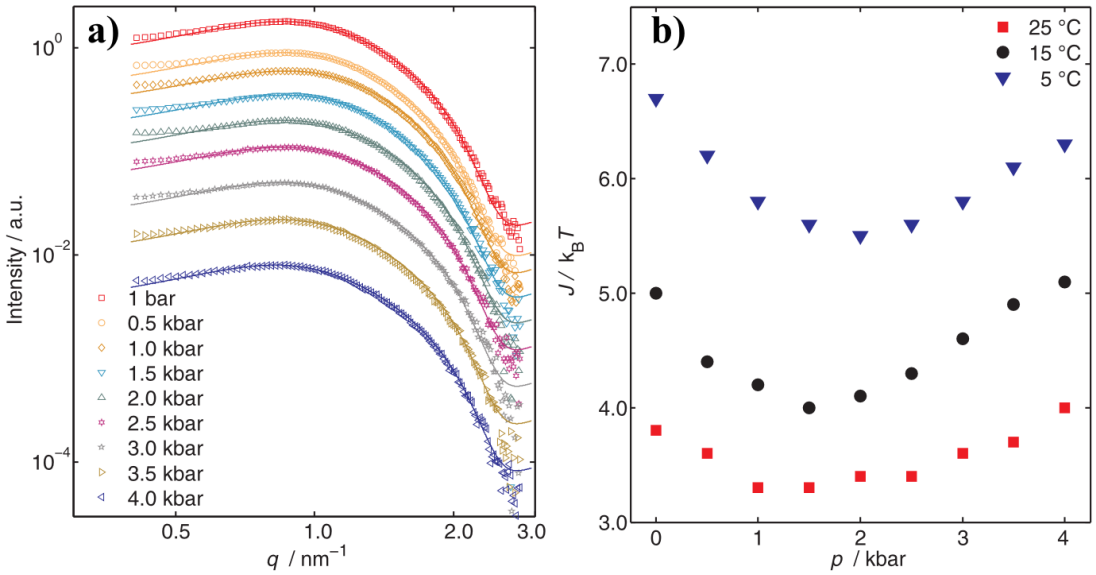

Figure 5.5: *Results of a 200 mg/mL lysozyme solution at $T = 25$ °C as a function of pressure. It was averaged over 3 data points. a) SAXS curves with corresponding refinements (solid lines). b) Strength of attraction, J, for different temperatures as a function of pressure.*

the pressure-dependent J curves is present reflecting the nonlinear influence of pressure. Decreasing the temperature results in an increase of the intermolecular attraction of the proteins. This temperature dependence is in accord with previous measurements at ambient pressure [Shukla et al., 2008]. The maximal error in J is given by the direct comparison of the results of the SAXS data obtained on two different beamlines.

The effect of pressure on the total intermolecular potential $V(r)$ for the highest ($T = 25$ °C) and the lowest ($T = 5$ °C) temperatures measured is shown in Fig. 5.4c) and d). For $T = 25$ °C the application of pressure results in a slight increase of the repulsion barrier, i.e. the maximum of $V(r)$ for $r > \sigma$, up to 1.0 kbar. Further increasing the pressure leads to a slight reduction of the repulsion barrier. Decreasing the temperature down to $T = 5$ °C reduces the repulsion barrier as J becomes larger. A similar pressure-dependence as for the higher temperature is present.

SAXS measurements were also performed on higher protein concentrations ($c_P = 200$ mg/mL). The resulting scattering curves are shown in Fig. 5.5a). Increasing the protein amount within the solutions leads to a shift of the correlation peak from $q_{corr} = (0.750 \pm 0.015)$ nm^{-1} to $q_{corr} = (0.850 \pm 0.015)$ nm^{-1} at ambient pressure. This is due to the higher protein density leading to a decrease of the average protein-protein distance. Furthermore, a slight decrease of strength of attraction, J, is accompanied by the higher concentration. Such a type of decrease of protein attraction was reported previously [Malfois et al., 1996]. The pressure-dependence is similar to that of the lower concentrated solution (Fig. 5.5b)).

5.1.1 Discussion

The SAXS data presented exhibit a nonlinear pressure dependence of the protein-protein interaction in concentrated lysozyme solutions. Up to pressures of 1.5 - 2.0 kbar the interaction becomes more repulsive. Raising the pressure furthermore leads to an increase of the attraction again, i.e. a minimum of the attraction strength J is present. This occurs for the whole temperature and concentration range studied. To determine the underlying mechanism of this pressure dependence one has to note that structural changes of the protein as well as of the protein's effective charge can be ruled out. No unfolding of lysozyme was observed for all solution conditions studied as is reflected by the form factor and FTIR measurements [Schroer et al., 2011]. Furthermore, as a pressure-insensitive buffer solution was used, no change of the pH value and thus of the protein's charge Z should have happened. In addition, all pressure dependencies of the solutions properties were taken into account (ϵ_r, λ_D). Therefore, one is left with the pressure dependence of the water structure and its influence on the protein-protein interaction.

Different transport properties of water have been shown to change nonmonotonically with pressure. For instance, the diffusion coefficient of water shows a maximum at 2 kbar [Ludwig, 2001] and the shear viscosity a minimum at 1 - 2 kbar [Debenedetti, 2003]. Similarly, a minimum at 2 kbar was found in the stretching band maximum of liquid water by Raman spectroscopy measurements [Sun et al., 2003] corresponding to the behavior of the oxygen-oxygen distance r_{OO} at high pressure [Okhulkov et al., 1994]. These results indicate the presence of structural changes of water close to 2 kbar. More precisely, diffraction measurements revealed a volume reduction in water caused by a rapid and monotonic increase in the coordination number starting at 2 kbar, from 4 to 6.5 at 5 kbar, which can be attributed to the penetration of non-hydrogen bonded water molecules into the first hydration shell [Soper and Ricci, 2000, Weck et al., 2009, Katayama et al., 2010].

These structural changes in the kbar pressure range seem to coincide with the observed nonlinear pressure response of the protein-protein interaction potential $V(r)$. At pressures below about 2.0 kbar, pressure leads to a reduction of the intermolecular distances resulting in a decrease of J. Beyond this pressure threshold, the high-density structure and concomitant increased hydration repulsion of water may lead to the effective small increase of J and the slight increase of intermolecular distances. Thus, the collapse of the second hydration shell of water, i.e. the breaking of hydrogen bonds between the first and the second shell and changes in the coordination number, starting at about 2 kbar,

is reflected by pressure-dependence of the solvent mediated protein-protein interaction potential.

To clarify this interpretation of the SAXS results, additional measurements on protein solutions with different cosolvents added which alter the water structure should show a different effect of the pressure-depend interactions. Such measurements were performed using small biologically relevant molecules, so called osmolytes, and will be presented in the next section.

5.2 Effects of osmolytes on the pressure-dependent interactions

Organisms living in deep sea regions have to cope with the high pressure conditions up to 1 kbar [Daniel et al., 2006]. In particular, mechanisms have been evolved to protect the organisms' proteins against pressure-induced unfolding. Therefor, small organic molecules, so-called osmolytes are accumulated in their cells. Among these are amino acids, polyols and sugars (e.g., glycerol and trehalose), methylamines such as trimethylamine-N-oxide (TMAO), and urea [Yancey et al., 2002, Yancey, 2005]. For instance, TMAO has been found to enhance protein folding most efficiently. For example, its presence induces folding of the natively unfolded staphylococcal nuclease variant T62P [Baskakov and Bolen, 1998a] and inhibits pressure-induced unfolding of the wild type protein [Krywka et al., 2008]. In contrast, urea is a highly concentrated waste product in mammalian kidneys and destabilizes proteins. Both osmolytes, TMAO and urea, are present in marine elasmobranch fishes, like sharks and rays [Yancey et al., 2002, Yancey, 2005]. Notable, the osmolyte concentration was found to increase as a function of ocean's depth [Yancey et al., 2002, Yancey, 2005]. TMAO has been found to counteract the perturbations imposed by urea and hydrostatic pressure in deep-sea animals, most effectively at a 2:1 urea:TMAO ratio [Zou et al., 2002, Bennion and Daggett, 2004].

Different types of experimental and computer simulation studies have proposed that TMAO influences the local water structure which is assumed to be the underlying mechanism for its stabilizing effect [Bennion and Daggett, 2004, Paul and Patey, 2007, Panuszko et al., 2009, Wei et al., 2010]. As was shown in the previous chapter about high pressure effects on concentrated lysozyme solutions, the water mediated protein-protein interaction was largely affected by pressure. The collapse of the second hydration shell was proposed to be the reason of the nonlinear pressure dependence. As TMAO might affect the water structure, this should be manifested in a change of the pressure-dependent interaction potential. Moreover, concentrated protein solutions with different cosolvents added under high pressure conditions serve as model systems to study the protein-protein interaction present, for instance, in cells of deep sea organisms.

Due to this, high pressure SAXS experiments were conducted on concentrated lysozyme solutions. The cosolvents added are trimethylamine-N-oxide (TMAO, C_3H_9NO), urea (CH_4N_2O), and glycerol ($C_3H_8O_3$) (Fig. 5.6). The study was performed within a collaboration between the groups of Prof. Tolan and Prof. Winter (both TU Dortmund). The presented study will be published as: M.A. Schroer, Y. Zhai, D.C.F. Wieland, Ch.J. Sahle, J. Nase, M. Paulus, M. Tolan, R. Winter (2011). Exploring the Piezophilic Behavior of Natural Cosolvent Mixtures. *Angewandte Chemie International Edition.*

High pressure SAXS measurements on concentrated lysozyme solutions with differ-

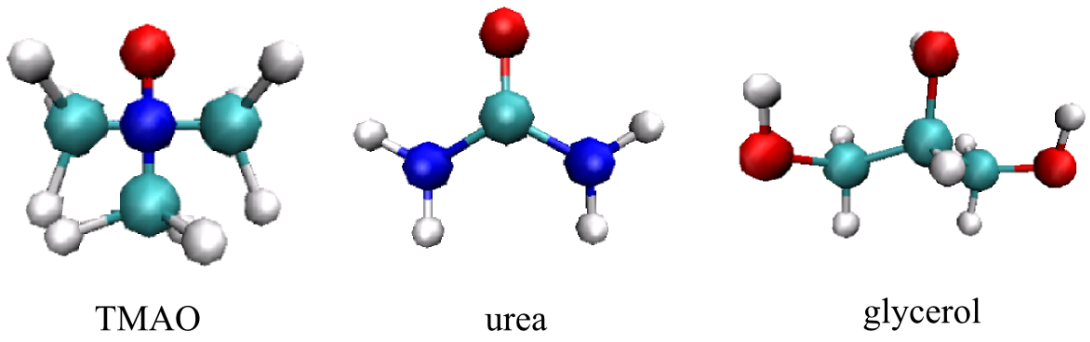

Figure 5.6: *Representation of the different cosolvents used, trimethylamine-N-oxide (TMAO), urea, and glycerol, drawn by VMD [Humphrey et al., 1996]. White balls represent hydrogen atoms, red ones oxygen, turquoise ones carbon, and blue ones nitrogen.*

detector	MARCCD165
number of pixels	2048 x 2048
wavelength λ / Å	1.381
exposure time / s	600
q-range /nm^{-1}	0.3 - 2.8

Table 5.2: *Experimental parameters of the SAXS setup used at beamline BW4, HASYLAB.*

ent osmolytes added were performed on beamline BW4, HASYLAB. The experimental parameter are given in Tab. 5.2. The high pressure equipment was used as described previously (see chapter 5.1). In a 25 mM bis-Tris buffer solution (pH 7.0), appropriate amounts of trimethylamine-N-oxide (TMAO), urea, and glycerol were dissolved to obtain solutions with cosolvent concentration, c_S, of 0.25 M, 0.5 M, and 1.0 M, respectively. In addition, different TMAO-urea mixtures and TMAO-glycerol mixtures were prepared. A summary of these is given in Tab. 5.3.

As was shown in the previous section, lysozyme dissolved in pure buffer solution does not unfold within the pressure range studied. In order to check that this is also the case when osmolytes are added to the solution, diluted protein solutions (c_P = 10 mg/mL) were studied. Especially the highest urea concentration used (c_S = 1.0 M) needs to be analyzed as this substance destabilizes proteins. The results of SAXS measurements on TMAO and urea (both c_S = 1.0 M) are depicted in Fig. 5.7. For both protein solutions no pressure-induced unfolding is detectable. The data can be refined using the form factor of a prolate ellipsoid of revolution similar to that obtained for pure buffer.

As no unfolding occurred for any of the cosolvents added, the SAXS curves obtained for concentrated lysozyme solutions (c_P = 100 mg/mL) could be analyzed using the similar approach as for the protein in pure buffer solution (chapter 5.1). A notable difference is the use of the proper dielectric numbers ϵ_r for the osmolyte solutions. These were measured separately and are given in Tab. 5.3. For the pressure dependence

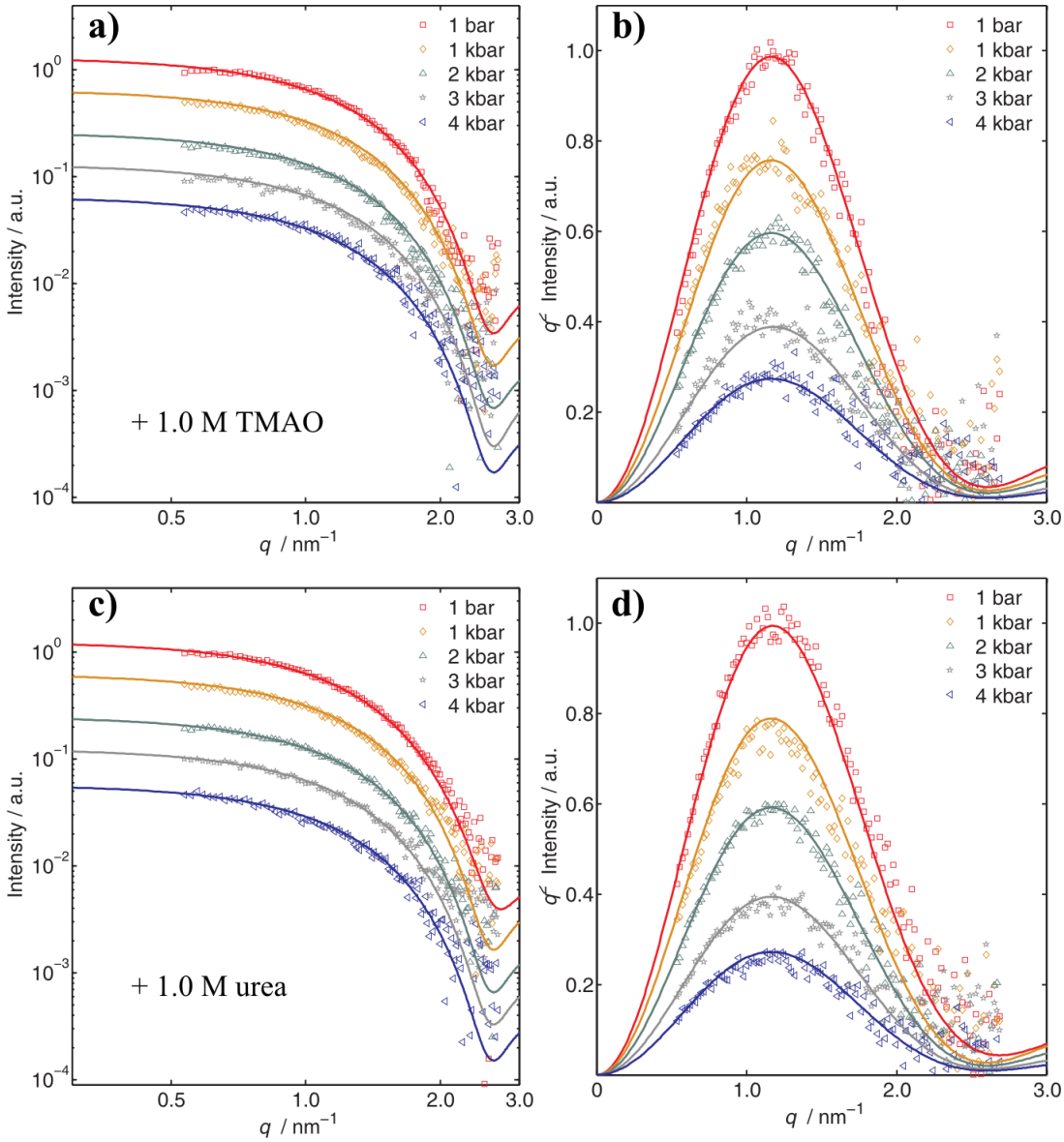

Figure 5.7: *Results of small angle X-ray scattering on a diluted lysozyme solution (c_P = 10 mg/mL) at T = 25 °C as a function of pressure for different cosolvents. a) With 1.0 M TMAO added (double logarithmic representation). b) Corresponding Kratky plot. c) With 1.0 M urea added (double logarithmic representation). d) Corresponding Kratky plot. Solid lines are refinements to the data employing the form factor of a prolate ellipsoid of revolution. It was averaged over 3 data points. No pressure-induced unfolding is present.*

cosolvent	ϵ_r
250 mM TMAO	77.39
500 mM TMAO	76.22
1.0 M TMAO	73.88
250 mM urea	79.26
500 mM urea	79.69
1.0 M urea	81.01
250 mM glycerol	78.48
500 mM glycerol	77.81
1.0 M glycerol	76.54
125 mM T + 500 mM U	73.67
250 mM T + 500 mM U	77.35
500 mM T + 500 mM U	71.06
250 mM T + 250 mM U	76.29
125 mM T + 125 mM U	76.76
250 mM T + 125 mM U	76.54
500 mM T + 125 mM U	73.56
500 mM T + 250 mM G	77.89
250 mM T + 250 mM G	76.94
250 mM T + 500 mM G	76.45

Table 5.3: *Experimentally obtained dielectric numbers, ϵ_r, of the osmolyte solutions. Herein, "T", "U", and "G" denote TMAO, urea, and glycerol. The typical error is 0.40.*

of ϵ_r a similar relation as for pure water was used [Floriano and Nascimento, 2004]. In addition, corrections to the calculated Debye screening length, λ_D, were needed to obtain proper refinements to the experimental data. Besides of this, the same parameters as for the pure buffer solutions were used, i.e. $Z = 8$, $\sigma = (29.9 \pm 0.5)$ Å, and $d = (2.7 \pm 0.2)$ Å.

Exemplary results of SAXS measurements on concentrated lysozyme solutions with different osmolytes as a function of pressure are shown in Fig. 5.8, together with the refinement to the data. In Fig. 5.8a) the scattering curves of the protein solution with 1.0 M TMAO added is depicted. The pronounced correlation peak due to the presence of a structure factor reflecting strong protein-protein interactions is visible. With increasing pressure up to about 2.5 kbar, a slight shift of the position of the correlation peak q_{corr} to higher q values is present. A further pressure increase reverses this effect to some extent. This reversal is however smaller than that for the pure buffer solution. The structure factors $S(q)$ were obtained from refinement. To highlight the pressure induced changes, the differences $\Delta S(q)$ introduced in the previous section are shown in Fig. 5.8b). The effect for pressures up to 2.5 kbar is much stronger than that of pressures beyond this threshold.

In the case of the chaotropic cosolvent urea ($c_S = 1.0$ M), the influence on the pressure-dependent protein-protein interaction is different (5.8c), d)). $\Delta S(q)$ shows a biphasic

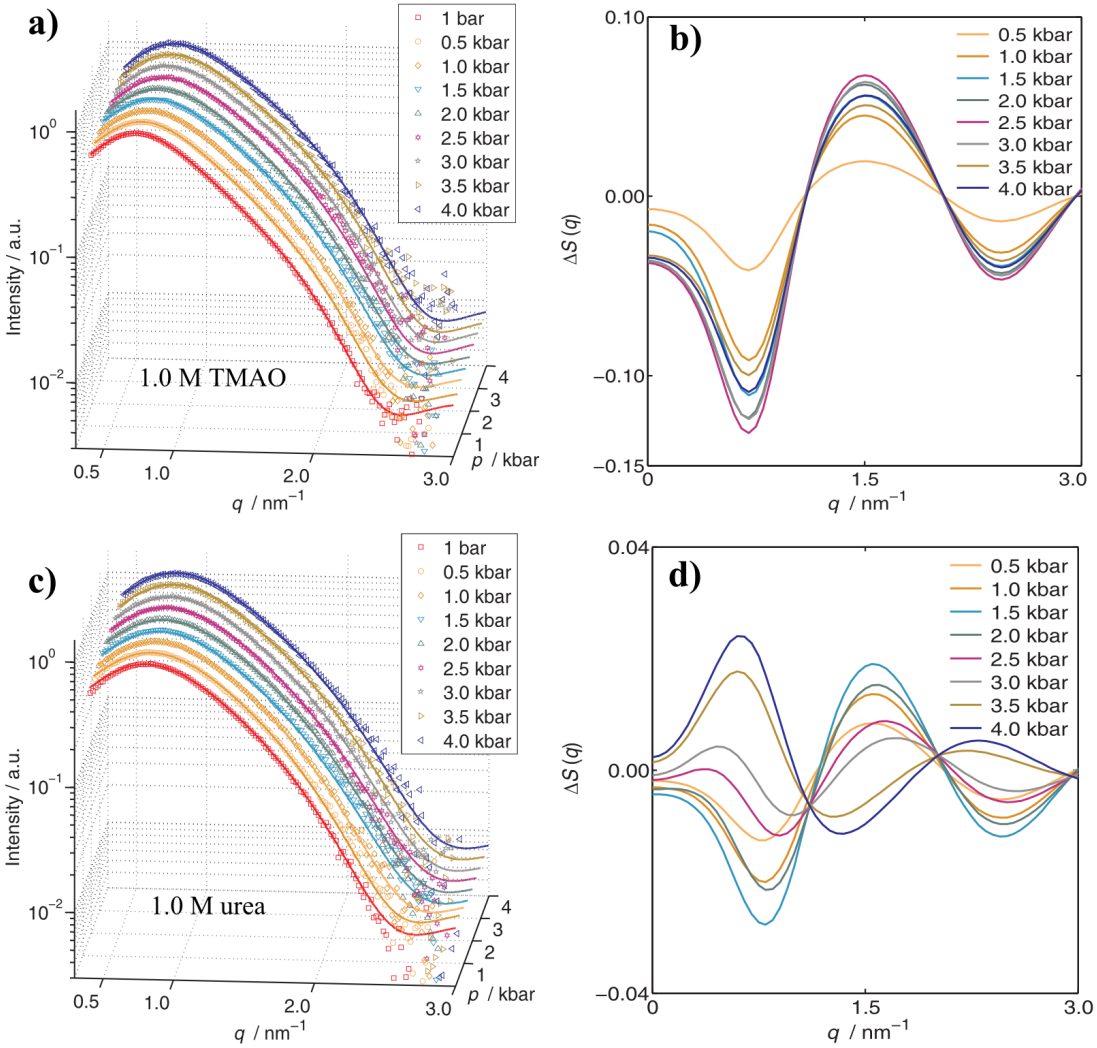

Figure 5.8: *Results of small angle X-ray scattering on a concentrated lysozyme solution (c_P = 100 mg/mL) at $T = 25\,°C$ as a function of pressure for different osmolytes. a) With 1.0 M TMAO added (double logarithmic representation). b) Corresponding $\Delta S(q)$ curves. c) With 1.0 M urea added (double logarithmic representation). d) Corresponding $\Delta S(q)$ curves. Solid lines are refinements to the data. It was averaged over 3 data points.*

pressure dependence and the amplitude changes are less pronounced than for the 1.0 M TMAO concentration. The influence of pressure for this substance is similar to that for the protein in pure buffer solution.

To highlight the influence of the different cosolvents studied on the pressure-dependent protein-protein interaction, the position of the correlation peak, q_{corr}, and the strength of attraction, J, are shown in Fig. 5.9. In the case of TMAO concentrations of 0.25 M and 0.50 M, at ambient pressure q_{corr} is similar to that of the buffer solution (Fig. 5.9a)). An increase in concentration results in a shift to smaller q_{corr} reflecting a slight enhancement of the average protein separation. Pressurizing induces a shift of the peak position to higher values which is much stronger than for the buffer. Beyond a pressure of 2.5 kbar, a slight decrease is visible.

In terms of the attraction strength, the addition of TMAO results in a marked increase of J with rising osmolyte concentration ($\Delta J = +2\ \mathrm{k_B}T$ for 1 M TMAO, Fig. 5.9b)) which has been previously reported [Niebuhr and Koch, 2005]. Increasing pressure results in a drastic decrease of J, up to a pressure of about 2.5 kbar. At higher pressures, no significant change of J is observed anymore. Consistently, J scales with the TMAO concentration. The addition of TMAO leads to a different pressure dependence of the interaction potential than for pure buffer. No strong nonlinear pressure effect is present. As the reason for this phenomenon was attributed to be the collapse of the second hydration shell of water, the SAXS results on TMAO solutions indicate that the collapse seems to be suppressed.

For the solutions with urea added, a concentration-dependent shift to higher q_{corr} occurs and thus shorter distances are present (Fig. 5.9c)). A similar pressure dependence as for the buffer solution is observable. Fig. 5.9d) depicts the pressure dependence of the strength of attraction, J, for different urea concentrations ($\Delta J =$ -1 $\mathrm{k_B}T$ for 1 M urea). With increasing urea concentration, the interaction becomes more repulsive. This decrease of J is in accord with previous ambient-pressure studies [Niebuhr and Koch, 2005, Ortore et al., 2008]. The pressure dependence of J is similar to that in the pure buffer solution. An increase in the amount of urea results in a systematic shift of J towards smaller values, only.

Finally, the effect of the kosmotropic cosolvent glycerol on q_{corr} and J is shown in Fig. 5.9e) and f), respectively. As reported previously, glycerol also leads to a decrease of the protein-protein attraction, similar to urea, but to a lesser extent [Javid et al., 2007b, Sinibaldi et al., 2007]. The effect of pressure on both q_{corr} and J is of similar magnitude as that for the buffer and the urea solutions. A slight shift of the minimum of J to 2.5 kbar can be seen for the glycerol solutions.

Hence, in contrast to urea and glycerol, which reduce only the strength of attraction

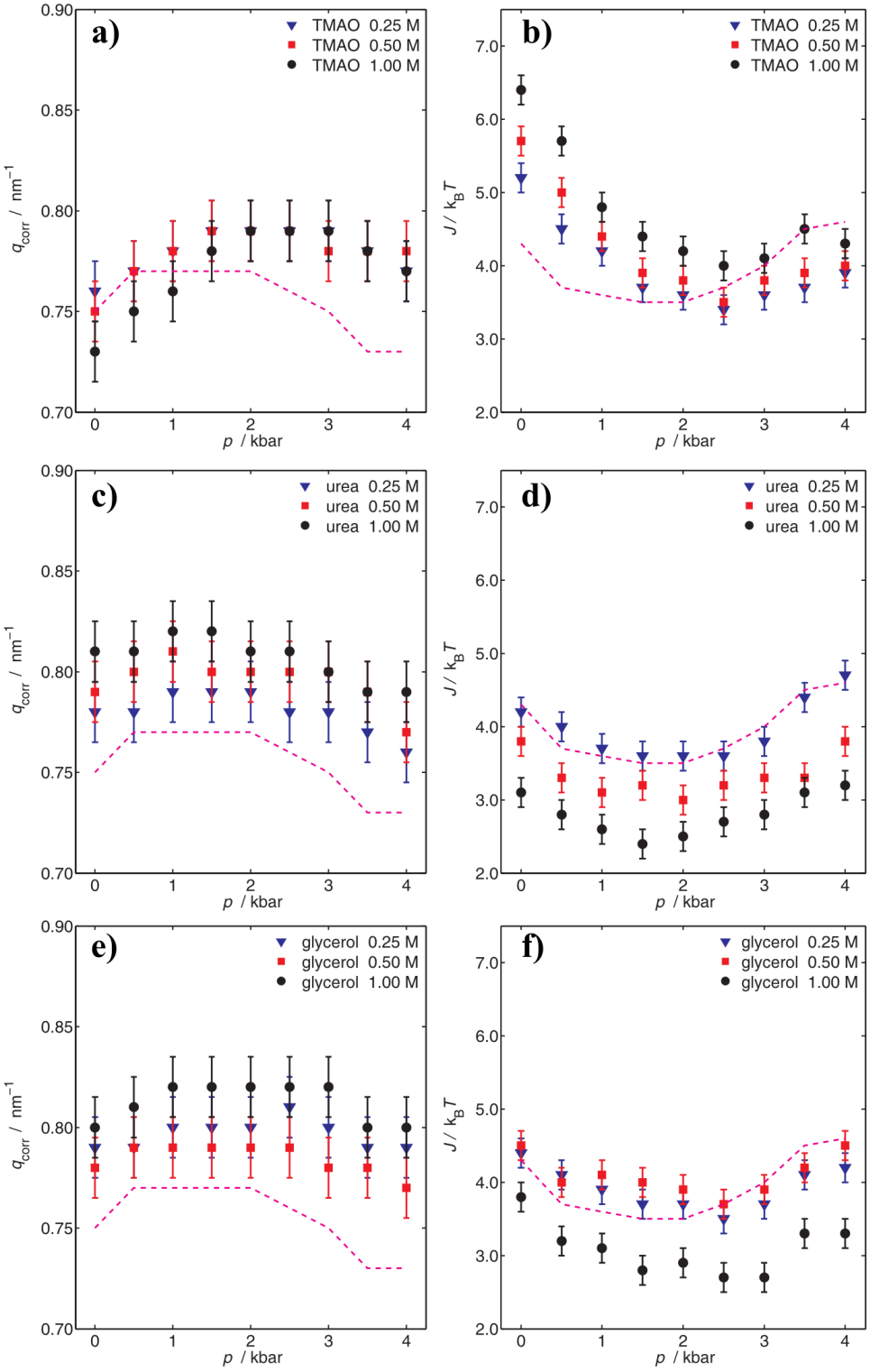

Figure 5.9: *Position of the correlation peak, q_{corr}, (left) and strength of attraction, J, (right) as a function of pressure and osmolyte concentration. a), b) For TMAO. c), d) For urea. e), f) For glycerol. The results for the pure buffer solution at $T = 25$ °C are given as dashed lines.*

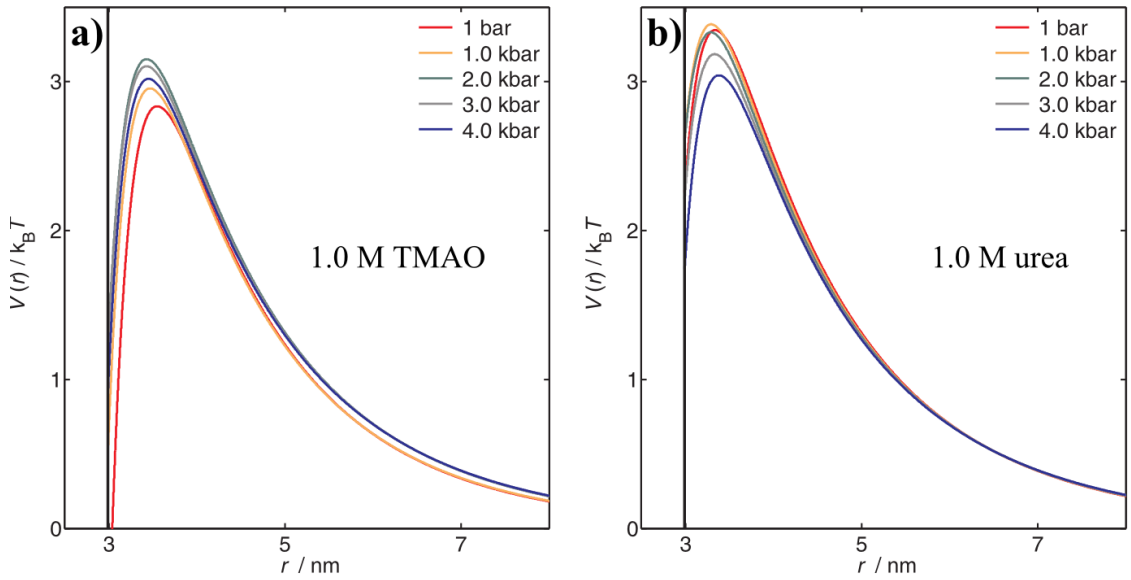

Figure 5.10: *Pressure-dependent protein-protein interaction potentials $V(r)$. a) With 1.0 M TMAO added. b) With 1.0 M urea added.*

but have no significant effect on the pressure sensitivity of J, TMAO drastically changes the pressure dependence of the protein intermolecular interaction.

For completeness, the interaction potentials $V(r)$ for 1.0 M TMAO and 1.0 M urea added are shown in Fig. 5.10. For TMAO (Fig. 5.10a), the repulsion barrier increases as the pressure is raised up to 2.0 kbar and shifts slightly to a smaller distance r. A further increase induces a decrease of the barrier again. However, this decline is much smaller than that present for urea (Fig. 5.10b). For this chaotropic cosolvent pressures up to 2 kbar lead to a slight increase of barrier which is followed by a much stronger decrease for higher pressures. This result for the destabilizing agent is similar to that of the pure solution (Fig. 5.4c)). Noteworthy, the differences in the Coulomb repulsion of the protein in the pure solution and in the cosolvent solutions also affect the interaction potential as the dielectric properties of the solvent, i.e. ϵ_r and the screening length, are different. Thus, the repulsion barrier for lysozyme in the TMAO solution is slightly higher than in the pure buffer solution although the attraction strength is greater. However, as for the pure solution, the repulsive part of interaction potential also shows a monotonic pressure dependence for the osmolyte solutions. Therefore, the effects of the additives on the pressure dependent interaction is due to their influence on the water structure.

SAXS measurements on different cosolvent mixtures were additionally performed to quantify the canceling of the different types of interaction and in particular to mimic the conditions present in deep-sea organisms (1:2 TMAO:urea mixtures) [Zou et al., 2002,

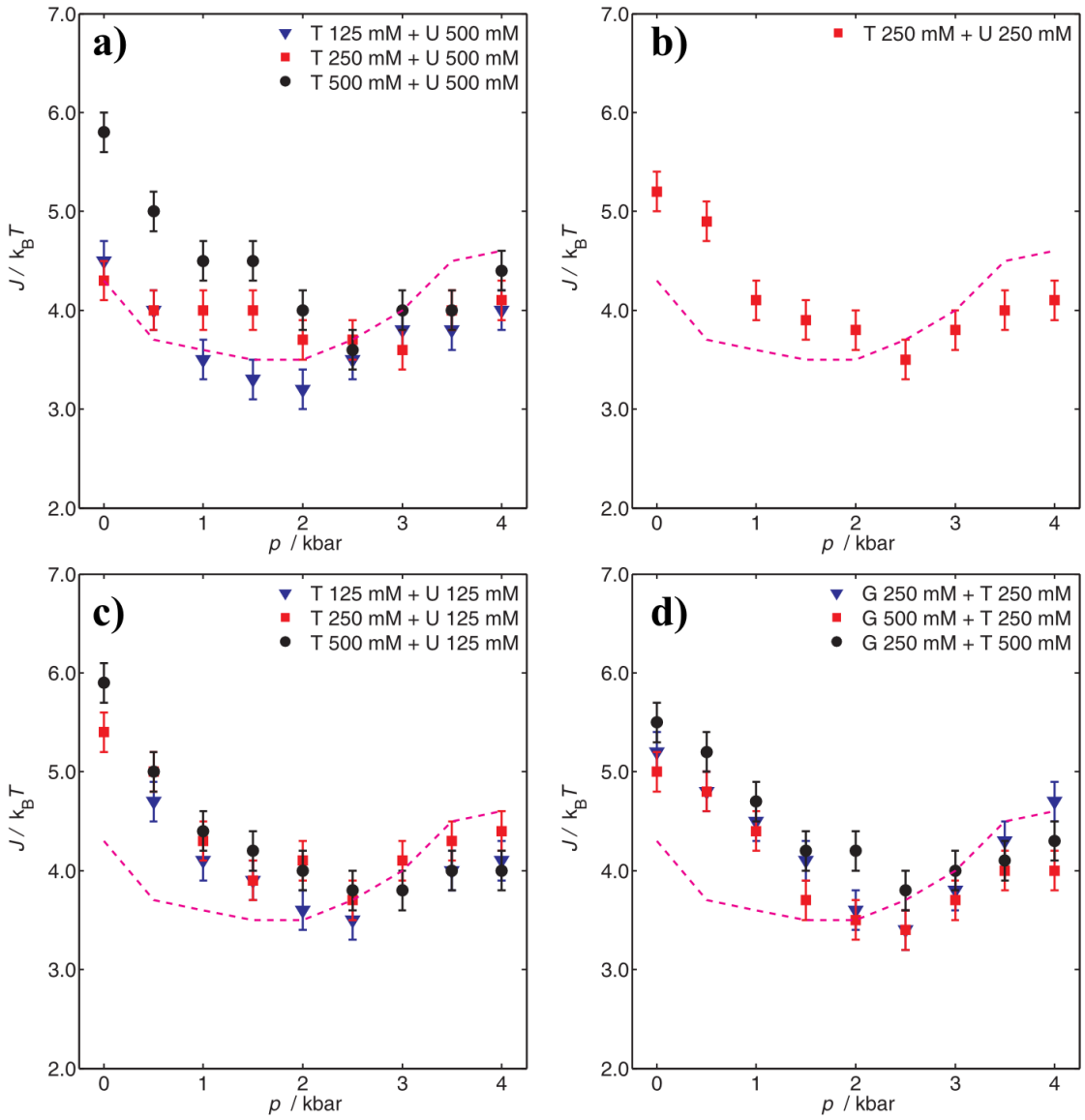

Figure 5.11: *Strength of attraction, J, for different osmolyte mixtures. Herein, "T", "U", and "G" denote TMAO, urea, and glycerol, respectively. Dashed lines are results for pure buffer solution.*

Bennion and Daggett, 2004]. The results are presented in Fig. 5.11.

For example, the results for a 0.5 M urea solution at different amounts of TMAO are shown in Fig. 5.11a). It can be seen that even in the presence of a low TMAO concentrations of 0.125 M, the tendency of urea to foster the repulsive nature of the intermolecular protein interaction is largely compensated by the addition of TMAO at ambient pressure. Up to a pressure of 2.5 kbar, the 0.5 M urea/0.125 M TMAO mixture displays a pressure dependence of J which is similar to that of the pure buffer solution (dashed line). At higher pressures, J is slightly below the value of the pure buffer solution, which is also observed for the pure TMAO solutions. An increase of the TMAO concentration in the urea-TMAO cosolvent mixture to 0.25 M causes a shift of the minimum of J from about 1 to 2 kbar. For the equimolar mixture (0.5 M TMAO/0.5 M urea), the data look similar to those of the pure 0.5 M TMAO solution. Thus, the strong and counteracting influence of TMAO on the intermolecular protein-protein interaction potential also under high pressure conditions is revealed.

Decreasing the urea concentration of the mixtures to 250 mM (Fig. 5.11b)) and to 125 mM (Fig. 5.11c)) consistently leads to similar results. Due to the lower amount of urea, the strong effect of TMAO dominates the pressure dependence of the attraction strength J. For mixtures of glycerol and TMAO, equal findings as for urea were obtained (Fig. 5.11d)) as glycerol has a similar, slightly weaker effect on the protein-protein interaction.

Within the collaboration additional differential scanning calorimetry (DSC) and pressure perturbation calorimetry (PPC) measurements were performed on lysozyme in the different cosolvent solutions and mixtures. Therein, a significant decrease of the temperature of the midpoint of unfolding, T_m, upon addition of urea, reflecting its destabilizing effect was found. Conversely, an increase of T_m is observed upon addition of TMAO. For the 1:1 and 2:1 urea:TMAO mixture, a counteracting behavior is observed.

5.2.1 Discussion

The presented high pressure SAXS study on concentrated lysozyme solutions in presence of natural osmolytes revealed that the pressure-dependent interaction potential is largely influenced by the type of cosolvent. In detail, urea and glycerol show the same pressure dependence as pure buffer solution whereas TMAO largely changes this. As the reason for the nonlinear pressure dependence in buffer solution was attributed to the collapse of the second hydration shell at about 2 kbar, changes of the pressure effect on the interaction are due to alterations of the water structure. Thus, the influence of the osmolytes on the solvent will be discussed.

According to experimental and molecular dynamics (MD) simulation studies, TMAO seems to enhance the number of strong hydrogen bonds of the water structure, i.e., serves as "water structure maker" [Bennion and Daggett, 2004, Paul and Patey, 2007, Panuszko et al., 2009, Wei et al., 2010]. More precisely, it was found that TMAO enhances the tetrahedral water structure [Wei et al., 2010] and leads to more order [Panuszko et al., 2009]. Notable, the second hydration shell is further outward than in pure water [Wei et al., 2010].

In the presence of proteins, a direct interaction between the protein and the osmolyte is disfavored. The depletion of TMAO from the protein surface (preferential exclusion) and the enhancement of the water structure gives rise to the increased protein stability as the cosolvent is added [Bennion and Daggett, 2004, Panuszko et al., 2009]. The mechanism of preferential exclusion was discussed in chapter 4.1.3. For a more structured water network, the direct interaction of the protein with single water molecules is reduced. As in particular the direct interaction of water molecules with the protein's carbonyl groups was assumed to lead to destabilization [Wei et al., 2010], the addition of TMAO thus stabilizes the protein. In contrast, urea was found to fit perfectly in water network [Panuszko et al., 2009, Wei et al., 2010] and thus does not alter the water structure.

The presence of TMAO increases the attractive part of the interaction potential, J, significantly, which is probably due to the marked change in solvent structural properties. Moreover, the data show that J is more pressure sensitive for the TMAO solutions than in pure buffer, resulting in a much steeper decay of the strength of attraction up to about 2.5 kbar. Different from the pure buffer solution, above 2 kbar, no significant changes of J are observed anymore, as pressure and TMAO have counteracting effects on the structural properties of water.

Conversely, such strong pressure dependence of J is not observed for the urea solution. The J curve is shifted to smaller values, only. This might be due to the fact that the water structure is not significantly perturbed in the presence of urea [Panuszko et al., 2009, Wei et al., 2010].

Glycerol is a stabilizing osmolyte such as TMAO. For the glycerol solutions studied,

only a minor influence on the interaction potential is detectable, i.e., the effect of glycerol on the intermolecular interaction is markedly different from TMAO, although both are stabilizing osmolytes. A small shift of the minimum of J is observed for the highest glycerol concentration, only. Stronger glycerol-water interactions are present for larger amounts of glycerol added to water [Dashnau et al., 2006]. Thus, using higher glycerol concentration should lead to a similar pressure dependence of J as TMAO.

The influence of the TMAO-urea mixtures on the protein-protein interaction significantly depends on the mixing ratio. In the case of the equimolar mixture, the influence of the strong kosmotropic cosolvent TMAO on the value and pressure dependence of J dominates. For the 1:4 and 1:2 TMAO:urea solutions, their influence on the pressure dependence on J are similar to the corresponding data for the pure buffer solution, i.e., the two cosolvents largely counteract each other. The cancellation of interactions is in good agreement with neutron scattering data indicating a direct interaction of urea with TMAO [Meersman et al., 2009, Meersman et al., 2011] that was found previously by MD simulations [Paul and Patey, 2007]. A 1:2 TMAO:urea mixture has also been found to be most effective in avoiding pressure-induced cellular stresses in deep-sea animals [Zou et al., 2002, Yancey, 2005]. For the TMAO-glycerol mixtures the dominant influence of TMAO persists as for TMAO-urea mixtures with lower amount of urea.

The presented SAXS study shows how the nonlinear pressure-dependent protein-protein interactions in dense protein solutions are affected by the type and amount of cosolvent and its influence on the water structure. Addition of urea increases the repulsive interaction between lysozyme molecules. Conversely, the addition of TMAO increases the attractive interaction. TMAO increases the amount of strong hydrogen bonds of water, causes a strengthening of the hydrogen bond network structure, and in its presence the second hydration shell of water moves slightly outward which is contrary to the effect of high pressure [Wei et al., 2010]. As a result, no increase of J is observed at pressures above 2 kbar. For urea-TMAO mixtures, a large counteracting effect on the intermolecular interaction, qualitatively similar to the effect on protein stability revealed from the calorimetric measurements, is observed.

These findings on the influence of osmolytes on the pressure-dependent interaction potential support the interpretations of the nonlinear pressure effect, i.e., it is due to the collapse of the second hydration shell at 2 kbar. Furthermore, the counteracting effect of TMAO and urea is reflected in the magnitude and pressure dependence of the strength of attraction J. Thus, studying the pressure dependence of the protein-protein interaction potential with different cosolutes added might be used in principle to check if these alter the water structure. For instance, using higher glycerol concentrations should give a similar result as for TMAO.

6 Summary and outlook

In the presented thesis, small angle X-ray scattering studies on proteins in solution are reported. Variation of the solution conditions allowed to induce structural changes which were monitored by the SAXS signal. Among the extreme conditions employed are high hydrostatic pressure, pH variation, and the addition of cosolvents. Furthermore, mutants of the protein staphylococcal nuclease as well as highly concentrated protein solutions were studied. Using this combined approach, structural transitions of the protein structure were studied for diluted protein solutions and changes of the protein-protein interaction for concentrated solutions.

SAXS measurements on diluted solutions of the hyperstable SNase variant Δ-PHS and its mutant Δ-PHS/V66K were performed at two pH values as a function of pressure. At these particular pH values, the Lys-66 residue of the mutant is either charged or uncharged. Depending on the charge state of this single residue, different structural changes are present. The charge state affects the protein stability significantly which was probed by high pressure perturbation. As high pressures favor the protein state with the lowest volume, this approach allows to gain information about the protein packing and protein's stability. Within this study, it was shown that all effects influenced by changing the pH value are solely attributed to the properties of the single Lys-66 residue. For the neutral state, the pressure-induced unfolded protein is still compact whereas it is largely expanded when the residue is charged. Additional NMR spectroscopy measurement performed within a collaboration allowed to localize the regions within the protein which are strongly influenced by pH and pressure. The combined study reveals how subtle changes within the protein structure can give rise to its high tolerance against insertion of ionizable residues and how small changes of the solution conditions drastically influence the thermodynamics of these types of proteins.

Similarly, electrostatic interactions within proteins were in focus of the study on the wild type SNase mutant T62P which is natively unfolded. Variation of the solution's pH value over a broad range revealed a structural transition of the wild type variant and T62P. For WT SNase, folding from an unfolded state at pH 2.0 with increasing pH into a fully folded one at pH 7.0 could be detected doubtlessly. In the case of the T62P variant, the transition from a random coil state into a folding intermediate

state was revealed. Notable is the high propensity of T62P to form aggregates. This was determined when changing the salt content in the solution. Different mechanisms known to influence the acid-induced unfolded state of WT SNase might also affect the mutant and its aggregation behavior and in particular the pH dependence of the folding process. Further SAXS measurements on higher diluted protein solutions might help to clarify this. At all conditions studied, especially including the lowest pH value and lowest salt content, T62P was not as highly extended as was calculated for a fully unfolded protein. Thus, this SAXS study indicates residual structure present also in a natively unfolded protein. Additional measurements using techniques which are sensitive to different structural properties will give a deeper insight into the type of residual structure.

The study on the ankyrin repeat domain of the *Drosophila* Notch receptor was conducted to get a deeper insight into the unfolding process of a linear, non-globular protein. Therefor, high pressures and different concentrations of destabilizing urea were used. As was obtained by the SAXS measurements, the protein in pure buffer is stable within the full pressure range explored. Addition of urea however leads to pressure-induced unfolding. The study showed that slightly different amounts of urea strongly affected the unfolded state, whose high plasticity was also revealed by other techniques.

SAXS measurements on concentrated solutions of the protein lysozyme allowed to study the pressure effect on the protein-protein interaction. The results show a nonlinear pressure dependence of interaction potential. This effect which is reflected by the strength of attraction is present for different temperatures and protein concentrations. Unfolding of the protein can be ruled out by additional SAXS measurements on diluted solutions and FTIR spectroscopy results. Furthermore, no change of the protein's effective charge occurs. Therefore, the reason of the nonlinear pressure dependence was attributed to the collapse of the second hydration shell. This sets in at 2 kbar which coincides with the minimum of the strength of attraction. SAXS measurements on protein solutions with different osmolytes added support this interpretation.

Osmolytes are small organic molecules present in organisms to compensate the effects of extreme environmental conditions such as high and low temperatures or high pressures. Especially the substance TMAO is present in deep sea organisms. The influence of TMAO, urea, and glycerol on the pressure-dependent interaction was studied. At ambient pressure, presence of these cosolvents influences the attraction strength as a function of cosolvent concentration. TMAO increases the attraction, urea and glycerol reduce it. High pressure SAXS measurements on proteins with TMAO added revealed a different pressure dependence of the interaction potential than for pure buffer. In contrast no effect was observed for urea and only a slight one for glycerol. As TMAO is

assumed to strengthen the water structure and thus counteracting the pressure-induced structural changes, this finding supports the interpretation of the nonlinear pressure effect. No change is seen for urea, as it fits perfectly into the water network leaving it unchanged. For higher glycerol concentrations also a change of the pressure dependence should occur as this substance affects the water structure. Mixture of TMAO-urea showed that TMAO even in low concentrations has a dominant influence on the interaction. Furthermore, for a 1:2 TMAO:urea mixture as it is present in deep sea organisms, a canceling of the effects of the two substances was found.

As was shown in this thesis, a combined approach of extreme conditions with small angle X-ray scattering as well as with other experimental techniques allows to study different interactions within proteins as well as between them. With this a better understanding of the complex process of protein folding can be obtained. Furthermore, simple models of crowded protein solutions can be investigated under conditions as they are present for instance in organisms living under extreme conditions. Future measurements on both diluted and concentrated protein solutions employing different external perturbation therefore will shed more light into these complex processes and interactions.

For example, studies on diluted solutions of T62P in combination with other techniques will give a deeper insight into the pH-induced structural transition observed. Furthermore, this approach might reveal the type of residual structure present at pH 2.0 in this natively unfolded protein.

High pressure SAXS measurements on concentrated protein solutions might also be used in principle to study the impact of cosolutes on the water structure as was done for TMAO. For instance, solutions with higher glycerol concentrations can be investigated and compared to the results of TMAO as it is known that glycerol also affects the water structure.

Using highly concentrated solutions of less stable proteins that unfold under high pressure like SNase, high pressure SAXS measurements might allow to access differences of the unfolding process compared to that in the diluted solutions. Furthermore, addition of stabilizing cosolvents will modulate both the unfolding and the interaction potential and thus allows to monitor the protein-protein interaction between different folding states of the protein.

Finally, not only the pressure-dependent interaction of proteins but also of colloids might be studied. As some of these can be fabricated with tailored properties like size or surface charge, molecular details of pressure effects on the interactions can be investigated in more detail.

Bibliography

[Alber, 1989] Alber, T. (1989). Mutational Effects On Protein Stability. *Annual Review of Biochemistry*, 58:765–798.

[Allen, 2008] Allen, J. P. (2008). *Biophysical Chemistry*. Wiley-Backwell.

[Als-Nielsen and McMorrow, 2001] Als-Nielsen, J. and McMorrow, D. (2001). *Elements of Modern X-Ray Physics*. Wiley, New York.

[Anfinsen, 1973] Anfinsen, C. B. (1973). Principles That Govern Folding of Protein Chains. *Science*, 181(4096):223–230.

[Asherie, 2004] Asherie, N. (2004). Protein crystallization and phase diagrams. *Methods*, 34(3):266–272.

[Baldwin, 1986] Baldwin, R. L. (1986). Temperature-dependence of the Hydrophobic Interaction In Protein Folding. *Proceedings of the National Academy of Sciences of the United States of America*, 83(21):8069–8072.

[Baldwin, 1996] Baldwin, R. L. (1996). How Hofmeister ion interactions affect protein stability. *Biophysical Journal*, 71(4):2056–2063.

[Baldwin et al., 2010] Baldwin, R. L., Frieden, C., and Rose, G. D. (2010). Dry molten globule intermediates and the mechanism of protein unfolding. *Proteins: Structure, Function, and Bioinformatics*, 78(13):2725–2737.

[Bale and Schmidt, 1984] Bale, H. D. and Schmidt, P. W. (1984). Small-angle X-ray-scattering Investigation of Submicroscopic Porosity With Fractal Properties. *Physical Review Letters*, 53(6):596–599.

[Barrick, 2009] Barrick, D. (2009). What have we learned from the studies of two-state folders, and what are the unanswered questions about two-state protein folding? *Physical Biology*, 6(1):015001.

[Baskakov and Bolen, 1998a] Baskakov, I. and Bolen, D. W. (1998a). Forcing thermodynamically unfolded proteins to fold. *Journal of Biological Chemistry*, 273(9):4831–4834.

[Baskakov and Bolen, 1998b] Baskakov, I. V. and Bolen, D. W. (1998b). Monitoring the sizes of denatured ensembles of staphylococcal nuclease proteins: Implications regarding m values, intermediates, and thermodynamics. *Biochemistry*, 37(51):18010–18017.

[Beamline ID02, 2011] Beamline ID02 (2011). ID2 High Brilliance Beamline - ESRF (Homepage): http://www.esrf.eu/UsersAndScience/Experiments/SCMatter/ID02. Date checked: 06.04.2011.

[Beaucage, 1995] Beaucage, G. (1995). Approximations leading to a unified exponential power-law approach to small-angle scattering. *Journal of Applied Crystallography*, 28:717–728.

[Beaucage, 1996] Beaucage, G. (1996). Small-angle scattering from polymeric mass fractals of arbitrary mass-fractal dimension. *Journal of Applied Crystallography*, 29:134–146.

[Bennion and Daggett, 2004] Bennion, B. J. and Daggett, V. (2004). Counteraction of urea-induced protein denaturation by trimethylamine N-oxide: A chemical chaperone at atomic resolution. *Proceedings of the National Academy of Sciences of the United States of America*, 101(17):6433–6438.

[Bonnete et al., 1999] Bonnete, F., Finet, S., and Tardieu, A. (1999). Second virial coefficient: Variations with lysozyme crystallization conditions. *Journal of Crystal Growth*, 196(2-4):403–414.

[Boonyaratanakornkit et al., 2002] Boonyaratanakornkit, B. B., Park, C. B., and Clark, D. S. (2002). Pressure effects on intra- and intermolecular interactions within proteins. *Biochimica Et Biophysica Acta-Protein Structure and Molecular Enzymology*, 1595(1-2):235–249.

[Boyer et al., 1999] Boyer, M., Roy, M. O., Jullien, M., Bonnete, F., and Tardieu, A. (1999). Protein interactions in concentrated ribonuclease solutions. *Journal of Crystal Growth*, 196(2-4):185–192.

[Bradley and Barrick, 2006] Bradley, C. M. and Barrick, D. (2006). The notch ankyrin domain folds via a discrete, centralized pathway. *Structure*, 14(8):1303–1312.

[Broccio et al., 2006] Broccio, M., Costa, D., Liu, Y., and Chen, S. H. (2006). The structural properties of a two-Yukawa fluid: Simulation and analytical results. *Journal of Chemical Physics*, 124(8):084501.

[Brooks et al., 2001] Brooks, C. L., Onuchic, J. N., and Wales, D. J. (2001). Statistical thermodynamics - Taking a walk on a landscape. *Science*, 293(5530):612–613.

[Brun et al., 2006] Brun, L., Isom, D. G., Velu, P., Garcia-Moreno, B., and Royer, C. A. (2006). Hydration of the folding transition state ensemble of a protein. *Biochemistry*, 45(11):3473–3480.

[Bryngelson et al., 1995] Bryngelson, J. D., Onuchic, J. N., Socci, N. D., and Wolynes, P. G. (1995). Funnels, Pathways, and the Energy Landscape of Protein-folding - A Synthesis. *Proteins-Structure, Function, and Genetics*, 21(3):167–195.

[Bunde and Havlin, 1991] Bunde, A. and Havlin, S., editors (1991). *Fractals and Disordered Systems*. Springer.

[Byrne and Stites, 2007] Byrne, M. P. and Stites, W. E. (2007). Thermal denaturations of staphylococcal nuclease wild-type and mutants monitored by fluorescence and circular dichroism are similar: Lack of evidence for other than a two state thermal denaturation. *Biophysical Chemistry*, 125(2-3):490–496.

[Calmettes et al., 1994] Calmettes, P., Durand, D., Desmadril, M., Minard, P., Receveur, V., and Smith, J. C. (1994). How Random Is A Highly Denatured Protein. *Biophysical Chemistry*, 53(1-2):105–113.

[Cardinaux et al., 2011] Cardinaux, F., Zaccarelli, E., Stradner, A., Bucciarelli, S., Farago, B., Egelhaaf, S. U., Sciortino, F., and Schurtenberger, P. (2011). Cluster-Driven Dynamical Arrest in Concentrated Lysozyme Solutions. *Journal of Physical Chemistry B*, 115(22):7227–7237.

[Carpenter and Mattice, 1977] Carpenter, D. K. and Mattice, W. L. (1977). Influence of Fluctuations In Electron-density On Excess Small-angle X-ray-scattering From Dilute-solutions of Macromolecules. *Biopolymers*, 16(1):67–80.

[Carra et al., 1994] Carra, J. H., Anderson, E. A., and Privalov, P. L. (1994). Thermodynamics of Staphylococcal Nuclease Denaturation. 1. The Acid-denatured State. *Protein Science*, 3(6):944–951.

[Castaneda et al., 2009] Castaneda, C. A., Fitch, C. A., Majumdar, A., Khangulov, V., Schlessman, J. L., and Garcia-Moreno, B. E. (2009). Molecular determinants of the pK(a) values of Asp and Glu residues in staphylococcal nuclease. *Proteins-Structure, Function, and Bioinformatics*, 77(3):570–588.

[Chalikian and Breslauer, 1998] Chalikian, T. V. and Breslauer, K. J. (1998). Thermodynamic analysis of biomolecules: A volumetric approach. *Current Opinion In Structural Biology*, 8(5):657–664.

[Chavez et al., 2004] Chavez, L. L., Onuchic, J. N., and Clementi, C. (2004). Quantifying the roughness on the free energy landscape: Entropic bottlenecks and protein folding rates. *Journal of the American Chemical Society*, 126(27):8426–8432.

[Chen et al., 2000] Chen, J. M., Lu, Z. Q., Sakon, J., and Stites, W. E. (2000). Increasing the thermostability of staphylococcal nuclease: Implications for the origin of protein thermostability. *Journal of Molecular Biology*, 303(2):125–130.

[Chimenti et al., 2011] Chimenti, M. S., Castaneda, C. A., Majumdar, A., and Garcia-Moreno, B. (2011). Structural Origins of High Apparent Dielectric Constants Experienced by Ionizable Groups in the Hydrophobic Core of a Protein. *Journal of Molecular Biology*, 405(2):361–377.

[Cotton et al., 1979] Cotton, F. A., Hazen, E. E., and Legg, M. J. (1979). Staphylococcal Nuclease - Proposed Mechanism of Action Based On Structure of Enzyme-thymidine 3',5'-bisphosphate-calcium Ion Complex At 1.5-Å Resolution. *Proceedings of the National Academy of Sciences of the United States of America*, 76(6):2551–2555.

[Croxton, 1975] Croxton, C. (1975). *Introduction to Liquid State Physics*. Wiley, London.

[Curtis and Lue, 2006] Curtis, R. A. and Lue, L. (2006). A molecular approach to bioseparations: Protein-protein and protein-salt interactions. *Chemical Engineering Science*, 61(3):907–923.

[Damjanovic et al., 2005] Damjanovic, A., Garcia-Moreno, B., Lattman, E. E., and Garcia, A. E. (2005). Molecular dynamics study of water penetration in staphylococcal nuclease. *Proteins: Structure, Function, and Bioinformatics*, 60(3):433–449.

[Damjanovic et al., 2007] Damjanovic, A., Schlessman, J. L., Fitch, C. A., Garcia, A. E., and Garcia-Moreno, B. (2007). Role of flexibility and polarity as determinants of the hydration of internal cavities and pockets in proteins. *Biophysical Journal*, 93(8):2791–2804.

[Damjanovic et al., 2008] Damjanovic, A., Wu, X. W., Garcia-Moreno, B., and Brooks, B. R. (2008). Backbone Relaxation Coupled to the Ionization of Internal Groups in Proteins: A Self-Guided Langevin Dynamics Study. *Biophysical Journal*, 95(9):4091–4101.

[Daniel et al., 2006] Daniel, I., Oger, P., and Winter, R. (2006). Origins of life and biochemistry under high-pressure conditions. *Chemical Society Reviews*, 35(10):858–875.

[Dashnau et al., 2006] Dashnau, J. L., Nucci, N. V., Sharp, K. A., and Vanderkooi, J. M. (2006). Hydrogen bonding and the cryoprotective properties of glycerol/water mixtures. *Journal of Physical Chemistry B*, 110(27):13670–13677.

[Dawydow, 1981] Dawydow, A. S. (1981). *Quantenmechanik*. VEB Deutscher Verlag der Wissenschaften, 6. edition.

[Debenedetti, 2003] Debenedetti, P. G. (2003). Supercooled and glassy water. *Journal of Physics-Condensed Matter*, 15(45):R1669–R1726.

[Debye, 1915] Debye, P. (1915). Zerstreuung von Röntgenstrahlen. *Annalen der Physik*, 46:809.

[Debye, 1947] Debye, P. (1947). Molecular-weight Determination By Light Scattering. *Journal of Physical and Colloid Chemistry*, 51(1):18–32.

[Debye and Bueche, 1949] Debye, P. and Bueche, A. M. (1949). Scattering By An Inhomogeneous Solid. *Journal of Applied Physics*, 20(6):518–525.

[Denisov et al., 2004] Denisov, V. P., Schlessman, J. L., Garcia-Moreno, B., and Halle, B. (2004). Stabilization of internal charges in a protein: Water penetration or conformational change? *Biophysical Journal*, 87(6):3982–3994.

[Diamond, 1974] Diamond, R. (1974). Real-space Refinement of Structure of Hen Egg-white Lysozyme. *Journal of Molecular Biology*, 82(3):371.

[Dill, 1990] Dill, K. A. (1990). Dominant Forces In Protein Folding. *Biochemistry*, 29(31):7133–7155.

[Dill and Chan, 1997] Dill, K. A. and Chan, H. S. (1997). From Levinthal to pathways to funnels. *Nature Structural Biology*, 4(1):10–19.

[Dill et al., 2008] Dill, K. A., Ozkan, S. B., Shell, M. S., and Weikl, T. R. (2008). The protein folding problem. *Annual Review of Biophysics*, 37:289–316.

[Dinner et al., 2000] Dinner, A. R., Sali, A., Smith, L. J., Dobson, C. M., and Karplus, M. (2000). Understanding protein folding via free-energy surfaces from theory and experiment. *Trends In Biochemical Sciences*, 25(7):331–339.

[Dobson, 2003] Dobson, C. M. (2003). Protein folding and misfolding. *Nature*, 426(6968):884–890.

[Dobson et al., 1998] Dobson, C. M., Sali, A., and Karplus, M. (1998). Protein folding: A perspective from theory and experiment. *Angewandte Chemie International Edition*, 37(7):868–893.

[Dumetz et al., 2008] Dumetz, A. C., Chockla, A. M., Kaler, E. W., and Lenhoff, A. M. (2008). Protein phase behavior in aqueous solutions: Crystallization, liquid-liquid phase separation, gels, and aggregates. *Biophysical Journal*, 94(2):570–583.

[Dyson and Wright, 2005] Dyson, H. J. and Wright, P. E. (2005). Intrinsically unstructured proteins and their functions. *Nature Reviews Molecular Cell Biology*, 6(3):197–208.

[Ellis, 2001] Ellis, R. J. (2001). Macromolecular crowding: obvious but underappreciated. *Trends In Biochemical Sciences*, 26(10):597–604.

[Ellis and Hartl, 1999] Ellis, R. J. and Hartl, F. U. (1999). Principles of protein folding in the cellular environment. *Current Opinion In Structural Biology*, 9:102–110.

[Ellis and Minton, 2003] Ellis, R. J. and Minton, A. P. (2003). Cell biology - join the crowd. *Nature*, 425(6953):27–28.

[Feigin and Svergun, 1987] Feigin, L. A. and Svergun, D. I. (1987). *Structure Analysis by Small-Angle X-Ray and Neutron Scattering.* Plenum Press, London.

[Fersht and Daggett, 2002] Fersht, A. R. and Daggett, V. (2002). Protein folding and unfolding at atomic resolution. *Cell*, 108(4):573–582.

[Fink et al., 1994] Fink, A. L., Calciano, L. J., Goto, Y., Kurotsu, T., and Palleros, D. R. (1994). Classification of Acid Denaturation of Proteins - Intermediates and Unfolded States. *Biochemistry*, 33(41):12504–12511.

[Fink et al., 1993] Fink, A. L., Calciano, L. J., Goto, Y., Nishimura, M., and Swedberg, S. A. (1993). Characterization of the Stable, Acid-induced, Molten Globule-like State of Staphylococcal Nuclease. *Protein Science*, 2(7):1155–1160.

[Fischetti et al., 2003] Fischetti, R. F., Rodi, D. J., Mirza, A., Irving, T. C., Kondrashkina, E., and Makowski, L. (2003). High-resolution wide-angle x-ray scattering of protein solutions: effect of beam dose on protein integrity. *Journal of Synchrotron Radiation*, 10:398–404.

[Fitzkee and Garcia-Moreno E., 2008] Fitzkee, N. C. and Garcia-Moreno E., B. (2008). Electrostatic effects in unfolded staphylococcal nuclease. *Protein Science*, 17(2):216–227.

[Fitzkee and Rose, 2004] Fitzkee, N. C. and Rose, G. D. (2004). Reassessing random-coil statistics in unfolded proteins. *Proceedings of the National Academy of Sciences of the United States of America*, 101(34):12497–12502.

[Floriano and Nascimento, 2004] Floriano, W. B. and Nascimento, M. A. C. (2004). Dielectric constant and density of water as a function of pressure at constant temperature. *Brazilian Journal of Physics*, 34(1):38–41.

[Franke and Svergun, 2009] Franke, D. and Svergun, D. I. (2009). DAMMIF, a program for rapid ab-initio shape determination in small-angle scattering. *Journal of Applied Crystallography*, 42:342–346.

[Frye et al., 1996] Frye, K. J., Perman, C. S., and Royer, C. A. (1996). Testing the correlation between Δ A and Δ V of protein unfolding using m value mutants of staphylococcal nuclease. *Biochemistry*, 35(31):10234–10239.

[Frye and Royer, 1998] Frye, K. J. and Royer, C. A. (1998). Probing the contribution of internal cavities to the volume change of protein unfolding under pressure. *Protein Science*, 7(10):2217–2222.

[Garcia-Moreno et al., 1997] Garcia-Moreno, B., Dwyer, J. J., Gittis, A. G., Lattman, E. E., Spencer, D. S., and Stites, W. E. (1997). Experimental measurement of the effective dielectric in the hydrophobic core of a protein. *Biophysical Chemistry*, 64(1-3):211–224.

[Glatter, 1977] Glatter, O. (1977). New Method For Evaluation of Small-angle Scattering Data. *Journal of Applied Crystallography*, 10(OCT1):415–421.

[Glatter, 1979] Glatter, O. (1979). Interpretation of Real-space Information From Small-angle Scattering Experiments. *Journal of Applied Crystallography*, 12(APR):166–175.

[Glatter, 2002] Glatter, O. (2002). The Inverse Scattering Problem in Small-Angle Scattering. In Lindner, P. and Zemb, T., editors, *Neutrons, X-Ray and Light: Scattering Methods Applied to Soft Condensed Matter*, chapter 4, page 73. Elsevier Science.

[Goodisman and Brumberger, 1973] Goodisman, J. and Brumberger, H. (1973). Über die Zulässigkeit der Subtraktion der Lösungsmittelstreuung von der Streuung der Lösungen bei Röntgenkleinwinkelstreuungsmessungen. *Monatshefte für Chemie*, 104:598.

[Goto et al., 1990a] Goto, Y., Calciano, L. J., and Fink, A. L. (1990a). Acid-induced Folding of Proteins. *Proceedings of the National Academy of Sciences of the United States of America*, 87(2):573–577.

[Goto et al., 1990b] Goto, Y., Takahashi, N., and Fink, A. L. (1990b). Mechanism of Acid-induced Folding of Proteins. *Biochemistry*, 29(14):3480–3488.

[Gouyet, 1996] Gouyet, J.-F. (1996). *Physics and Fractal Structures*. Springer.

[Grimson, 1983] Grimson, M. J. (1983). Small-angle Scattering From Colloidal Dispersions. *Journal of the Chemical Society-Faraday Transactions*, 79:817–832.

[Guinier and Fournet, 1955] Guinier, A. and Fournet, G. (1955). *Small-Angle Scattering of X-Rays*. Wiley, New York.

[Hall and Minton, 2003] Hall, D. and Minton, A. P. (2003). Macromolecular crowding: qualitative and semiquantitative successes, quantitative challenges. *Biochimica Et Biophysica Acta-Proteins and Proteomics*, 1649(2):127–139.

[Hammersley et al., 1996] Hammersley, A. P., Svensson, S. O., Hanfland, M., Fitch, A. N., and Hausermann, D. (1996). Two-dimensional detector software: From real detector to idealised image or two-theta scan. *High Pressure Research*, 14(4-6):235–248.

[Hansen and Hayter, 1982] Hansen, J. P. and Hayter, J. B. (1982). A Rescaled MSA Structure Factor For Dilute Charged Colloidal Dispersions. *Molecular Physics*, 46(3):651–656.

[Hansen and McDonald, 1986] Hansen, J. P. and McDonald, I. R. (1986). *Theory of Simple Liquids*. Academic Press, UK, 2. edition.

[Harpaz et al., 1994] Harpaz, Y., Gerstein, M., and Chothia, C. (1994). Volume Changes On Protein-folding. *Structure*, 2(7):641–649.

[Harrison and Durbin, 1985] Harrison, S. C. and Durbin, R. (1985). Is There A Single Pathway For the Folding of A Polypeptide-chain. *Proceedings of the National Academy of Sciences of the United States of America*, 82(12):4028–4030.

[Hawley, 1971] Hawley, S. A. (1971). Reversible Pressure-temperature Denaturation of Chymotrypsinogen. *Biochemistry*, 10(13):2436–2442.

[Hayter and Penfold, 1981] Hayter, J. B. and Penfold, J. (1981). An Analytic Structure Factor For Macroion Solutions. *Molecular Physics*, 42(1):109–118.

[Heins et al., 1967] Heins, J. N., Suriano, J. R., Taniuchi, H., and Anfinsen, C. B. (1967). Characterization of A Nuclease Produced By Staphylococcus Aureus. *Journal of Biological Chemistry*, 242(5):1016.

[Hendriks et al., 1999] Hendriks, J., Hoff, W. D., Crielaard, W., and Hellingwerf, K. J. (1999). Protonation deprotonation reactions triggered by photoactivation of photoactive yellow protein from Ectothiorhodospira halophila. *Journal of Biological Chemistry*, 274(25):17655–17660.

[Heremans and Smeller, 1998] Heremans, K. and Smeller, L. (1998). Protein structure and dynamics at high pressure. *Biochimica Et Biophysica Acta-Protein Structure and Molecular Enzymology*, 1386(2):353–370.

[Hosemann, 1939] Hosemann, R. (1939). Theorie der Röntgenstrahlenstreuung an Partikelhaufen. Aufstellung des Aggregationsdiagrammes. *Zeitschrift für Physik*, 113:751.

[Huang et al., 1993] Huang, T. C., Toraya, H., N., B. T., and Wu, Y. (1993). X-ray-powder Diffraction Analysis of Silver Behenate, A Possible Low-angle Diffraction Standard. *Journal of Applied Crystallography*, 26:180–184.

[Hummer et al., 1998] Hummer, G., Garde, S., Garcia, A. E., Paulaitis, M. E., and Pratt, L. R. (1998). The pressure dependence of hydrophobic interactions is consistent with the observed pressure denaturation of proteins. *Proceedings of the National Academy of Sciences of the United States of America*, 95(4):1552–1555.

[Humphrey et al., 1996] Humphrey, W., Dalke, A., and Schulten, K. (1996). VMD: Visual molecular dynamics. *Journal of Molecular Graphics*, 14(1):33.

[Hyeon and Thirumalai, 2003] Hyeon, C. B. and Thirumalai, D. (2003). Can energy landscape roughness of proteins and RNA be measured by using mechanical unfolding experiments? *Proceedings of the National Academy of Sciences of the United States of America*, 100(18):10249–10253.

[Hynes and Fox, 1991] Hynes, T. R. and Fox, R. O. (1991). The Crystal-structure of Staphylococcal Nuclease Refined At 1.7 Å Resolution. *Proteins: Structure, Function, and Genetics*, 10(2):92–105.

[Isom et al., 2008] Isom, D. G., Cannon, B. R., Castaneda, C. A., Robinson, A., and Bertrand, G. M. E. (2008). High tolerance for ionizable residues in the hydrophobic interior of proteins. *Proceedings of the National Academy of Sciences of the United States of America*, 105(46):17784–17788.

[Isom et al., 2011] Isom, D. G., Castaneda, C. A., Cannon, B. R., and Garcia-Moreno, B. E. (2011). Large shifts in pk(a) values of lysine residues buried inside a protein. *Proceedings of the National Academy of Sciences of the United States of America*, 108(13):5260–5265.

[Israelachvili, 1985] Israelachvili, J. N. (1985). *Intermolecular and Surface Forces: With Applications to Colloidal and Biological Systems*. Academic Press (London), 2 edition.

[Javid et al., 2007a] Javid, N., Vogtt, K., Krywka, C., Tolan, M., and Winter, R. (2007a). Capturing the interaction potential of amyloidogenic proteins. *Physical Review Letters*, 99(2):028101.

[Javid et al., 2007b] Javid, N., Vogtt, K., Krywka, C., Tolan, M., and Winter, R. (2007b). Protein-protein interactions in complex cosolvent solutions. *ChemPhysChem*, 8(5):679–689.

[Kaler, 1995] Kaler, E. W. (1995). Small-Angle Scattering from Complex Fluids. In Brumberger, H., editor, *Modern Aspects of Small-Angle Scattering*, page 329. Kluwer Academic Publ., Dordrecht, Niederlande.

[Karp et al., 2010] Karp, D. A., Stahley, M. R., and Garcia-Moreno, E. B. (2010). Conformational Consequences of Ionization of Lys, Asp, and Glu Buried at Position 66 in Staphylococcal Nuclease. *Biochemistry*, 49(19):4138–4146.

[Kataoka et al., 1995] Kataoka, M., Nishii, I., Fujisawa, T., Ueki, T., Tokunaga, F., and Goto, Y. (1995). Structural Characterization of the Molten Globule and Native States of Apomyoglobin By Solution X-ray-scattering. *Journal of Molecular Biology*, 249(1):215–228.

[Katayama et al., 2010] Katayama, Y., Hattori, T., Saitoh, H., Ikeda, T., Aoki, K., Fukui, H., and Funakoshi, K. (2010). Structure of liquid water under high pressure up to 17 GPa. *Physical Review B*, 81(1):014109.

[Kauzmann, 1987] Kauzmann, . W. (1987). Protein Stabilization - Thermodynamics of Unfolding. *Nature*, 325(6107):763–764.

[Kim et al., 2011] Kim, J. M., Castaneda-Priego, R., Liu, Y., and Wagner, N. J. (2011). On the importance of thermodynamic self-consistency for calculating clusterlike pair correlations in hard-core double Yukawa fluids. *Journal of Chemical Physics*, 134(6):064904.

[Kirste and Porod, 1962] Kirste, R. and Porod, G. (1962). Röntgenkleinwinkelstreuung an kolloiden Systemen - asymptotisches Verhalten der Streukurven. *Kolloid-Zeitschrift und Zeitschrift Für Polymere*, 184:1.

[Kirste and Oberthür, 1982] Kirste, R. G. and Oberthür, R. C. (1982). Synthetic polymers in solution. In Glatter, O. and Kratky, O., editors, *Small Angle X-ray Scattering*, chapter 12, page 387. Academic Press, UK.

[Kitahara et al., 2011] Kitahara, R., Hata, K., Maeno, A., Akasaka, K., Chimenti, M. S., Garcia-Moreno, B., Schroer, M. A., Jeworrek, C., Tolan, M., Winter, R., Roche, J., Roumestand, C., Montet de Guillen, K., and Royer, C. A. (2011). Structural plasticity of staphylococcal nuclease probed by perturbation with pressure and pH. *Proteins: Structure, Function, and Bioinformatics*, 79(4):1293–1305.

[Klein, 2002] Klein, R. (2002). Interacting colloidal suspensions. In Lindner, P. and Zemb, T., editors, *Neutrons, X-Ray and Light: Scattering Methods Applied to Soft Condensed Matter*, chapter 14, page 351. Elsevier Science.

[Kohn et al., 2004] Kohn, J. E., Millett, I. S., Jacob, J., Zagrovic, B., Dillon, T. M., Cingel, N., Dothager, R. S., Seifert, S., Thiyagarajan, P., Sosnick, T. R., Hasan, M. Z., Pande, V. S., Ruczinski, I., Doniach, S., and Plaxco, K. W. (2004). Random-coil behavior and the dimensions of chemically unfolded proteins. *Proceedings of the National Academy of Sciences of the United States of America*, 101(34):12491–12496.

[Kotlarchyk and Chen, 1983] Kotlarchyk, M. and Chen, S. H. (1983). Analysis of Small-angle Neutron-scattering Spectra From Polydisperse Interacting Colloids. *Journal of Chemical Physics*, 79(5):2461–2469.

[Kratky, 1982] Kratky, O. (1982). Natural high polymers in the dissolved and solid state. In Glatter, O. and Kratky, O., editors, *Small Angle X-ray Scattering*, chapter 11, page 361. Academic Press, UK.

[Kratky and Porod, 1948] Kratky, O. and Porod, G. (1948). Die Abhängigkeit der Röntgen-Kleinwinkelstreuung von Form und Größe der kolloiden Teilchen in verdünnten Systemen, III. *Acta Physica Austriaca*, 2:133.

[Krywka, 2008] Krywka, C. (2008). *Ein Aufbau für Röntgenkleinwinkelstreuung an Protein-Lösungen an der Synchrotronstrahlungsquelle DELTA*. PhD thesis, TU Dortmund.

[Krywka et al., 2006] Krywka, C., Paulus, M., Sternemann, C., Volmer, M., Remhof, A., Nowak, G., Nefedov, A., Poter, B., Spiegel, M., and Tolan, M. (2006). The new diffractometer for surface X-ray diffraction at beamline BL9 of DELTA. *Journal of Synchrotron Radiation*, 13:8–13.

[Krywka et al., 2007] Krywka, C., Sternemann, C., Paulus, M., Javid, N., Winter, R., Al-Sawalmih, A., Yi, S. B., Raabe, D., and Tolan, M. (2007). The small-angle and wide-angle X-ray scattering set-up at beamline BL9 of DELTA. *Journal of Synchrotron Radiation*, 14:244–251.

[Krywka et al., 2008] Krywka, C., Sternemann, C., Paulus, M., Tolan, M., Royer, C., and Winter, R. (2008). Effect of Osmolytes on Pressure-induced Unfolding of Proteins: A High-Pressure SAXS Study. *ChemPhysChem*, 9(18):2809–2815.

[Kuehner et al., 1999] Kuehner, D. E., Engmann, J., Fergg, F., Wernick, M., Blanch, H. W., and Prausnitz, J. M. (1999). Lysozyme net charge and ion binding in concentrated aqueous electrolyte solutions. *Journal of Physical Chemistry B*, 103(8):1368–1374.

[Lassalle et al., 2000] Lassalle, M. W., Yamada, H., and Akasaka, K. (2000). The pressure-temperature free energy-landscape of staphylococcal nuclease monitored by H-1 NMR. *Journal of Molecular Biology*, 298(2):293–302.

[Le Bolloc'h et al., 2002] Le Bolloc'h, D., Livet, F., Bley, F., Schulli, T., Veron, M., and Metzger, T. H. (2002). X-ray diffraction from rectangular slits. *Journal of Synchrotron Radiation*, 9:258–265.

[Leeson et al., 2000] Leeson, D. T., Gai, F., Rodriguez, H. M., Gregoret, L. M., and Dyer, R. B. (2000). Protein folding and unfolding on a complex energy landscape. *Proceedings of the National Academy of Sciences of the United States of America*, 97(6):2527–2532.

[Lide, 2003] Lide, D., editor (2003). *CRC Handbook of Chemistry and Physics*. CRC Press, 84. edition.

[Lindner, 2002] Lindner, P. (2002). Scattering experiments: Experimental aspects, initial data reduczion and absolute calibration. In Lindner, P. and Zemb, T., editors, *Neutrons, X-Ray and Light: Scattering Methods Applied to Soft Condensed Matter*, chapter 2, page 23. Elsevier Science.

[Lindner and Zemb, 2002] Lindner, P. and Zemb, T., editors (2002). *Neutrons, X-Ray and Light: Scattering Methods Applied to Soft Condensed Matter*. Elsevier Science.

[Liu et al., 2005] Liu, Y., Chen, W. R., and Chen, S. H. (2005). Cluster formation in two-Yukawa fluids. *Journal of Chemical Physics*, 122(4):044507.

[Liu et al., 2011] Liu, Y., Porcar, L., Chen, J. H., Chen, W. R., Falus, P., Faraone, A., Fratini, E., Hong, K. L., and Baglioni, P. (2011). Lysozyme protein solution with an intermediate range order structure. *Journal of Physical Chemistry B*, 115(22):7238–7247.

[Löffler et al., 2007] Löffler, G., Petrides, P. E., and Heinrich, P. C., editors (2007). *Biochemie & Pathobiochemie*. Springer, 8 edition.

[Ludwig, 2001] Ludwig, R. (2001). Water: From clusters to the bulk. *Angewandte Chemie International Edition*, 40(10):1808–1827.

[Luecke et al., 1999] Luecke, H., Schobert, B., Richter, H. T., Cartailler, J. P., and Lanyi, J. K. (1999). Structure of bacteriorhodopsin at 1.55 Angstrom resolution. *Journal of Molecular Biology*, 291(4):899–911.

[Maeno et al., 2009] Maeno, A., Matsuo, H., and Akasaka, K. (2009). The pressure-temperature phase diagram of hen lysozyme at low pH. *Biophysics*, 5:1–9.

[Malfois et al., 1996] Malfois, M., Bonnete, F., Belloni, L., and Tardieu, A. (1996). A model of attractive interactions to account for fluid-fluid phase separation of protein solutions. *Journal of Chemical Physics*, 105(8):3290–3300.

[Martin and Hurd, 1987] Martin, J. E. and Hurd, A. J. (1987). Scattering from fractals. *Journal of Applied Crystallography*, 20:61–78.

[Matthews, 1993] Matthews, C. R. (1993). Pathways of Protein-folding. *Annual Review of Biochemistry*, 62:653–683.

[May, 2002] May, R. P. (2002). Biological applications of small-angle neutron scattering. In Lindner, P. and Zemb, T., editors, *Neutrons, X-Ray and Light: Scattering Methods Applied to Soft Condensed Matter*, chapter 19, page 463. Elsevier Science.

[Meersman et al., 2009] Meersman, F., Bowron, D., Soper, A. K., and Koch, M. H. J. (2009). Counteraction of Urea by Trimethylamine N-Oxide Is Due to Direct Interaction. *Biophysical Journal*, 97(9):2559–2566.

[Meersman et al., 2011] Meersman, F., Bowron, D., Soper, A. K., and Koch, M. H. J. (2011). An X-ray and neutron scattering study of the equilibrium between trimethylamine N-oxide and urea in aqueous solution. *Physical Chemistry Chemical Physics*, 13(30):13765–13771.

[Meersman et al., 2006] Meersman, F., Dobson, C. M., and Heremans, K. (2006). Protein unfolding, amyloid fibril formation and configurational energy landscapes under high pressure conditions. *Chemical Society Reviews*, 35(10):908–917.

[Mello and Barrick, 2004] Mello, C. C. and Barrick, D. (2004). An experimentally determined protein folding energy landscape. *Proceedings of the National Academy of Sciences of the United States of America*, 101(39):14102–14107.

[Mello et al., 2005] Mello, C. C., Bradley, C. M., Tripp, K. W., and Barrick, D. (2005). Experimental characterization of the folding kinetics of the notch ankyrin domain. *Journal of Molecular Biology*, 352(2):266–281.

[Mitra et al., 2007] Mitra, L., Hata, K., Kono, R., Maeno, A., Isom, D., Rouget, J. B., Winter, R., Akasaka, K., Garcia-Moreno, B., and Royer, C. A. (2007). V-i-Value analysis: A pressure-based method for mapping the folding transition state ensemble of proteins. *Journal of the American Chemical Society*, 129(46):14108–14109.

[Mitra et al., 2006] Mitra, L., Smolin, N., Ravindra, R., Royer, C., and Winter, R. (2006). Pressure perturbation calorimetric studies of the solvation properties and the thermal unfolding of proteins in solution - experiments and theoretical interpretation. *Physical Chemistry Chemical Physics*, 8(11):1249–1265.

[Mittelbach, 1964] Mittelbach, P. (1964). Zur Röntgenkleinwinkelstreuung verdünnter kolloider Systeme VIII. Diskussion des Streuverhaltens regelmäßiger Körper und Methoden zur Bestimmung von Größe und Form kolloider Teilchen. *Acta Physica Austriaca*, 19:54.

[Mittelbach and Porod, 1962] Mittelbach, P. and Porod, G. (1962). Zur Röntgenkleinwinkelstreuung verdünnter kolloider Systeme VII. Die Berechnung der Streukurven von dreiachsigen Ellipsoiden. *Acta Physica Austriaca*, 15:122.

[Muschol and Rosenberger, 1997] Muschol, M. and Rosenberger, F. (1997). Liquid-liquid phase separation in supersaturated lysozyme solutions and associated precipitate formation/crystallization. *Journal of Chemical Physics*, 107(6):1953–1962.

[Nägele, 2008] Nägele, G. (2008). Theories of Fluid Microstructures. In Dhont, J. K. G., Gompper, G., Nägele, G., Richter, D., and Winkler, R. G., editors, *39th IFF Spring School 2008: "Soft Matter: From Synthetic to Biological Materials"*, chapter B 2. Forschungszentrum Jülich.

[Narayanan and Liu, 2003] Narayanan, J. and Liu, X. Y. (2003). Protein interactions in undersaturated and supersaturated solutions: A study using light and x-ray scattering. *Biophysical Journal*, 84(1):523–532.

[Narayanan et al., 2001] Narayanan, T., Diat, O., and Bosecke, P. (2001). SAXS and USAXS on the high brilliance beamline at the ESRF. *Nuclear Instruments & Methods In Physics Research Section A-accelerators Spectrometers Detectors and Associated Equipment*, 467:1005–1009.

[Neuman et al., 1973] Neuman, R. C., Kauzmann, W., and Zipp, A. (1973). Pressure-dependence of Weak Acid Ionization In Aqueous Buffers. *Journal of Physical Chemistry*, 77(22):2687–2691.

[Niebuhr and Koch, 2005] Niebuhr, M. and Koch, M. H. J. (2005). Effects of urea and trimethylamine-N-oxide (TMAO) on the interactions of lysozyme in solution. *Biophysical Journal*, 89(3):1978–1983.

[Nishimura et al., 2001] Nishimura, C., Uversky, V. N., and Fink, A. L. (2001). Effect of salts on the stability and folding of staphylococcal nuclease. *Biochemistry*, 40(7):2113–2128.

[Okhulkov et al., 1994] Okhulkov, A. V., Demianets, Y. N., and Gorbaty, Y. E. (1994). X-ray-scattering In Liquid Water At Pressures of Up To 7.7 Kbar - Test of A Fluctuation Model. *Journal of Chemical Physics*, 100(2):1578–1588.

[Oregon State University, 2008] Oregon State University (2008). Oregon State University - Department of Crop and Soil Science: http://cropandsoil.oregonstate.edu/classes/css430/lecture%209-07/figure-09-03.JPG. Date checked: 30.07.2008.

[Ornstein and Zernike, 1914] Ornstein, L. S. and Zernike, F. (1914). Accidental deviations of density and opalescence at the critical point of a simple substance. *Koninklijke Nederlandse Akademie van Wetenschappen Amsterdam Proc. Sec. Sci.*, 17:793.

[Orthaber et al., 2000] Orthaber, D., Bergmann, A., and Glatter, O. (2000). SAXS experiments on absolute scale with Kratky systems using water as a secondary standard. *Journal of Applied Crystallography*, 33:218–225.

[Ortore et al., 2008] Ortore, M. G., Sinibaldi, R., Spinozzi, F., Carsughi, F., Clemens, D., Bonincontro, A., and Mariani, P. (2008). New Insights into Urea Action on Proteins: A SANS Study of the Lysozyme Case. *Journal of Physical Chemistry B*, 112(41):12881–12887.

[Ortore et al., 2009] Ortore, M. G., Spinozzi, F., Mariani, P., Paciaroni, A., Barbosa, L. R. S., Amenitsch, H., Steinhart, M., Ollivier, J., and Russo, D. (2009). Combining structure and dynamics: Non-denaturing high-pressure effect on lysozyme in solution. *Journal of the Royal Society Interface*, 6:S619–S634.

[Paliwal et al., 2004] Paliwal, A., Asthagiri, D., Bossev, D. P., and Paulaitis, M. E. (2004). Pressure denaturation of staphylococcal nuclease studied by neutron small-angle scattering and molecular simulation. *Biophysical Journal*, 87(5):3479–3492.

[Panick et al., 1998] Panick, G., Malessa, R., Winter, R., Rapp, G., Frye, K. J., and Royer, C. A. (1998). Structural characterization of the pressure-denatured state and unfolding/refolding kinetics of staphylococcal nuclease by synchrotron small-angle X-ray scattering and Fourier-transform infrared spectroscopy. *Journal of Molecular Biology*, 275(2):389–402.

[Panick et al., 1999] Panick, G., Vidugiris, G. J. A., Malessa, R., Rapp, G., Winter, R., and Royer, C. A. (1999). Exploring the temperature-pressure phase diagram of staphylococcal nuclease. *Biochemistry*, 38(13):4157–4164.

[Panuszko et al., 2009] Panuszko, A., Bruzdziak, P., Zielkiewicz, J., Wyrzykowski, D., and Stangret, J. (2009). Effects of Urea and Trimethylamine-N-oxide on the Properties of Water and the Secondary Structure of Hen Egg White Lysozyme. *Journal of Physical Chemistry B*, 113(44):14797–14809.

[Paul and Patey, 2007] Paul, S. and Patey, G. N. (2007). Structure and interaction in aqueous urea-trimethylamine-N-oxide solutions. *Journal of the American Chemical Society*, 129(14):4476–4482.

[Paulus et al., 2008] Paulus, M., Lietz, D., Sternemann, C., Shokuie, K., Evers, F., Tolan, M., Czeslik, C., and Winter, R. (2008). An access to buried interfaces: The X-ray reflectivity set-up of BL9 at DELTA. *Journal of Synchrotron Radiation*, 15:600–605.

[Pedersen, 2002] Pedersen, J. (2002). Modelling of small-angle scattering: Data from colloids and polymer systems. In Lindner, P. and Zemb, T., editors, *Neutrons, X-Ray and Light: Scattering Methods Applied to Soft Condensed Matter*, chapter 16, page 391. Elsevier Science.

[Perlich et al., 2010] Perlich, J., Rubeck, J., Botta, S., Gehrke, R., Roth, S. V., Ruderer, M. A., Prams, S. M., Rawolle, M., Zhong, Q., Korstgens, V., and Müller-Buschbaum, P. (2010). Grazing incidence wide angle x-ray scattering at the wiggler beamline BW4 of HASYLAB. *Review of Scientific Instruments*, 81(10):105105.

[Perrett and Zhou, 2002] Perrett, S. and Zhou, J. M. (2002). Expanding the pressure technique: Insights into protein folding from combined use of pressure and chemical denaturants. *Biochimica Et Biophysica Acta-Protein Structure and Molecular Enzymology*, 1595(1-2):210–223.

[Pietsch et al., 2004] Pietsch, U., Holý, V., and Baumbach, T. (2004). *High Resolution X-Ray Scattering*. Springer, 2. edition.

[Porod, 1948] Porod, G. (1948). Die Abhängigkeit der Röntgen-Kleinwinkelstreuung von Form und Grösse der kolloiden Teilchen in verdünnten Systemen, IV. *Acta Physica Austrica*, 2:255.

[Porod, 1951] Porod, G. (1951). Die Röntgenkleinwinkelstreuung Von Dichtgepackten Kolloiden Systemen. 1. *Kolloid-Zeitschrift und Zeitschrift Für Polymere*, 124(2):83–114.

[Porod, 1952] Porod, G. (1952). Die Röntgenkleinwinkelstreuung Von Dichtgepackten Kolloiden Systemen. 2. *Kolloid-Zeitschrift und Zeitschrift Für Polymere*, 125(2):108–122.

[Porod, 1982] Porod, G. (1982). General theory. In Glatter, O. and Kratky, O., editors, *Small Angle X-ray Scattering*, chapter 2, page 17. Academic Press, UK.

[Ravindra and Winter, 2003] Ravindra, R. and Winter, R. (2003). On the temperature - pressure free-energy landscape of proteins. *ChemPhysChem*, 4(4):359–365.

[RCSB Protein Data Bank, 2000] RCSB Protein Data Bank (2000). www.pdb.org.

[Roth et al., 2006] Roth, S. V., Dohrmann, R., Dommach, M., Kuhlmann, M., Kroger, I., Gehrke, R., Walter, H., Schroer, C., Lengeler, B., and Müller-Buschbaum, P. (2006). Small-angle options of the upgraded ultrasmall-angle x-ray scattering beamline BW4 at HASYLAB. *Review of Scientific Instruments*, 77(8):085106.

[Rothschild and Mancinelli, 2001] Rothschild, L. J. and Mancinelli, R. L. (2001). Life in extreme environments. *Nature*, 409(6823):1092–1101.

[Rouget et al., 2011] Rouget, J. B., Aksel, T., Roche, J., Saldana, J. L., Garcia, A. E., Barrick, D., and Royer, C. A. (2011). Size and Sequence and the Volume Change of Protein Folding. *Journal of the American Chemical Society*, 133(15):6020–6027.

[Rouget et al., 2010] Rouget, J. B., Schroer, M. A., Jeworrek, C., Puhse, M., Saldana, J. L., Bessin, Y., Tolan, M., Barrick, D., Winter, R., and Royer, C. A. (2010). Unique Features of the Folding Landscape of a Repeat Protein Revealed by Pressure Perturbation. *Biophysical Journal*, 98(11):2712–2721.

[Royer, 2002] Royer, C. A. (2002). Revisiting volume changes in pressure-induced protein unfolding. *Biochimica Et Biophysica Acta-Protein Structure and Molecular Enzymology*, 1595(1-2):201–209.

[Royer et al., 1993] Royer, C. A., Hinck, A. P., Loh, S. N., Prehoda, K. E., Peng, X. D., Jonas, J., and Markley, J. L. (1993). Effects of Amino-acid Substitutions On the Pressure Denaturation of Staphylococcal Nuclease As Monitored By Fluorescence and Nuclear-magnetic-resonance Spectroscopy. *Biochemistry*, 32(19):5222–5232.

[Sarupria et al., 2010] Sarupria, S., Ghosh, T., Garcia, A. E., and Garde, S. (2010). Studying pressure denaturation of a protein by molecular dynamics simulations. *Proteins: Structure, Function, and Bioinformatics*, 78(7):1641–1651.

[Schlessman et al., 2008] Schlessman, J. L., Abe, C., Gittis, A., Karp, D. A., Dolan, M. A., and Garcia-Moreno, B. E. (2008). Crystallographic study of hydration of an internal cavity in engineered proteins with buried polar or ionizable groups. *Biophysical Journal*, 94(8):3208–3216.

[Schmidt, 1991] Schmidt, P. W. (1991). Small-angle Scattering Studies of Disordered, Porous and Fractal Systems. *Journal of Applied Crystallography*, 24:414–435.

[Schmitz, 1993] Schmitz, K. S. (1993). *Macroions in Solution and Colloidal Suspension*. VCH Publishers, Inc.

[Schrödinger, LLC, 2008] Schrödinger, LLC (2008). The PyMOL Molecular Graphics System, Version 0.99rc6,.

[Schroer, 2008] Schroer, M. (2008). Röntgenkleinwinkelstreuung an dem Protein Staphylokkoken Nuklease und dessen Mutanten. Diploma thesis, TU Dortmund. (unpublished).

[Schroer et al., 2011] Schroer, M. A., Markgraf, J., Wieland, D. C. F., Sahle, C. J., Möller, J., Paulus, M., Tolan, M., and Winter, R. (2011). Nonlinear Pressure Dependence of the Interaction Potential of Dense Protein Solutions. *Physical Review Letters*, 106(17):178102.

[Schroer et al., 2010] Schroer, M. A., Paulus, M., Jeworrek, C., Krywka, C., Schmacke, S., Zhai, Y., Wieland, D. C. F., Sahle, C. J., Chimenti, M., Royer, C. A., Garcia-Moreno, B., Tolan, M., and Winter, R. (2010). High-Pressure SAXS Study of Folded and Unfolded Ensembles of Proteins. *Biophysical Journal*, 99(10):3430–3437.

[Schurtenberger, 2002a] Schurtenberger, P. (2002a). Contrast and contrast variation in neutron, x-ray and light scattering. In Lindner, P. and Zemb, T., editors, *Neutrons, X-Ray and Light: Scattering Methods Applied to Soft Condensed Matter*, chapter 7, page 145. Elsevier Science.

[Schurtenberger, 2002b] Schurtenberger, P. (2002b). Static properties of polymers. In Lindner, P. and Zemb, T., editors, *Neutrons, X-Ray and Light: Scattering Methods Applied to Soft Condensed Matter*, chapter 11, page 259. Elsevier Science.

[Seemann et al., 2001] Seemann, H., Winter, R., and Royer, C. A. (2001). Volume, expansivity and isothermal compressibility changes associated with temperature and pressure unfolding of staphylococcal nuclease. *Journal of Molecular Biology*, 307(4):1091–1102.

[Selkoe, 2003] Selkoe, D. J. (2003). Folding proteins in fatal ways. *Nature*, 426(6968):900–904.

[Semisotnov et al., 1996] Semisotnov, G. V., Kihara, H., Kotova, N. V., Kimura, K., Amemiya, Y., Wakabayashi, K., Serdyuk, I. N., Timchenko, A. A., Chiba, K., Nikaido, K., Ikura, T., and Kuwajima, K. (1996). Protein globularization during folding. A study by synchrotron small-angle X-ray scattering. *Journal of Molecular Biology*, 262(4):559–574.

[Sharma and Sharma, 1977] Sharma, R. V. and Sharma, K. C. (1977). Structure Factor and Transport Properties of Dense Fluids Having Molecules With Square-well Potential - Possible Generalization. *Physica A*, 89(1):213–218.

[Sherman and Stadtmuller, 1987] Sherman, W. F. and Stadtmuller, A. A. (1987). *Experimental Techniques in High-Pressure Research*. John Wiley & Sons Inc.

[Shukla et al., 2008] Shukla, A., Mylonas, E., Di Cola, E., Finet, S., Timmins, P., Narayanan, T., and Svergun, D. I. (2008). Absence of equilibrium cluster phase in concentrated lysozyme solutions. *Proceedings of the National Academy of Sciences of the United States of America*, 105(13):5075–5080.

[Silva et al., 2001] Silva, J. L., Foguel, D., and Royer, C. A. (2001). Pressure provides new insights into protein folding, dynamics and structure. *Trends In Biochemical Sciences*, 26(10):612–618.

[Sinha, 1989] Sinha, S. K. (1989). Scattering from fractal structures. *Physica D*, 38(1-3):310–314.

[Sinibaldi et al., 2007] Sinibaldi, R., Ortore, M. G., Spinozzi, F., Carsughi, F., Frielinghaus, H., Cinelli, S., Onori, G., and Mariani, P. (2007). Preferential hydration of lysozyme in water/glycerol mixtures: A small-angle neutron scattering study. *Journal of Chemical Physics*, 126(23):235101.

[Sinibaldi et al., 2008] Sinibaldi, R., Ortore, M. G., Spinozzi, F., Funari, S. D., Teixeira, J., and Mariani, P. (2008). SANS/SAXS study of the BSA solvation properties in aqueous urea

solutions via a global fit approach. *European Biophysics Journal With Biophysics Letters*, 37(5):673–681.

[Sinko et al., 2008] Sinko, K., Torma, V., and Kovacs, A. (2008). SAXS investigation of porous nanostructures. *Journal of Non-Crystalline Solids*, 354(52-54):5466–5474.

[Smeller, 2002] Smeller, L. (2002). Pressure-temperature phase diagrams of biomolecules. *Biochimica Et Biophysica Acta-Protein Structure and Molecular Enzymology*, 1595(1-2):11–29.

[Sobry and Ciccariello, 2002] Sobry, R. and Ciccariello, S. (2002). Background subtraction and moments of the microscopic density fluctuation. *Journal of Applied Crystallography*, 35:220–227.

[Soper and Ricci, 2000] Soper, A. K. and Ricci, M. A. (2000). Structures of high-density and low-density water. *Physical Review Letters*, 84(13):2881–2884.

[Sosnick and Barrick, 2011] Sosnick, T. R. and Barrick, D. (2011). The folding of single domain proteins - have we reached a consensus? *Current Opinion In Structural Biology*, 21(1):12–24.

[Spalla, 2002] Spalla, O. (2002). General theorems in small-angle scattering. In Lindner, P. and Zemb, T., editors, *Neutrons, X-Ray and Light: Scattering Methods Applied to Soft Condensed Matter*, chapter 3, page 49. Elsevier Science.

[Stadler et al., 2010] Stadler, A. M., Schweins, R., Zaccai, G., and Lindner, P. (2010). Observation of a Large-Scale Superstructure in Concentrated Hemoglobin Solutions by Using Small Angle Neutron Scattering. *Journal of Physical Chemistry Letters*, 1(12):1805–1808.

[Stradner et al., 2004] Stradner, A., Sedgwick, H., Cardinaux, F., Poon, W. C. K., Egelhaaf, S. U., and Schurtenberger, P. (2004). Equilibrium cluster formation in concentrated protein solutions and colloids. *Nature*, 432(7016):492–495.

[Stribeck, 2007] Stribeck, N. (2007). *X-ray Scattering of Soft Matter*. Springer Berlin Heidelberg New York.

[Sun et al., 2003] Sun, Q., Zheng, H. F., Xu, J. A., and Hines, E. (2003). Raman spectroscopic studies of the stretching band from water up to 6 kbar at 290 K. *Chemical Physics Letters*, 379(5-6):427–431.

[Svergun, 1992] Svergun, D. I. (1992). Determination of the Regularization Parameter In Indirect-transform Methods Using Perceptual Criteria. *Journal of Applied Crystallography*, 25:495–503.

[Svergun, 1999] Svergun, D. I. (1999). Restoring low resolution structure of biological macromolecules from solution scattering using simulated annealing. *Biophysical Journal*, 76(6):2879–2886.

[Svergun and Koch, 2003] Svergun, D. I. and Koch, M. H. J. (2003). Small-angle scattering studies of biological macromolecules in solution. *Reports On Progress In Physics*, 66(10):1735–1782.

[Svergun et al., 2009] Svergun, D. I., Semyenuk, A., and Gajda, M. J. (2009). GNOM manual: http://www.embl-hamburg.de/biosaxs/manual_gnom.html. Date checked: 08.08.2011.

[Takayama et al., 2008] Takayama, Y., Castaneda, C. A., Chimenti, M., Garcia-Moreno, B., and Iwahara, J. (2008). Direct evidence for deprotonation of a lysine side chain buried in the hydrophobic core of a protein. *Journal of the American Chemical Society*, 130(21):6714.

[Takayasu, 1990] Takayasu, H. (1990). *Fractals in the physical sciences*. Manchester University Press.

[Tardieu et al., 1999] Tardieu, A., Le Verge, A., Malfois, M., Bonnete, F., Finet, S., Ries-Kautt, M., and Belloni, L. (1999). Proteins in solution: from x-ray scattering intensities to interaction potentials. *Journal of Crystal Growth*, 196(2-4):193–203.

[Timasheff, 1993] Timasheff, S. N. (1993). The Control of Protein Stability and Association By Weak-interactions With Water - How Do Solvents Affect These Processes. *Annual Review of Biophysics and Biomolecular Structure*, 22:67–97.

[Timmann et al., 2009] Timmann, A., Dohrmann, R., Schubert, T., Schulte-Schrepping, H., Hahn, U., Kuhlmann, M., Gehrke, R., Roth, S. V., Schropp, A., Schroer, C., and Lengeler, B. (2009). Small angle x-ray scattering with a beryllium compound refractive lens as focusing optic. *Review of Scientific Instruments*, 80(4):046103.

[Tucker et al., 1978] Tucker, P. W., Hazen, E. E., and Cotton, F. A. (1978). Staphylococcal Nuclease Reviewed - Prototypic Study In Contemporary Enzymology. 1. Isolation - Physical and Enzymatic Properties. *Molecular and Cellular Biochemistry*, 22(2-3):67–77.

[Uversky, 2002] Uversky, V. N. (2002). Natively unfolded proteins: A point where biology waits for physics. *Protein Science*, 11(4):739–756.

[Uversky, 2009] Uversky, V. N. (2009). Intrinsically Disordered Proteins and Their Environment: Effects of Strong Denaturants, Temperature, pH, Counter Ions, Membranes, Binding Partners, Osmolytes, and Macromolecular Crowding. *Protein Journal*, 28(7-8):305–325.

[Uversky et al., 2000] Uversky, V. N., Gillespie, J. R., and Fink, A. L. (2000). Why are "natively unfolded" proteins unstructured under physiologic conditions? *Proteins: Structure, Function, and Genetics*, 41(3):415–427.

[Uversky et al., 1999] Uversky, V. N., Karnoup, A. S., Khurana, R., Segel, D. J., Doniach, S., and Fink, A. L. (1999). Association of partially-folded intermediates of staphylococcal nuclease induces structure and stability. *Protein Science*, 8(1):161–173.

[Uversky et al., 1998a] Uversky, V. N., Karnoup, A. S., Segel, D. J., Seshadri, S., Doniach, S., and Fink, A. L. (1998a). Anion-induced folding of Staphylococcal nuclease: Characterization of multiple equilibrium partially folded intermediates. *Journal of Molecular Biology*, 278(4):879–894.

[Uversky et al., 1998b] Uversky, V. N., Segel, D. J., Doniach, S., and Fink, A. L. (1998b). Association-induced folding of globular proteins. *Proceedings of the National Academy of Sciences of the United States of America*, 95(10):5480–5483.

[Vidugiris et al., 1996] Vidugiris, G. J. A., Truckses, D. M., Markley, J. L., and Royer, C. A. (1996). High-pressure denaturation of staphylococcal nuclease proline-to-glycine substitution mutants. *Biochemistry*, 35(12):3857–3864.

[Voet et al., 2006] Voet, D., Voet, J. D., and W., P. C. (2006). *Fundamentals of Biochemistry. Life at the molecular level*. Wiley.

[Weck et al., 2009] Weck, G., Eggert, J., Loubeyre, P., Desbiens, N., Bourasseau, E., Maillet, J. B., Mezouar, M., and Hanfland, M. (2009). Phase diagrams and isotopic effects of normal and deuterated water studied via x-ray diffraction up to 4.5 GPa and 500 K. *Physical Review B*, 80(18):180202.

[Wei et al., 2010] Wei, H. Y., Fan, Y. B., and Gao, Y. Q. (2010). Effects of Urea, Tetramethyl Urea, and Trimethylamine N-Oxide on Aqueous Solution Structure and Solvation of Protein Backbones: A Molecular Dynamics Simulation Study. *Journal of Physical Chemistry B*, 114(1):557–568.

[Wignall et al., 1990] Wignall, G. D., Lin, J. S., and Spooner, S. (1990). Reduction of parasitic scattering in small-angle x-ray-scattering by a 3-pinhole collimating system. *Journal of Applied Crystallography*, 23:241–245.

[Winter et al., 2007] Winter, R., Lopes, D., Grudzielanek, S., and Vogtt, K. (2007). Towards an understanding of the temperature/pressure configurational and free-energy landscape of biomolecules. *Journal of Non-equilibrium Thermodynamics*, 32(1):41–97.

[Winter and Noll, 1998] Winter, R. and Noll, F. (1998). *Methoden der Biophysikalischen Chemie*. Teubner Studienbücher.

[Woenckhaus et al., 2001] Woenckhaus, J., Kohling, R., Thiyagarajan, P., Littrell, K. C., Seifert, S., Royer, C. A., and Winter, R. (2001). Pressure-jump small-angle x-ray scattering detected kinetics of staphylococcal nuclease folding. *Biophysical Journal*, 80(3):1518–1523.

[Yancey, 2005] Yancey, P. H. (2005). Organic osmolytes as compatible, metabolic and counteracting cytoprotectants in high osmolarity and other stresses. *Journal of Experimental Biology*, 208(15):2819–2830.

[Yancey et al., 2002] Yancey, P. H., Blake, W. R., and Conley, J. (2002). Unusual organic osmolytes in deep-sea animals: Adaptations to hydrostatic pressure and other perturbants. *Comparative Biochemistry and Physiology A-molecular and Integrative Physiology*, 133(3):667–676.

[Yoshikawa et al., 1998] Yoshikawa, S., Shinzawa-Itoh, K., Nakashima, R., Yaono, R., Yamashita, E., Inoue, N., Yao, M., Fei, M. J., Libeu, C. P., Mizushima, T., Yamaguchi, H., Tomizaki, T., and Tsukihara, T. (1998). Redox-coupled crystal structural changes in bovine heart cytochrome c oxidase. *Science*, 280(5370):1723–1729.

[Zernike and Prins, 1927] Zernike, F. and Prins, J. A. (1927). Die Beugung von Röntgenstrahulng in Flüssigkeiten als Effekt der Molekülanordnung. *Zeitschrift für Physik*, 41:184.

[Zhang et al., 2008] Zhang, F., Skoda, M. W. A., Jacobs, R. M. J., Zorn, S., Martin, R. A., Martin, C. M., Clark, G. F., Weggler, S., Hildebrandt, A., Kohlbacher, O., and Schreiber, F. (2008). Reentrant condensation of proteins in solution induced by multivalent counterions. *Physical Review Letters*, 101(14):148101.

[Zhang et al., 2007] Zhang, F. J., Skoda, M. W. A., Jacobs, R. M. J., Martin, R. A., Martin, C. M., and Schreiber, F. (2007). Protein interactions studied by SAXS: Effect of ionic strength and protein concentration for BSA in aqueous solutions. *Journal of Physical Chemistry B*, 111(1):251–259.

[Zhang et al., 2010] Zhang, F. J., Weggler, S., Ziller, M. J., Ianeselli, L., Heck, B. S., Hildebrandt, A., Kohlbacher, O., Skoda, M. W. A., Jacobs, R. M. J., and Schreiber, F. (2010). Universality of protein reentrant condensation in solution induced by multivalent metal ions. *Proteins: Structure, Function, and Bioinformatics*, 78(16):3450–3457.

[Zhang et al., 2011] Zhang, F. J., Zocher, G., Sauter, A., Stehle, T., and Schreiber, F. (2011). Novel approach to controlled protein crystallization through ligandation of yttrium cations. *Journal of Applied Crystallography*, 44:755–762.

[Zheng and Sosnick, 2010] Zheng, Z. Z. and Sosnick, T. R. (2010). Protein Vivisection Reveals Elusive Intermediates in Folding. *Journal of Molecular Biology*, 397(3):777–788.

[Zou et al., 2002] Zou, Q., Bennion, B. J., Daggett, V., and Murphy, K. P. (2002). The molecular mechanism of stabilization of proteins by TMAO and its ability to counteract the effects of urea. *Journal of the American Chemical Society*, 124(7):1192–1202.

[Zweifel and Barrick, 2001a] Zweifel, M. E. and Barrick, D. (2001a). Studies of the ankyrin repeats of the Drosophila melanogaster Notch receptor. 1. Solution conformational and hydrodynamic properties. *Biochemistry*, 40(48):14344–14356.

[Zweifel and Barrick, 2001b] Zweifel, M. E. and Barrick, D. (2001b). Studies of the ankyrin repeats of the Drosophila melanogaster Notch receptor. 2. Solution stability and cooperativity of unfolding. *Biochemistry*, 40(48):14357–14367.

[Zweifel et al., 2003] Zweifel, M. E., Leahy, D. J., Hughson, F. M., and Barrick, D. (2003). Structure and stability of the ankyrin domain of the Drosophila Notch receptor. *Protein Science*, 12(11):2622–2632.

Publications

- Feroughi, O. M., Sternemann, C., Sahle, Ch. J., Schroer, M. A., Sternemann, H., Conrad, H., Hohl, A., Seidler, G. T., Bradley, J., Fister, T. T., Balasubramanian, M., Sakko, A., Pirkkalainen, K., Hämäläinen, K., and Tolan M. (2010). Phase separation and Si nanocrystal formation in bulk SiO studied by x-ray scattering. *Applied Physics Letters*, 96:081912.

- Rouget, J.-B., Schroer, M. A., Jeworrek, C., Pühse, M., Saldana, J. L., Bessin, Y., Tolan, M., Barrick, D., Winter, R., and Royer, C. A. (2010). Unique Features of the Folding Landscape of a Repeat Protein Revealed by Pressure Perturbation. *Biophysical Journal*, 98:2712-2721.

- Schroer, M. A., Paulus, M., Jeworrek, C., Krywka, C., Schmacke, S., Zhai, Y., Wieland, D. C. F., Sahle, Ch. J., Chimenti, M., Royer, C. A., Garcia-Moreno, B., Tolan, M., and Winter, R. (2010). High-Pressure SAXS Study of Folded and Unfolded Ensembles of Proteins. *Biophysical Journal*, 99:3430-3437.

- Kitahara, R., Hata, K., Maeno, A., Akasaka, K., Chimenti, M., Garcia-Moreno E., B., Schroer, M. A., Jeworrek, C., Tolan, M., Winter, R., Roche, J., Roumestand, C., Montet de Guillen, K., and Royer, C. A. (2011). Structural plasticity of staphylococcal nuclease probed by perturbation with pressure and pH. *Proteins: Structure, Function, and Bioinformatics*, 79:1293-1305.

- Schroer, M. A., Markgraf, J., Wieland, D. C. F., Sahle, Ch. J., Möller, J., Paulus, M., Tolan, M., and Winter, R. (2011). Nonlinear Pressure Dependence of the Interaction Potential of Dense Protein Solutions. *Physical Review Letters*, 106:178102.

- Arslan, H. K., Shekhah, O. I., Wieland, D. C. F., Paulus, M., Sternemann, C., Schroer, M. A., Tiemeyer, S., Tolan, M., Fischer, R. A., and Wöll, C. (2011). Intercalation in Layered Metal-Organic Frameworks: Reversible Inclusion of an Extended π-System. *Journal of the American Chemical Society*, 133, 8158-8161.

- Schroer, M. A., Zhai., Y., Wieland, D. C. F., Sahle, Ch. J., Nase, J., Paulus, M., Tolan, M., and Winter, R. (2011). Exploring the Piezophilic Behavior of Natural Cosolvent Mixtures. *Angewandte Chemie International Edition*, accepted for publication.

- Wieland, D. C. F., Paulus, M., Schroer, M. A., Tolan, M., Degen, P., and Rehage, R. (2011). Manipulating thin polymer films by change of the pH-value. *Journal of Applied Physics*, accepted for publication.

- Möller, J., Cebi, M., Schroer, M. A., Paulus, M., Degen, P., Sahle, Ch. J., Wieland, D. C. F., Leick, S., Nyrow, A., Rehage, H., and Tolan, M. (2011). Dissolution of iron oxide nanoparticles inside polymer nanocapsules. *Physical Chemistry Chemical Physics*, accepted for publication.

Acknowledgments

The last words of this thesis are dedicated to those persons who helped to successfully complete it.

At first I thank Prof. Metin Tolan for giving me the opportunity to write my thesis in his group and to work freely on this interesting interdisciplinary research topic. Moreover, I am grateful for letting me attend different workshops and conferences.

Similarly I am thankful to Prof. Roland Winter not only for co-supervising my thesis but also for his advice within the last years that largely helped to obtain much of the interesting phenomena presented herein. Furthermore, I want to thank him for involving me into the different collaborations.

I thank Dr. Michael Paulus and Dr. Christian Sternemann for their advice and help within the last years.

I am indebted to my dear friends Christoph Sahle and Florian Wieland for their unfailing help during all the beam times at the different synchrotrons and during everyday life in the office. Without them, large parts of this thesis would not have been possible.

I want to thank all persons who helped during the beamtimes, namely Dr. Michael Paulus, Dr. Christina Krywka, Andre Steffen, Sebastian Tiemeyer, Johannes Möller, and Dr. Julia Nase, and all others who I may have forgotten.

The local contacts of BW4, HASYLAB, Dr. Jan Perlich and Dr. Andreas Timmann, and I02, ESRF, Dr. Michael Sztucki and Dr. Shirley Callow, who helped during the beamtimes are kindly acknowledged.

I want to thank all members of the group of Prof. Winter with whom I was allowed to work with during the last years. Thanks to Christoph Jeworrek for his help with the high pressure equipment and to Yong Zhai and Jonas Markgraf for performing the calorimetric measurements and the FTIR spectroscopy measurements, respectively.

I also thank Dr. Reiner Große for his help with the measurements of the dielectric permittivities of the osmolyte solutions.

I want to thank the collaboration partners, Prof. Catherine A. Royer, Prof. Bertrand Garcia-Moreno, Prof. Doug Barrick, and Prof. Kazuyuki Akasaka, and all of their coworkers for proving the different proteins studied, the excellent work, and for involving me into the collaboration.

For proof-reading I am thankful to Dr. Michael Paulus, Dr. Julia Nase, Johannes Möller, Christoph Sahle, and Sabrina Hoffmann.

I am indebted to my dear friend Sabrina Hoffmann for the wonderful atmosphere in our office and it was a pleasure for me to share this office with Sebastian Tiemeyer for the last years. I thank all former and present members of the chair Experimentelle Physik I for help and a nice atmosphere within office times, beam times, and extra-curricular events. In particular I thank Dr. Stefanie Duffe, Dr. Julia Nase, Dr. Felix Lehmkühler, Dr. Michael Paulus, and Priv.-Doz. Heinz Hövel for fruitful and funny discussions. I am very glad that Johannes Möller continues my work competently.

The DFG and BMBF are acknowledged for financial support.

I am indebted to all my friends only to name Florian Wieland, Christoph Sahle, Sabrina Hoffmann, Rüdiger Stirnberg, Daniel Brenner, and Felix Spennemann for their dear friendship within the last years.

Last but not least, I am thankful to my dear family to whom this thesis is dedicated. I want to thank my parents, Peter Schroer and Ok-Young Rohbeck-Schroer, my grandmother Marianne Schroer, and my brother Carsten Schroer for their encouragement and love. Moreover, I want to thank my father for inspiring me to be interested in many fields as he is, and my brother for supporting my interest in chemistry. These two aspects largely contributed to the successfully finishing of my thesis.

Eidesstattliche Erklärung

Ich versichere hiermit an Eides statt, dass ich die vorliegende Dissertation mit dem Titel „Small angle X-ray scattering studies on proteins under extreme conditions“ selbständig und ohne unzulässige fremde Hilfe erbracht habe. Ich habe keine anderen als die angegebenen Quellen und Hilfsmittel benutzt sowie wörtlich und sinngemäße Zitate kenntlich gemacht. Die Arbeit hat in gleicher oder ähnlicher Form noch keiner Prüfungsbehörde vorgelegen.

Dortmund, den

_____

(Martin A. Schroer)